

LIMITED DUCTILITY DESIGN
OF
REINFORCED CONCRETE COLUMNS

A report submitted in partial fulfilment
of the requirements for the degree of
Master of Engineering at the University
of Canterbury, Christchurch, New Zealand

by

M.T. SOESIANAWATI

1986

ABSTRACT

This report describes an experimental and analytical investigation of the strength and ductility of reinforced concrete columns.

Four columns of square cross-section were tested under axial compression loading and cyclic lateral loading applied at mid-height which simulated seismic loading.

The main variable investigated was the quantity of transverse confining steel used, which ranged between 17 to 46 percent of the NZS 3101:1982 recommended quantity for ductile detailing.

The experimental results are reported in the form of lateral load-displacement and lateral load-curvatures hysteresis loops, curvature profiles, transverse steel strain distributions and concrete compressive strains.

The results are discussed and compared with the analytical predictions. A modified equation for the quantity of confining reinforcement in rectangular columns is recommended. Conclusions are made regarding the ductility available from columns containing substantially less transverse confining reinforcement than recommended by the New Zealand concrete design code.

ACKNOWLEDGEMENTS

The material presented in this report is based on the research work carried out in the Department of Civil Engineering, University of Canterbury.

Firstly, I express my special gratitude to Professor R. Park, the Head of Department and the main supervisor for this project, for his invaluable advice, helpful guidance and particularly for a great deal of encouragement throughout the project.

My special gratitude is also due to Dr. M.J.N. Priestley, the co-supervisor for this project, for all his invaluable guidance and advice.

I am very thankful for the assistance given by the Senior Technical Officer, Mr. N.W. Prebble, and all the technical staff of the Civil Engineering Department. Special thanks are due to Messrs. P.F. Coursey, V.A. Scott, G.E. Hill, D.J. McPherson and G.H. Clarke for their contribution towards the construction and testing of the reinforced concrete column specimens, and to H.H. Crowther for arranging the purchase of materials and equipment.

I wish to thank the academic staff and graduate students of the Civil Engineering Department for their advice and assistance throughout the project.

The financial assistance provided by the National Roads Board is very gratefully acknowledged.

Thanks are also due to Ms. L. Leonard for her tracing assistance and to Mr. L.H. Gardner for the photographic processing. My special thanks are due to Mrs. D.E. Ball for typing the manuscript and for her friendly helpfulness.

Finally, I express my deepest gratitude to my parents, sisters and brothers for their precious support and encouragement.

CONTENTS

	Page
ABSTRACT	i
ACKNOWLEDGEMENTS	ii
CONTENTS	iii
NOTATION	viii
 CHAPTER ONE : <u>INTRODUCTION</u>	 1
1.1 SEISMIC DESIGN PHILOSOPHY	1
1.2 PREVIOUS NEW ZEALAND RESEARCH ON COLUMN AND PILE DUCTILITY	1
1.3 BACKGROUND AND SCOPE OF RESEARCH	2
 CHAPTER TWO : <u>DESIGN, CONSTRUCTION AND INSTRUMENTATION OF COLUMN UNITS</u>	 4
2.1 INTRODUCTION	4
2.2 DESIGN OF COLUMN UNITS	4
2.2.1 General Description	4
2.2.2 Unit Size	4
2.2.3 Longitudinal Reinforcement	6
2.2.4 Transverse Reinforcement	6
2.3 CONSTRUCTION OF THE COLUMN UNITS	13
2.3.1 Mould	13
2.3.2 Fabrication of Reinforcing Cage	13
2.3.3 Placing of Concrete	15
2.4 INSTRUMENTATION OF THE COLUMN UNITS	19
2.4.1 Load and Displacement	19
2.4.2 Column Curvature	20
2.4.3 Transverse Strains	20
2.4.4 Data Acquisition	24
 CHAPTER THREE : <u>MATERIAL PROPERTIES OF COLUMN UNITS</u>	 25
3.1 INTRODUCTION	25
3.2 STEEL TENSION TESTING	25
3.3 CONCRETE STRENGTH	28
3.3.1 Compression Tests	28
3.3.2 Bending Test	28

CHAPTER FOUR	: <u>CODE REQUIREMENTS FOR AMOUNT OF TRANSVERSE REINFORCEMENT</u>	30
4.1	INTRODUCTION	30
4.2	TRANSVERSE REINFORCEMENT FOR CONCRETE CONFINEMENT	30
4.2.1	New Zealand Concrete Design Code Provisions	30
4.2.2	Comparison of New Zealand Concrete Design Code Equation and the Modified Equation with the Quantities of Transverse Reinforcement Provided in the Column Units	33
4.3	TRANSVERSE REINFORCEMENT TO PREVENT PREMATURE BUCKLING OF LONGITUDINAL REINFORCEMENT	34
4.3.1	New Zealand Concrete Design Code Provisions	34
4.3.2	Comparison of New Zealand Concrete Design Code Requirements with the Quantities of Transverse Reinforcement Provided in the Column Units	35
4.4	TRANSVERSE REINFORCEMENT FOR SHEAR	35
4.4.1	New Zealand Concrete Design Code Provisions	35
4.4.2	Comparison of New Zealand Concrete Design Code Requirements and Shear Strength of Columns	36
4.5	CONCLUDING REMARKS	38
CHAPTER FIVE	: <u>ANALYTICAL INVESTIGATION OF THE COLUMN UNITS</u>	39
5.1	INTRODUCTION	39
5.2	THEORETICAL CONSIDERATIONS	39
5.3	ANALYTICAL STRESS-STRAIN RELATIONSHIPS FOR CONCRETE	41
5.3.1	Stress-strain Relationship for Concrete Proposed by Kent and Park with Modifications	41
5.3.2	Stress-strain Relationship for Concrete Proposed by Mander, Priestley and Park	43

	Page
5.3.3 Comparison of the Models	45
5.4 ANALYTICAL STRESS-STRAIN RELATIONSHIP FOR LONGITUDINAL REINFORCING STEEL	48
5.5 MOMENT-CURVATURE ANALYSES FOR COLUMN UNITS	48
5.5.1 Monotonic Moment-Curvature Analysis	48
5.5.2 Cyclic Moment-Curvature Analysis	50
5.5.3 Design Charts for Ductility	51
5.6 THEORETICAL YIELD CURVATURE AND YIELD DISPLACEMENT	51
CHAPTER SIX : <u>TESTING PROCEDURE</u>	53
6.1 INTRODUCTION	53
6.2 TEST PREPARATION	53
6.2.1 Installation of Column Units	53
6.2.2 Loading Frame	56
6.2.3 Concrete Compression Test	57
6.3 COLUMN TESTING	57
CHAPTER SEVEN : <u>EXPERIMENTAL RESULTS AND OBSERVATIONS</u>	61
7.1 INTRODUCTION	61
7.2 ASPECTS OF THE INVESTIGATION	61
7.3 THE PERFORMANCE OF COLUMN UNIT 1	67
7.4 THE PERFORMANCE OF COLUMN UNIT 2	82
7.5 THE PERFORMANCE OF COLUMN UNIT 3	98
7.6 THE PERFORMANCE OF COLUMN UNIT 4	112
7.7 CONCLUDING REMARKS	127
CHAPTER EIGHT : <u>DISCUSSION OF THE EXPERIMENTAL RESULTS</u>	129
8.1 INTRODUCTION	129
8.2 ASPECTS OF THE DISCUSSION AND COMPARISONS OF THE EXPERIMENTAL RESULTS WITH THE ANALYTICAL INVESTIGATIONS	129
8.2.1 General Behaviour	129
8.2.2 Moment-Curvature Relationships	129
8.2.3 Yield Curvature and Yield Displacement	130
8.2.4 Ultimate Curvature and Available Curvature Ductility Factor	136
8.2.5 Flexural Overstrength Factor	138

8.2.6	Lateral Load-Displacement Hysteresis Loops	141
8.2.7	Available Displacement Ductility Factor	146
8.2.8	Maximum Displacement and Maximum Drift	148
8.2.9	Equivalent Plastic Hinge Length	149
8.2.10	Spalling Strain and Maximum Compressive Strain	149
8.3	COMPARISON OF THE PERFORMANCE OF UNITS 1 AND 2 WITH THE COLUMN UNITS TESTED BY ANG ET AL	151
8.4	CONCLUDING REMARKS	153
CHAPTER NINE	: <u>ANALYTICAL INVESTIGATION OF RECTANGULAR COLUMNS WITH THE PROPOSED MODIFIED CODE QUANTITY OF TRANSVERSE REINFORCEMENT FOR CONFINEMENT</u>	155
9.1	INTRODUCTION	155
9.2	MOMENT-CURVATURE ANALYSES FOR RECTANGULAR COLUMNS WITH THE QUANTITY OF TRANSVERSE REIN- FORCEMENT AS GIVEN BY THE MODIFIED EQUATION	155
9.2.1	General Description	155
9.2.2	Analytical Moment-Curvature Relationships	157
9.3	COMPARISON OF THE ANALYTICAL CYCLIC MOMENT- CURVATURE HYSTERESIS LOOPS AND THE AVAILABLE CURVATURE DUCTILITY FACTORS FOR RECTANGULAR COLUMNS CONTAINING THE PROPOSED MODIFIED CODE VALUE OF TRANSVERSE REINFORCEMENT WITH CIRCULAR COLUMNS CONTAINING THE CODE RECOMMENDED QUANTITY OF SPIRAL CONFINING STEEL.	161
9.4	CONCLUDING REMARKS	167
CHAPTER TEN	: <u>CONCLUSIONS AND RECOMMENDATIONS</u>	169
10.1	CONCLUSIONS	169
10.2	RECOMMENDATIONS FOR FUTURE RESEARCH	170
REFERENCES		172
APPENDIX A	: <u>COMPUTER PROGRAMS</u>	175
A.1	GENERAL	175
A.2	UNITS	175

A.3	SOURCE LISTING OF SSCONCRETE	176
A.4	SOURCE LISTING OF SSSTEEL	181
A.5	COMPUTER PROGRAM MMPHI	183
A.5.1	Description	183
A.5.2	Data Deck	183
A.5.3	Source Listing	188

APPENDIX B : APPLICATION OF THE DESIGN CHARTS BY ZAHN TO
OBTAIN THE FLEXURAL STRENGTH AND DUCTILITY
OF THE COLUMN UNITS

B.1	AVAILABLE CURVATURE DUCTILITY	201
B.2	IDEAL FLEXURAL STRENGTH AND FLEXURAL OVERSTRENGTH FACTOR	206

NOTATION

ΣA_b	=	sum of areas of longitudinal bars
A_c	=	area of concrete core of section measured to outside of peripheral spiral or hoop
A_{ci}	=	area of i th concrete lamina
A_g	=	gross area of section
A_s	=	area of tension reinforcement
A_{sb}	=	area of transverse reinforcement bar
A_{sh}	=	total effective area of hoop bars and supplementary cross ties in direction under consideration with spacing s_h
A_{sj}	=	area of j th steel level
A_{st}	=	total area of longitudinal reinforcement
A_t	=	area of one leg of hoop or cross tie
A_v	=	total area of shear reinforcement parallel to direction of shear force within spacing s_h
b	=	width of column section, in the design charts
b''	=	dimension of concrete core of section measured perpendicular to the direction of the hoop bars to outside of peripheral hoop, in rectangular columns
b_c	=	width of concrete core of section measured to centreline of peripheral hoop
b_w	=	width of column section
c	=	distance from extreme compression fibre to neutral axis
D	=	overall diameter of circular column section
d	=	distance from extreme compression fibre to centroid of tension reinforcement
d_b	=	reinforcing bar diameter
d_s	=	diameter of spiral
E_c	=	modulus of elasticity of concrete
E_s	=	modulus of elasticity of steel
E_{sec}	=	f'_{cc}/ϵ_{cc} in Popovics' equation

E_{sh}	=	strain-hardening modulus of steel
EI	=	effective flexural rigidity of column section
f_c	=	longitudinal stress in concrete
f'_c	=	compressive cylinder strength of concrete
f'_{cc}	=	peak longitudinal compressive stress of the stress-strain curve of confined concrete
f'_{ci}	=	concrete stress in i th lamina
f'_{co}	=	peak longitudinal compressive stress of the stress-strain curve of unconfined concrete
f'_l	=	effective lateral confining stress acting on concrete
f_r	=	modulus of rupture of concrete
f_r	=	effective lateral confining stress acting on concrete, in the design charts
f_{sj}	=	steel stress in j th level
f_s	=	stress in steel
f_{su}	=	ultimate tensile strength of steel
f_y	=	yield strength of longitudinal reinforcing steel
f_{yh}	=	yield strength of transverse reinforcing steel
g	=	distance between extreme steel layers in long faces, in the design charts
H	=	lateral load
H_i	=	lateral load at ideal column strength
H_{max}	=	maximum lateral load occurred during testing
h	=	overall depth of column section
h''	=	dimension of concrete core section measured perpendicular to the direction of the hoop bars to outside of peripheral hoop
h''	=	dimension of concrete core of section measured perpendicular to the direction of the hoop bars to centreline of peripheral hoop, in the Mander et al model
h_c	=	depth of concrete core of section measured to centreline of peripheral hoop

K	=	strength enhancement factor for confined concrete
K_{m0}	=	flexural strength enhancement factor, Fig. B.7
K_{m1}	=	flexural strength enhancement factor, Fig. B.8
K_{m2}	=	flexural strength enhancement caused by the additional confinement provided by adjacent member
K_{m3}	=	flexural strength enhancement to allow for strain hardening of steel
k_e	=	confinement effectiveness coefficient based on the area of effectively confined concrete core
k_e^*	=	confinement effectiveness coefficient based on the first moment of area of effectively confined concrete core
L_o	=	gauge length of reinforcing steel
ℓ	=	distance from section of maximum moment to point of contraflexure
ℓ'	=	distance from mid-height of column to point of contraflexure
ℓ_p/h	=	non-dimensional equivalent plastic hinge length
$(\ell_p/h)_{av}$	=	average of non-dimensional equivalent plastic hinge lengths measured at the first and second potentiometer levels
M	=	moment
\overline{M}	=	average of the magnitude of the experimental moments measured at the positive and negative peaks of the first cycle at $\mu_n = 2$
M_{code}	=	flexural strength calculated using the code approach, in the design charts
M_i	=	ideal flexural column strength calculated using the code approach
M_i	=	ideal flexural column strength, in the design charts
M_{max}	=	maximum moment
M_y	=	moment calculated at first yield of longitudinal reinforcement
m	=	$f_y/0.85f'_c$

n	=	number of hoop legs crossing the section per hoop set
n_c	=	number of concrete laminae
n_s	=	number of steel levels
P	=	compressive concentric load on column
p	=	strain hardening power
P_e	=	axial compression load on column due to design gravity and seismic loading
P_o	=	ideal axial load compressive strength when the load is applied with zero eccentricity
r	=	$E_c / (E_c - E_{sec})$ in Popovics' equation
S_o	=	cross sectional area of reinforcing steel
s'	=	clear spacing between hoop bars in which arching action of concrete develops
s_h	=	centre-to-centre spacing of hoop sets
t	=	age of concrete
V_c	=	shear force resisted by concrete shear resisting mechanisms
V_i	=	ideal shear strength of column ($= V_c + V_s$)
V_o	=	design shear force at overstrength flexural capacity
V_s	=	shear force resisted by steel reinforcement
V_u	=	shear force at ideal flexural capacity
v_b	=	basic nominal shear stress carried by concrete
v_c	=	ideal shear stress provided by concrete
w	=	centre-to-centre spacing between longitudinal bars
w'	=	clear spacing between longitudinal bars in which arching action of concrete develops
x	=	$\epsilon_c / \epsilon_{cc}$ in Popovics' equation
y_{ci}	=	distance from extreme compression fibre to the centre of i th concrete lamina
y_{sj}	=	distance from extreme compression fibre to j th steel level
Z	=	slope of linear falling branch, for unconfined concrete
Z_m	=	slope of linear falling branch, for confined concrete

α	=	$\rho_s / \rho_{s \text{ code}}$
β	=	b/h , in the design charts
γ	=	curvature ductility modification factor
γ_{cover}	=	factor to allow for the influence of relative cover thickness on curvature ductility
$\gamma f'_c$	=	factor to allow for the influence of concrete cylinder strength on curvature ductility
γf_y	=	factor to allow for the influence of steel grade of longitudinal bars on curvature ductility
γf_{yh}	=	factor to allow for the influence of steel grade of confining steel on curvature ductility
Δ	=	lateral displacement of column
Δ_b	=	lateral displacement for the bottom half of column, including the rotation of central stub
Δ_t	=	lateral displacement for the top half of column, including the rotation of central stub
Δ_{max}	=	maximum lateral displacement occurred during testing
$\Delta_{\text{max}}/\ell'$	=	maximum drift
Δ_p	=	plastic deformation
Δ_y	=	yield displacement
Δ_y'	=	displacement at first yield of longitudinal reinforcement
Δ_y^*	=	initial experimental yield displacement
ϵ_c	=	concrete strain
ϵ_{cc}	=	compressive strain in confined concrete corresponding to f'_{cc}
ϵ_{cm}	=	concrete strain in extreme compression fibre
ϵ_{cmax}	=	maximum compressive strain of concrete
ϵ_{co}	=	compressive strain in unconfined concrete corresponding to f'_{co}
ϵ_s	=	strain in steel
ϵ_{sf}	=	steel strain at fracture
ϵ_{sh}	=	steel strain at the commencement of strain-hardening

ϵ_{spall}	=	spalling strain of cover concrete
ϵ_{su}	=	ultimate steel strain
ϵ_{y}	=	steel strain at first yield
θ	=	rotation of central stub
μ	=	displacement ductility factor
μ_{n}	=	nominal displacement ductility factor
μ_{r}	=	real displacement ductility factor
ρ_{cc}	=	ratio of volume of longitudinal steel to volume of concrete core, measured to the centreline of perimeter hoop
ρ_{s}	=	ratio of volume of transverse reinforcement to volume of concrete core
ρ_{t}	=	area of longitudinal reinforcement divided by gross area of column section
$\rho_{\text{t}}^{\text{m}}$	=	mechanical reinforcing ratio
ρ_{w}	=	$A_{\text{s}}/b_{\text{w}}d$
ϕ	=	strength reduction factor
ϕ	=	curvature
ϕ_{b}	=	curvature measured in the potentiometers gauge nearest the central stub, below the stub
ϕ_{t}	=	curvature measured in the potentiometers gauge nearest the central stub, above the stub
ϕ_{u}	=	ultimate curvature
ϕ_{y}	=	yield curvature
ϕ_{y}'	=	curvature calculated at first yield of longitudinal reinforcement
ϕ_{y}^*	=	curvature corresponding to Δ_{y}^*
$\phi_{\text{u}}/\phi_{\text{y}}$	=	available curvature ductility
$(\phi_{\text{u}}/\phi_{\text{y}})_{\text{b}}$	=	available curvature ductility obtained from the basic design chart, Fig. B.2

CHAPTER ONE

INTRODUCTION

1.1 SEISMIC DESIGN PHILOSOPHY

When designing an earthquake resistant structure economic considerations usually require that the large seismic energy input be absorbed and dissipated through large but controllable inelastic deformations of the structure.

To achieve adequate inelastic deformation capacity without significant strength degradation, namely ductility, the sources of potential structural brittle failure should be eliminated. In the case of a reinforced concrete structure, it is necessary to prevent premature crushing and shear of concrete, sudden cracking and simultaneous fracturing of steel (as in the case of members with extremely low reinforcement ratio), loss of bond and anchorage of reinforcement, premature crushing and/or splitting of the cover concrete accompanied by local buckling of the longitudinal bars, and the possibility of dynamic instability resulting from large lateral drifts. Also, degradation of strength under seismic cyclic loading must be minimized or delayed long enough to permit survival of the structure. The elimination of these types of undesirable failure is the aim of the seismic provisions of the New Zealand codes for reinforced concrete^(1,2).

1.2 PREVIOUS NEW ZEALAND RESEARCH ON COLUMN AND PILE DUCTILITY

Much of the structural research at the University of Canterbury has been directed towards an assessment of the strength and ductility of reinforced concrete columns and bridge piers of different cross sections, containing different amounts and configurations of flexural and confining reinforcement. Some laboratory tests on prestressed concrete and steel-encased reinforced concrete piles have also been carried out.

Except for some hollow reinforced concrete bridge piers tested by Mander⁽³⁾ and prestressed concrete piles tested by Pam⁽⁴⁾, most of the tests have been conducted to investigate the performance of columns and piles detailed for full ductility under simulated seismic loading. These tests have led to the requirements for transverse reinforcement in the columns and piles detailed for full ductility specified by the New Zealand concrete design code NZS 3101:1982⁽²⁾. The tests have demonstrated that

the quantities of transverse reinforcement recommended in the code⁽²⁾ resulted in an available displacement ductility factor of at least eight in the columns and piles.

1.3 BACKGROUND AND SCOPE OF RESEARCH

According to the New Zealand concrete design code NZS 3101:1982⁽²⁾ the volumetric ratio of transverse reinforcement in the form of spirals or circular hoops in the potential plastic hinge regions of columns in seismic design should not be less than

$$\rho_s = 0.45 \left(\frac{A_g}{A_c} - 1 \right) \frac{f'_c}{f_{yh}} \left(0.5 + 1.25 \frac{P_e}{\phi f'_c A_g} \right) \quad (1.1)$$

or

$$\rho_s = 0.12 \frac{f'_c}{f_{yh}} \left(0.5 + 1.25 \frac{P_e}{\phi f'_c A_g} \right) \quad (1.2)$$

whichever is greater, where A_g is gross area of column cross section, A_c is area of concrete core of section measured to outside of peripheral hoop, f'_c is concrete compressive strength, f_{yh} is yield strength of transverse hoops, P_e is axial compression load due to design gravity and seismic loading and ϕ is strength reduction factor.

The code⁽²⁾ also requires that for arrangements of rectangular hoops, the total effective area of transverse hoops A_{sh} in each principal direction in the potential plastic hinge regions of columns in seismic design should not be less than

$$A_{sh} = 0.3 s_h h'' \left(\frac{A_g}{A_c} - 1 \right) \frac{f'_c}{f_{yh}} \left(0.5 + 1.25 \frac{P_e}{\phi f'_c A_g} \right) \quad (1.3)$$

or

$$A_{sh} = 0.12 s_h h'' \frac{f'_c}{f_{yh}} \left(0.5 + 1.25 \frac{P_e}{\phi f'_c A_g} \right) \quad (1.4)$$

whichever is greater, where s_h is centre-to-centre spacing of hoop sets, h'' is dimension of concrete core of the section measured perpendicular to the direction of the hoop bars and to the outside of the perimeter hoop, and the other notation is as for columns with spirals or circular hoops.

The NZS 3101⁽²⁾ equations result in a greater volume of rectangular hoop steel being required for columns than spiral or circular hoop steel. One objective of this study is to investigate the applicability of a proposed modification of Eq. 1.4, involving the replacement of the numerical coefficient 0.12 by 0.08. This proposed modification results from

matching Eqs. 1.4 and 1.2 in the same manner as Eqs. 1.3 and 1.1 are matched^(5,6). The modified Eq. 1.4 is then

$$A_{sh} = 0.08 s_h h'' \frac{f'_c}{f_{yh}} \left(0.5 + 1.25 \frac{P_e}{\phi f'_c A_g} \right) \quad (1.5)$$

Another objective of this study is to investigate the behaviour columns with reduced quantities of transverse reinforcement. It is of interest to assess the performance of this type of column, since the provisions for transverse reinforcement in the concrete design code⁽²⁾ not include any indication of the levels of ductility available from columns designed with various quantities of transverse reinforcement.

CHAPTER TWO

DESIGN, CONSTRUCTION AND INSTRUMENTATION
OF COLUMN UNITS

2.1 INTRODUCTION

The experimental research for this project was also carried out using the DARTEC 10 MN universal testing machine at the University of Canterbury.

Four column units with square cross sections were designed and constructed. The column units were held in position under constant axial compression load while reversible lateral load was applied at the mid-height of the column units (see Fig. 2.1).

2.2 DESIGN OF COLUMN UNITS

2.2.1 General Description

The main variable investigated in this experimental program was the amount of rectangular transverse hoop reinforcement provided in each column unit. Another variable was the level of axial compression load applied, namely $0.1 f'_c A_g$ for Unit 1 and $0.3 f'_c A_g$ for Units 2, 3 and 4.

Details of the transverse reinforcement are described in detail in Section 2.2.4. Units 1 and 2 were to check experimentally and analytically the use of the area of transverse hoops A_{sh} given by the modified Eq. 1.5, while Units 3 and 4 were to check experimentally and analytically the ductility available from columns with less transverse reinforcement than that given by the modified equation.

2.2.2 Unit Size

Based on the consideration that the maximum height of column units that can be tested in the DARTEC testing machine is about 4 m, four column units of 3.9 m high and of 400 x 400 mm square cross section were designed. Fig. 2.1 shows applied loads and dimensions of column units, which were similar in overall dimensions and longitudinal reinforcement to Units 3 and 4 of the columns tested by Ang et al⁽⁷⁾.

Each column unit was subjected to axial compression load and was laterally loaded through a heavily reinforced stub at mid-height. The reversible horizontal load on the stub was applied by either load control-

led or displacement controlled 1 MN hydraulic jack.

The distribution of bending moment in the upper and lower halves of each column unit was similar to that in a column between the point of maximum moment and the point of contraflexure. The central stub modelled the effect of a pier or pile cap, footing or beam.

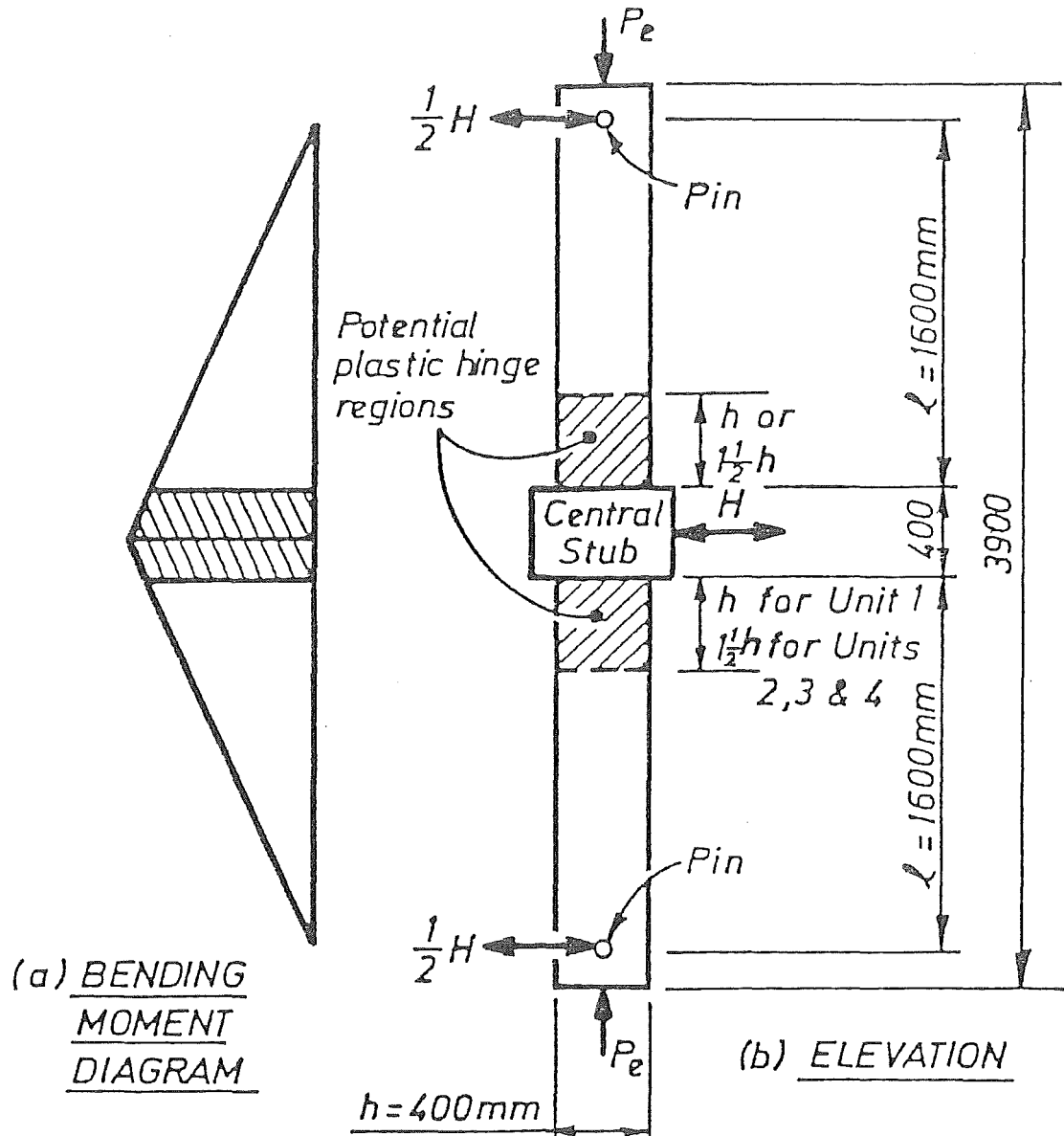


Fig. 2.1 : APPLIED LOADS AND DIMENSIONS OF COLUMN UNITS

2.2.3 Longitudinal Reinforcement

Twelve 16 mm diameter Grade 380 deformed bars (12 HD 16) were used as longitudinal reinforcing steel for all column units giving a reinforcement ratio ρ_t of 0.0151.

The steel was uniformly distributed around the peripheral of the section (see Fig. 2.2).

2.2.4 Transverse Reinforcement

As discussed previously in Section 1.3, the New Zealand concrete design code NZS 3101:1982⁽²⁾ (Clause 6.5.4.3b) requires in seismic design that in potential plastic hinge regions for columns with arrangements of rectangular hoop reinforcement the total effective area A_{sh} should not be less than

$$A_{sh} = 0.3 s_h h'' \left[\frac{A_g}{A_c} - 1 \right] \frac{f'_c}{f_{yh}} \left[0.5 + 1.25 \frac{P_e}{\phi f'_c A_g} \right] \quad (2.1)$$

or

$$A_{sh} = 0.12 s_h h'' \frac{f'_c}{f_{yh}} \left[0.5 + 1.25 \frac{P_e}{\phi f'_c A_g} \right] \quad (2.2)$$

whichever is the greater. The notation used in Eqs. 2.1 and 2.2 may be seen in the Notation.

Also, Section 1.3 pointed out that the purpose of the present project is to investigate the possibility of modifying Eq. 2.2 by replacing "0.12" by "0.08" as proposed previously^(5,6). The modified equation is then

$$A_{sh} = 0.08 s_h h'' \frac{f'_c}{f_{yh}} \left[0.5 + 1.25 \frac{P_e}{\phi f'_c A_g} \right] \quad (2.3)$$

The reason for this modification is discussed in Section 4.2.

Eq. 2.3 will govern the amount of transverse reinforcing steel required in the plastic hinge regions if 0.08 is greater than $0.3 \left(\frac{A_g}{A_c} - 1 \right)$, i.e. if A_g/A_c is less than 1.267. Consequently, for Eq. 2.3 to be critical, the cover to hoops has to be such that $\frac{A_g}{A_c} < 1.267$

where A_g = gross area of column cross section = $400 \times 400 \text{ mm}^2$

A_c = area of concrete core of section measured to outside of peripheral transverse steel = h''^2 (see Fig. 2.2)

$$\therefore \frac{A_g}{A_c} = \left(\frac{400}{h''} \right)^2 < 1.267$$

$$\text{or } h'' > 355 \text{ mm}$$

Hence, for Eq. 2.3 to be critical for the column units of this project, the cover to hoops should not be greater than 22.5 mm. In the columns tested the cover to hoops used was 13 mm.

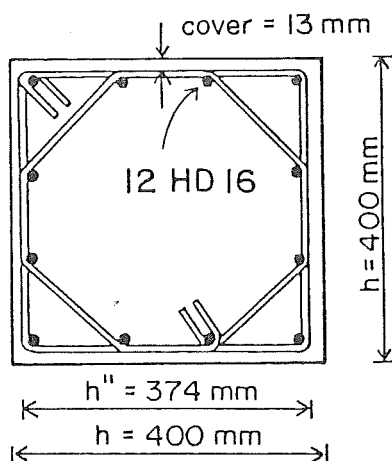


Fig. 2.2 : CROSS SECTION OF COLUMN UNITS

As illustrated in Fig. 2.2, sets of overlapping square and octagonal hoops were used as transverse reinforcement for all column units. It has been previously demonstrated that square columns with hoop arrangements of this type require less transverse reinforcement volume than square columns with sets of overlapping square and rectangular hoops^(5,6,8).

The New Zealand concrete design code NZS 3101:1982⁽²⁾ also requires in seismic design that the centre-to-centre spacing of the hoop sets s_h in the plastic hinge regions of columns shall not exceed the smaller of

- (i) one-fifth of the least lateral dimension of cross section, i.e. $s_h = 0.2h = 0.2 \times 400 = 80 \text{ mm}$, or
- (ii) six times the diameter of the longitudinal bar to be restrained, i.e. $s_h = 6d_b = 6 \times 16 = 96 \text{ mm}$, or
- (iii) $s_h = 200 \text{ mm}$.

From these requirements, $s_h \leq 6d_b$ was used as the governing limitation of spacings of transverse reinforcement in the design of these column units. The $6d_b$ limitation of spacing has proved in past tests⁽⁶⁾ to effectively prevent premature buckling of longitudinal bars when undergoing yield reversals in tension and compression during cyclic loading. It is well known that such stress reversals in the yield range cause a reduction in the tangent modulus of the steel at relatively low stresses, due to the Bauschinger effect, and therefore closely spaced transverse steel providing lateral support is required to prevent buckling of longitudinal steel⁽²⁾.

The requirement of $s_h \leq 0.2h$ specified by the New Zealand code⁽²⁾ could be considered in the light of recent test results⁽⁶⁾ to be a little conservative. The use of the $6d_b$ limitation for these test column units resulted in a centre-to-centre spacing of hoop sets of $s_h = 0.24h$. Hence the test results were also to give an indication as to whether an increase of s_h to about one-quarter of the column dimension could lead to satisfactory performance.

Following on the above considerations, the design of transverse reinforcement for all column units was as follows. In the modified design equation, Eq. 2.3, the strength reduction factor ϕ was taken as unity for all column units and compressive strength of concrete f'_c was assumed to be 30 MPa. For sets of overlapping square and octagonal hoops, $A_{sh} = (2 + \sqrt{2}) A_{sb}$ where A_{sb} is the area of transverse reinforcing bar. The actual measured yield strength of the transverse reinforcement was used.

Units 1 and 2 were designed using Eq. 2.3 and for column load levels of $P_e / \phi f'_c A_g = 0.1$ and 0.3 .

Unit 1 : $P_e / \phi f'_c A_g = 0.1$

Use R7 as transverse reinforcement, $A_{sh} = 131.4 \text{ mm}^2$.

From steel tension testing (refer to Section 3.2), the yield strength f_{yh} for R7 was 364 MPa.

From Eq. 2.3:

$$\frac{A_{sh}}{s_h} = 0.08 \times 374 \times \frac{30}{364} (0.5 + 1.25 \times 0.1)$$

$$= 1.541$$

$$\therefore s_h = \frac{131.4}{1.541} = 85.3, \text{ say } \underline{s_h = 85 \text{ mm}}$$

Unit 2 : $P_e / \phi f'_c A_g = 0.3$

Use R8 as transverse reinforcement, $A_{sh} = 171.6 \text{ mm}^2$.

From steel tension testing, it was found that f_{yh} for R8 was 360 MPa.

Thus,

$$\frac{A_{sh}}{s_h} = 0.08 \times 374 \times \frac{30}{360} (0.5 + 1.25 \times 0.3) \\ = 2.182$$

$$\therefore s_h = \frac{171.6}{2.182} = 78.7, \text{ say } \underline{s_h = 78 \text{ mm}}$$

Units 3 and 4 were designed to contain $\frac{2}{3}$ and $\frac{1}{3}$ of A_{sh} given by Eq. 2.3 respectively, and $P_e / \phi f'_c A_g = 0.3$.

Unit 3 : $P_e / \phi f'_c A_g = 0.3$

Use R7 as transverse reinforcement, $A_{sh} = 131.4 \text{ mm}^2$
 $f_{yh} = 364 \text{ MPa}$

$$\frac{A_{sh}}{s_h} = \frac{2}{3} \times 0.08 \times 374 \times \frac{30}{364} (0.5 + 1.25 \times 0.3) \\ = 1.438$$

$$\therefore s_h = 91.3, \text{ say } \underline{s_h = 91 \text{ mm}}$$

Unit 4 : $P_e / \phi f'_c A_g = 0.3$

Use R6 as transverse reinforcement, $A_{sh} = 96.5 \text{ mm}^2$
 From steel tension testing, f_{yh} for R6 was 255 MPa.

Thus,

$$\frac{A_{sh}}{s_h} = \frac{1}{3} \times 0.08 \times 374 \times \frac{30}{255} (0.5 + 1.25 \times 0.3) \\ = 1.027$$

$$\therefore \underline{s_h = 94 \text{ mm}}$$

According to NZS 3101:1982⁽²⁾, the spacing of transverse reinforcement outside the potential plastic hinge regions, shall not exceed twice that in the potential plastic hinge regions nor $0.5d$ where d is the distance from extreme compression fibre to centroid of tension reinforcement. Therefore, for Units 1, 2 and 3, the spacings of transverse reinforcement outside plastic hinge regions were 170, 156 and 182 mm respectively. For Unit 4, the spacing was governed by $0.5d$, i.e. 186 mm.

Also, according to NZS 3101:1982⁽²⁾, the length of the potential plastic hinge region for axial load levels of less than or equal to

$0.3\phi f'_c A_g$ is taken as the longer cross-section dimension (400 mm) or where the moment exceeds 80% of the maximum moment (320 mm), whichever is greater. For axial load levels higher than $0.3\phi f'_c A_g$, the potential plastic hinge region is taken as 50% greater than the above requirement. The lengths of the potential plastic hinge regions were taken as 400 mm for Unit 1 and 600 mm for Units 2, 3 and 4.

The arrangement of reinforcement for all column units are shown in Figs. 2.3 and 2.4 respectively. Table 2.1 summarizes the details of the column units.

Table 2.1 : DETAILS OF COLUMN UNITS

Unit	$\frac{P_e}{f'_c A_g}$	Longitudinal Reinforcement ^(a)		Transverse Reinforcement				
		Diameter (mm)	f_y (MPa)	Diameter (mm)	f_{yh} (MPa)	Spacing ^(b) s_h (mm)	% of current code ^(c) equation	% of modified ^(d) equation
1	0.1	HD16	446	R7	364	85	67	100
2	0.3	HD16	446	R8	360	78	67	101
3	0.3	HD16	446	R7	364	91	45	67
4	0.3	HD16	446	R6	255	94	22	33

(a) $\rho_t = 0.0151$

(b) Spacing of transverse reinforcement in potential plastic hinge regions

(c) $A_{sh} = 0.12 s_h h'' \frac{f'_c}{f_{yh}} \left(0.5 + 1.25 \frac{P_e}{\phi f'_c A_g} \right)$

(d) $A_{sh} = 0.08 s_h h'' \frac{f'_c}{f_{yh}} \left(0.5 + 1.25 \frac{P_e}{\phi f'_c A_g} \right)$

(e) $\phi = 1$ is assumed in all equations.

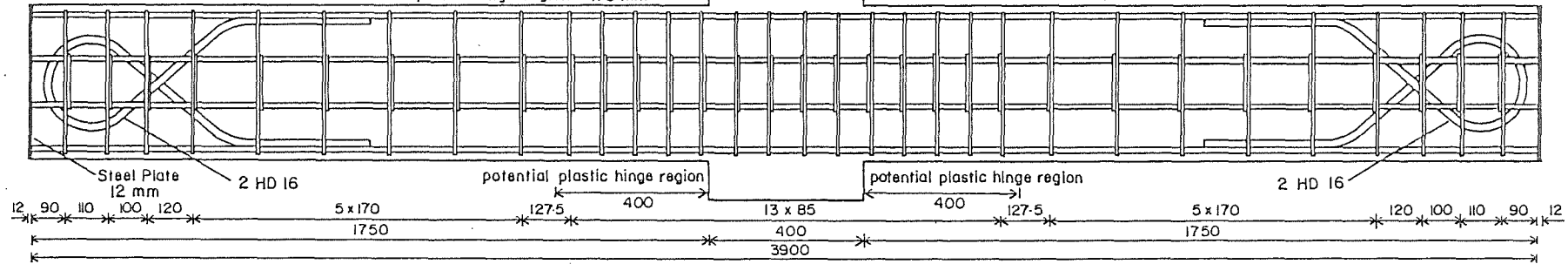
The arrangement of the reinforcement in the central stub for all column units is shown in Fig. 2.5. As mentioned in Section 2.2.2, the central stub needs to be heavily reinforced. This is to ensure that the stub remains in the elastic range during testing and hence that yielding will occur in the potential plastic hinge regions during the testing. The main bars making up the supplementary cage for the central stub were of 12 mm diameter Grade 380 steel.

UNIT 1

$$P_a = 0.1 f'_c A_g$$

Longitudinal reinforcing steel: 12 HD 16

Transverse reinforcing steel: R7, spacing: In the plastic hinge region = 85 mm
outside plastic hinge region = 170 mm

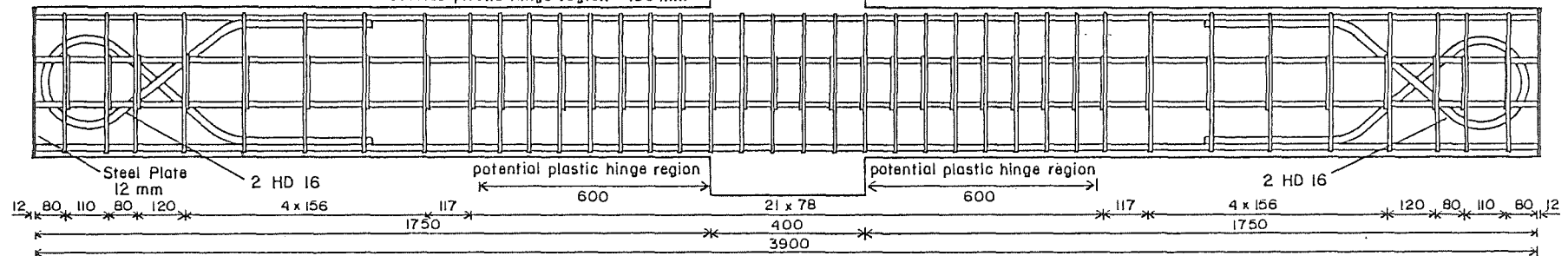


UNIT 2

$$P_a = 0.3 f'_c A_g$$

Longitudinal reinforcing steel: 12 HD 16

Transverse reinforcing steel: R8, spacing: In the plastic hinge region = 78 mm
outside plastic hinge region = 156 mm



Note: all dimensions in mm
Reinforcement in the central stub is not shown

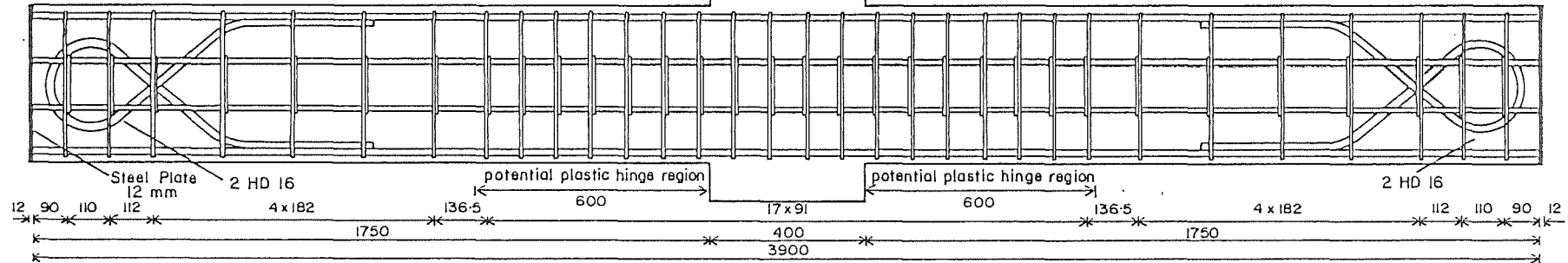
Fig. 2.3: THE ARRANGEMENT OF REINFORCEMENT IN UNITS 1 AND 2

UNIT 3

$$P_e = 0.3 f'_c A_g$$

Longitudinal reinforcing steel: 12 HD 16

Transverse reinforcing steel: R7, spacing: in the plastic hinge region = 91 mm
outside plastic hinge region = 182 mm

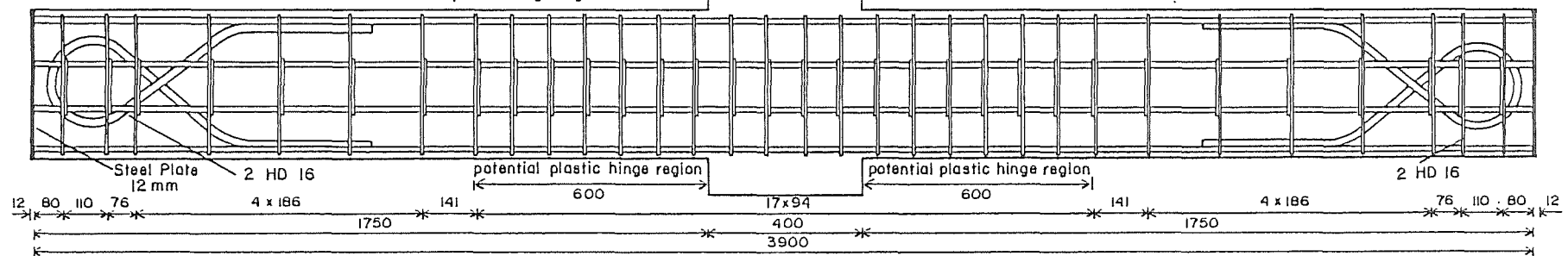


UNIT 4

$$P_e = 0.3 f'_c A_g$$

Longitudinal reinforcing steel: 12 HD 16

Transverse reinforcing steel: R6, spacing: in the plastic hinge region = 94 mm
outside plastic hinge region = 186 mm



Note: all dimensions in mm
Reinforcement in the central stub is not shown

Fig. 2.4 : THE ARRANGEMENT OF REINFORCEMENT IN UNITS 3 AND 4

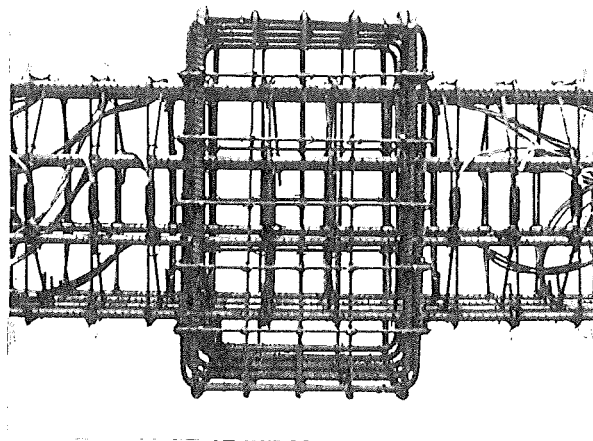


Fig. 2.5 : THE ARRANGEMENT OF REINFORCEMENT IN THE CENTRAL STUB
FOR ALL COLUMN UNITS

2.3 CONSTRUCTION OF THE COLUMN UNITS

2.3.1 Mould

Two plywood moulds were constructed. Steel channel sections were used to form a stiff base. The moulds were also stiffened with angle sections along the edges and held in position with screws and rods across the top and bottom. The moulds were painted to prevent water absorption during curing of the concrete.

2.3.2 Fabrication of Reinforcing Cage

The fabrication of each reinforcing cage was commenced by tying some transverse hoops to the longitudinal bars. The two 400 x 400 x 12 mm steel end plates, which had pre-bored holes to locate the longitudinal bars, were then welded to the longitudinal bars at each end of the cage. Finally, all the transverse hoops were fixed to the longitudinal bars by tying wire and the reinforcement in the central stub constructed. The reinforcing cages of all column units are shown in Fig. 2.6.

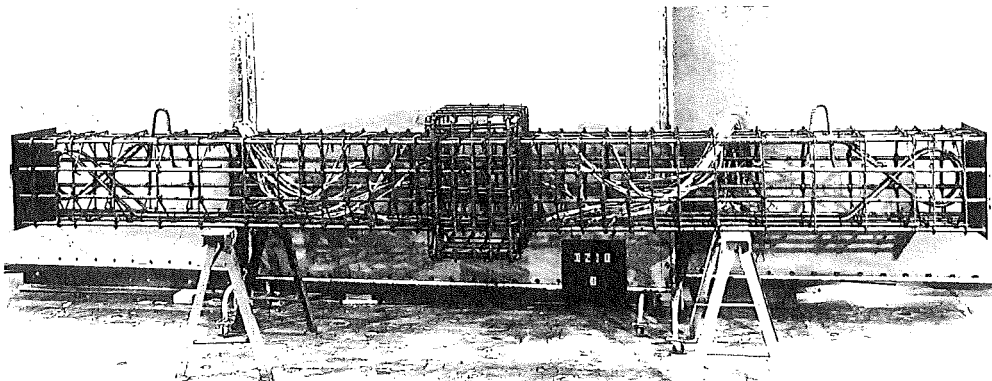
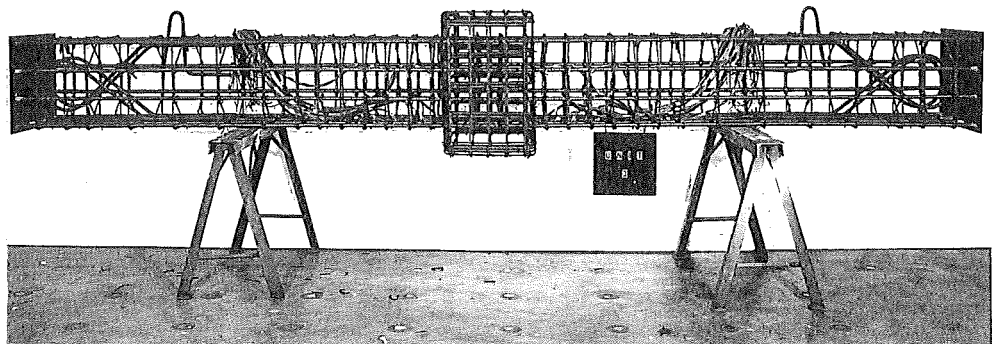
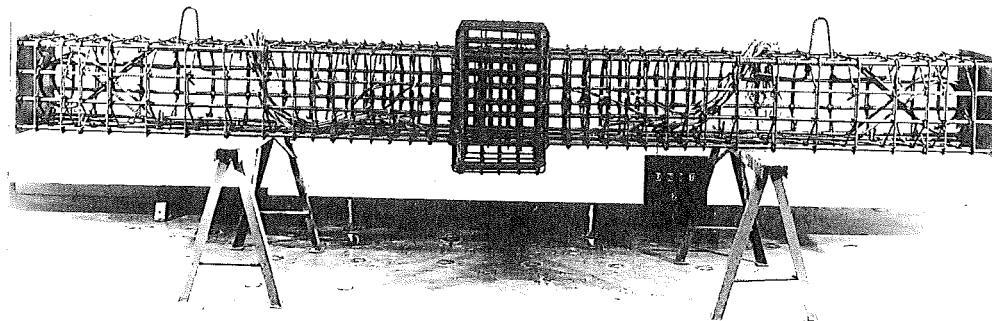
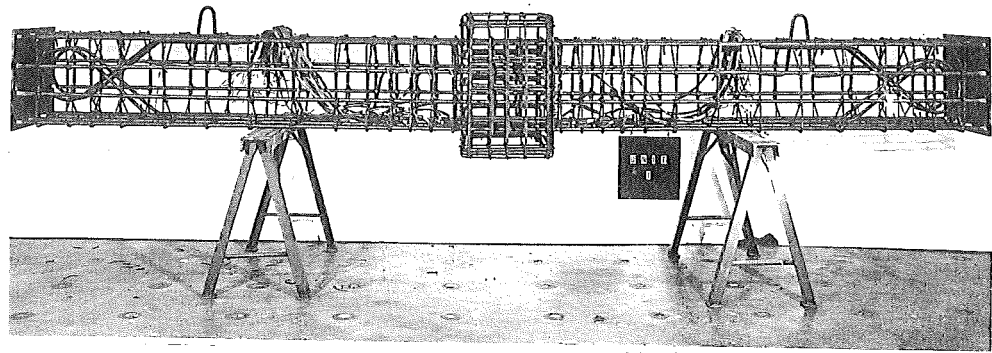


Fig. 2.6 : REINFORCING CAGES OF COLUMN UNITS 1 TO 4

To control any cracking of concrete around the location of the two reaction pins at the column ends, the spacing of transverse reinforcing steel was reduced in the vicinity of the pins. Also two ∞ shaped reinforcing bars were placed around the pin locations. Fig. 2.7 shows a close up view of the reinforcement in the vicinity of the pin together with the lifting hook. Each reaction pin was located in a 55 mm diameter steel tube cast in the concrete (see Fig. 2.8).

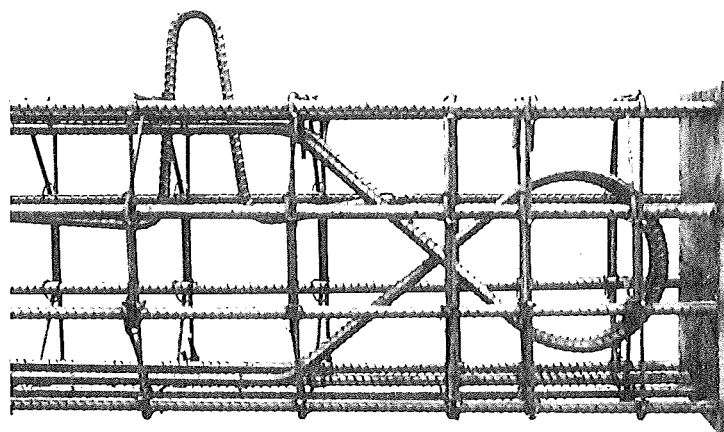


Fig. 2.7 : CLOSE UP VIEW OF THE REINFORCEMENT IN THE VICINITY OF THE LOCATION OF THE REACTION PIN TOGETHER WITH THE LIFTING HOOK

2.3.3 Placing of Concrete

Prior to the placing of the reinforcing cage in the mould, the interior surfaces of the mould were oiled to facilitate the removal of the column units after curing. After the completed reinforcing cage was placed in the mould two 55 mm diameter steel tubes were located at the position of the reaction pins.

After the mould sides were installed, any gap along joining edges was sealed and the holding rods tightened to prevent the mould from moving apart during vibration. Where necessary, wooden wedges were also used for the same purpose.

The 12 mm diameter steel rods, which were to pass through the columns to hold the potentiometers, were positioned at the appropriate locations and screwed to prevent any movement. The potentiometer rods had tips which were made of polystyrene, so that they could easily be removed before installing the potentiometers. The polystyrene tips enabled voids around the ends of the rods in the cover concrete to be formed.

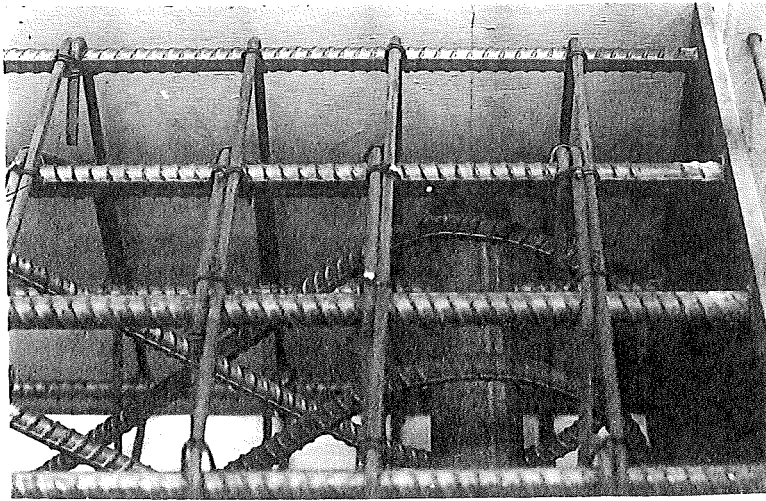


Fig. 2.8 : STEEL TUBE AT THE POSITION OF PIN

Four 16 mm diameter anchor bars, for lifting the column unit into the testing machine, were also placed in each column unit before casting the concrete. Also, four 32 mm diameter plastic tubes were positioned passing through the central stub, to be used for attaching the lateral load jack by bolts during the tests.

The spaghetti which protected the strain gauge wires during construction were tied into bundles and were positioned as far away from plastic hinge regions as possible.

Fig. 2.9 shows the completed reinforcing cages in the moulds, ready for pouring the concrete. The column units were cast in the horizontal position.

The concrete was provided by a local ready-mix supplier and was ordered to have a specified compressive strength of 30 MPa, a maximum aggregate size of 12 mm, and a slump of 75 mm.

From each batch of concrete was cast two column units, twelve 200 x 100 mm diameter cylinders and three 400 mm long x 120 mm square prisms. Units 2 and 4 were cast from the first batch and Units 1 and 3 from the second batch. Prior to pouring the concrete from each batch, a slump test was carried out according to the procedure specified in the NZS 3109:1980⁽⁹⁾ Section 9.3. The slump measured was 55 mm.

Fig. 2.10 shows the concrete being placed. Compaction was achieved by mechanical vibration.

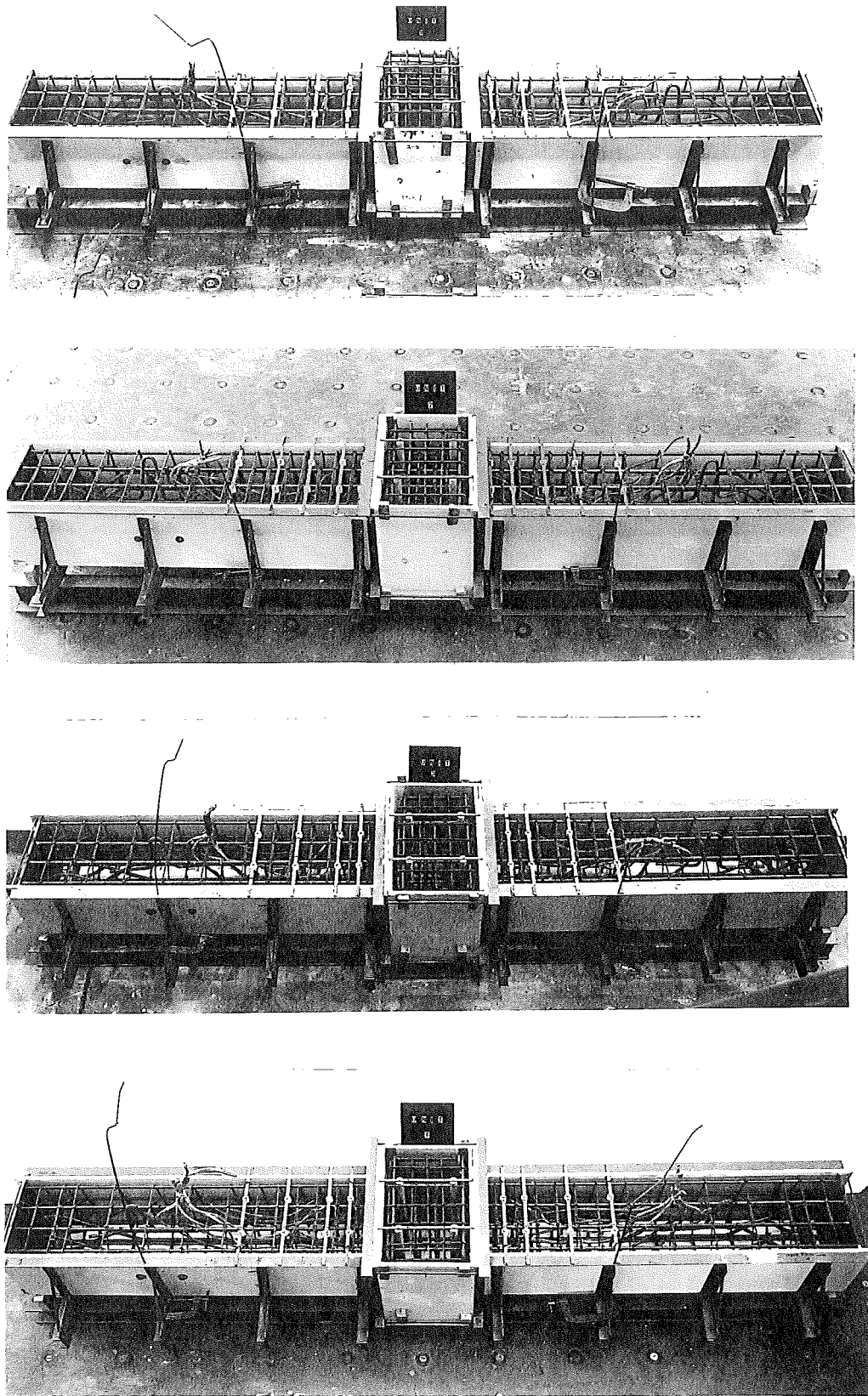


Fig. 2.9 : THE COMPLETED REINFORCING CAGES IN THE MOULDS

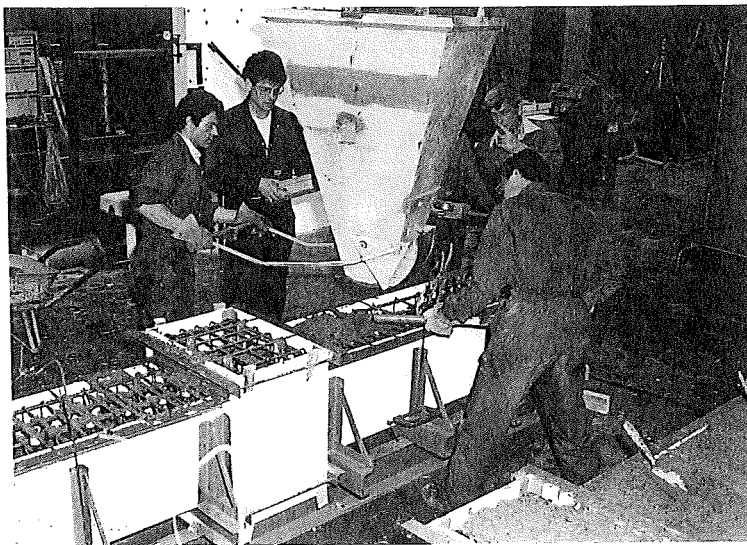
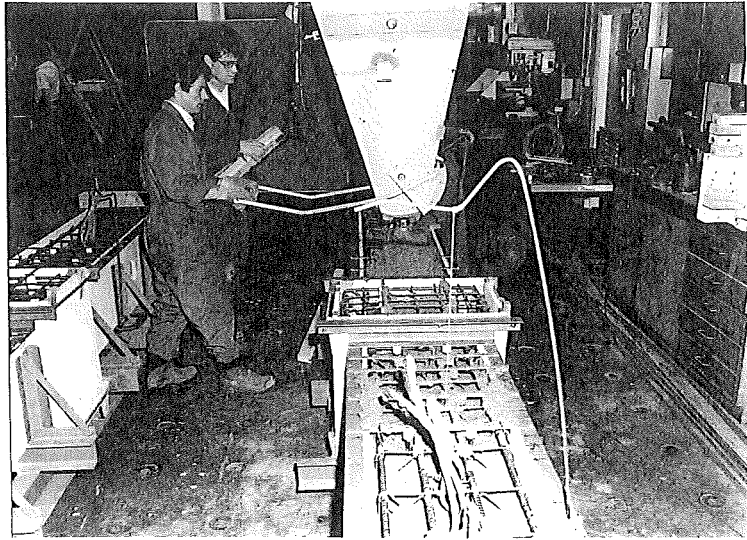


Fig. 2.10 : PLACING THE CONCRETE

On the completion of placing the concrete, the top surface of the columns was trowelled smooth, covered with damp sacks and polythene, and kept moist for seven days. Then, the column units were stripped from the moulds and were given a coat of white paint to facilitate crack identification during testing.

The test cylinders and prisms were cast in steel moulds and were compacted using a vibrating table. As with the column units, the top surfaces of the specimens were troweled smooth, covered with damp sacks and polythene and kept moist. After one day the specimens were removed from their moulds and were placed to cure in a fog room at 20°C and 100 percent relative humidity until tested.

2.4 INSTRUMENTATION OF THE COLUMN UNITS

2.4.1 Load and Displacement

The 10 MN capacity DARTEC universal testing machine was used to apply the axial compression load to the column unit, while the lateral load was applied through 1 MN hydraulic jack which was connected to the steel plates at the central stub by means of four 25 mm diameter high strength bolts. The lateral load applied by the hydraulic jack was measured by a load cell which was calibrated using an Avery Universal Testing Machine to an accuracy of ± 1 kN prior to testing. Details of the loading arrangement are described in Chapter 6.

Three 300 mm travel SAKAE 20 FLP 300 Ohm linear potentiometers were installed to measure lateral displacements on one side of the central stub. The central potentiometer measured the mid-height lateral displacement and it was calibrated with a digital volt meter (DVM) to give a displacement record with an accuracy of ± 0.075 mm. The upper and lower potentiometers were used to measure the rotation of the central stub. Fig. 2.11 shows these three potentiometers bearing against a 40 x 5 mm flat steel strip at the face of the central stub.

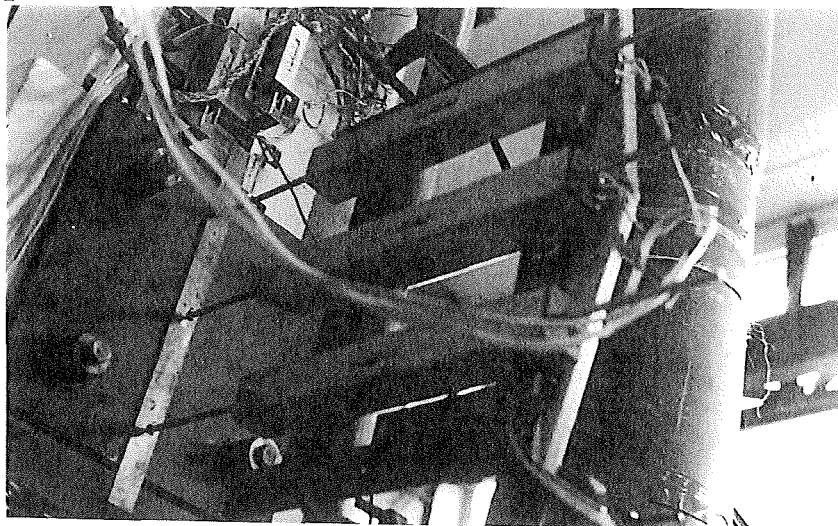


Fig. 2.11: LINEAR POTENTIOMETERS AT THE CENTRAL STUB

2.4.2 Column Curvatures

Ten pairs of linear potentiometers of either 50 mm travel or 30 mm travel, aligned vertically at five levels above and below the central stub (see Fig. 2.14), were used to enable column curvatures and longitudinal strains to be calculated. The potentiometers were supported on steel brackets which were attached to the 12 mm diameter transverse steel rods which passed through the concrete. As mentioned in Section 2.3.3, these steel rods had polystyrene tips at both ends, which when removed formed voids around the ends of the rods. This was to ensure that when the cover concrete crushed the measurements would not be affected. Also, for accurate measurements the steel rods were not to be affected by deformations of the longitudinal bars or transverse hoops, which meant ensuring that there was clearance between the rods and transverse hoops. For this reason, the gauge lengths of some potentiometers at the same level varied slightly from one column unit to another, depending on the hoop spacing. Fig. 2.12 shows the positions of the transverse steel rods for each column unit.

From the column curvatures computed from the potentiometer readings, core strains and longitudinal bar strains could be calculated assuming that plane sections of the columns remained plane after bending (Bernoulli's principle).

2.4.3 Transverse Strains

To measure the strains on the transverse reinforcement 5 mm SHOWA N11-FA-5-120-11 electrical resistance strain gauges with a gauge factor of 2.11 were attached to the octagonal and the square hoops at four different levels above and below the central stub, as shown in Fig. 2.13. For each position, the gauges were attached in pairs (see Fig. 2.13b), one on each side of the bar, and the average of strains measured were taken as the actual strains. This averaging eliminated the effect of bar bending and ensured that only axial strains were measured. The pair of gauges perpendicular to the direction of lateral loading, designated A and B, monitored steel strains due to confinement of the concrete. To measure strains due to shear in the column the pair of gauges, designated C and D, were fixed to the hoops parallel to the direction of lateral loading.

Before affixing the strain gauges, the hoop surfaces where the strain gauges would be placed, were prepared by first smoothing the steel with emery paper and then thoroughly cleaning with Methyl Ethyl Ketone. The strain gauges were attached with LOCTITE Cyanoacrylate adhesive 496 and joined to SHOWA SFG-5T self adhesive terminals. The gauges were then

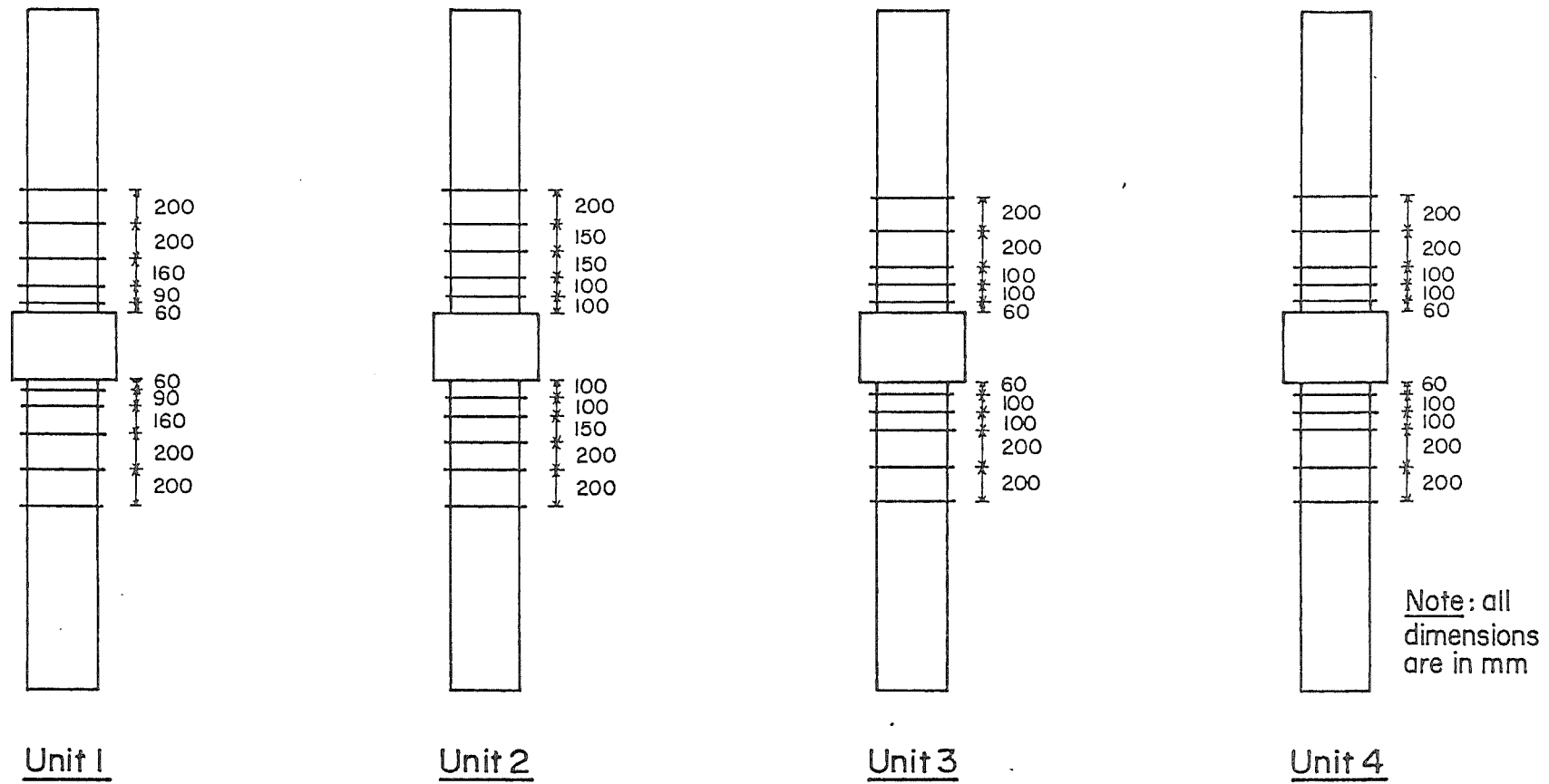


Fig. 2.12 : POSITIONS OF THE TRANSVERSE STEEL RODS USED FOR HOLDING THE POTENTIOMETERS MEASURING COLUMN CURVATURES

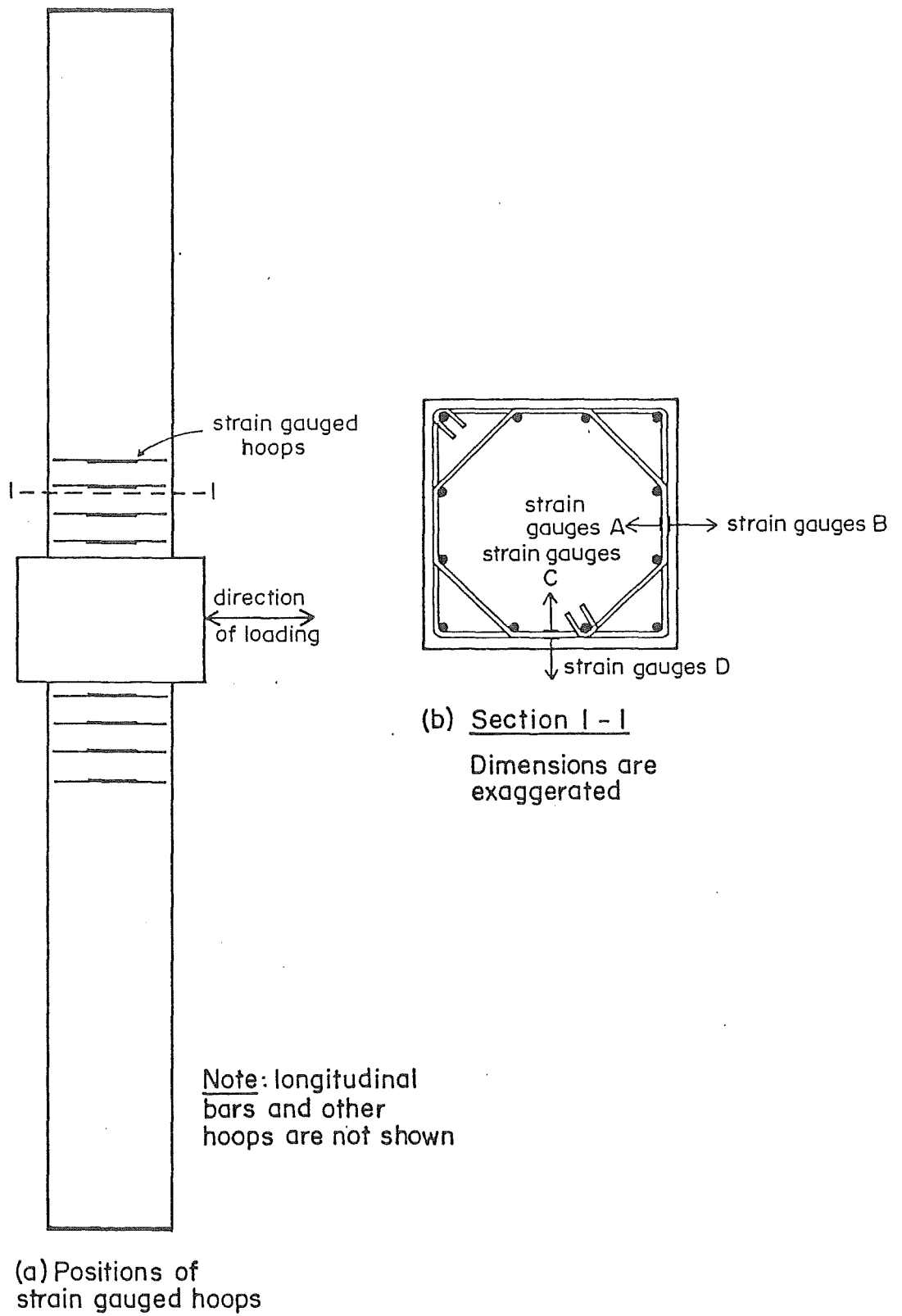


Fig. 2.13: POSITIONS OF HOOPS WITH STRAIN GAUGES

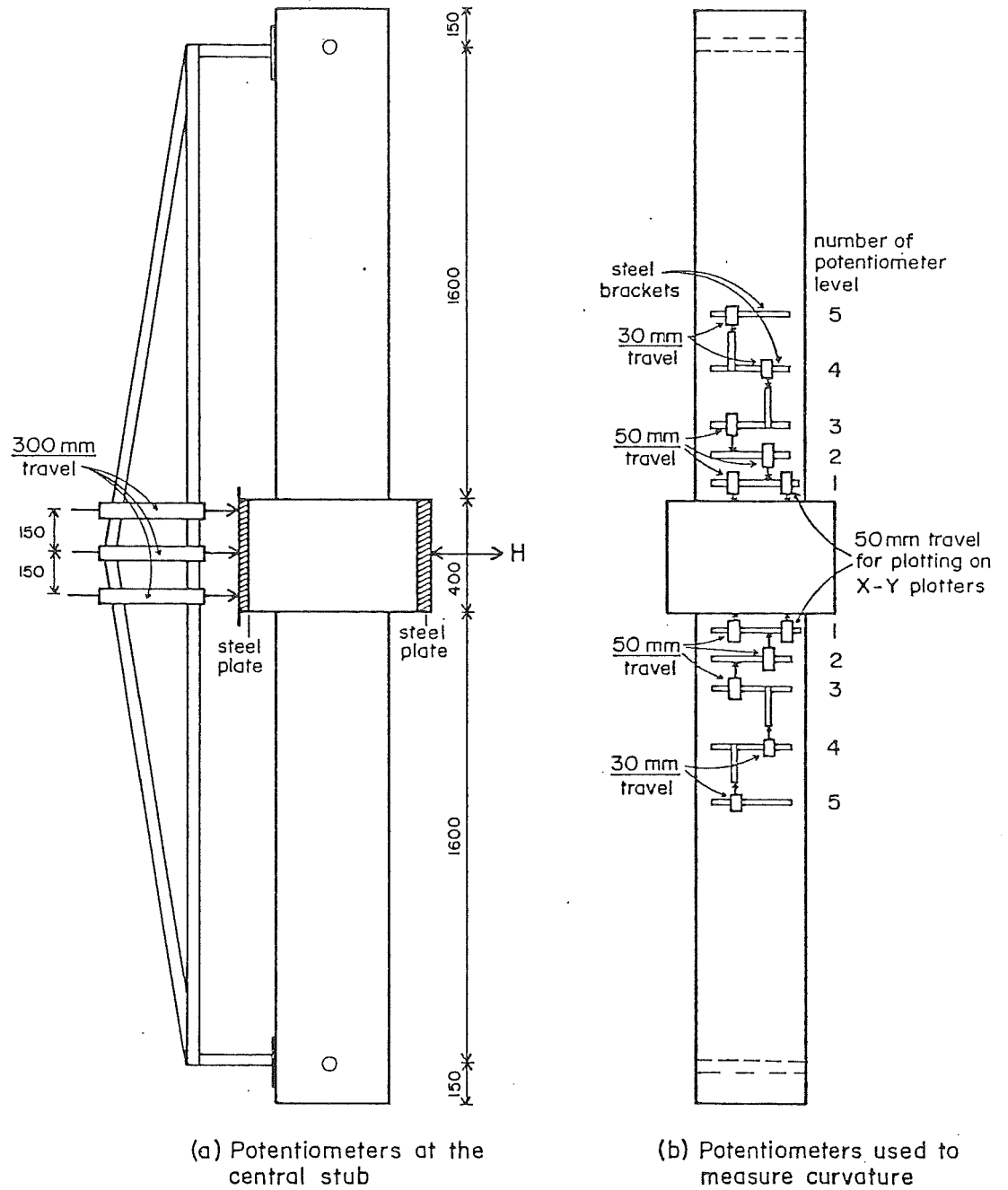


Fig. 2.14 : POTENTIOMETER LOCATIONS AND LEVEL NUMBERS

waterproofed with at least four layers of SHINKOH SN/4 coating cement and finally they were protected by two layers of SCOTCH 3M vinyl mastic tape. Strain gauge wires were threaded through electrical spaghetti which was double tied to the hoop close to the strain gauges providing protection to the wires during construction of column units.

It should be noted that the strain gauges were attached to the hoops before the fabrication of reinforcing cages.

2.4.4 Data Acquisition

The lateral load, measured by the load cell adjacent to the jack, was recorded on three X-Y plotters. During testing the plotters were used to give a continuous record of:

- (a) Load-displacement, where the displacement was measured at the mid-height of the column unit. This was recorded by a WATANABE WX 4421 X-Y plotter.
- (b) Load-top column curvature at level 1 and load-bottom column curvature at level 1, where the curvatures were measured by taking into account the difference in voltage readings between the two potentiometers which were positioned at the same level. These were recorded by HEWLETT-PACKARD X-Y plotters. Fig. 2.14 shows the potentiometer locations and the level numbers.

At selected points during testing, the output voltages of all linear potentiometers and strain gauges were recorded using a SOLARTRON Data Logger. From these records, longitudinal and transverse strains together with curvature profiles could be calculated.

CHAPTER THREE

MATERIAL PROPERTIES OF COLUMN UNITS

3.1 INTRODUCTION

In order to assess the actual strength of the column units, it was necessary to measure the strength properties of the materials. Tensile tests for the reinforcing steel, and compression and bending tests for the concrete, were carried out.

3.2 STEEL TENSION TESTING

From randomly selected samples of each diameter reinforcing steel, six monotonic tensile tests were carried out. Strains were measured using a Batty extensometer. The gauge lengths for these tests were based on the British Standard BS18:Part 2:1971 Section 5⁽¹⁰⁾, that is $L_0 = 5.65\sqrt{S_0}$, where L_0 and S_0 are the gauge length and the cross sectional area of reinforcing steel. The average stress-strain curves for the transverse reinforcing steel and the longitudinal reinforcing steel are plotted in Figs. 3.1 and 3.2 respectively.

The transverse reinforcing steel used was plain round bars of Grade 275, namely R7 for Units 1 and 3, R8 for Unit 2 and R6 for Unit 4. It can be seen from Fig. 3.1 that the yield strength of the R6 bars of 255 MPa obtained from the tensile tests was lower than expected, while the yield strengths of the R7 and R8 bars (364 and 360 MPa, respectively) were much higher than expected. All of the stress-strain curves for the transverse reinforcing steel exhibited an initial linear elastic portion but had no well-defined yield points. According to BS18:1971⁽¹⁰⁾ and ASTM specifications⁽¹¹⁾, for steel lacking a well defined yield point, the yield strength is taken as the stress corresponding to a strain of 0.005.

The longitudinal reinforcing steel was deformed bars of Grade 380, namely HD 16 for all column units. Fig. 3.2 shows that the yield strength of the HD 16 bars of 446 MPa was higher than specified. The stress-strain curve for the longitudinal reinforcing steel indicated an initial linear elastic portion, a yield plateau (i.e. a yield point beyond which the strain increases with little or no increase in stress) and a strain-hardening range in which stress increases non-linearly with strain.

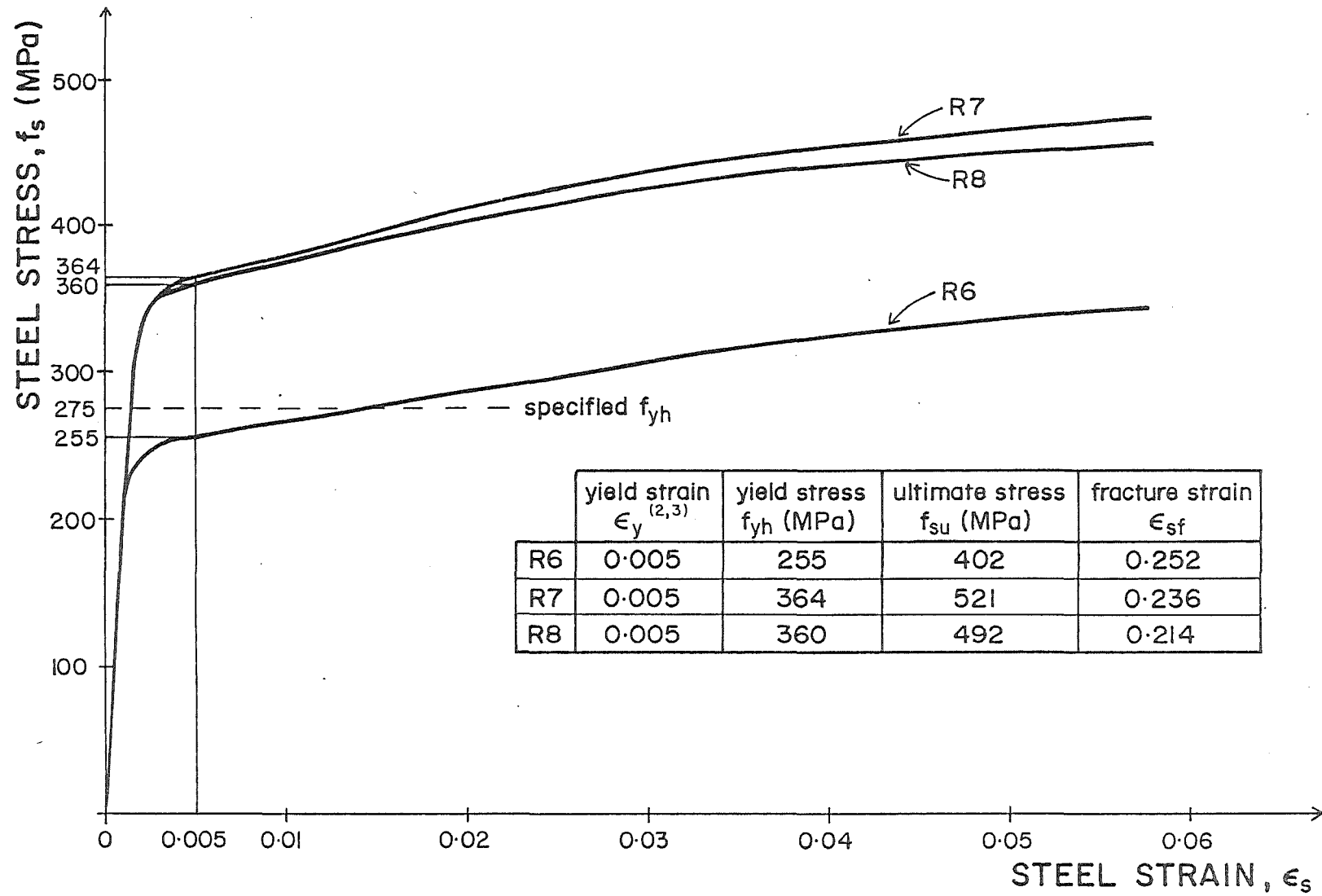


Fig. 3.1 : STRESS-STRAIN CURVES FOR TRANSVERSE REINFORCING STEEL

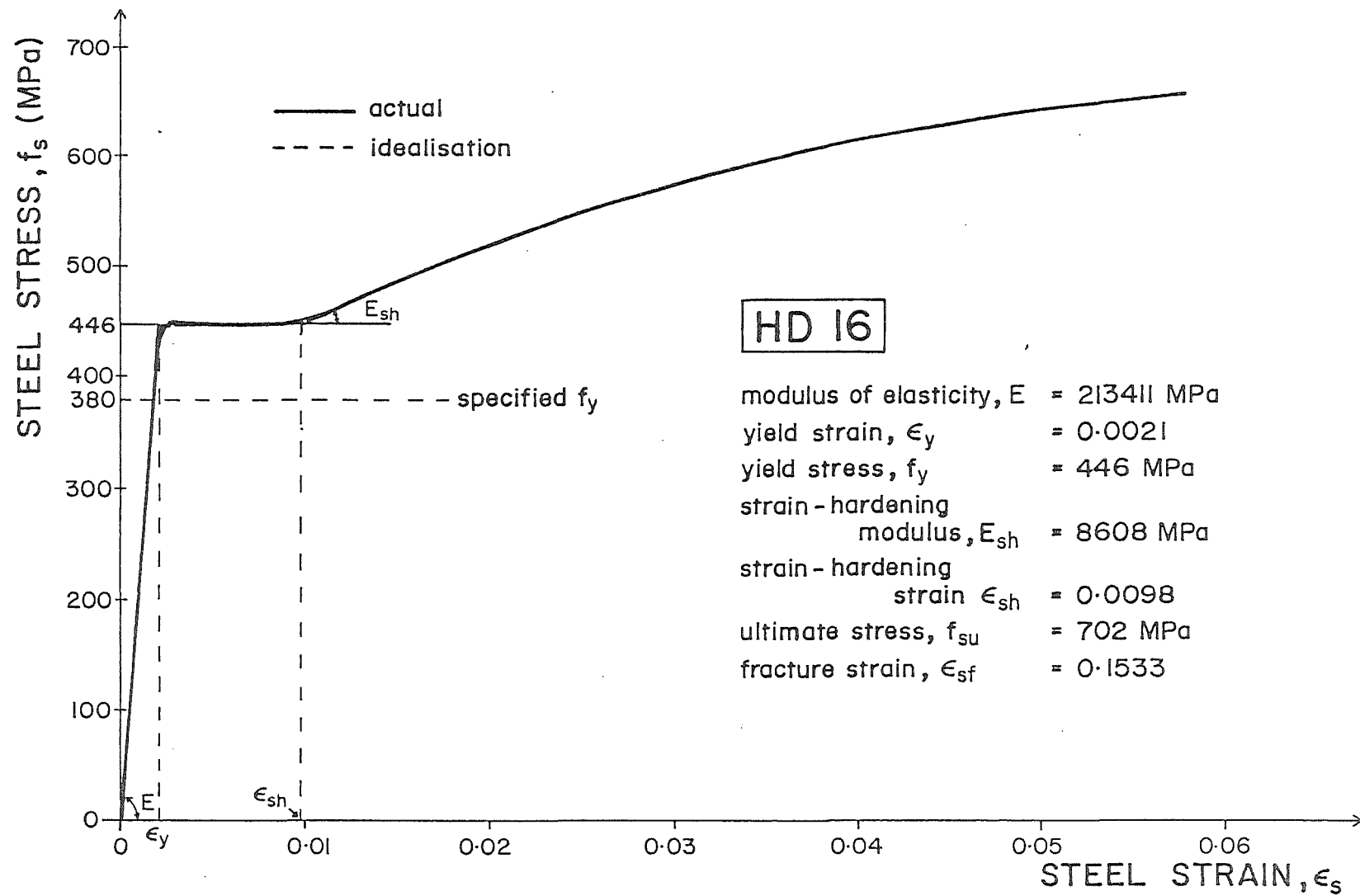


Fig. 3.2 : STRESS-STRAIN CURVE FOR LONGITUDINAL REINFORCING STEEL

Unfortunately a complete stress-strain curve to fracture was not obtained from the tests. As a result, the steel stresses for strain higher than 0.0575 and the ultimate strain had to be estimated.

Since steel compression tests were not carried out, it was assumed that the behaviour of longitudinal reinforcing steel in compression was identical with that in tension⁽¹²⁾.

3.3 CONCRETE STRENGTH

3.3.1 Compression Tests

The compressive strength of the concrete was obtained from 200 x 100 mm diameter concrete cylinders. The cylinders were tested according to the procedure specified in NZS 3112:Part 2:1980⁽¹³⁾ Section 6.

As mentioned in Section 2.3.3, from each batch of concrete two column units and twelve cylinders were cast. Three cylinders were tested at 7 days, three at 28 days, and three at the day of testing each column unit. Table 3.1 summarizes the cylinder strengths for the two concrete batches.

Table 3.1 : CONCRETE CYLINDER STRENGTH

Unit	Batch	Days	Cylinder Strength f'_c (MPa)
1	1	7	37
		28	43.5
		40 (test)	46.5
2	2	7	35
		28	40
		48 (test)	44
3	1	7	37
		28	43.5
		33 (test)	44
4	2	7	35
		28	40
		38 (test)	40

3.3.2 Bending Test

The tensile strength of concrete, generally less than 20% of the compressive strength, can be obtained directly from tension specimens. However, because of the difficulties of holding the specimens to achieve

axial tension, and the uncertainties of secondary stresses induced by the holding devices, the direct tension test is infrequently used⁽¹²⁾.

In this project the tensile strength of concrete was evaluated by means of bending tests conducted on plain concrete beams with a 120 mm square cross section and 400 mm length. The bending tests were conducted on three specimens for each batch of concrete and were carried out at the age of 28 days. The tests were conducted according to the procedure specified in NZS 3112 Part 2:1980⁽¹³⁾ Section 7.

The tensile strength in flexure known as the modulus of rupture, f_r is computed from the flexural formula M/Z , where M is the bending moment at the failure of the specimen and Z is the section modulus of the concrete cross section.

The modulus of rupture results from bending tests for the two concrete batches are summarized in Table 3.2.

Table 3.2 : CONCRETE MODULUS OF RUPTURE

Batch	Modulus of Rupture f_r (MPa)
1	$4.71 = 0.745\sqrt{f'_c}$
2	$5.59 = 0.848\sqrt{f'_c}$

According to NZS 3101:1982⁽²⁾, the modulus of rupture of concrete may be calculated from $f_r = 0.6 f'_c$ MPa in Clause 4.4.1.3 (a lower limit for deflection calculations) and $f_r = 1.0 f'_c$ MPa in Clause 13.3.7.2 (an upper limit for flexural strength calculations). Table 3.2 indicates that the values of modulus of rupture obtained from the tests are between those code values.

For the theoretical moment-curvature analyses conducted later the tensile strength of concrete was taken into account and the stress-strain curve in tension was idealised as a straight line up to the modulus of rupture. Within this range the modulus of elasticity in tension was assumed to be the same as in compression.

CHAPTER FOUR

CODE REQUIREMENTS FOR AMOUNT OF
TRANSVERSE REINFORCEMENT

4.1 INTRODUCTION

To ensure that the available ductility of a reinforced concrete column exceeds the ductility demand during a severe earthquake, it is necessary to provide sufficient transverse reinforcement in the potential plastic hinge regions to confine the concrete in the compression zone, to prevent buckling of longitudinal bars, and to provide shear resistance.

In this chapter the requirements of the New Zealand concrete design code NZS 3101:1982⁽²⁾ for transverse reinforcement will be discussed and the amount of transverse reinforcement placed in each of the column unit tested will be compared with the code amounts.

4.2 TRANSVERSE REINFORCEMENT FOR CONCRETE CONFINEMENT

4.2.1 New Zealand Concrete Design Code Provisions

A sufficient quantity of closely spaced transverse reinforcement is necessary to effectively confine the concrete. The requirement of the New Zealand concrete design code NZS 3101:1982⁽²⁾ that in the potential plastic hinge regions the centre-to-centre spacing of transverse reinforcement should not exceed one-fifth of the diameter or cross section of the member to ensure a close enough spacing for adequate confinement of concrete by arching action between the transverse reinforcement.

With regard to quantity of transverse reinforcement, as previously noted in Section 1.3, the New Zealand code⁽²⁾ requires that the volumetric ratio of transverse reinforcement in the form of spirals or circular hoops in the potential plastic hinge regions of columns in seismic design should not be less than

$$\rho_s = 0.45 \left[\frac{A_g}{A_c} - 1 \right] \frac{f'_c}{f_{yh}} \left[0.5 + 1.25 \frac{P_e}{\phi f'_c A_g} \right] \quad (4.1)$$

or

$$\rho_s = 0.12 \frac{f'_c}{f_{yh}} \left[0.5 + 1.25 \frac{P_e}{\phi f'_c A_g} \right] \quad (4.2)$$

whichever is greater, where A_g is gross area of column cross section, A_c is area of concrete core of section measured to outside of peripheral hoop, f'_c is concrete compressive strength, f_{yh} is yield strength of transverse hoops, P_e is axial compression load due to design gravity

and seismic loading and ϕ is strength reduction factor.

The code also requires that for arrangements of rectangular hoops, the total effective area of transverse hoops A_{sh} in each principal direction in the potential plastic hinge regions of columns in seismic design should not be less than

$$A_{sh} = 0.3 s_h h'' \left(\frac{A_g}{A_c} - 1 \right) \frac{f'_c}{f_{yh}} \left(0.5 + 1.25 \frac{P_e}{\phi f'_c A_g} \right) \quad (4.3)$$

or

$$A_{sh} = 0.12 s_h h'' \frac{f'_c}{f_{yh}} \left(0.5 + 1.25 \frac{P_e}{\phi f'_c A_g} \right) \quad (4.4)$$

whichever is greater, where s_h is centre-to-centre spacing of hoop sets, h'' is dimension of concrete core of the section measured perpendicular to the direction of the hoop bars to the outside of the perimeter hoop and the other notation is as for columns with spirals or circular hoops.

Eqs. 4.1 to 4.4 are based on the SEAOC⁽¹⁴⁾ equations, but with a modification factor $(0.5 + 1.25 P_e / \phi f'_c A_g)$ to account for the effect of axial load. The modification factor was derived from theoretical moment-curvature analyses^(12,15,16,17), using idealised stress-strain curves for the longitudinal reinforcing steel and for concrete confined by either rectangular or circular shaped confining steel.

It should be noted that Eqs. 4.1 and 4.3 are the basic equations for ρ_s and A_{sh} . Eqs. 4.2 and 4.4 give the lower limiting values for ρ_s and A_{sh} and become critical for columns when $(A_g/A_c - 1)$ is small, that is for larger columns.

The amount of transverse reinforcement required by Eqs. 4.1 to 4.4 increases with the axial load level because a high axial load means a large neutral axis depth which in turn means that the flexural strength of the column is more dependent on the contribution of the compressive stress block. Thus, the higher the axial load, the more important it becomes to maintain the strength and ductility of the compressed concrete, thus leading to a greater quantity of transverse steel.

Also, as previously mentioned in Section 1.3, the code equations, Eqs. 4.1 to 4.4 result in a greater volume of rectangular hoop steel being required for columns than spiral or circular hoop steel. This feature will now be examined. From Eqs. 4.1 and 4.3 it is evident that the ratio of A_{sh} for rectangular columns to ρ_s for circular columns is given by

$$\frac{\rho_s}{A_{sh}} = \frac{0.45}{0.3 s_h h''} \quad (4.5)$$

Let A_{sb} be the area of the transverse reinforcement bar used in both columns. Then for the rectangular column

$$A_{sh} = n A_{sb} \quad (4.6)$$

where n is number of rectangular hoop legs or cross ties crossing the section per hoop set, and for the circular column

$$\rho_s = \frac{4 A_{sb}}{d_s s_h} \quad (4.7)$$

where d_s is the diameter of spiral or circular hoop

$$\begin{aligned} \therefore \frac{2 A_{sb} \text{ for circular column}}{n A_{sb} \text{ for rectangular column}} &= \frac{\rho_s d_s s_h / 2}{A_{sh}} \\ &= \frac{\rho_s d_s s_h}{2 A_{sh}} \\ &= \frac{0.45}{0.3 s_h h''} \frac{d_s s_h}{2} \\ &= 0.75 d_s / h'' \end{aligned} \quad (4.8)$$

Now, the transverse confining force applied in each direction is proportional to the total area of the transverse bar in that direction, which is $n A_{sb}$ for the rectangular column and $2 A_{sb}$ for the circular column. If each column has the same width of concrete to be confined, i.e. $h'' = d_s$, it is evident that the ratio of these total transverse bar areas for the two columns is a measure of the ratio of the confining pressure for the columns. Eq. 4.8 shows, therefore, that according to the NZS 3101:1982⁽²⁾ equations, the efficiency of the confining pressure of the transverse hoop legs in the rectangular column is 75% of that of the transverse spiral in the circular column. The difference between spirals and rectangular hoops arises because spirals apply a continuous confining pressure to the concrete around their circumference. Whereas rectangular hoops are less efficient since they apply confining forces only in the vicinity of the hoop legs because the pressure of the concrete tends to bend hoop sides outwards.

If the ratio of ρ_s / A_{sh} is determined from Eqs. 4.2 and 4.4, rather than Eqs. 4.1 and 4.3, it is found that the efficiency factor is 50% rather than 75%. There is no reason for this lower efficiency factor

and the anomaly is inherited from the SEAOC code⁽¹⁴⁾. It should be possible to modify Eq. 4.4 by replacing the numerical coefficient 0.12 by 0.08, thus matching Eqs. 4.4 and 4.2 in the same manner as Eqs. 4.3 and 4.1 are matched^(5,6). The modified equation is then

$$A_{sh} = 0.08 s_h h'' \frac{f'_c}{f_{yh}} \left[0.5 + 1.25 \frac{P_e}{\phi f'_c A_g} \right] \quad (4.9)$$

According to NZS 3101⁽²⁾, it is anticipated that the amounts of confining steel recommended by Eqs. 4.1 to 4.4 will ensure that the column is capable of reaching a displacement ductility factor of at least 8. This level of available ductility has been demonstrated by laboratory tests at the University of Canterbury^(18,19). However, the code provisions⁽²⁾ do not include an indication of the levels of ductility available from columns designed with lesser amounts of transverse reinforcement than given by Eqs. 4.1 to 4.4. In some cases in design a lower available ductility than that provided by the code equations may be adequate. Equations for the amount of transverse reinforcement necessary in design for "limited ductility" need to be established by theoretical and experimental studies.

4.2.2 Comparison of New Zealand Concrete Design Code Equation and the Modified Equation with the Quantities of Transverse Reinforcement Provided in the Column Units

Details of the transverse reinforcement provided in each column unit tested in this study are given in Section 2.2.4. The transverse reinforcement was designed using the actual measured yield strengths f_{yh} of that steel. The compressive strength of the concrete f'_c was assumed to be 30 MPa. From Table 3.1, it can be seen that the actual measured compressive strength of the concrete at the time of testing the column units was much higher than specified.

Table 4.1 shows the amount of transverse reinforcement provided in each column unit as a percentage of the amount recommended by the code equation, Eq. 4.4, and the modified equation, Eq. 4.9., calculated using the actual measured values for f_{yh} and f'_c . It is evident that tests would give an indication of the ductility available when smaller quantities of transverse reinforcement than the code specified amounts are present in columns.

Table 4.1 : AMOUNT OF TRANSVERSE REINFORCEMENT IN EACH COLUMN UNIT AS A PERCENTAGE OF THE AMOUNTS SPECIFIED BY THE CURRENT CODE EQUATION AND THE MODIFIED EQUATION

Unit	$\frac{P_e}{f'_c A_g}$	Measured f'_c (a) (MPa)	Amount of Transverse Reinforcement	
			% of current code equation (b)	% of modified equation (c)
1	0.1	46.5	43.1	64.7
2	0.3	44	45.8	68.8
3	0.3	44	30.4	45.6
4	0.3	40	16.7	25.0

(a) measured f'_c at the day of testing

$$(b) A_{sh} = 0.12 s_h h'' \frac{f'_c}{f_{yh}} \left(0.5 + 1.25 \frac{P_e}{\phi f'_c A_g} \right)$$

$$(c) A_{sh} = 0.08 s_h h'' \frac{f'_c}{f_{yh}} \left(0.5 + 1.25 \frac{P_e}{\phi f'_c A_g} \right)$$

(d) $\phi = 1$ is assumed in all equations.

4.3 TRANSVERSE REINFORCEMENT TO PREVENT PREMATURE BUCKLING OF LONGITUDINAL REINFORCEMENT

4.3.1 New Zealand Concrete Design Code Provisions

According to the New Zealand concrete design code NZS 3101:1982⁽²⁾ the yield force in the hoop or cross tie should at least equal one-sixteenth of the yield force of the longitudinal bar or bars it is to restrain. This requirement may be written as

$$A_t = \frac{\sum A_b f_y}{16 f_{yh}} \quad (4.10)$$

where A_t = area of the leg hoop or cross tie, $\sum A_b$ = sum of the areas of the longitudinal bars reliant on the tie, f_y = yield strength of longitudinal bars and f_{yh} = yield strength of hoops.

It is also required that the centre-to-centre spacing of hoop sets should not exceed six longitudinal bar diameters.

4.3.2 Comparison of New Zealand Concrete Design Code Requirements with the Quantities of Transverse Reinforcement Provided in the Column Units

The cross section of the column units is shown in Fig. 2.2. It is evident that the intermediate longitudinal bars of the cross section are not as well restrained as the corner longitudinal bars, since each corner longitudinal bar is restrained from outward buckling by a full transverse bar yield force whereas each intermediate longitudinal bar is restrained from outward buckling by $(1/\sqrt{2})$ times a full transverse bar yield force.

The yield force of each HD16 longitudinal bar used was 89.6 kN. Thus the minimum yield force required from each interior (octagonal) hoop was $89.6/16 = 5.6$ kN. The yield force of each octagonal hoop actually provided in Units 1, 2, 3 and 4 was 14.0, 18.0, 14.0 and 7.2 kN, respectively. Therefore the transverse reinforcement of the column units satisfied the code requirement for restraint of longitudinal bars.

4.4 TRANSVERSE REINFORCEMENT FOR SHEAR

4.4.1 New Zealand Concrete Design Code Provisions

As mentioned in Section 4.1, the transverse reinforcement in potential plastic hinge regions of a column has also to provide shear resistance.

As a shear failure is non-ductile, resulting in rapid strength and stiffness degradation under seismic cyclic loading, it is essential that premature shear failure, either within the plastic hinge regions or elsewhere does not occur.

The current New Zealand design philosophy is to ensure against shear failure by using a capacity design approach. That is, the design shear force used for columns is that resulting from plastic hinging in the frame when the flexural overstrength capacity is reached at the plastic hinges.

According to the New Zealand concrete design code NZS 3101:1982⁽²⁾, in the end region of the column where plastic hinging occurs, the shear stress taken by the concrete v_c is assumed to be zero unless the minimum design axial compression force produces an average stress in excess of $0.1f'_c$ over the gross concrete area. The assumption of $v_c = 0$ for small axial load levels is in order to take into account the possible deterioration of the shear carried by the concrete during high intensity cyclic loading. Reversal of moment in plastic hinge regions causes a

reduction in the shear transferred by the concrete across the compression zone and in the shear force carried by aggregate interlock and dowel action.

4.4.2 Comparison of New Zealand Concrete Design Code Requirements and Shear Strength of Columns

Following on the above considerations, the shear carrying capacity of each column units will be checked as follows. From Fig. 2.1 it is obvious that the theoretical ideal flexural strength M_i is related to the lateral load at the mid-height of the column H_i when M_i is developed by (neglecting $P-\Delta$ moment) the following equation:

$$H_i = 2M_i/\ell \quad (4.11)$$

where $\ell = 1.6$ m. The shear force V_u corresponding to the development of the ideal flexural strength, is $V_u = \frac{1}{2} H_i$. Assuming that the flexural overstrength factor is 1.3, the design shear force V_o is then

$$V_o \geq 1.3 V_u \quad (4.12)$$

In the concrete design code NZS 3101:1982⁽²⁾, the ideal shear strength of a column V_i is based on the ACI approach⁽²⁰⁾ of considering separately the shear carried by concrete V_c and the shear carried by the shear reinforcement V_s . Thus the requirement is

$$V_i = V_c + V_s \geq V_o \quad (4.13)$$

(a) Shear carried by concrete

The shear carried by the concrete is given by

$$V_c = v_c b_w d \quad (4.14)$$

where v_c is the nominal shear stress carried by the concrete, b_w is the width of the column and d is the effective depth. Different expressions for v_c apply for the plastic hinge regions of a column and for regions outside plastic hinges where inelastic curvature will not occur.

(i) In the plastic hinge region:

For Unit 1, where $P_e/\phi f'_c A_g = 0.1$

$$v_c = 0 \quad (4.15)$$

For Units 2, 3 and 4, where $P_e/\phi f'_c A_g = 0.3$

$$v_c = 4 v_b \sqrt{\frac{P_e}{\phi f'_c A_g} - 0.1} \quad (4.16)$$

in which v_b is the basic concrete shear stress and is given by

$$v_b = (0.07 + 10\rho_w) \sqrt{f'_c} \leq 0.2\sqrt{f'_c} \quad (4.17)$$

$$\text{where } \rho_w = \frac{A_s}{b_w d} \quad (4.18)$$

and A_s is area of tension reinforcement, b_w is the width of the column and d is the effective depth of the column.

(ii) Outside plastic hinge regions:

$$v_c = 1 + \left[\frac{3P_e}{\phi f'_c A_g} \right] v_b \quad (4.19)$$

(b) Shear carried by shear reinforcement

The shear carried by the shear reinforcement is expressed by

$$v_s = \frac{A_v f_{yh} d}{s_h} \quad (4.20)$$

where A_v is total area of shear reinforcement parallel to the direction of the shear force.

Table 4.2 summarizes the shear carrying capacity of all column units. Note that $\phi = 1$ is assumed in all calculations.

Table 4.2 : THE SHEAR STRENGTH OF THE COLUMN UNITS IN KILONEWTONS

Unit	$\frac{P_e}{f'_c A_g}$	V_o Eq.4.12	In plastic hinge regions			Outside plastic hinge regions		
			$V_c^{(a)}$	V_s Eq.4.20	V_i $=V_c + V_s$	$V_c^{(b)}$	V_s Eq.4.20	V_i $=V_c + V_s$
1	0.1	246	0	209	209	264	105	369
2	0.3	330	266	294	560	283	147	430
3	0.3	330	267	196	463	283	98	381
4	0.3	312	255	98	353	270	49	319

(a) Value of v_c calculated from Eq. 4.16

(b) Value of v_c calculated from Eq. 4.19.

From Table 4.2, it can be seen that the shear capacity V_i in the plastic hinge regions of Units 2, 3 and 4 is larger than the design shear force V_o . In the case of Unit 1, the shear capacity is smaller than the design shear force. Hence, the test results from Unit 1 were also to

give a possible indication as to whether the code recommendation of $v_c = 0$ for small axial load levels is overly conservative or not. Outside plastic regions, all units satisfied the code shear strength requirements, as is evident from Table 4.2.

4.5 CONCLUDING REMARKS

The quantities of transverse reinforcement provided in the column units are compared with the NZS 3101:1982⁽²⁾ requirements in Table 4.3.

Table 4.3 : QUANTITIES OF TRANSVERSE REINFORCEMENT IN
UNITS 1 TO 4 COMPARED WITH THE CODE REQUIREMENTS

Unit	$\frac{P_e}{f'_c A_g}$	f'_c MPa	f_{yh} MPa	Transverse Reinforcement		
				Concrete Confinement	Antibuckling	Shear in Plastic Hinge Region
				$\frac{\text{Actual } A_{sh}}{\text{Code } A_{sh}}$	$\frac{\text{Actual tie force}}{16 \text{ Long. bar force}}$	$\frac{\text{Calculated Shear Strength}}{\text{Design Shear Force}}$
1	0.1	46.5	364	0.43	2.50	0.85
2	0.3	44	360	0.46	3.21	1.70
3	0.3	44	364	0.30	2.50	1.40
4	0.3	40	255	0.17	1.29	1.13

(a) For longitudinal reinforcement $\rho_t = 1.51\%$ and $f_y = 446$ MPa

(b) Spacing of transverse reinforcement in potential plastic hinge regions:

Unit 1 R7 @ $s_h = 85 \text{ mm} = 5.3d_b = 0.21h$

Unit 2 R8 @ $s_h = 78 \text{ mm} = 4.9d_b = 0.20h$

Unit 3 R7 @ $s_h = 91 \text{ mm} = 5.7d_b = 0.23h$

Unit 4 R6 @ $s_h = 94 \text{ mm} = 5.9d_b = 0.24h$

ANALYTICAL INVESTIGATION OF THE COLUMN UNITS

5.1 INTRODUCTION

When undertaking moment-curvature analyses for members subjected to combined flexure and axial load, it is necessary to use constitutive models which accurately trace the stress-strain path of the materials used.

In this chapter, analytical models for both confined and unconfined concrete and of reinforcing steel will be described. These models are based on previous research at the University of Canterbury^(21,18,22,3).

The moment-curvature relationship of the column units will be investigated analytically using three approaches, namely monotonic moment-curvature analysis, cyclic moment-curvature analysis, and design charts for ductility. Comparison between these approaches and experimental results will be discussed in Section 8.2.

5.2 THEORETICAL CONSIDERATIONS

Theoretical moment-curvature relationships for reinforced concrete sections with flexure and axial load can be derived on the basis of assumptions similar to those used for the determination of the flexural strength. It is assumed that plane sections before bending remain plane after bending and that the stress-strain curves for concrete and steel are known. The curvatures associated with a range of bending moments and axial loads may be found using these assumptions and from the requirements of strain compatibility and equilibrium of forces.

The stress-strain relationship for confined concrete can be used to determine the compressive stress distribution in the core concrete for a given extreme fibre compressive strain while the cover concrete follows the stress-strain relationship for unconfined concrete and is assumed to cease carrying load when the spalling strain is reached.

To compute the moment-curvature relationship for a given column section and axial load level, it is convenient to divide the concrete section into a number of discrete laminae, where the long sides being parallel to the neutral axis of bending. Each laminae then contained an area of cover and core concrete. Similarly, the longitudinal reinforcing bars are divided into a discrete number of layers or levels, where each level contains a specified area of reinforcing steel. The stresses in

the cover concrete, core concrete and steel in each lamina can be found from the stress-strain relationships. It is assumed that the strain in the lamina is that at the mid-depth of the lamina. Fig. 5.1 shows the idealisation of the column unit section.

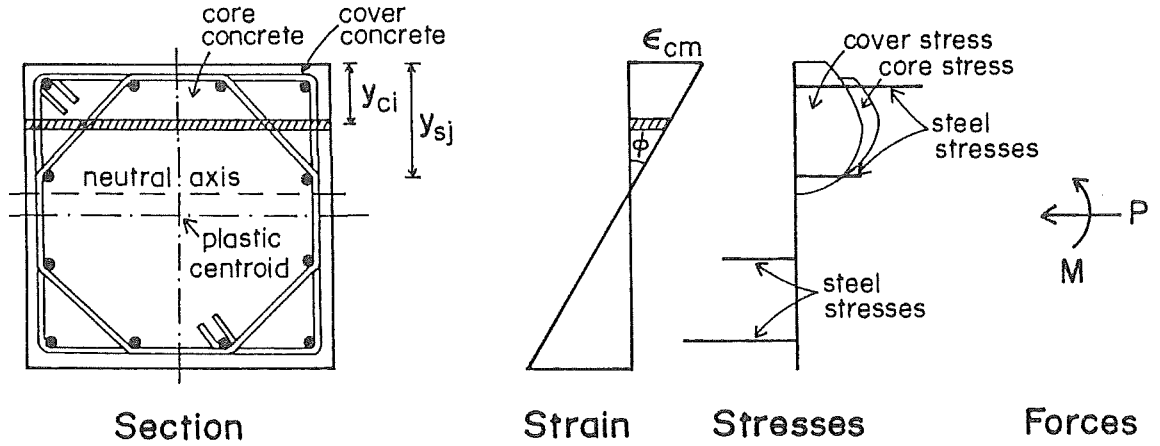


Fig. 5.1 : COLUMN SECTION WITH STRAIN AND STRESS DISTRIBUTION

The theoretical moment-curvature relationship for a given axial load level P may be determined by incrementing the concrete strain in the extreme compression fibre ϵ_{cm} .

For each value of ϵ_{cm} , the neutral axis depth, c , is estimated and the strains in the laminae determined. The stresses in the laminae are then calculated and the force equilibrium equation is checked. An iterative procedure is used to determine the neutral axis depth c which for the extreme fibre strain ϵ_{cm} satisfies the force equilibrium equation

$$P = \sum_{i=1}^{n_c} f_{ci} A_{ci} + \sum_{j=1}^{n_s} f_{sj} A_{sj} \quad (5.1)$$

where n_c and n_s are the number of concrete laminae and steel levels of area A_{ci} and A_{sj} respectively. f_{ci} and f_{sj} are the stresses in the i th concrete laminae and j th steel level.

The moment M corresponding to the value of ϵ_{cm} , the axial load P and the determined neutral axis depth c , is then determined by taking moments about the plastic centroidal axis

$$M = \sum_{i=1}^{n_c} f_{ci} A_{ci} \left(\frac{h}{2} - y_{ci} \right) + \sum_{j=1}^{n_s} f_{sj} A_{sj} \left(\frac{h}{2} - y_{sj} \right) \quad (5.2)$$

where h is depth of section. The curvature corresponding to M is given by $\phi = \epsilon_{cm}/c$.

By carrying out the calculation for M and ϕ for a range of ϵ_{cm} values, the moment-curvature curve can be plotted.

5.3 ANALYTICAL STRESS-STRAIN RELATIONSHIPS FOR CONCRETE

5.3.1 Stress-strain Relationship for Concrete Proposed by Kent and Park with Modifications

In 1971, Kent and Park⁽²¹⁾ developed a stress-strain model for concrete confined by rectangular hoops. The equations for the Kent-Park model are as follows:

Ascending Branch: $\epsilon_c \leq 0.002$

$$f_c = f'_c \left[\frac{2\epsilon_c}{0.002} - \left(\frac{\epsilon_c}{0.002} \right)^2 \right] \quad (5.3)$$

where ϵ_c is concrete compression strain and f'_c is concrete cylinder strength. This ascending branch curve is represented by a second-degree parabola. The confined concrete strength is assumed to be unaffected by confinement.

Falling Branch: $\epsilon_c > 0.002$

$$f_c = f'_c [1 - Z(\epsilon_c - 0.002)] \quad (5.4)$$

but not less than $0.2 f'_c$

$$\text{where } Z = \frac{0.5}{\epsilon_{50u} + \epsilon_{50h} - 0.002} \quad (5.5)$$

$$\epsilon_{50u} = \frac{3 + 0.29 f'_c}{145 f'_c - 1000} \quad (f'_c \text{ in MPa units}) \quad (5.6)$$

$$\epsilon_{50h} = \frac{3}{4} \rho_s \sqrt{\frac{h''}{s_h}} \quad (5.7)$$

This curve is taken as a straight line in which the slope Z is a function of concrete cylinder strength f'_c , the volume ratio of hoop steel measured to the outside of perimeter hoops ρ_s , and the ratio of width of confined concrete to hoop spacing h''/s_h . ϵ_{50h} gives the additional ductility due to confinement and is taken as zero for unconfined concrete.

Based on the experimental results that the strength of the core concrete was enhanced due to transverse hoop reinforcement Park et al⁽¹⁸⁾ and Scott et al⁽²²⁾ proposed a modified form of the original Kent-Park model. In the Modified Kent-Park analytical relationship the maximum stress attained, Kf'_c is assumed to be reached at a strain of $0.002K$, and the

stress strain relation is

For $\epsilon_c \leq 0.002 K$

$$f_c = K f'_c \left[\frac{2\epsilon_c}{0.002 K} - \left(\frac{\epsilon_c}{0.002 K} \right)^2 \right] \quad (5.8)$$

For $\epsilon_c > 0.002 K$

$$f_c = K f'_c [1 - Z_m (\epsilon_c - 0.002 K)] \quad (5.9)$$

but not less than $0.2 K f'_c$

$$\text{in which } K = 1 + \frac{\rho_s f_{yh}}{f'_c} \quad (5.10)$$

$$\text{and } Z_m = \frac{0.5}{\frac{3 + 0.29 f'_c}{145 f'_c - 1000} + \frac{3}{4} \rho_s \sqrt{\frac{h''}{s_h}} - 0.002 K} \quad (5.11)$$

where K is strength enhancement factor for confined concrete, f_{yh} is yield strength of transverse reinforcing steel and Z_m defines the slope of linear falling branch.

The shapes of the stress-strain curves given by the modified Kent-Park model are shown in Fig. 5.2.

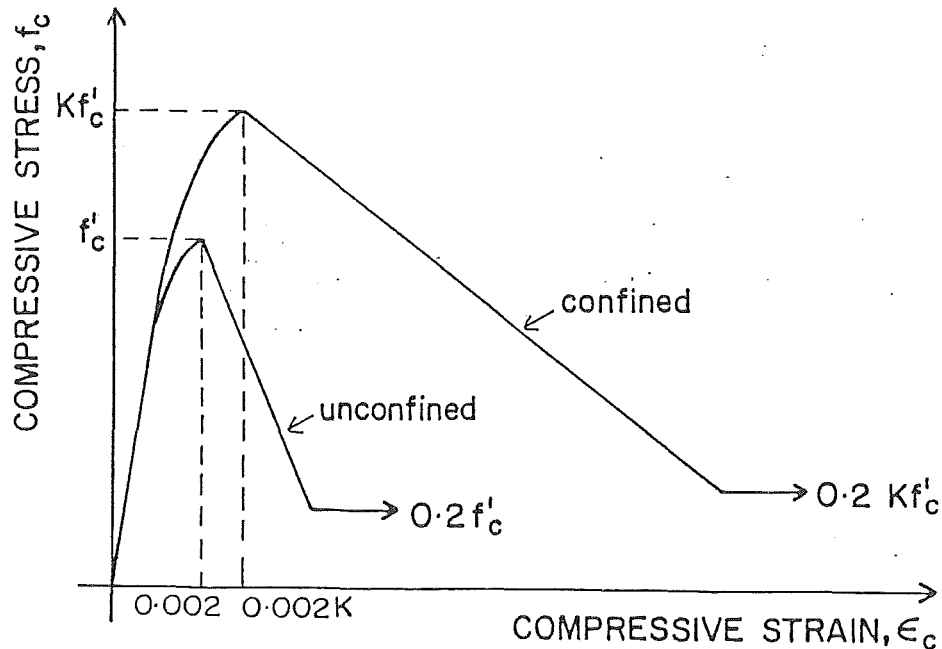


Fig. 5.2 : CONCRETE COMPRESSIVE STRESS-STRAIN CURVES GIVEN BY
MODIFIED KENT-PARK MODEL (21,18,22)

5.3.2 Stress-Strain Relationship for Concrete Proposed by Mander, Priestley and Park

An analytical model for longitudinal compressive stress in concrete proposed by Mander et al⁽³⁾ is shown in Fig. 5.3. The model is based on an equation suggested by Popovics⁽²³⁾

$$f_c = \frac{f'_{cc} \times r}{r - 1 + x^r} \quad (5.12)$$

$$\text{in which } x = \epsilon_c / \epsilon_{cc} \quad (5.13)$$

$$r = \frac{E_c}{E_c - E_{sec}} \quad (5.14)$$

$$E_c = 5000 \sqrt{f'_{co}} \quad (5.15)$$

$$E_{sec} = \frac{f'_{cc}}{\epsilon_{cc}} \quad (5.16)$$

where f'_{cc} is the peak longitudinal compressive stress of the stress-strain curve for confined concrete, ϵ_{cc} is the strain at peak concrete strength, E_c is the initial tangent modulus of elasticity of concrete, f'_{co} is unconfined compressive strength of concrete, f_c and ϵ_c are concrete compressive stress and strain respectively.

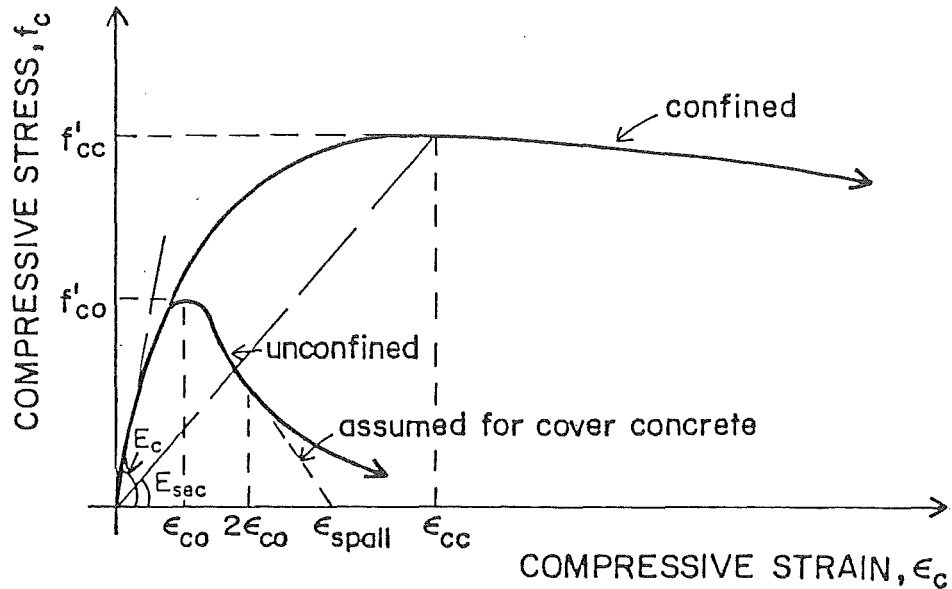


Fig. 5.3 : CONCRETE COMPRESSIVE STRESS-STRAIN CURVES GIVEN BY MODEL OF MANDER, PRIESTLEY AND PARK⁽³⁾

The advantage of using Eq. 5.12 is that it obviates the need for separate rising and falling branch relations. Also, it can be used for different section shapes with any transverse reinforcing configuration.

For square columns with the arrangement of hoops shown in Fig. 2.2:

$$f'_{cc} = f'_{co} \left[-1.254 + 2.254 \sqrt{1 + 7.94 \frac{f'_l}{f'_c} - \frac{2f'_l}{f'_{co}}} \right] \quad (5.17)$$

$$\text{in which } f'_l = k_e \frac{(2 + \sqrt{2}) A_{sb} f_{yh}}{s_h h''} \quad (5.18)$$

$$\text{and } \epsilon_{cc} = \epsilon_{co} \left[1 + 5 \left(\frac{f'_{cc}}{f'_{co}} - 1 \right) \right] \quad (5.19)$$

where ϵ_{co} is longitudinal compressive strain in concrete corresponding to unconfined compressive strength of concrete f'_{co} , f'_l is effective lateral confining stress, h'' = width of the confined core measured to the centreline of the perimeter hoop, A_{sb} = area of hoop bar, s_h = centre-to-centre spacing of hoop sets, f_{yh} is yield strength of transverse steel and k_e is confinement effectiveness coefficient and is determined from

$$k_e = 1 - \frac{\Sigma(w'_1)^2/6}{h''^2} \frac{(1 - 0.5 s'/h'')^2}{(1 - \rho_{cc})} \quad (5.20)$$

where w' and s' are clear transverse spacing between longitudinal bars and clear longitudinal spacing between hoop bars in which arching action of the concrete develops, h'' is width of the columns measured to the centreline of the perimeter hoop and ρ_{cc} is ratio of volume of longitudinal steel to volume of concrete core, measured to the centreline of the perimeter hoop.

The model of Mander et al includes equations which take into account the age of the concrete when assessing the compressive strength and strain of the concrete. The unconfined compressive strength of the concrete f'_{co} is expressed in terms of the 28-day concrete cylinder strength $(f'_c)_{28d}$, as follows:

$$\frac{(f'_{co})_t}{(f'_c)_{28d}} = \frac{t}{2.5 + 0.93t} \quad (5.21)$$

where t is the age of the concrete in days. The strain at the maximum unconfined concrete strength $(\epsilon_{co})_t$, is given by

$$\frac{(\epsilon_{co})_t}{\epsilon_{co}} = \frac{4.0 + 0.85t}{2.5 + 0.93t} \quad (5.22)$$

5.3.3 Comparison of the Models

Figs. 5.4 to 5.7 show the analytical stress-strain relationships for the confined and unconfined concrete of each of the four column units derived for the arrangements of transverse reinforcement in the columns and the measured values of f'_c and f_{yh} .

It can be seen that the model proposed by Mander et al⁽³⁾ gives a higher peak strength f'_{cc} and a higher strain at peak stress ϵ_{cc} than the modified Kent-Park model for all column units. Table 5.1 summarizes the values of the peak strength f'_{cc} and the corresponding strain ϵ_{cc} predicted by the two models.

Table 5.1 : CONFINED STRENGTH AND CONFINED STRAIN AT PEAK STRESS
FOR ALL COLUMN UNITS

Unit	$\frac{A_{sh}}{s_h} \left(\frac{\text{mm}^2}{\text{mm}} \right)$	f'_c (MPa)	Modified Kent-Park Model		Mander et al Model	
			f'_{cc} (MPa)	ϵ_{cc}	f'_{cc} (MPa)	ϵ_{cc}
1	1.546	46.5	49.6	0.00213	51.44	0.00358
2	2.20	44	48.4	0.00220	51.20	0.00457
3	1.444	44	46.9	0.00213	50.74	0.00358
4	1.027	40	41.5	0.00207	44.02	0.00284

Also, at higher strains, the model by Mander et al predicts higher stresses than the modified Kent-Park model, except for Unit 4, where at very high strains, the stresses predicted using the model by Mander et al are slightly lower (see Fig. 5.7).

From Figs. 5.4 to 5.7 it is evident that the most significant parameter affecting the shape of the confined stress-strain curve is the quantity of confining reinforcement. As the volumetric ratio of confining reinforcement increases, the confined strength of the concrete, f'_{cc} and the longitudinal strain at which this strength developed, ϵ_{cc} increases and the slope of falling branch decreases. For Unit 2 which contains the largest amount of transverse reinforcement the slope of falling branch is the least steep, while for Unit 4 which contains the smallest amount of transverse reinforcement the slope is steepest.

For unconfined concrete the Kent-Park⁽²¹⁾ model simply assumed that the peak of unconfined compressive stress is the same as concrete cylinder strength f'_c and this occurs at the strain of 0.002, while the Mander model⁽³⁾ takes into account the age of the concrete to determine the unconfined compressive strength and the strain at which this strength developed.

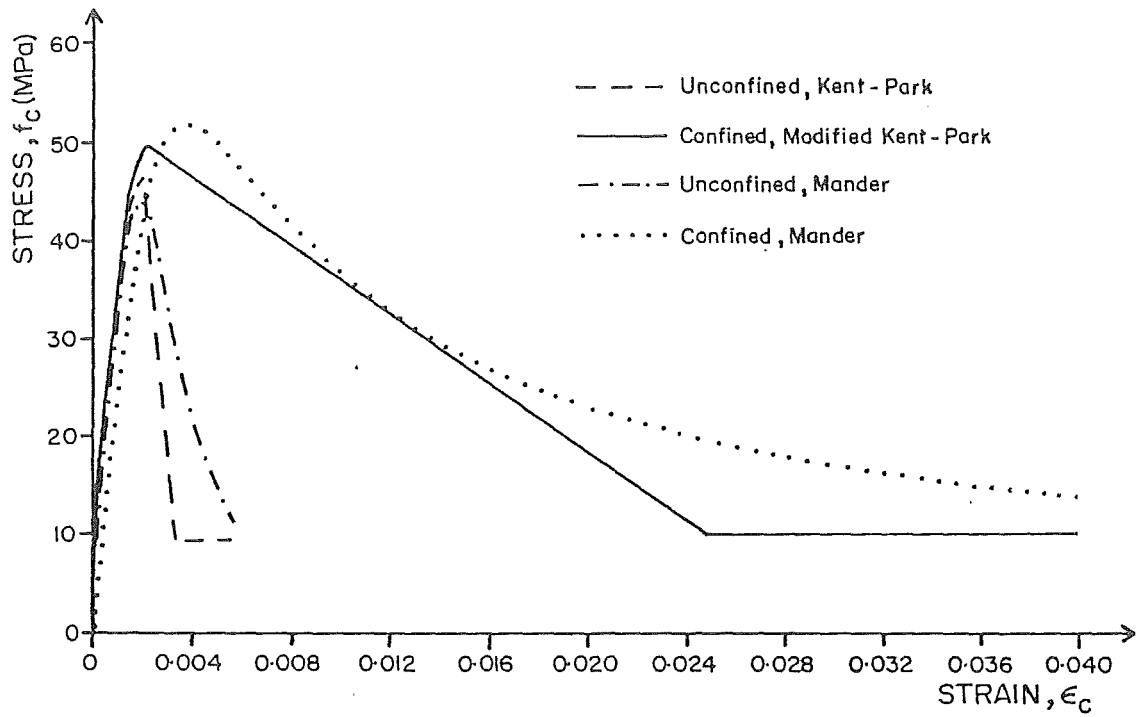


Fig. 5.4 : ANALYTICAL STRESS-STRAIN CURVES FOR CONCRETE FOR UNIT 1

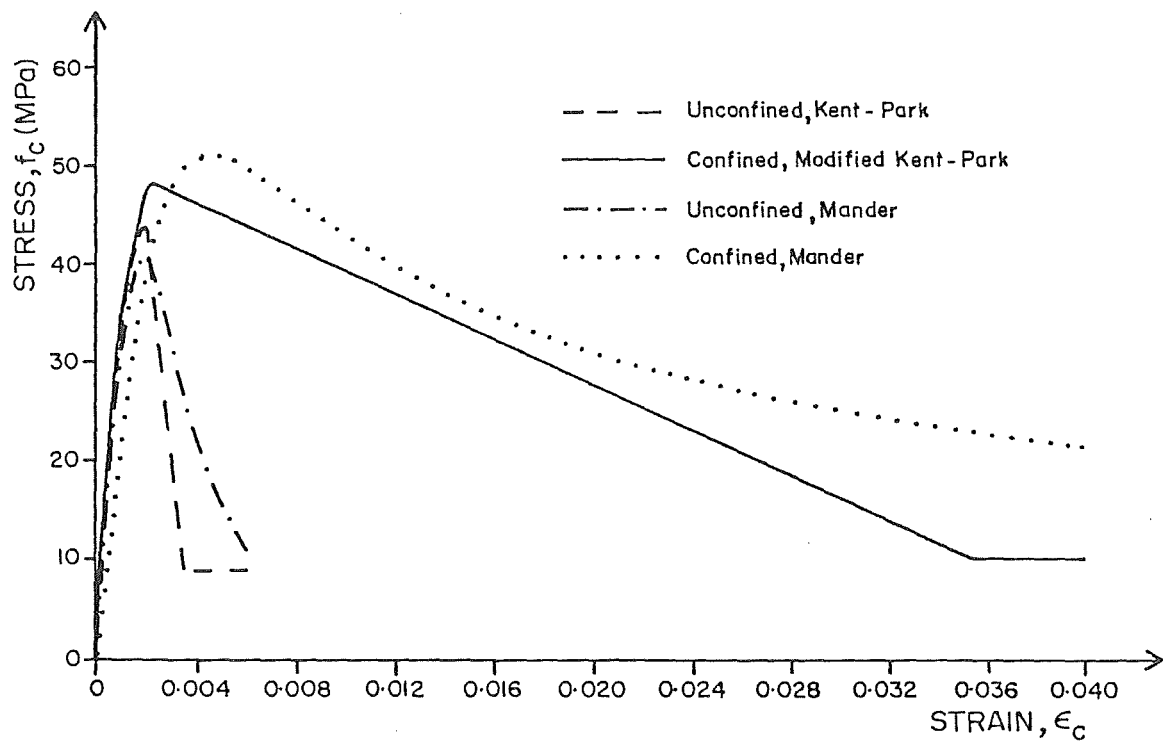


Fig. 5.5 : ANALYTICAL STRESS-STRAIN CURVES FOR CONCRETE FOR UNIT 2

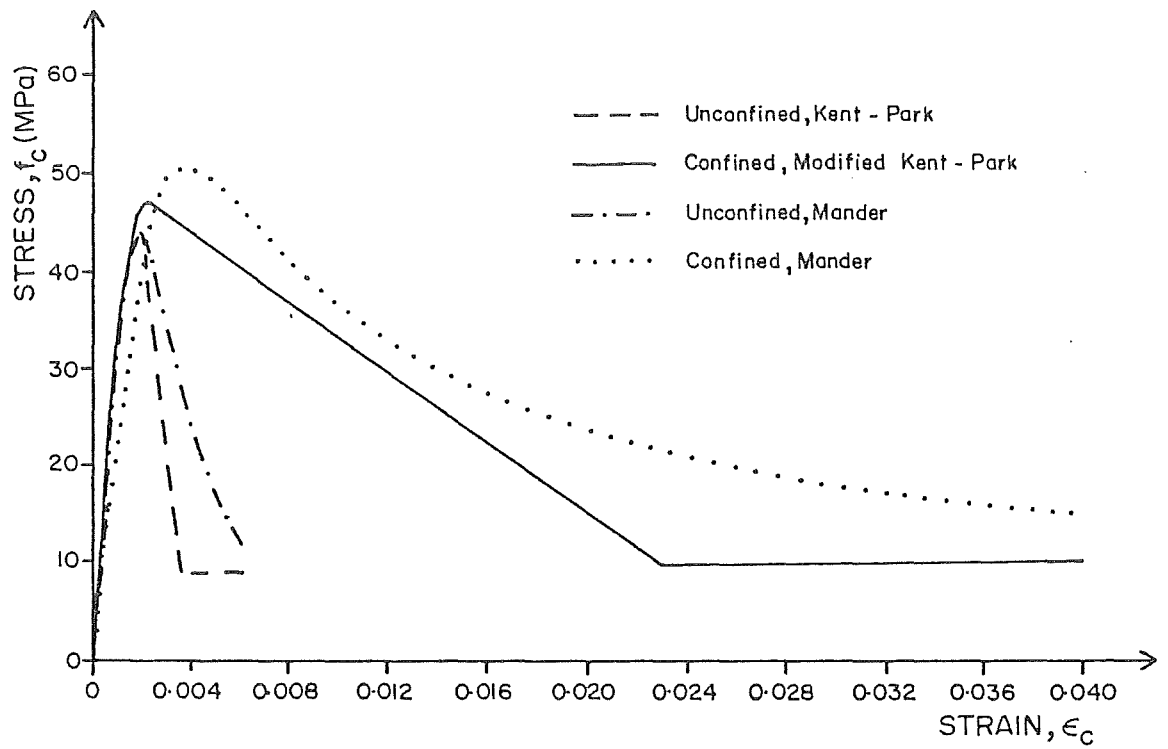


Fig. 5.6 : ANALYTICAL STRESS-STRAIN CURVES FOR CONCRETE FOR UNIT 3

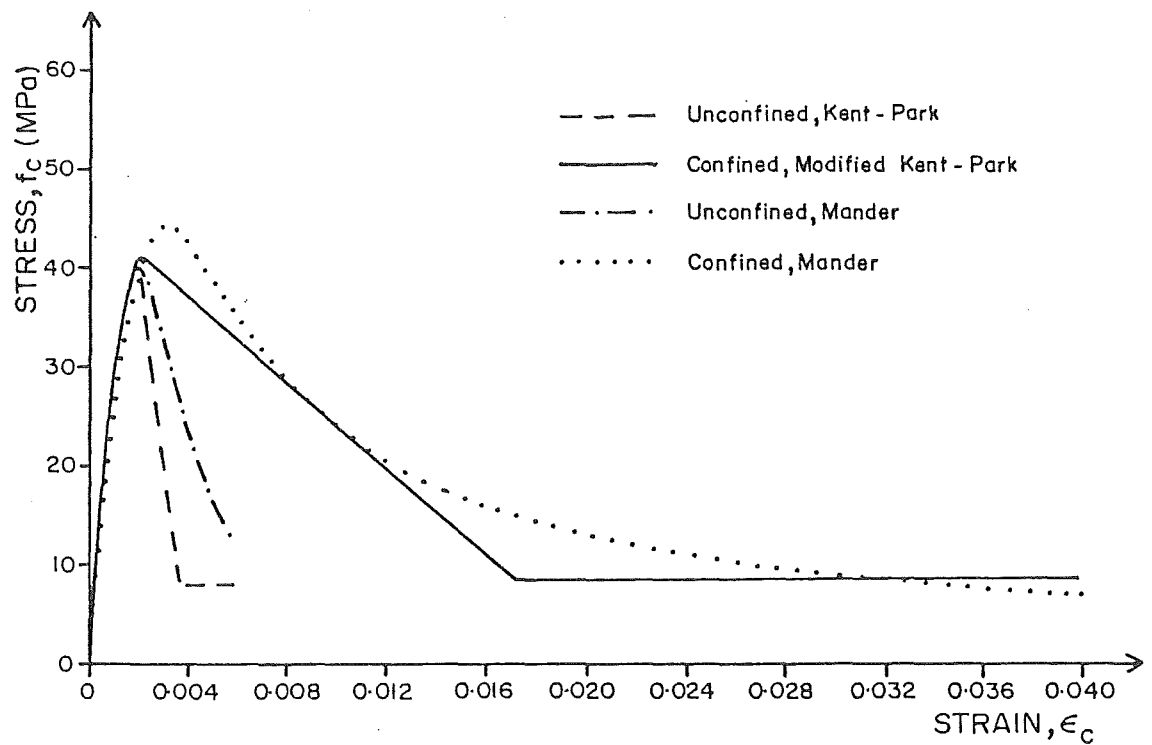


Fig. 5.7 : ANALYTICAL STRESS-STRAIN CURVES FOR CONCRETE FOR UNIT 4

5.4 ANALYTICAL STRESS-STRAIN RELATIONSHIP FOR LONGITUDINAL REINFORCING STEEL

The monotonic tension stress-strain relationship proposed by Mander et al⁽³⁾ was used for longitudinal reinforcing steel. It was assumed that the monotonic stress-strain behaviour of longitudinal reinforcing steel in compression was identical to that in tension.

Fig. 5.8 illustrates the stress-strain relationship fitted to the measured properties of the longitudinal reinforcing steel. The stress-strain relationship is defined by the following equations:

$$\begin{aligned} \text{Elastic Branch:} \quad 0 \leq \epsilon_s \leq \epsilon_y \\ f_s = E_s \epsilon_s \end{aligned} \quad (5.23)$$

where ϵ_s and f_s are steel tensile strain and stress respectively, ϵ_y is yield strain, i.e. $\epsilon_y = f_y / E_s$, f_y is yield stress and E_s is modulus of elasticity of steel.

$$\begin{aligned} \text{Yield Plateau:} \quad \epsilon_y < \epsilon_s \leq \epsilon_{sh} \\ f_s = f_y \end{aligned} \quad (5.24)$$

$$\begin{aligned} \text{Strain-hardening Branch:} \quad \epsilon_{sh} < \epsilon_s \leq \epsilon_{su} \\ f_s = f_{su} - (f_{su} - f_y) \left[\frac{\epsilon_{su} - \epsilon_s}{\epsilon_{su} - \epsilon_{sh}} \right]^P \end{aligned} \quad (5.25)$$

$$\text{in which} \quad P = E_{sh} \left[\frac{\epsilon_{su} - \epsilon_{sh}}{f_{su} - f_y} \right] \quad (5.26)$$

where P is the strain-hardening power, ϵ_{sh} and E_{sh} are strain-hardening strain and modulus respectively, and f_{su} and ϵ_{su} are ultimate tensile stress and strain respectively.

Numerical values for the stress-strain relation obtained from the tensile tests on the samples of the reinforcing bar are listed in Fig. 5.8.

5.5 MOMENT-CURVATURE ANALYSES FOR COLUMN UNITS

5.5.1 Monotonic Moment-Curvature Analysis

As discussed in Section 5.2, to derive theoretical moment-curvature relationships for reinforced concrete sections, it is necessary to know the stress-strain curves for concrete and steel. Using the stress-strain

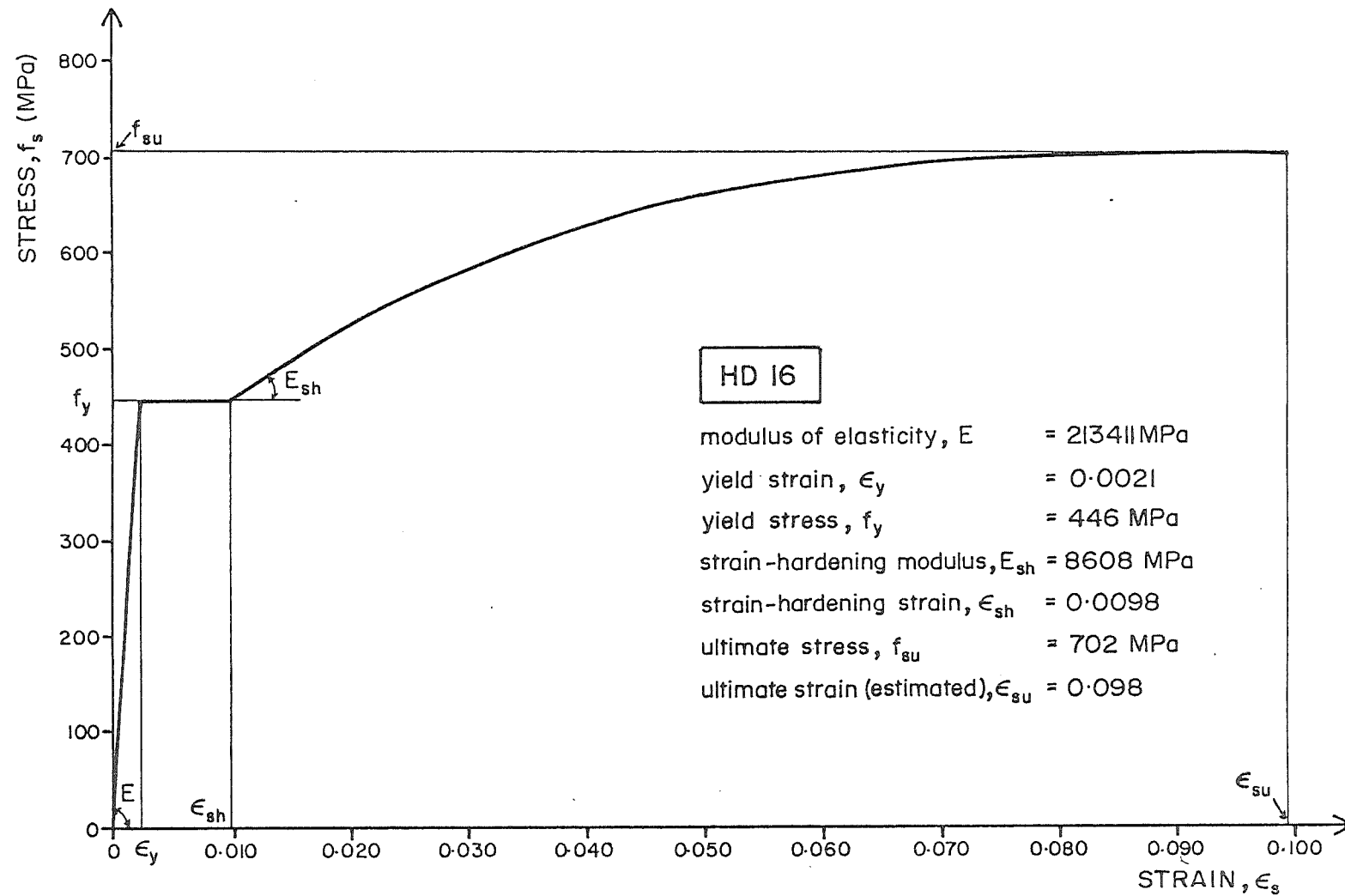


Fig. 5.8 : ANALYTICAL STRESS-STRAIN CURVE FOR LONGITUDINAL STEEL

relationships for cover and core concrete and longitudinal reinforcing steel described in Sections 5.3 and 5.4, a computer program MMPHI was developed to obtain the monotonic moment curvature response of a rectangular column under combined flexure and axial load. The listings of the program MMPHI together with the programs SSConcrete and SSSteel to determine the stress-strain curves for concrete and steel are given in Appendix A. The programs were written in FORTRAN IV language and a BURROUGHS 6900 computer was used to run the programs.

In Section 5.2 it was indicated that in order to determine the moment and curvature corresponding to a given value of concrete strain at the extreme compression fibre ϵ_{cm} , it is necessary to first determine the neutral axis depth c which satisfies the force equilibrium equation (Eq. 5.1). It is clear, that an iterative procedure is needed to find the neutral axis depth and the bisection technique was used in the program. By finding the moment and curvature corresponding to a range of ϵ_{cm} values, the moment-curvature curve for the reinforced concrete column can be plotted.

The analytical monotonic moment-curvature relationship derived for each column unit is compared with the experimental results in Section 8.2.

5.5.2 Cyclic Moment-Curvature Analysis

A computer program COLUMN was developed by Mander et al⁽³⁾ to obtain the moment-curvature response of a reinforced concrete column under combined axial load and cyclic flexure. Complete descriptions of the program can be found in Section 7.4.2 of Ref. 3.

Briefly, the program considers the stress-strain relationships of concrete and steel under cyclic loading. Also, it included energy balance calculations to predict the ultimate compressive strain of confined concrete, defined as the longitudinal compressive strain in the concrete corresponding to first fracture of the transverse reinforcement. To determine this strain the work done on the concrete core is compared with the strain energy capacity of the transverse hoops. When the total work done on the concrete core just exceeds the strain energy capacity provided by the transverse reinforcement, the fracture strain of the hoop will have been reached and the concrete compressive strain corresponding to hoop fracture can be calculated.

The shear deformation of the column is also evaluated and some additional plastic curvature from penetration of the yielding longitudinal reinforcing steel is also considered.

This theoretical approach is compared with the experimental results of column units in Section 8.2.

5.5.3 Design Charts for Ductility

Based on cyclic moment-curvature analysis, design charts for flexural strength and ductility of reinforced concrete columns have been developed by Zahn⁽²⁴⁾. The design charts are for solid and hollow circular sections as well as for solid rectangular sections.

The charts can be used either to determine the amount of transverse reinforcement required for a given curvature ductility factor or to check the available curvature ductility factor in a column with a certain amount of transverse reinforcement.

The main variables which were investigated by Zahn et al, which influence the available curvature ductility factor ϕ_u/ϕ_y of a reinforced concrete column, are the axial load P_e , the longitudinal reinforcement content ρ_t , the concrete cylinder strength f'_c , the yield strength of both the longitudinal and the transverse steel f_y and f_{yh} and the relative thickness of the concrete cover.

The application of the design charts to the column units is illustrated in Appendix B. In Section 8.2, the available curvature ductility factor of each column unit is checked analytically using the charts.

5.6 THEORETICAL YIELD CURVATURE AND YIELD DISPLACEMENT

The theoretical yield curvature ϕ_y of a reinforced concrete section is defined by the expression

$$\phi_y = \phi'_y \frac{M_i}{M_y} \quad (5.27)$$

in which M_i is the ideal (theoretical) moment capacity calculated using the code⁽²⁾_i approach which assumes an ultimate concrete compressive strain of 0.003 and a rectangular concrete compressive stress block, M_y is the moment calculated at the first yield of the longitudinal steel and ϕ'_y is the corresponding curvature at the first yield of the longitudinal steel. The definition of the yield curvature is illustrated in Fig. 5.9.

Similarly, the yield displacement Δ_y is defined by

$$\Delta_y = \Delta'_y \frac{M_i}{M_y} \quad (5.28)$$

For the column units tested, if no rotation occurs at the centre stub,

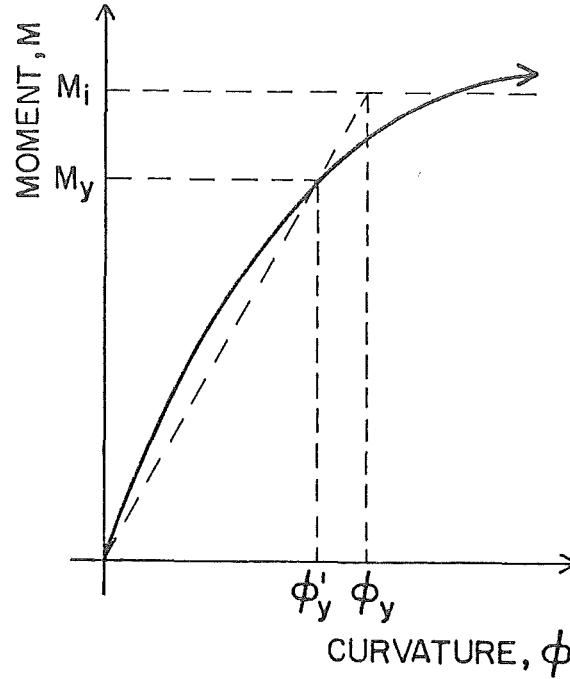


Fig. 5.9 : DEFINITION OF YIELD CURVATURE ϕ_y

$$\Delta'_Y = \frac{M_Y \ell^2}{3EI} \quad (5.29)$$

where ℓ is the distance from the section of maximum moment to the point of contraflexure and EI is effective flexural rigidity of the column section.

The total displacement Δ divided by the yield displacement Δ_Y is defined as the displacement ductility factor μ , that is

$$\mu = \frac{\Delta}{\Delta_Y} \quad (5.30)$$

The definitions of yield curvature and yield displacement given by Eqs. 5.27 and 5.28 have been conventionally used at the University of Canterbury. These definitions are based on the premise, that when the moment-curvature relation is rounded as in Fig. 5.9, the "yield point" is best defined by assuming elastic behaviour up to the ideal (theoretical) strength, as in the case of elasto-plastic behaviour.

CHAPTER SIX

TESTING PROCEDURE

6.1 INTRODUCTION

The testing procedure for column units used in this project was similar to those for the columns tested by Ang et al⁽⁷⁾ and by some previous researchers at the University of Canterbury.

As mentioned in Section 2.4.1, the axial compression load was applied by the DARTEC testing machine and the lateral load was applied through a 1 MN hydraulic jack. Using this jack, only quasi-static tests can be carried out.

6.2 TEST PREPARATION

6.2.1 Installation of Column Units

The column unit was first aligned with the DARTEC testing machine and placed in a horizontal position on a pair of trolleys. The column was then manually pulled towards the machine along a steel plate path. Once the top end of the column was under the machine, two 3-tonne chain-block hooks were attached to the lifting brackets near the top end of the unit (see Fig. 6.1). Then the column unit was winched and rotated into the

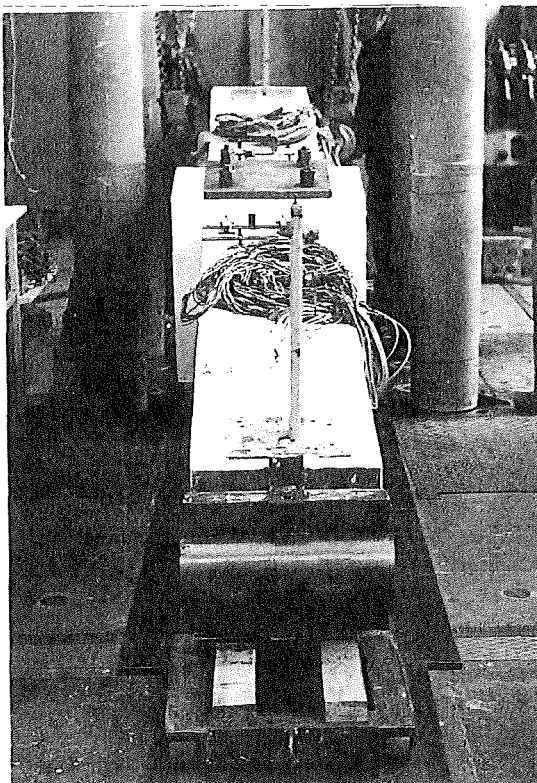


Fig. 6.1 : A COLUMN UNIT BEING PULLED TO POSITION UNDER THE TESTING MACHINE

vertical position with the bottom end riding freely on its trolley. The bottom pair of the rollers and scalloped plate were next fixed while the column unit was suspended from the chain-blocks. The top pair were fixed before the column unit was pulled into its final position. The plates were then adjusted and plastered. A small amount of axial load was used to hold the column unit while the lateral loading frame with the jack was lifted and pinned to the column. A column unit installed in the DARTEC machine is shown in Fig. 6.2. Next the calibration of the data recording devices was carried out. The column unit and the loading frame were left suspended from the chain blocks until testing commenced. During testing, the chain blocks were slackened.

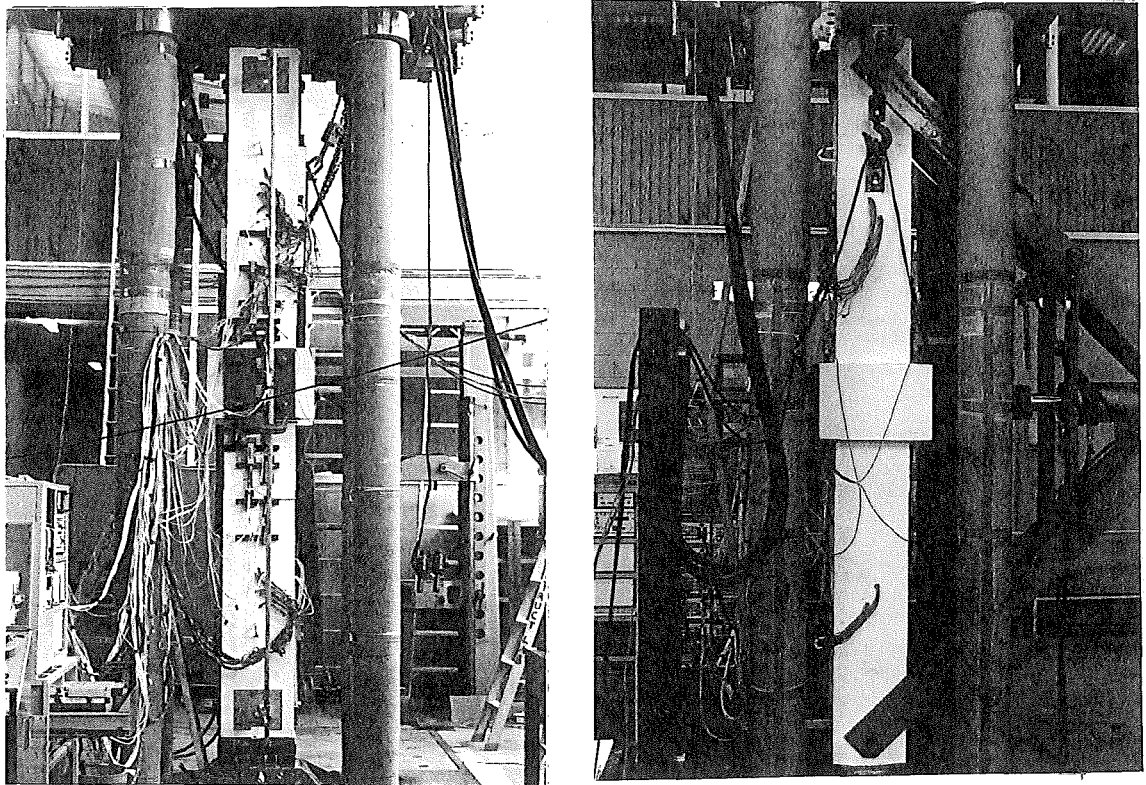


Fig. 6.2 : OVERALL VIEW OF A COLUMN UNIT IN THE DARTEC TESTING
MACHINE READY TO BE TESTED

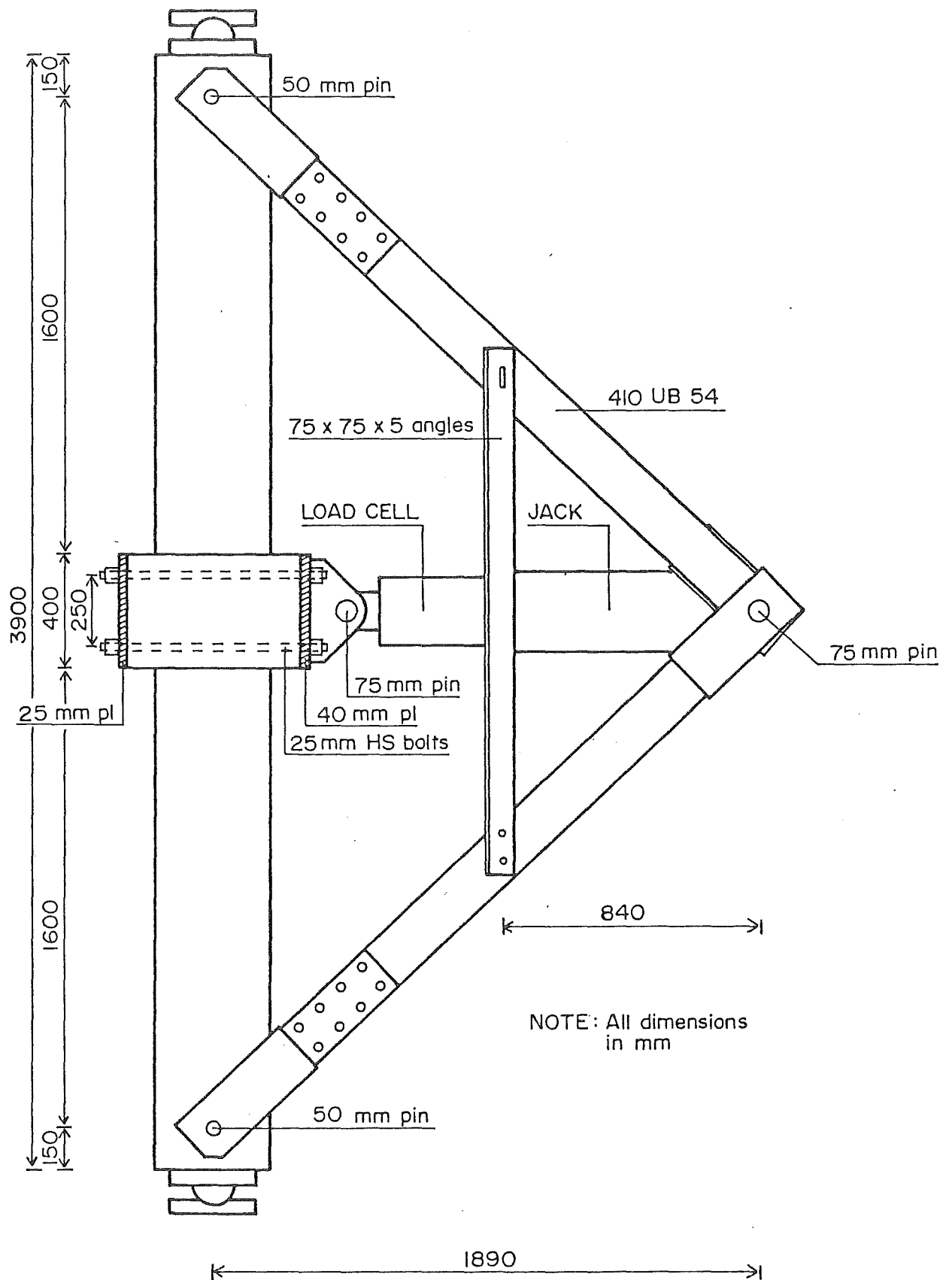


Fig. 6.3 : LATERAL LOADING FRAME AND COLUMN UNIT

6.2.2 Loading Frame

The loading frame used for applying the lateral load consisted of two inclined arms with a hydraulic jack acting along the line of bisection. The hydraulic jack was connected to both inclined arms by a 75 mm diameter steel pin. The end of each arm was connected to the column unit by a 50 mm diameter steel pin that passed through the arm and the steel tube at each end of the unit. Fig. 6.3 shows the loading frame and the column unit. Full details of the loading frame were included in Ang's report⁽⁷⁾.

The ends of the column units were designed as hinge supports, hence, they need to be allowed to rotate freely during the test. To achieve this, at each end, a steel plate with a semi-circular steel roller was bolted to two angle sections which in turn were welded to the end plate of the unit. The matching scalloped plates were bolted to the DARTEC loading patterns.

From Fig. 6.3, it is clear that the lateral load applied to the column unit will introduce an additional component of axial load. This is also shown by the force diagram in Fig. 6.4. Hence, the axial load applied by the DARTEC testing machine had to be adjusted at each lateral load increment to compensate for that effect and thus to ensure that the axial load applied to the column unit was maintained constant. When the lateral

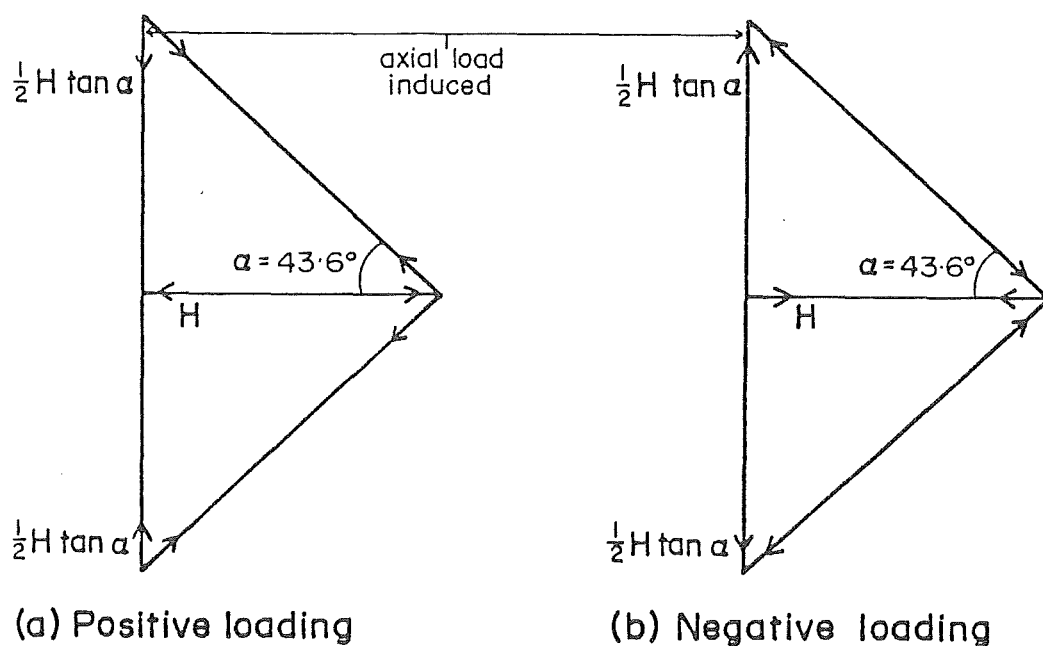


Fig. 6.4 : FORCE DIAGRAM FOR LATERAL LOADING FRAME

load applied was in compression (pushed condition), which is defined as positive loading, the axial load applied by the DARTEC machine had to be decreased. When the lateral load was in tension (pulled condition) the axial load applied by the DARTEC machine had to be increased.

The lateral load was applied through a 1 MN double-acting hydraulic jack which has an actual capacity of 1120 kN in compression and 840 kN in tension, and has 400 mm travel. The jack was connected to the steel plates at the central stub by means of a 75 mm steel pin. These plates were held against the central stub by four 25 mm diameter high-strength bolts passed through the plastic tubes cast in the stub, and bolted at both ends (see Fig. 6.3). The loading frame and the jack were assembled as one unit with minor adjustment of the jack level available through a slotted hole connection in the two angle sections which kept the jack in position.

6.2.3 Concrete Compression Test

Just prior to testing the column units, compressive tests were carried out on the 200 x 100 mm diameter concrete cylinders to determine the concrete strength. The ideal flexural strength M_i of the column was calculated using the measured concrete and steel strengths. An ultimate compression strain of 0.003 and the Code⁽²⁾ concrete rectangular compressive stress block were used in calculating M_i .

6.3 COLUMN TESTING

Once the ideal flexural strength M_i is known, the theoretical ultimate load, i.e. lateral load at ideal strength H_i could be calculated.

An initial loading cycle to approximately 75 percent of the ideal column flexural strength was applied in both the positive and negative directions. From the resulting load displacement graph, an experimental value for the yield displacement Δ_y^* , was obtained by extrapolating a straight line from the origin through the peak load-displacement coordinate at $0.75 H_i$ to the theoretical ultimate load H_i (neglecting P- Δ effect). This is illustrated in Fig. 6.5. The yield displacement Δ_y^* used in the tests was the average of the values found for loading in each direction.

For Units 1, 2 and 3, the displacement history used during the tests, followed a similar pattern to those used in the previous projects.

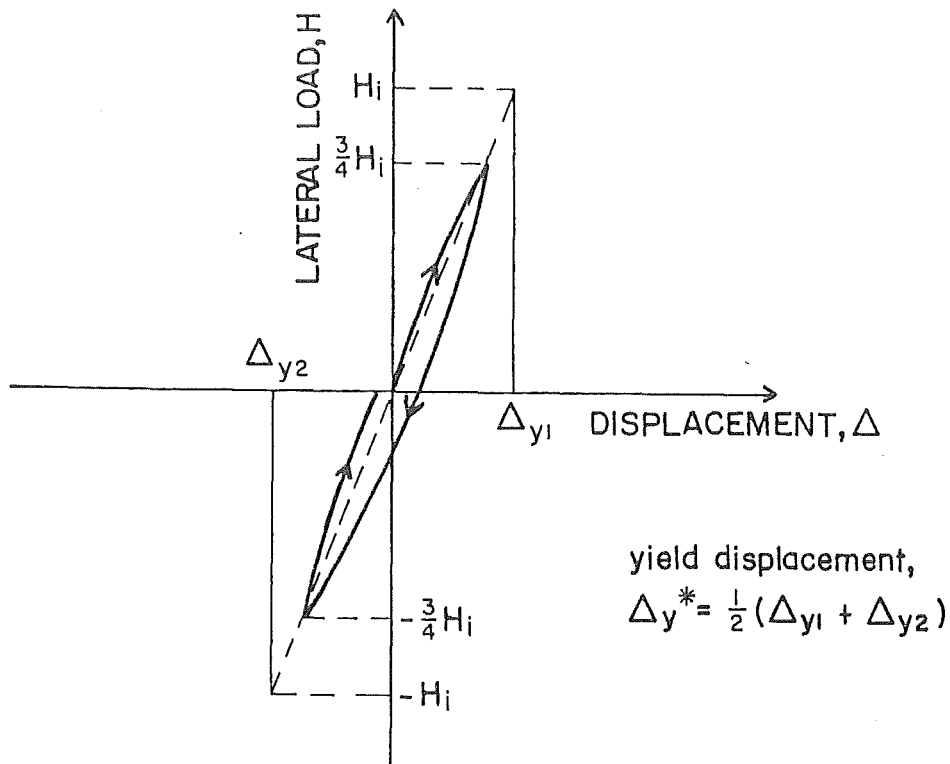


Fig. 6.5 : DETERMINATION OF EXPERIMENTAL VALUE OF YIELD
 DISPLACEMENT, Δ_y^*

This basically consisted of one complete cycle to displacement ductility factor μ_n of 0.75 and two complete cycles to each of $\mu_n = 2, 4, 6, 8$, etc. until complete failure resulted or the test had to be terminated for other reasons. The displacement history used for Units 1, 2 and 3 is shown in Fig. 6.6a.

For Unit 4, which contained only a small amount of transverse reinforcement (refer to Section 2.2.4), a lower available ductility was expected. Therefore, to extract more useful information from the test, it was considered more appropriate for the displacement history illustrated in Fig. 6.6b to be used. This consisted of one complete cycle of $\mu_n = 0.75$ and two complete cycles to each of $\mu_n = 1, 2, 3, 4$, etc.

During each loading cycle, when the stiffness of column units was sufficiently high, the test was carried out using load controlled increments of one-quarter of the theoretical ultimate load (neglecting P-Δ effect). When the stiffness was low the test was carried out using displacement controlled increments. Typically increments of one-half of the

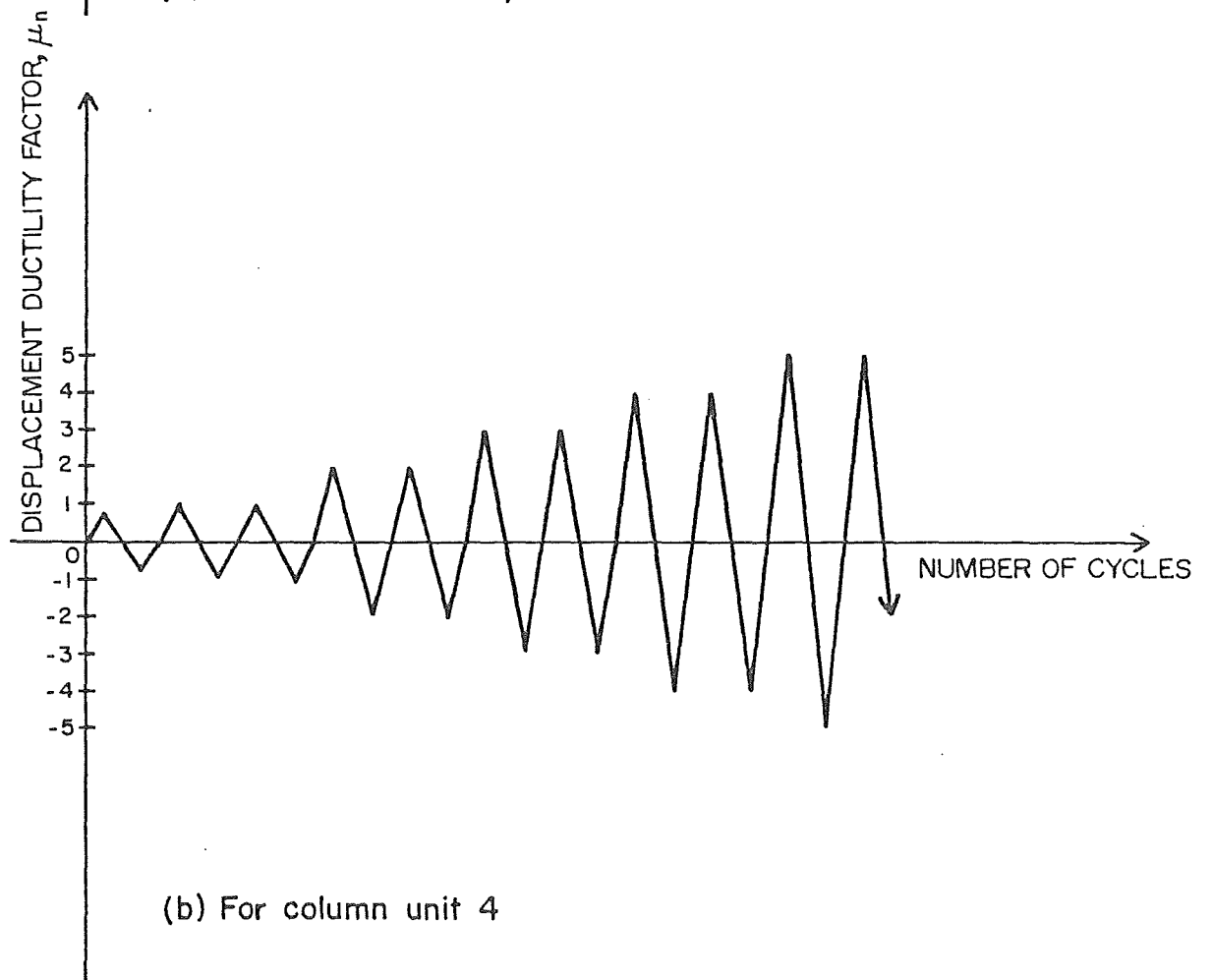
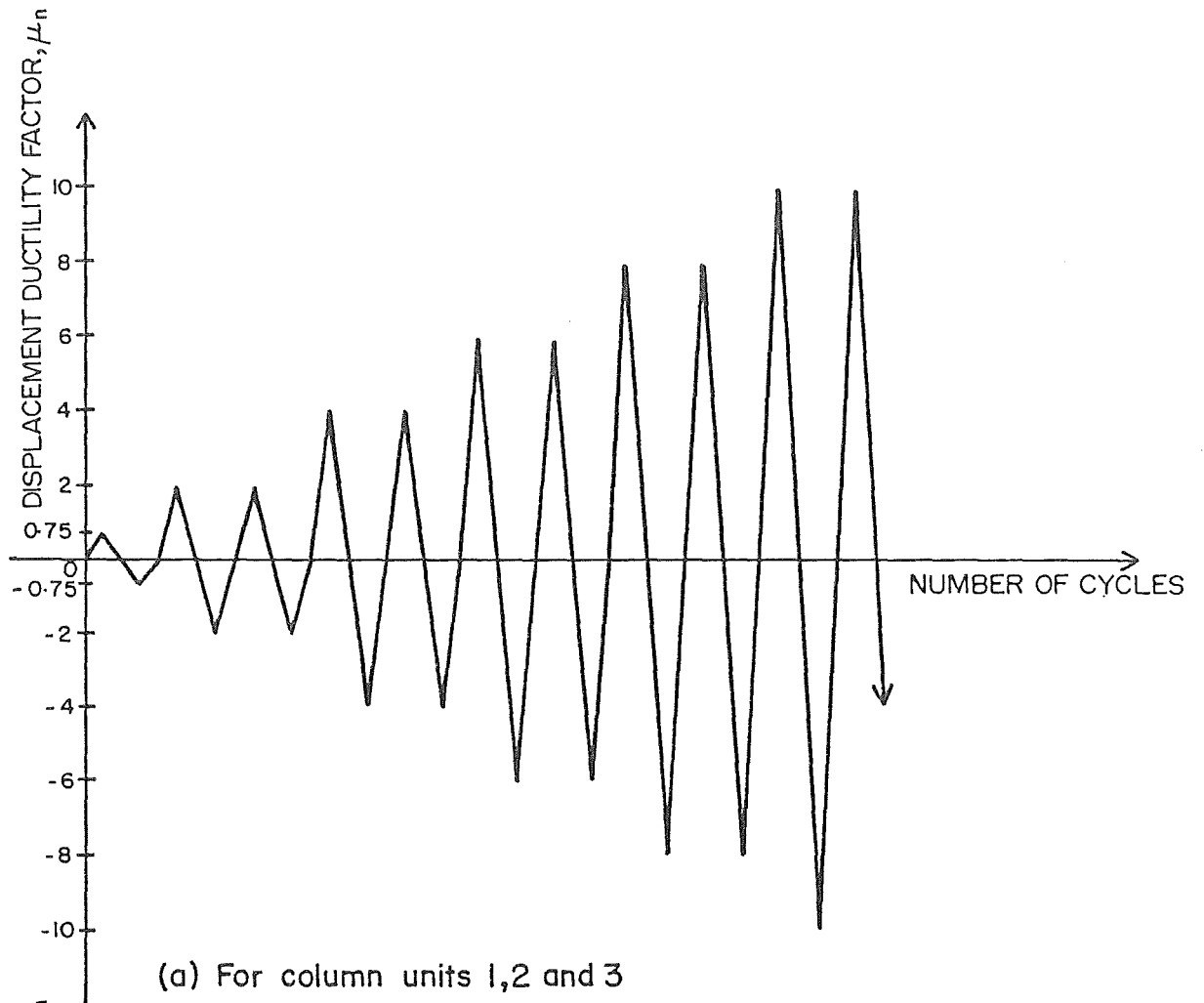


Fig. 6.6 : LOAD AND DISPLACEMENT HISTORIES

yield displacement were used, up to the desired displacement.

At the peak of each loading cycle, cracks in the concrete were marked, photographs were taken and the strain gauge and potentiometer readings were recorded by the SOLARTRON data logger. Also, between the displacement peaks of each cycle, readings were taken on the data logger at position of zero lateral load.

The hysteresis loops obtained from the tests were not actually as smooth as plotted in Chapter 7. At each displacement controlled increment, creep of the column units caused the lateral load jack to lose some load. Similarly at each load controlled increment, creep of the column unit caused the deflection to increase. Another effect was the axial load adjustment necessary at the end of each increment, although this would have had a much smaller influence than creep. The curves plotted represent the envelope of the load-deflection and load-curvatures behaviour for each cycle.

CHAPTER SEVEN

EXPERIMENTAL RESULTS AND OBSERVATIONS

7.1 INTRODUCTION

The experimental results obtained in the column tests are presented in this chapter. The four column units tested were subjected to static cyclic lateral loading and constant axial compressive load in a DARTEC testing machine.

The test units have been described in earlier chapters. The details of the units will be summarized when presenting the experimental results.

Finally, concluding remarks on the experimental results are given.

7.2 ASPECTS OF THE INVESTIGATION

The performance of each column unit during the testing is described in detail in the following sections. For each unit the following aspects are reported:

(i) General Observations

A general description of the behaviour of each column unit during testing is presented.

(ii) Hysteretic Performance

Hysteresis curves, which were directly plotted during the testing are presented. The hysteresis curves plotted for each unit are a lateral load-displacement graph ($H-\Delta$) and two lateral load-curvature graphs (i.e. lateral load-top column curvature ($H-\phi_t$) and lateral load-bottom column curvature ($H-\phi_b$)), where ϕ_t and ϕ_b are the curvatures measured in the potentiometers gauge nearest the central stub above and below the central stub. Superimposed on the measured lateral load displacement curves of these figures is the theoretical ideal lateral load capacity H_i of the column unit plotted as dashed lines. Obviously, the lines drop as the displacement increases owing to the secondary moment ($P-\Delta$) effect.

Also, a brief description of each column unit is presented. This is the level of axial load applied P_e , the transverse hoops provided in the potential plastic hinge regions, the total effective area of hoops A_{sh} compared both to the current code equation and to the modified equation. The experimental yield displacement Δ_y^* and the maximum

lateral load reached during the testing H_{\max} are also listed.

The nominal and real displacement ductility factors μ_n and μ_r are presented on the figures. An explanation of the definition of these ductility factors is given below. In most of the column units tested, the plastic rotation occurred unsymmetrically either above or below the central stub, particularly at higher displacement ductility factors. This unsymmetrical rotation led to a concentration of the rotation in the plastic hinge which had formed first and it was clearly visible in the last stages of testing. Fig. 7.1 shows the implication of unsymmetrical plastic hinging which results in a rotation θ of the central stub.

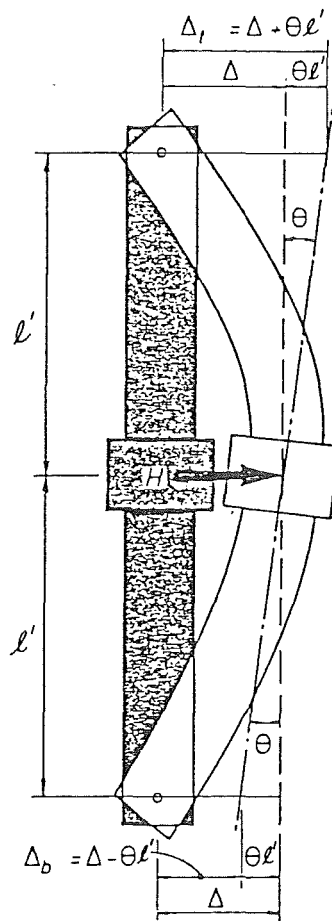


Fig. 7.1 : IMPLICATION OF THE ROTATION OF THE CENTRAL STUB

To account for the concentration of the plastic rotation in one plastic hinge of the column unit, the quantity of $\theta l'$ has to be added to the horizontal displacement Δ measured by the potentiometer at the middle of the stub. The rotation θ was calculated from the difference in the

displacements measured by the two linear potentiometers at the top and bottom positions on the stub. The displacement ductility factor calculated from $(\Delta + \theta \ell')/\Delta_y$ is referred to as the real displacement ductility factor μ_r , and that calculated from Δ/Δ_y^* is referred to as the nominal displacement ductility factor μ_n , where Δ_y^* and Δ_y are yield displacements as defined below.

(1) Δ_y^* was defined previously in Section 6.3. In summary, Δ_y^* was calculated at the beginning of the test of the column unit by linearly extrapolating from the origin through the load-displacement coordinate at $0.75 H_i$ to the theoretical ultimate load H_i which corresponds to the theoretical flexural strength M_i . The yield displacement Δ_y^* was taken as the average of the values so found at H_i for loading in each direction (see Fig. 6.5).

(2) Δ_y was calculated using the actual (measured) flexural strength of the column unit in each loading direction. That is, when the moments measured at the peaks of the first half cycles to $\mu_n = +2$ and $\mu_n = -2$ were known, the yield displacement used in subsequent loading could be refined by linear extrapolation as follows:

$$\Delta_y = \Delta_y^* \frac{\bar{M}}{M_i} \quad (7.1)$$

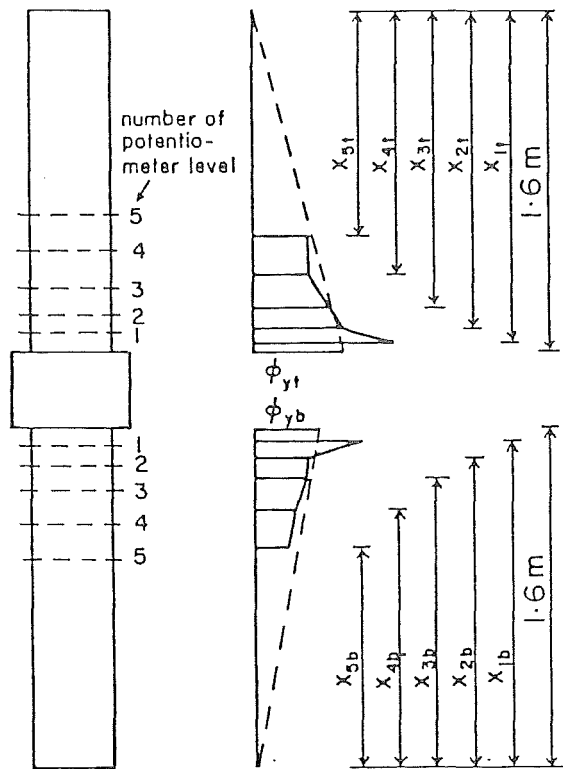
where \bar{M} is the average of the magnitude of the experimental moments measured at the positive and negative peaks of the first cycle at $\mu_n = 2$.

(iii) Curvature Distribution, Curvature Ductility and Equivalent Plastic Hinge Length

Curvature profiles for the column units are plotted at the displacement ductility factor peaks. The curvature values are plotted at the mid-point of the successive gauge lengths and joined by straight lines.

The general trend for the measured curvature profiles was an increase in curvature as the displacement ductility factor was increased. Some irregularity of the curvature profiles existed due to the random nature of the flexural crack formation.

To calculate the experimental curvature ductility factor available in the column units, it is necessary to define the experimental yield curvature ϕ_y . Fig. 7.2 shows a typical example of the curvatures measured by pairs of potentiometers over the five gauge lengths along each top and bottom half of the column adjacent to the central stub when the lateral displacement at the middle of the central stub was Δ_y^* .



$$\phi_{yt} = \frac{1}{4} \sum_{it=2}^5 \phi_{it} \frac{1.6}{x_{it}} \quad (7.2)$$

$$\phi_y^* = \frac{1}{2} (\phi_{yt} + \phi_{yb}) \quad (7.4)$$

$$\phi_{yb} = \frac{1}{4} \sum_{ib=2}^5 \phi_{ib} \frac{1.6}{x_{ib}} \quad (7.3)$$

Fig. 7.2 : DEFINITION OF EXPERIMENTAL YIELD CURVATURE ϕ_y

During the tests it was observed that the curvatures immediately above and below the central stub (i.e. the curvatures at potentiometer level 1) were overproportionally large compared to those measured at the other levels. This was already noticeable when the displacement at the middle of the stub was equal to Δ_y^* , and was because the gauge lengths at level 1 actually include a pronounced crack at the face of the stub due to relative displacements between the longitudinal reinforcing steel and the concrete inside the central stub, namely yield penetration. Consequently the yield curvature cannot be calculated accurately by simply averaging the curvatures at level 1. Instead, it is more appropriate, if the curvatures measured at levels 2 to 5 when the central displacement was equal to $\pm \Delta_y^*$ were extrapolated to the top and bottom face of the stub, respectively, assuming a triangular curvature distribution as shown in Fig. 7.2. All the extrapolated curvatures so found for both faces of the stub and for both loading directions were averaged to define the curvature ϕ_y^* , corresponding to the preliminary yield displacement Δ_y^* .

The experimental yield curvature ϕ_y was then found by extrapolating the value ϕ_y^* to the measured moment \bar{M} , in the same manner as described for the experimental yield displacement Δ_y . Therefore

$$\phi_y = \phi_y^* \frac{\bar{M}}{M_i} \quad (7.5)$$

The equivalent plastic hinge length ℓ_p may be found from the plastic displacement Δ_p , by taking the first moment of area of an idealised rectangular distribution of the plastic curvature about the point of contraflexure of the column. Fig. 7.3 illustrates the assumed curvature distribution for the column. Then

$$\Delta_p = (\mu_r - 1)\Delta_y = (\phi_u - \phi_y) \ell_p (\ell - 0.5\ell_p) \quad (7.6)$$

in which $(\phi_u - \phi_y)\ell_p$ is the plastic rotation and ℓ is the distance from the section of maximum moment to the point of contraflexure (1600 mm).

By rearranging Eq. 7.6 it can be shown that

$$\frac{\ell_p}{h} = \frac{\ell}{h} \left[1 - \sqrt{1 - \frac{2(\mu_r - 1)\Delta_y/\ell^2}{\phi_u - \phi_y}} \right] \quad (7.7)$$

where h is the overall depth of the column (400 mm).

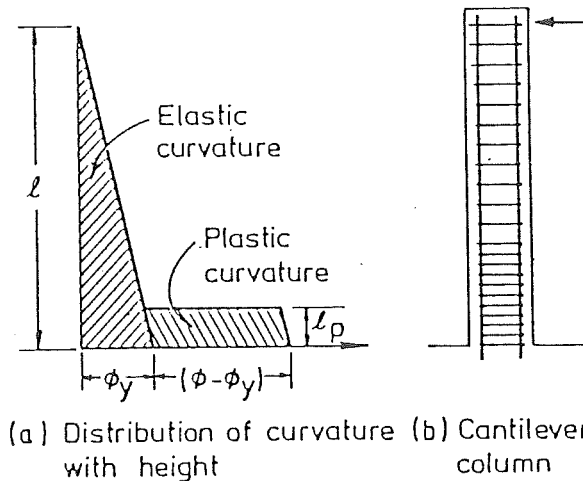


Fig. 7.3 : IDEALISED CURVATURE DISTRIBUTION FOR THE COLUMN

In the following sections the non-dimensional equivalent plastic hinge lengths ℓ_p/h are calculated using ϕ_u at the first and second gauge lengths respectively and an average $(\ell_p/h)_{av}$, found by averaging the two values of ℓ_p/h , is also given.

(iv) Measured Strain Profile

The profiles of the transverse strains in the hoops, which were monitored by the electrical resistance strain gauges, are plotted at the successive positive and negative displacement ductility peaks. The strains measured by the strain gauges at each level are joined by straight lines.

As mentioned previously in Section 2.4.3, the positions of the strain gauges designated A and B were as shown in Fig. 2.13, i.e. at the nearer side to the loading frame. Therefore, during positive loading, this side was in longitudinal compression and these strain gauges measured the tensile strains in the hoops resulting from confining the concrete. During negative loading, this side was in longitudinal tension and the tensile strains measured by these strain gauges reduced. This may be explained as follows. During positive loading the longitudinal compressive strains in the concrete caused lateral expansion of the concrete and as a result transverse tensile strains were measured by the strain gauges on the hoops, namely confining strains. During negative loading the longitudinal tensile strains in the concrete would reduce the lateral expansion of the concrete, but not to zero since much of it would have been due to internal micro cracking. Hence even for negative loading some tensile strain would be recorded by these strain gauges.

The profiles of the longitudinal compressive strains at the extreme fibre of the core concrete are also presented. For positive loading the profiles are plotted together with the tensile strains measured in the hoops due to confinement, while for negative loading the profiles are plotted together with the transverse tensile strains induced in the hoops in the tension zone. These longitudinal compressive strains at the extreme fibre of the core concrete at the successive positive and negative displacement ductility peaks were calculated by linear interpolation of the longitudinal strains measured by each pair of linear potentiometers at a given level. The compressive strain values are plotted at the mid-point of the successive gauge lengths and joined by straight lines. It is more appropriate to measure the dimensions of the core concrete to the centreline of the peripheral hoop. However, the core concrete was measured to the outside of the peripheral hoop as defined by the code⁽²⁾.

Finally, the transverse strains on the hoop sides parallel to the direction of loading, which measured the hoop strains due to shear in the column, are presented.

7.3 THE PERFORMANCE OF COLUMN UNIT 1

Unit 1 properties:

Axial load level $P_e = 0.1 f'_c A_g$

Concrete compressive strength $f'_c = 46.5 \text{ MPa}$

Transverse hoops in the potential plastic hinge regions = R7 - 85 mm

Yield strength of the transverse reinforcing steel $f_y = 364 \text{ MPa}$

Total effective area of the transverse hoops A_{sh}
 $= 43.1\%$ of the current code value, Eq. 4.4, or
 64.7% of the proposed modified code value, Eq. 4.9.

Lateral load at the ideal strength $H_i = 378 \text{ kN}$.

(i) General Observations

Flexural cracks in the column were first detected adjacent to the upper and lower faces of the central stub at about 50 percent of the ideal column flexural strength. Further cracking occurred as the lateral load increased. The initial elastic cycle was taken up to ± 75 percent of the ideal strength. The extent of cracking at the end of the elastic cycle is shown in Fig. 7.4, and at the second cycle of $\mu_n = -2$ in Fig. 7.5. The cracks tended to increase in length and width as the peak displacements were increased in subsequent load cycles.

The first sign of the cover concrete beginning to spall was observed at approximately 150 mm above and below the central stub during the first cycle of $\mu_n = 4$. Spalling occurred when the concrete compressive strain was about 0.013. Fig. 7.6 exhibits the unit at the second cycle of $\mu_n = 4$.

The cover concrete spalled more severely at the first cycle of $\mu_n = 6$ in the vicinity of the upper and lower faces of the stub. During the second cycle of $\mu_n = 6$ the transverse hoops at the second potentiometer levels and the corner longitudinal bar became visible. Fig. 7.7 shows the unit at the second cycle of $\mu_n = -6$.

At the second cycle of $\mu_n = 8$, buckling of the longitudinal bars at the top plastic hinge had just commenced. The unit at this cycle is shown in Fig. 7.8. From the strain gauge readings recorded by the data



Fig. 7.4 : EXTENT OF CRACKING
IN UNIT 1 AT THE END
OF ELASTIC CYCLE



Fig. 7.5 : UNIT 1, AT THE SECOND CYCLE
OF $\mu_n = -2$



Fig. 7.6 : CRACKING AND SPALLING
IN UNIT 1 AT $\mu_n = 4$

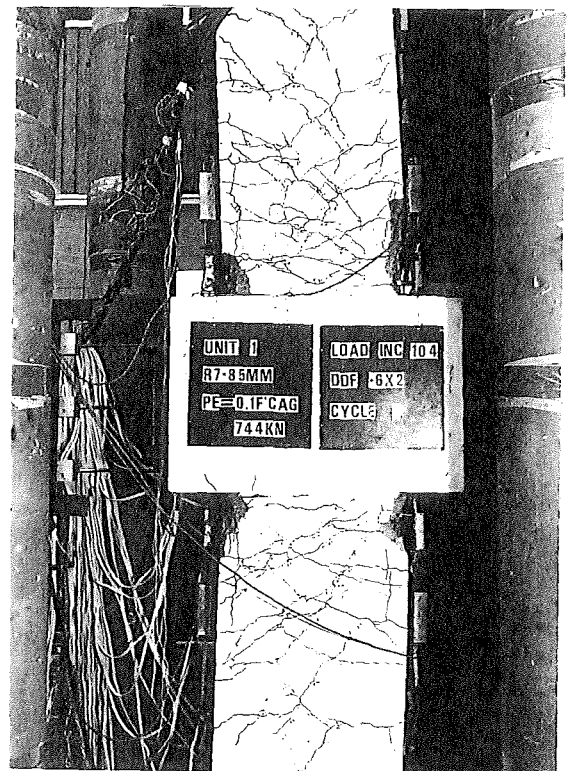


Fig. 7.7 : UNIT 1, AFTER COMPLETION
OF TWO CYCLES OF $\mu_n = -6$



Fig. 7.8 : UNIT 1, AT THE SECOND
CYCLE OF $\mu_n = 8$



Fig. 7.9 : UNIT 1, AT THE DISPLACEMENT
PEAK OF THE FIRST CYCLE OF
 $\mu_n = 10$



Fig. 7.10 : AFTER COMPLETING ONE
CYCLE OF $\mu_n = 10$



Fig. 7.11 : UNIT 1, AT THE SECOND
CYCLE OF $\mu_n = 10$

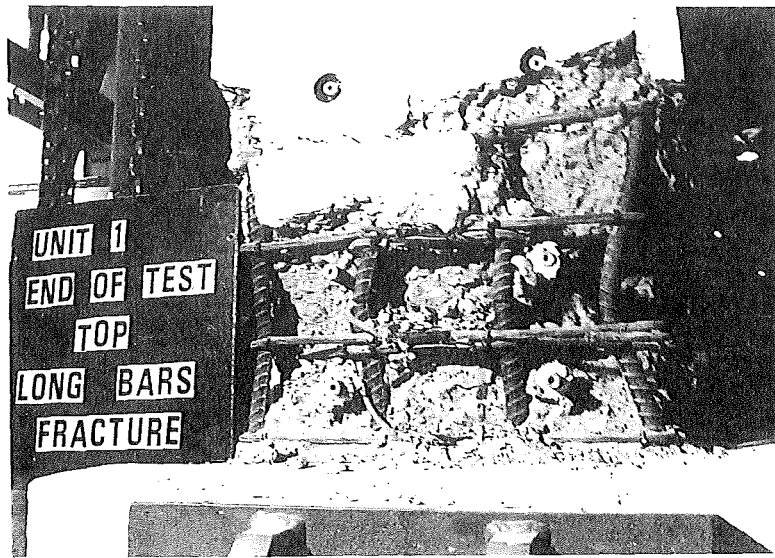


Fig. 7.12 : LONGITUDINAL BARS FRACTURED AT THE END OF TESTING OF UNIT 1

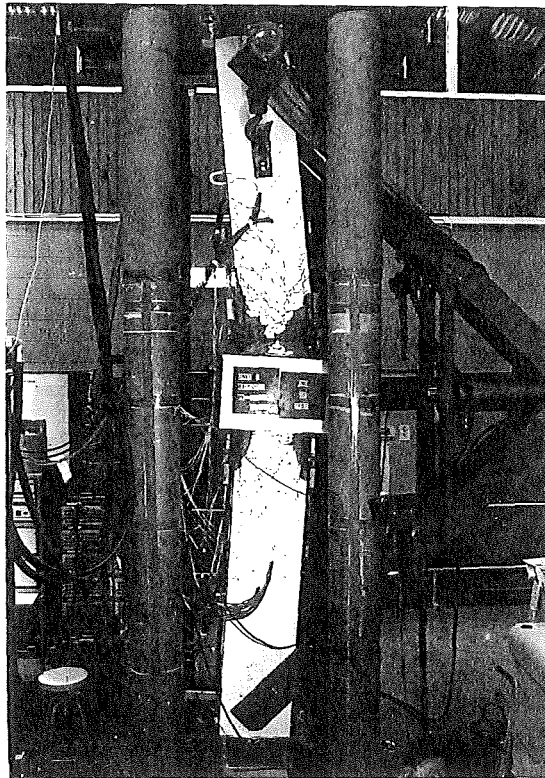


Fig. 7.13 : OVERALL VIEW OF UNIT 1 AT THE END OF THE TESTING

logger, it was evident that the strains due to shear measured in some of the hoops of the column were quite high. At the completion of this cycle, i.e. at zero lateral load, the axial shortening of the column was 5.41 mm.

Although crushing of the core concrete was visible at the first cycle of $\mu_n = 10$, the transverse hoops were still effectively preventing buckling of the longitudinal bars. The unit at this stage is shown in Fig. 7.9. Also, the lateral load capacity at this cycle was still 15 percent in excess of the theoretical ultimate capacity (see Fig. 7.14).

The anchorage bends at the ends of the octagonal hoops at the top plastic hinge, opened up at the first cycle of $\mu_n = -10$. This resulted in the commencement of strength degradation of the column. Fig. 7.10 shows the unit at this stage.

At the second cycle of $\mu_n = 10$, buckling of the longitudinal bars was quite significant as shown in Fig. 7.11 and the lateral load capacity also dropped quite significantly compared to that in previous cycles.

The excursion to the second cycle of $\mu_n = -10$ resulted in fracture of some of the longitudinal bars. The test of the unit was terminated at the second cycle of $\mu_n = -10$, by which stage the lateral load capacity had dropped to 47 percent of the theoretical ultimate capacity. At the end of the testing, low cycle fatigue fracture of two longitudinal bars at the top plastic hinge was observed as in Fig. 7.12. The overall view of the unit at the end of the testing is shown in Fig. 7.13.

(ii) Hysteretic Performance

The lateral load-displacement graph, the lateral load-top column curvature graph and the lateral load-bottom column curvature graph are shown in Figs. 7.14, 7.15 and 7.16 respectively. It can be seen that the hysteresis loops show very good energy dissipating characteristics and stability. With increasing displacement ductility, some stiffness degradation is apparent. Very little degradation of strength occurred on the second complete cycle at a constant ductility factor until $\mu_n = 10$ was reached.

The experimental ultimate (maximum) load H_{max} occurred at $\mu_n = 2$ and was 402 kN, giving a flexural overstrength factor M_{max}/M_i of 1.11, where M_i is the ideal (theoretical) flexural strength calculated using the measured material strengths.

Pinching of the hysteresis loops commenced at $\mu_n = 4$. It is known that pinching is a characteristic of the hysteresis loops for columns with low levels of axial load. Pinching is due to compressive

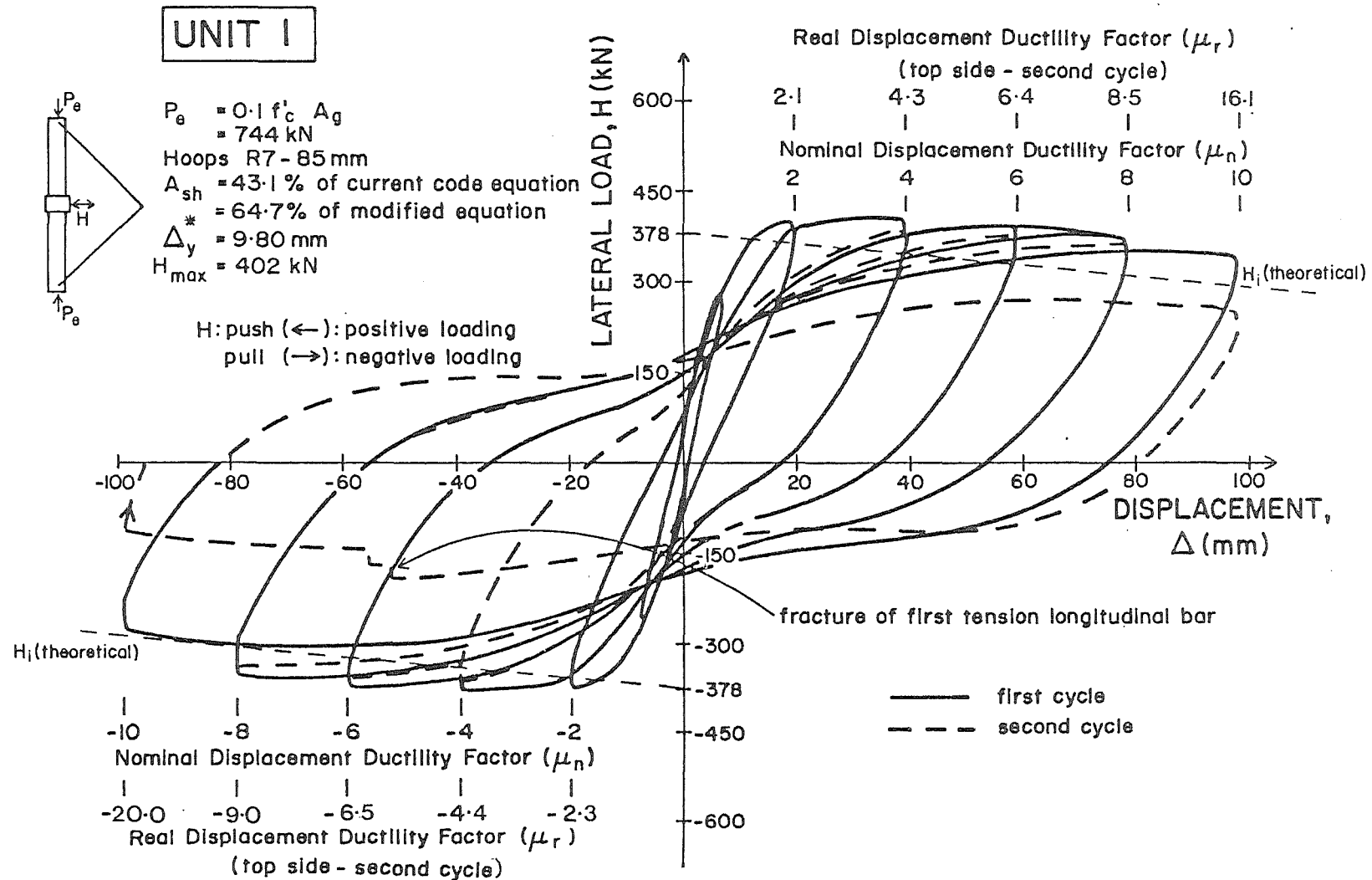


Fig. 7.14 : EXPERIMENTAL LATERAL LOAD-DISPLACEMENT HYSTERESIS LOOPS FOR COLUMN UNIT 1

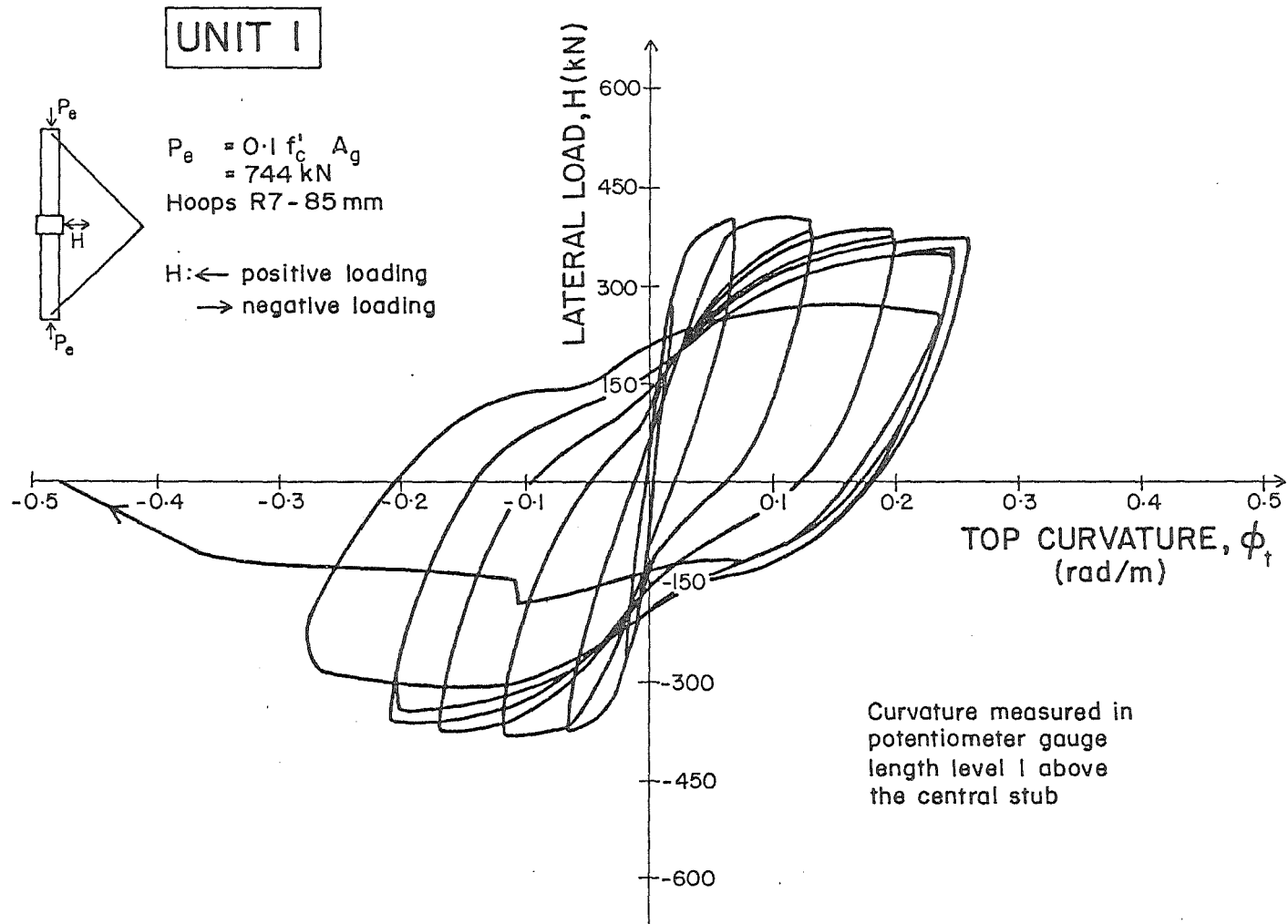


Fig. 7.15 : EXPERIMENTAL LATERAL LOAD-TOP COLUMN CURVATURE HYSTERESIS LOOPS FOR COLUMN UNIT 1

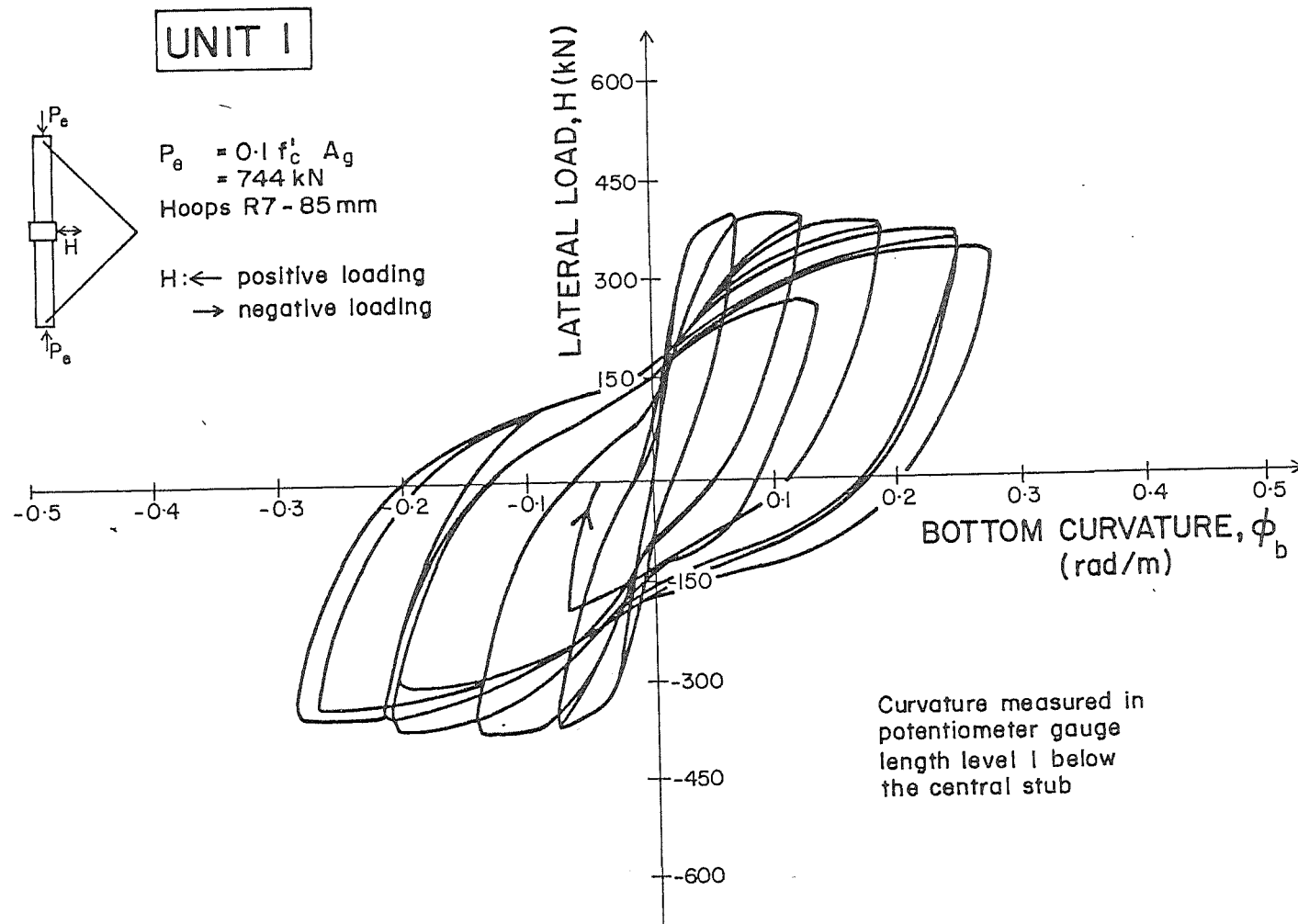


Fig. 7.16 : EXPERIMENTAL LATERAL LOAD-BOTTOM COLUMN CURVATURE HYSTERESIS LOOPS FOR COLUMN UNIT 1

axial load and flexure causing the closure of open cracks in the compression zone. The open cracks were there as a result of the plastic tensile extension of the steel which occurred during the half cycle of loading in the previous direction.

As mentioned previously, the flexural capacity was still 15 percent in excess of the theoretical flexural capacity at the first cycle to a nominal displacement ductility $\mu_n = 10$ or a real displacement ductility $\mu_r = 11.2$, although the transverse hoops provided in the column was only 43 percent of the code⁽²⁾ requirements.

The maximum lateral displacement, $\Delta + \theta \ell'$ where θ is the stub rotation and $\ell' = 1.8 \text{ m}$, was calculated for the top half of the column as 91 mm. Hence the maximum drift measured, $(\Delta + \theta \ell')/\ell'$, was 5.1 percent.

(iii) Curvature Distribution, Curvature Ductility and Equivalent Plastic Hinge Length

The measured curvature profiles for Unit 1 are shown in Fig. 7.17. The profiles are plotted at the positive and negative displacement ductility peaks of $\mu_n = 2, 4, 6, 8$ and 10. It can be seen that the curvatures are quite uniformly distributed over the top and bottom plastic hinge region. Only at the later stage of the testing was the plastic rotation more concentrated at the top plastic hinge region.

Using the procedure described in Section 7.2, the experimental yield curvature ϕ_y was found to be $10.14 \times 10^{-3} \text{ rad/m}$. The ultimate curvature was taken as the curvature measured in the first potentiometer level ϕ_{ul} , at the top plastic hinge region in the second cycle of $\mu_n = -8$ when the measured flexural strength had reduced to not less than 80% of the theoretical ideal strength. From the potentiometer reading, ϕ_{ul} was calculated to be 0.2014 rad/m . The available curvature ductility ϕ_{ul}/ϕ_y is then 19.9.

It should be noted that the heavily reinforced central stub provided some confinement to the column concrete immediately above and below the stub. Consequently, the critical sections of the column for flexure would have been at about $0.5h$ from the stub or approximately at the second potentiometer level. Thus, the curvature at this level increased more rapidly than the curvature at the first potentiometer level, particularly at higher displacement ductility factors when the stiffness of the column decreased significantly. If the curvature at the second potentiometer level was considered as the ultimate curvature, i.e. $\phi_{u2} = 0.2426 \text{ rad/m}$, the available curvature ductility factor $\phi_{u2}/\phi_y = 23.9$,

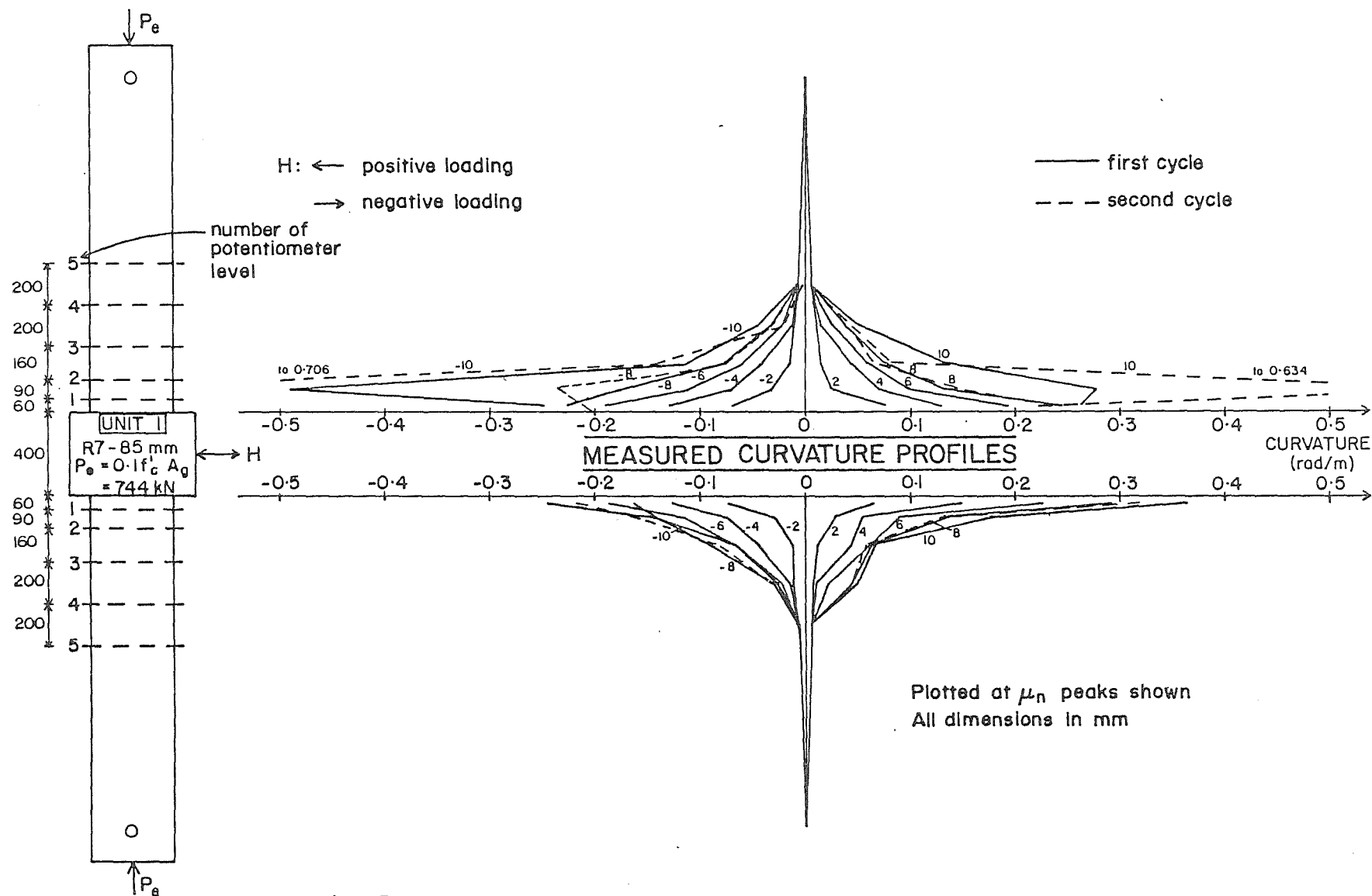


Fig. 7.17: MEASURED CURVATURE PROFILES FOR COLUMN UNIT 1

which is larger than ϕ_{ul}/ϕ_y .

The equivalent plastic hinge lengths ℓ_p calculated from Eq. 7.7 are 0.29 h or 116 mm and 0.23 h or 92 mm for the curvature ductility factors ϕ_u/ϕ_y of 19.9 and 23.9 respectively, giving an average plastic hinge length $(\ell_p/h)_{av}$ of 0.26 h (104 mm).

(iv) Measured Strain Profiles

The profiles of the longitudinal compressive strains at the extreme fibre of the core concrete, together with the transverse confining strains and the transverse tensile strains in the tension zone in the hoops, are presented in Figs. 7.18 and 7.19, respectively. The compressive strains in the core concrete increased as the column curvature increased. It can be seen that the maximum concrete compressive strain occurred at the second potentiometer level at the top plastic hinge, and was found to be 0.050 at the second cycle of $\mu_n = \pm 8$.

The concrete compressive strain in turn caused a lateral expansion of the concrete inducing tensile strains in the transverse hoops which confined the concrete. It has been noted that the central stub also provided a confining effect to the column concrete adjacent to the stub. The confinement provided by the stiff central stub was significant, since as can be seen from Fig. 7.18, yielding of the transverse hoops did not occur at the face of the stub but only occurred at the second level of octagonal hoops at the displacement ductility of 10. At this stage, crushing of concrete penetrated the core very significantly. However, the yielding hoops still effectively provided lateral restraint to the longitudinal bars and prevented buckling.

The compressive strain profiles of the core concrete are plotted for positive and negative displacement ductilities of $\mu_n = 2, 4, 6, 8$ and 10, and the measured strains in the hoops are plotted at $\mu_n = 2, 8$ and 10 in both directions of loading.

Measured strain profiles in the hoops due to shear at the successive positive and negative displacement ductility peaks are shown in Figs. 7.20 and 7.21, respectively. As mentioned previously, the critical section for flexure appeared to be about 0.5 h from the central stub. Yielding of the transverse hoops due to shear also occurred in the vicinity of this critical section at a high displacement ductility factor. Up to $\mu_n = 8$, yielding of transverse hoops due to shear did not occur at the top plastic hinge region, where the damage mostly occurred. This indicated that the concrete mechanisms did make a contribution in resisting shear, although according to the concrete design code NZS 3101:1982⁽²⁾,

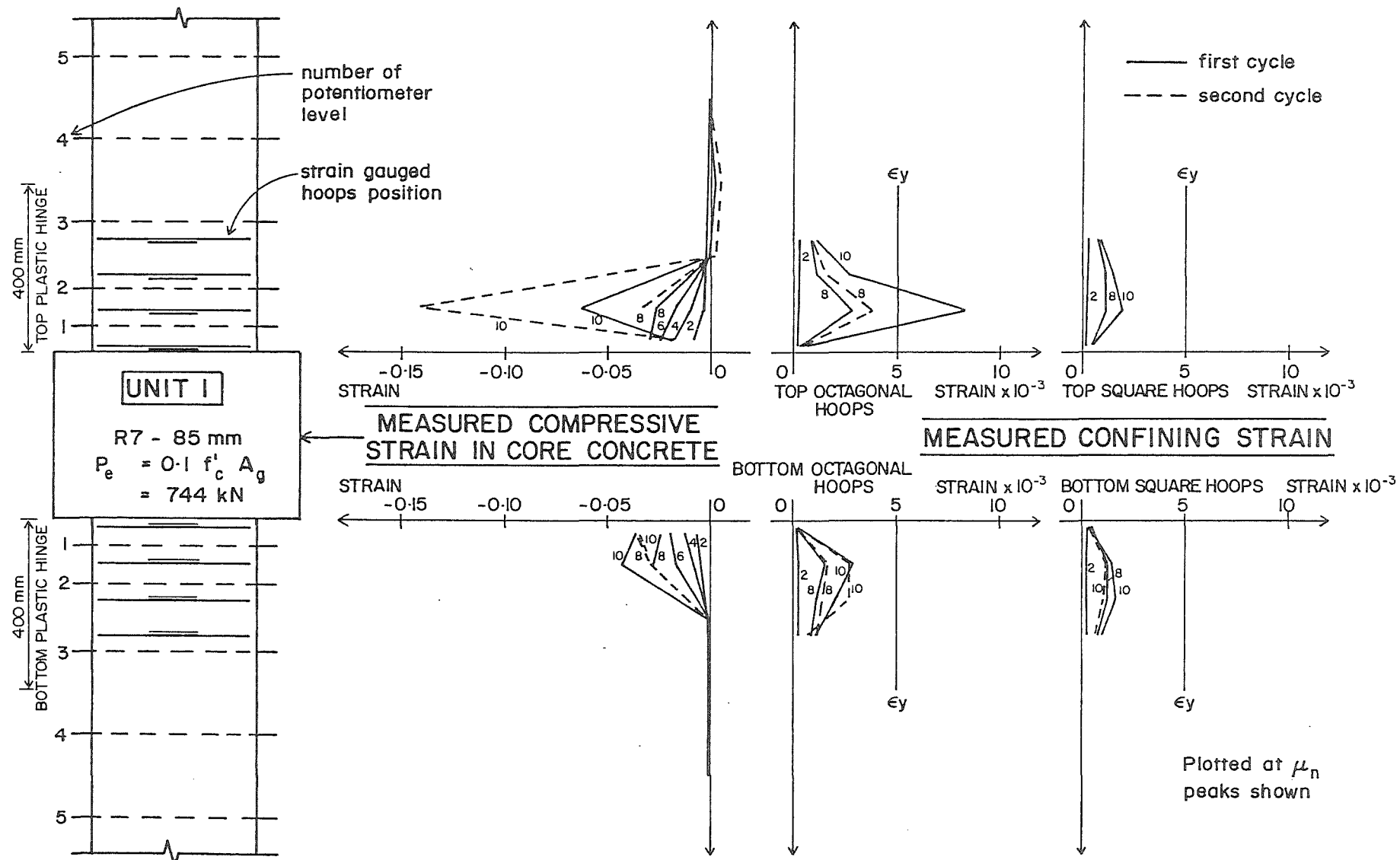


Fig. 7.18 : MEASURED COMPRESSIVE STRAINS IN THE CORE CONCRETE AND MEASURED STRAINS IN THE HOOPS DUE TO CONFINEMENT AT THE POSITIVE LOADING PEAKS FOR COLUMN UNIT 1

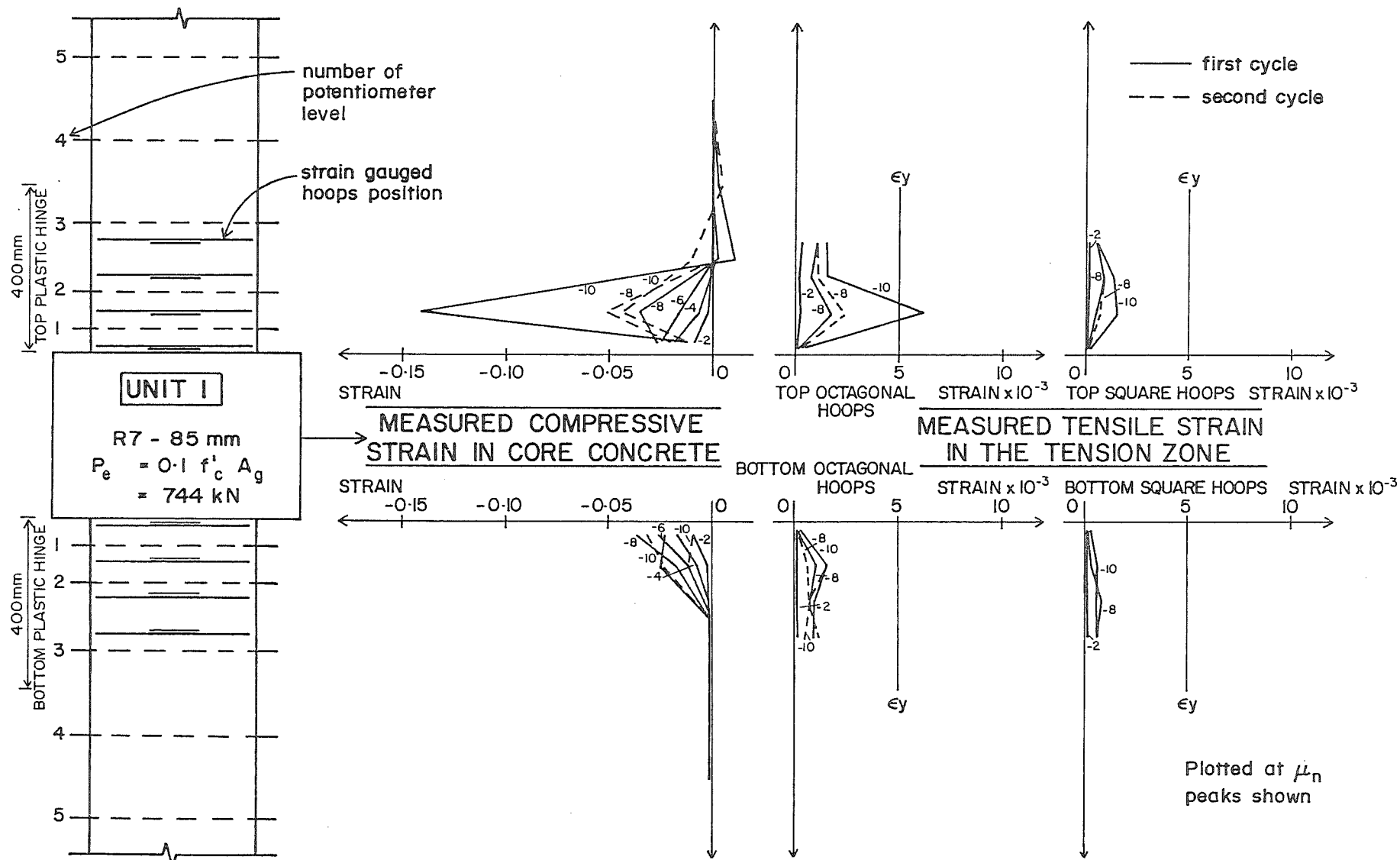


Fig. 7.19 : MEASURED COMPRESSIVE STRAINS IN THE CORE CONCRETE AND MEASURED TENSILE STRAINS IN THE HOOPS IN THE TENSION ZONE AT THE NEGATIVE LOADING PEAKS FOR COLUMN UNIT 1

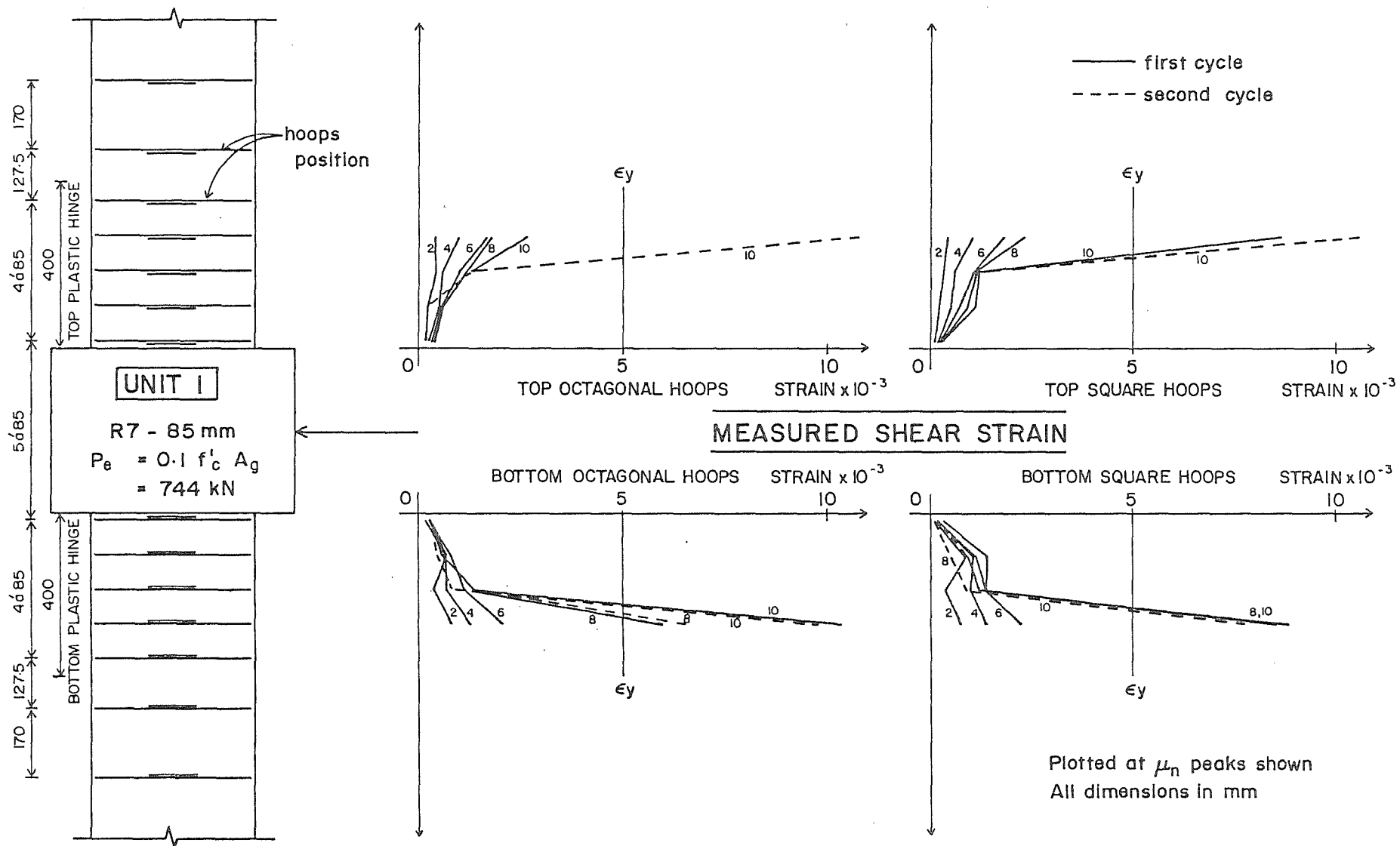


Fig. 7.20 : MEASURED STRAINS IN THE HOOPS DUE TO SHEAR AT THE POSITIVE LOADING PEAKS FOR COLUMN UNIT 1

the shear strength provided by the concrete, V_c , is taken as zero in a column with a low level of axial load. Moreover, as noted previously, at the end of the test of this unit there was fracture of some longitudinal bars due to flexural yielding. There were no indications of shear failure during the test.

7.4 THE PERFORMANCE OF COLUMN UNIT 2

Unit 2 properties:

Axial load levels $P_e = 0.3 f'_c A_g$

Concrete compressive strength $f'_c = 44$ MPa

Transverse hoops in the potential plastic hinge regions = R8 - 78 mm

Yield strength of the transverse reinforcing steel $f_{yh} = 360$ MPa

Total effective area of the transverse hoops A_{sh}
 = 45.8% of the current code value, Eq. 4.4, or
 68.8% of the proposed modified code value, Eq. 4.9.

Lateral load at the ideal strength $H_i = 508$ kN.

(i) General Observations

The first cycle was in the elastic range, up to ± 75 percent of the ideal column strength. Flexural cracks first appeared at the top and bottom sides of the central stub when the lateral load was about 60 percent of the theoretical ultimate load. The extent of cracking at the completion of the elastic cycle is shown in Fig. 7.22. Significant cracks were observed in the first cycle of $\mu_n = 2$. During the second cycle, the existing cracks were not significantly different from those at the first cycle. The crack pattern after two cycles of $\mu_n = 2$ is shown in Fig. 7.23.

The first sign of spalling of the cover concrete was observed in both plastic hinge regions, at the first cycle of $\mu_n = 4$. The spalling of the cover concrete extended over a region 300 mm from the stub and occurred when the concrete compressive strain was about 0.013. Fig. 7.24 shows the unit after the completion of $\mu_n = 4$.

The spalling of the cover concrete increased significantly, particularly at the bottom plastic hinge, during the first cycle of $\mu_n = 6$. The corner longitudinal bars and the transverse hoops then became visible. The existing cracks widened and some new cracks appeared at the second cycle of $\mu_n = 6$. At zero lateral load, the axial shortening of the column was measured to be 2.4 mm. Fig. 7.25 shows the unit at the second cycle of $\mu_n = -6$.

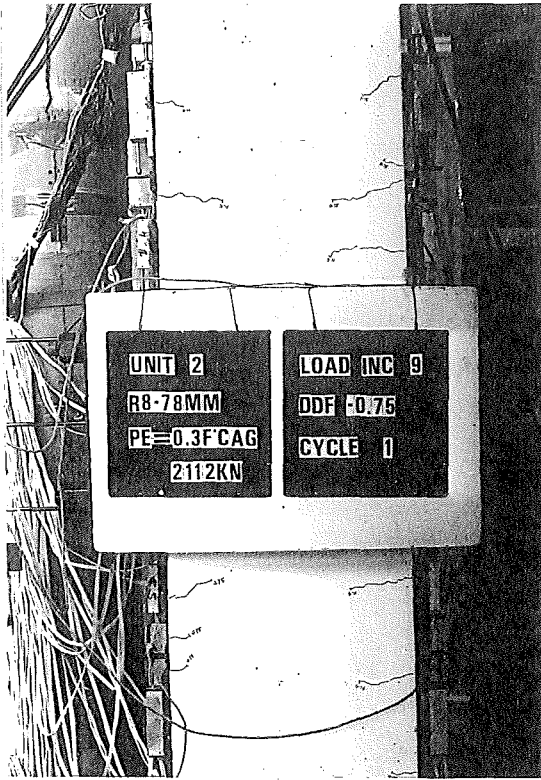


Fig. 7.22 : END OF ELASTIC CYCLE OF
UNIT 2



Fig. 7.23 : UNIT 2 AT THE SECOND CYCLE
OF $\mu_n = -2$



Fig. 7.24 : UNIT 2 AFTER TWO CYCLES
OF $\mu_n = 4$

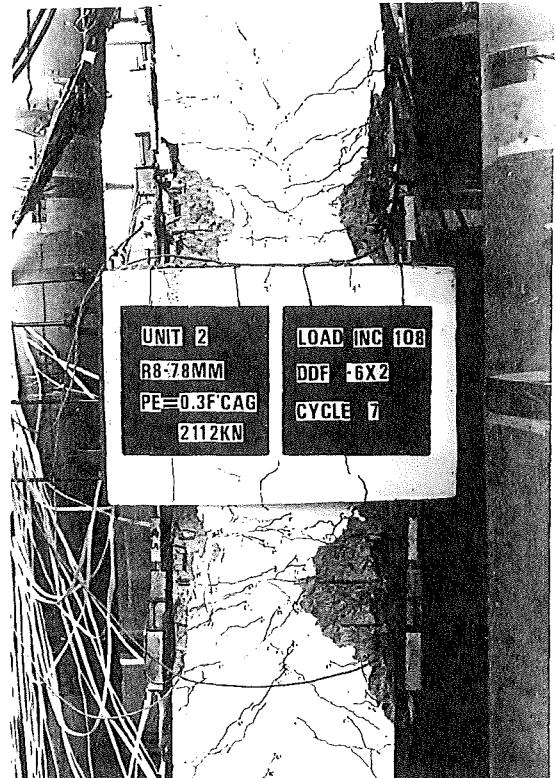


Fig. 7.25 : LONGITUDINAL BARS AND
TRANSVERSE HOOPS BECAME
VISIBLE AT $\mu_n = -6$

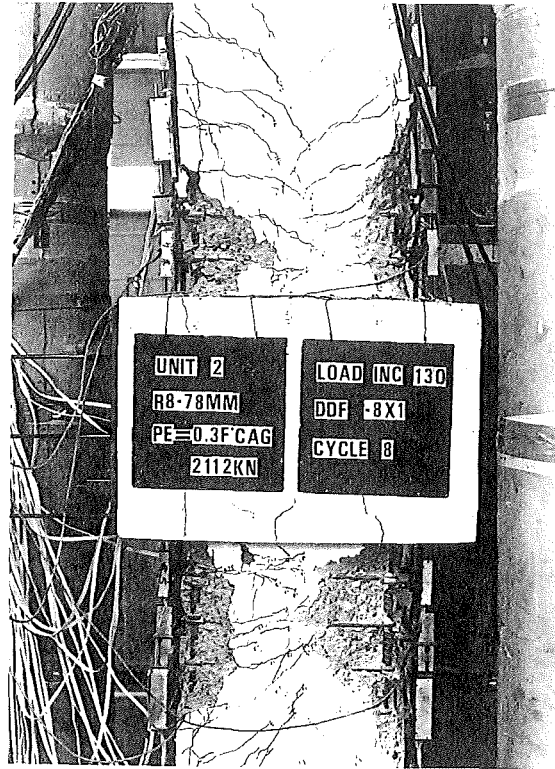


Fig. 7.26 : UNIT 2 AT THE FIRST CYCLE OF $\mu_n = -8$



Fig. 7.27 : CLOSE UP VIEW OF THE BOTTOM HINGE AT $\mu_n = 8$ (SECOND CYCLE)

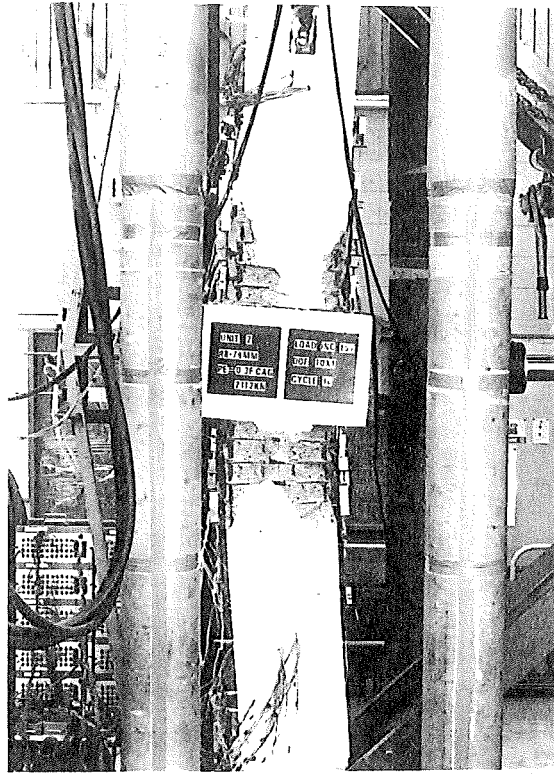


Fig. 7.28 : UNIT 2 AT THE FIRST CYCLE OF $\mu_n = 10$



Fig. 7.29 : CLOSE UP VIEW OF THE BOTTOM HINGE AT $\mu_n = 10$

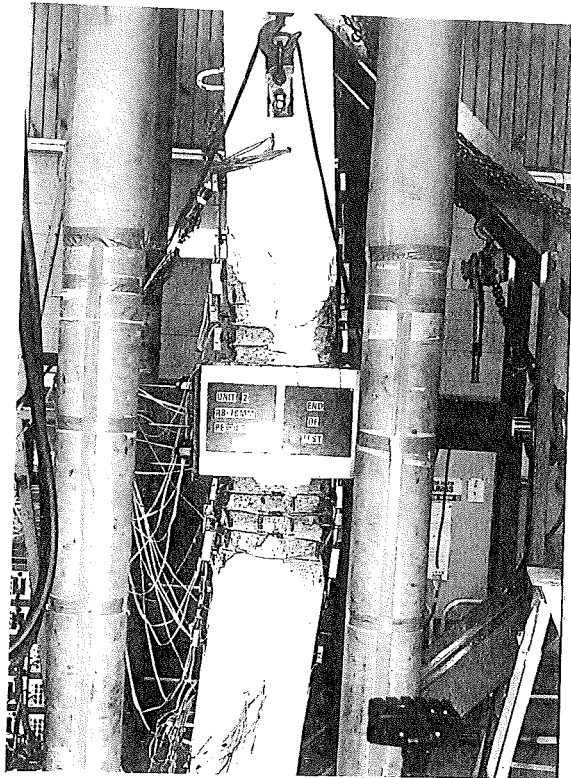


Fig. 7.30 : END OF TESTING OF UNIT 2

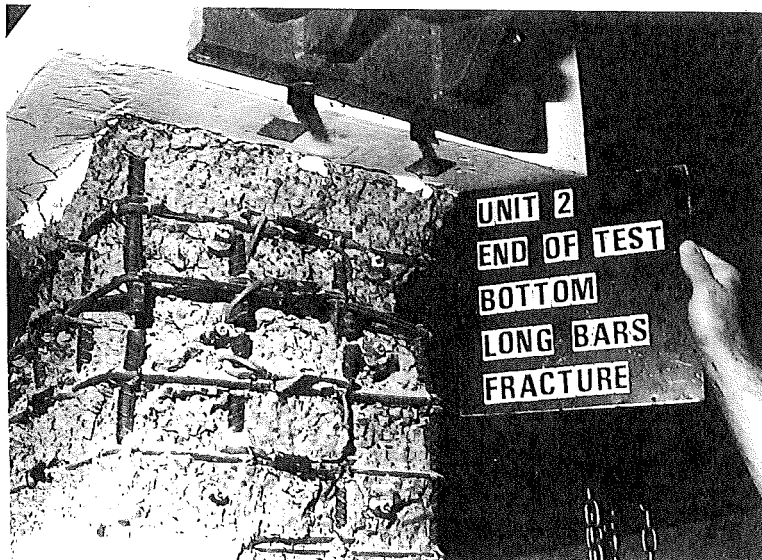


Fig. 7.31 : LONGITUDINAL BARS FRACTURED AT THE END OF THE TESTING

At the first cycle of $\mu_n = 8$, the cover concrete spalled severely and buckling of the longitudinal bars commenced beneath the stub, resulting in more concentrated rotation at the bottom plastic hinge as shown in Fig. 7.26. However, the load carrying capacity of the column was still 6 percent in excess of the theoretical ideal ultimate capacity (see Fig. 7.32). Buckling of the longitudinal bars was more visible at the second cycle of $\mu_n = 8$, as shown in Fig. 7.27, and resulted in some degradation of the lateral load capacity. At $\mu_n = -8$, the damage was visibly more concentrated at the top plastic hinge at the opposite side of the column to that in the bottom plastic hinge. This feature is also illustrated in the lateral load-curvature graphs where for the positive load cycle, the plastic rotation was more concentrated at the bottom plastic hinge, while for the negative load cycle the plastic rotation was more concentrated at the top plastic hinge (see Figs. 7.33 and 7.34).

The overall view of the unit at the displacement peak of the first cycle of $\mu_n = 10$ is shown in Fig. 7.28 and a close up view of the bottom plastic hinge is illustrated in Fig. 7.29.

At the load cycle to $\mu_n = 10$ the lateral load capacity dropped significantly, but there were no signs of a sudden failure. This indicated that the unit behaved in a ductile manner, although the transverse hoops provided in the unit were only 46 percent of the code⁽²⁾ required quantity.

The load excursion to $\mu_n = -10$ caused the corner longitudinal bars to fracture, followed by the fracture of all longitudinal bars at the extreme tensile fibre. The test was terminated when the lateral load capacity was only 25 percent of the theoretical ultimate load. Fig. 7.30 shows the unit at the end of the testing and a close up view of the bottom plastic hinge is shown in Fig. 7.31. The axial shortening of the column at the end of the testing was 11.1 mm.

(ii) Hysteretic Performance

Figs. 7.32, 7.33 and 7.34 show the experimental lateral load-displacement and the lateral load-column curvature graphs. It can be seen that very good energy dissipating characteristics were achieved. This desired ductile response is clearly indicated in the well rounded load-displacement hysteresis loops. A little strength degradation occurred at the second loading cycle to the similar displacement ductility factor. The strength degraded more significantly when $\mu_n = \pm 8$ was applied.

The maximum lateral load achieved during the test was $H_{\max} = 562 \text{ kN}$ and it occurred at the displacement peak of the first cycle of $\mu_n = 2$.

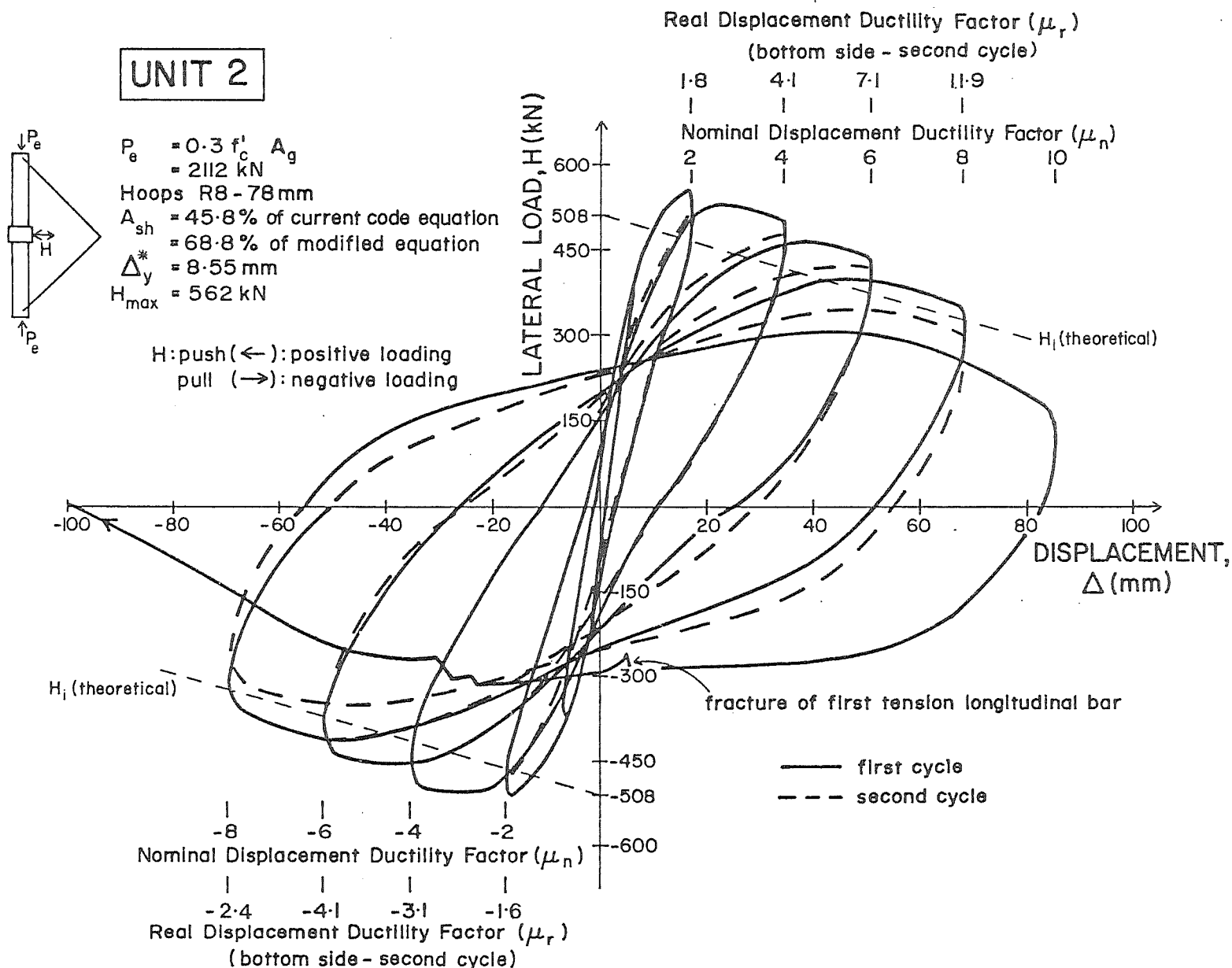


Fig. 7.32: EXPERIMENTAL LATERAL LOAD-DISPLACEMENT HYSTERESIS LOOPS FOR COLUMN UNIT 2

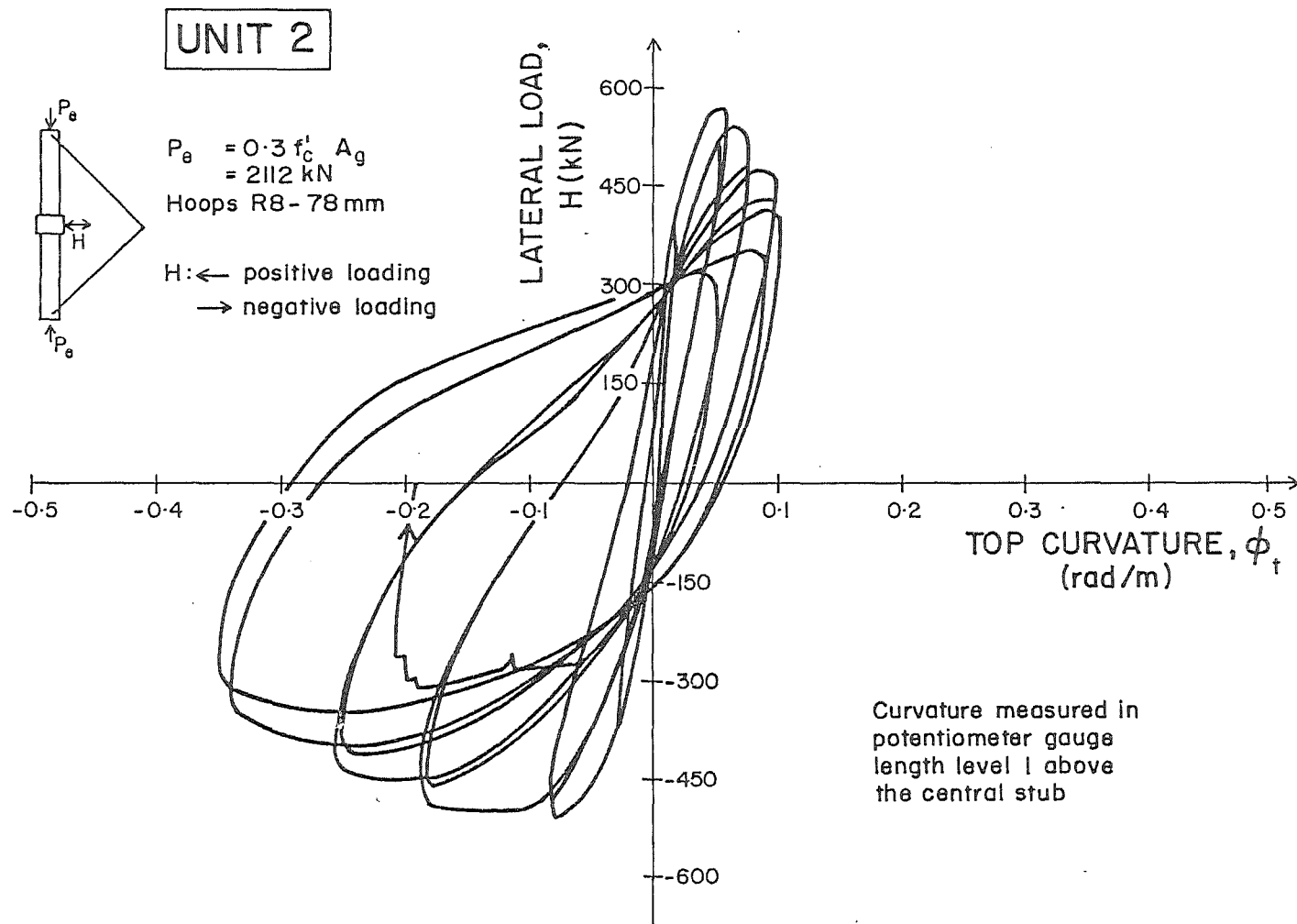


Fig. 7.33 : EXPERIMENTAL LATERAL LOAD-TOP COLUMN CURVATURE HYSTERESIS LOOPS FOR COLUMN UNIT 2

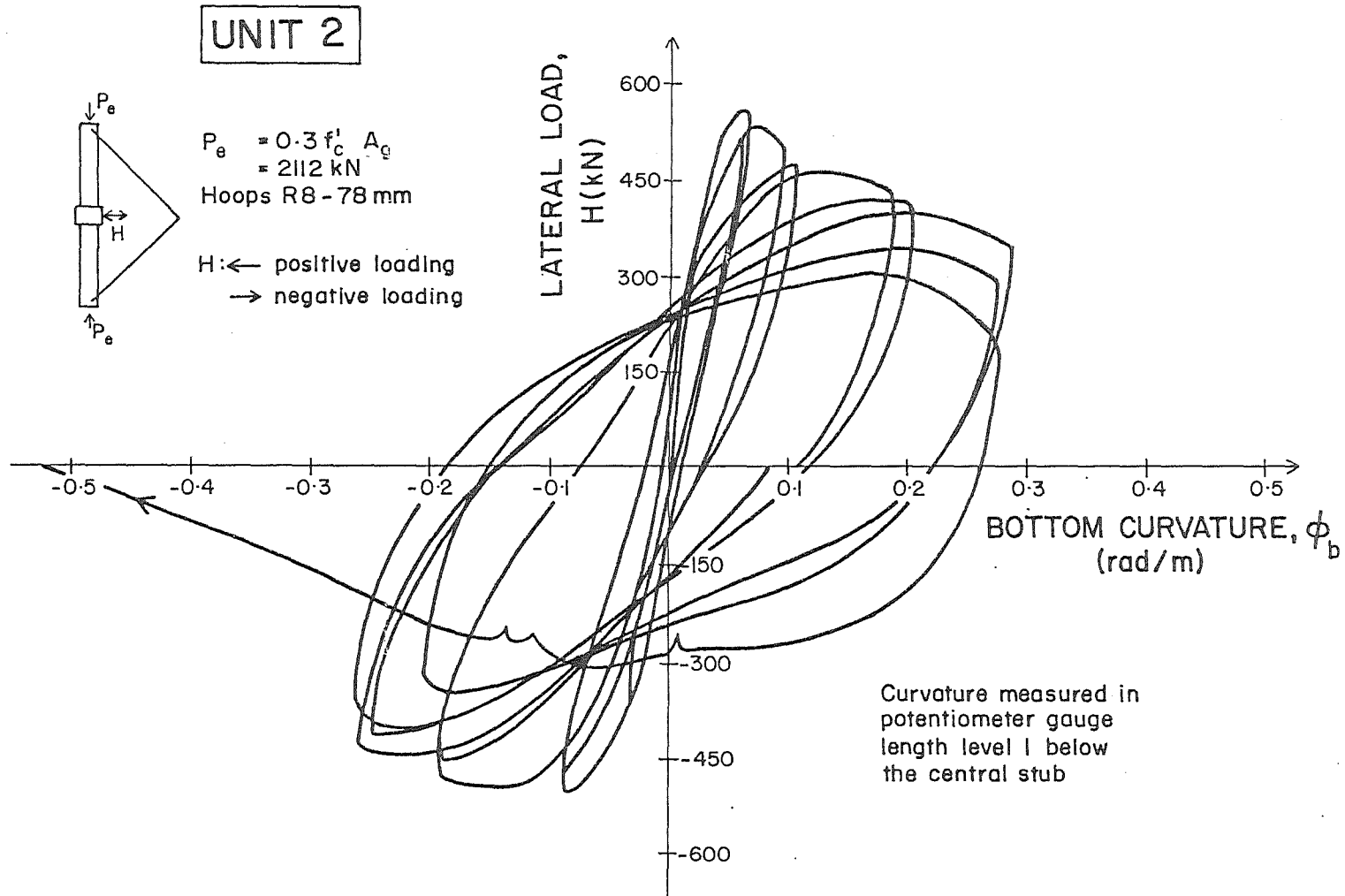


Fig. 7.34 : EXPERIMENTAL LATERAL LOAD-BOTTOM COLUMN CURVATURE HYSTERESIS LOOPS FOR COLUMN UNIT 2

The measured H_{\max} was 20 percent in excess of the lateral load at the ideal strength H_i , giving a flexural overstrength factor M_{\max}/M_i of 1.20.

The lateral load capacity of the second cycle of the nominal displacement ductility $\mu_n = 8$, or the real displacement ductility $\mu_r = 11.9$, was still 94% of the ideal column strength. This indicated that the column could achieve $\mu_n = 8$ without significant strength degradation.

The maximum lateral displacement $\Delta + \theta \ell'$, where θ is the stub rotation and $\ell' = 1.8$ m, was calculated for the bottom half of the column as 118 mm. Hence the maximum drift measured, $(\Delta + \theta \ell')/\ell'$, was 6.6 percent.

As mentioned previously, the inelastic deformations concentrated in the top plastic hinge during negative loading and in the bottom plastic hinge during positive loading. This is clearly shown in Figs. 7.33 and 7.34, particularly $\mu_n = 6$ and higher.

(iii) Curvature Distribution, Curvature Ductility and Equivalent Plastic Hinge Length

The measured curvature profiles for Unit 2 are presented in Fig. 7.35, and are plotted at the successive positive and negative displacement ductility peaks of $\mu_n = 2, 4, 6$ and 8 , and at the positive displacement peak of the first cycle of $\mu_n = 10$.

The different plastic hinge sides in which most of the damage occurred, as mentioned earlier, is also indicated in the measured curvature profiles.

The calculated experimental yield curvature ϕ_y was 11.10×10^{-3} rad/m. From the potentiometer readings at the second cycle to $\mu_n = 8$, the maximum curvature at the first potentiometer level ϕ_{u1} was calculated to be 0.1981 rad/m and the maximum curvature at the second potentiometer level ϕ_{u2} was 0.3124 rad/m, giving available curvature ductility factors of 17.9 and 28.1 respectively.

It should be noted that these maximum curvatures were taken as the curvatures at the second cycle of $\mu_n = -8$ when the measured flexural capacity had reduced to not less than 80% of the theoretical ideal capacity.

The equivalent plastic hinge length ℓ_p calculated from Eq. 7.7 are $0.41h$ or 164 mm and $0.24h$ or 96 mm for ϕ_u/ϕ_y of 17.9 and 28.1, respectively, resulting in an average plastic hinge length $(\ell_p/h)_{av}$ of 0.33h or 132 mm.

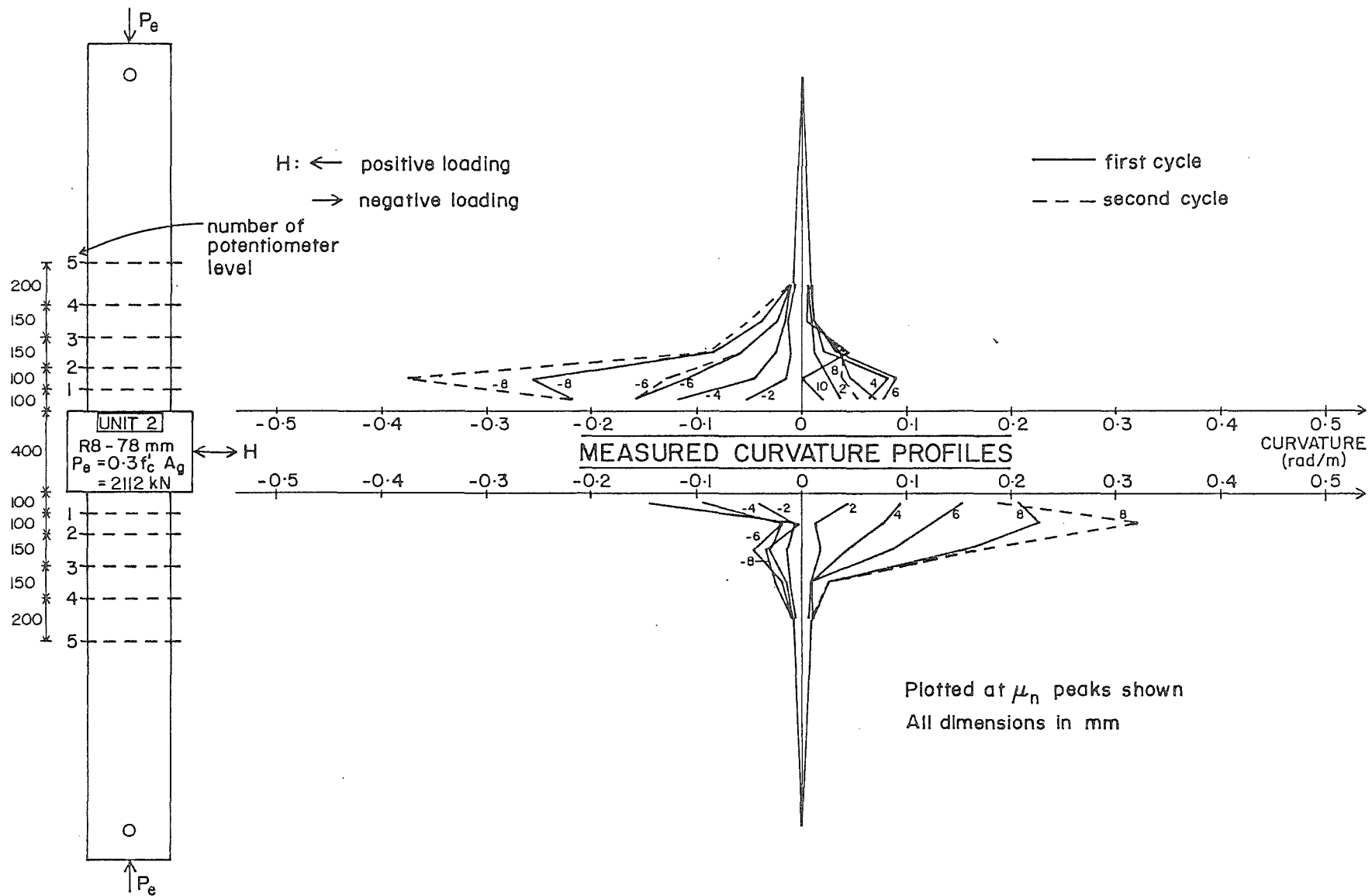


Fig. 7.35 : MEASURED CURVATURE PROFILES FOR COLUMN UNIT 2

(iv) Measured Strain Profiles

Figs. 7.36 and 7.37 illustrate the profiles of the longitudinal concrete compressive strains at the extreme fibre of the core concrete and the transverse strains in the hoops measuring both the confinement to the concrete and the tensile stress in the tension zone.

Again, the different sides of the concentration of the plastic rotation, in the top and the bottom plastic hinges, as mentioned previously resulted in the measured unsymmetrical compressive strain profiles shown in Figs. 7.36 and 7.37. Higher concrete compressive strains occurred at the top plastic hinge when the loading was in the negative direction and at the bottom plastic hinge when positive loading was applied. The maximum concrete compressive strain, calculated from the potentiometer readings at the second level, was found to be 0.110 during positive loading in the second cycle of $\mu_n = 8$ at the bottom hinge.

The profiles of the transverse strains in the hoops indicated that yielding of the hoops was not measured at the top plastic hinge. The reason was that during positive loading the plastic rotation was concentrated at the bottom plastic hinge. During negative loading the plastic rotation was concentrated at the top plastic hinge but the compression zone of the concrete was on the side of the column opposite to which the strain gauges were fixed on the hoops.

Yielding of the transverse hoops at the bottom plastic hinge did occur, commencing at displacement ductility factors of higher than 6. The hoops after yielding still provided very good confinement and prevented buckling of the longitudinal bars.

From the figures, it can also be seen that due to the heavily reinforced central stub, the critical section for flexure appeared at about 0.5 h from the section of maximum moment.

The concrete compressive strains and the transverse strains in the hoops are plotted at the successive positive and negative displacement ductility peaks of $\mu_n = 2, 4, 6$ and 8 and the positive peak of $\mu_n = 10$. For the square hoops at the top plastic hinge it is plotted at the peaks of $\mu_n = \pm 2, \pm 6, \pm 8$ and 10.

The measured hoop strain profiles due to shear at the successive positive and negative displacement ductility peaks are shown in Figs. 7.38 and 7.39 respectively. Yielding of the transverse hoops due to shear did not occur. It is evident that the concrete shear resisting mechanisms provided very good shear resistance.

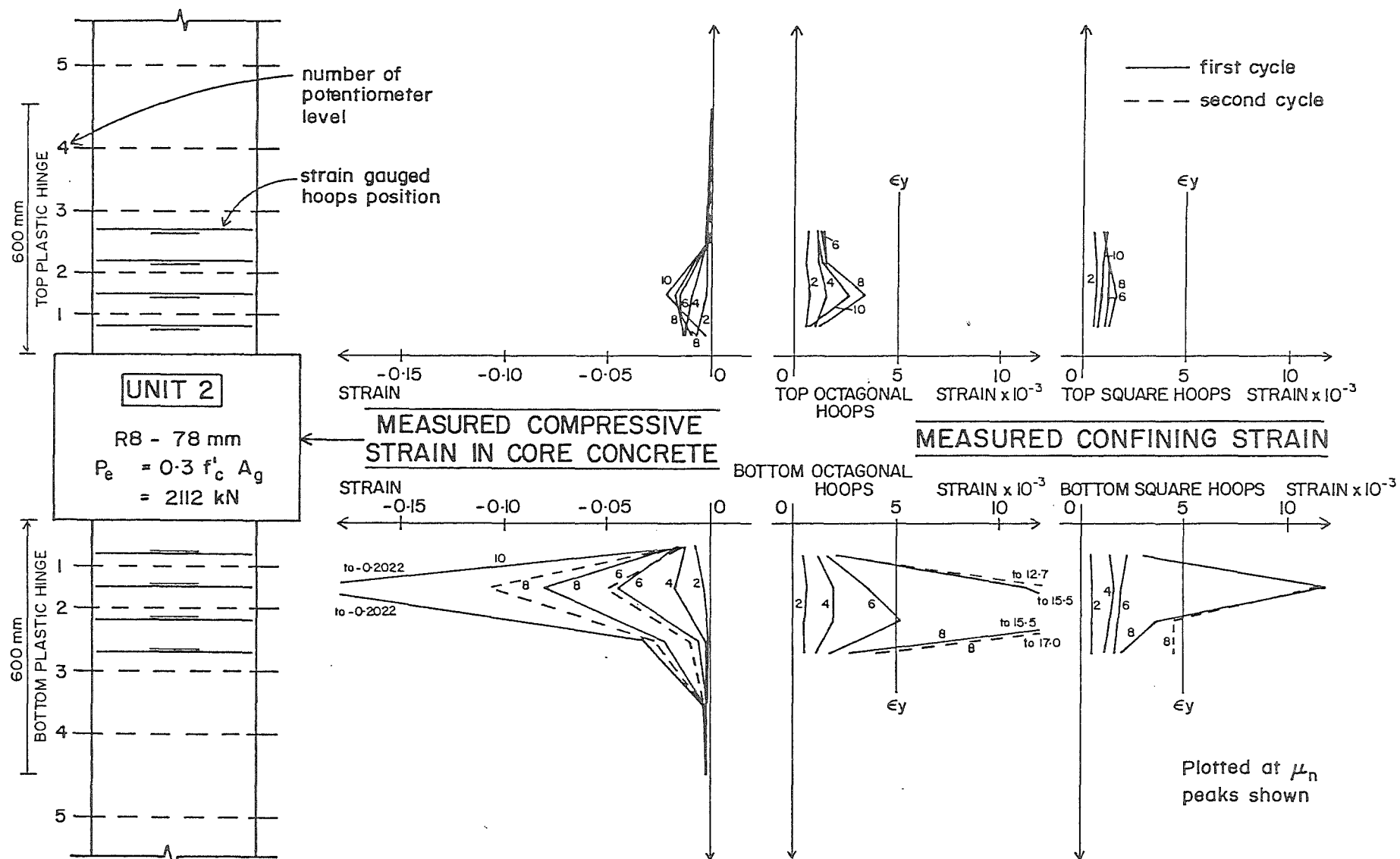


Fig. 7.36 : MEASURED COMPRESSIVE STRAINS IN THE CORE CONCRETE AND MEASURED STRAINS IN THE HOOPS
 DUE TO CONFINEMENT AT THE POSITIVE LOADING PEAKS FOR COLUMN UNIT 2

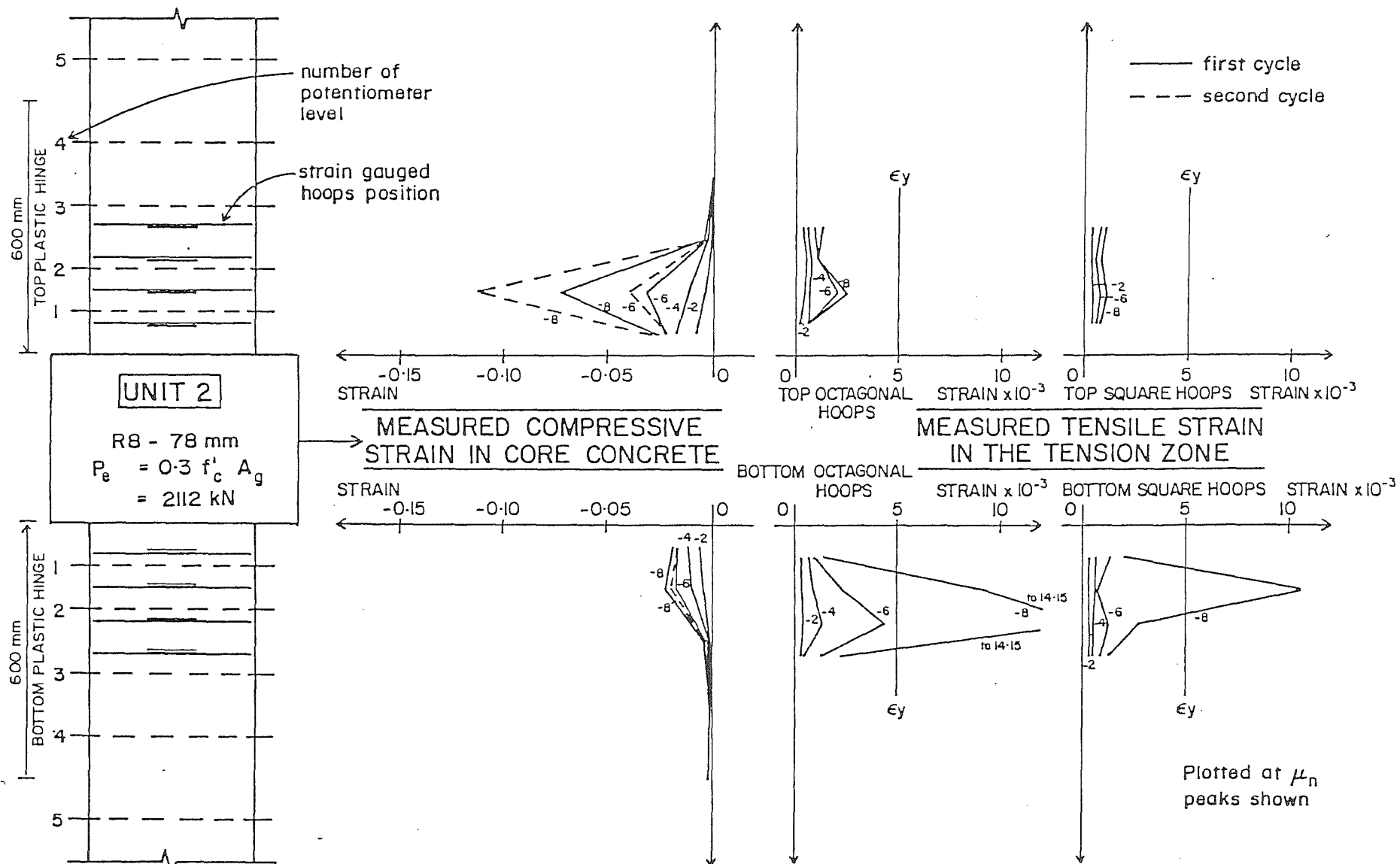


Fig. 7.37 : MEASURED COMPRESSIVE STRAINS IN THE CORE CONCRETE AND MEASURED TENSILE STRAINS IN THE HOOPS IN THE TENSION ZONE AT NEGATIVE LOADING PEAKS FOR COLUMN UNIT 2

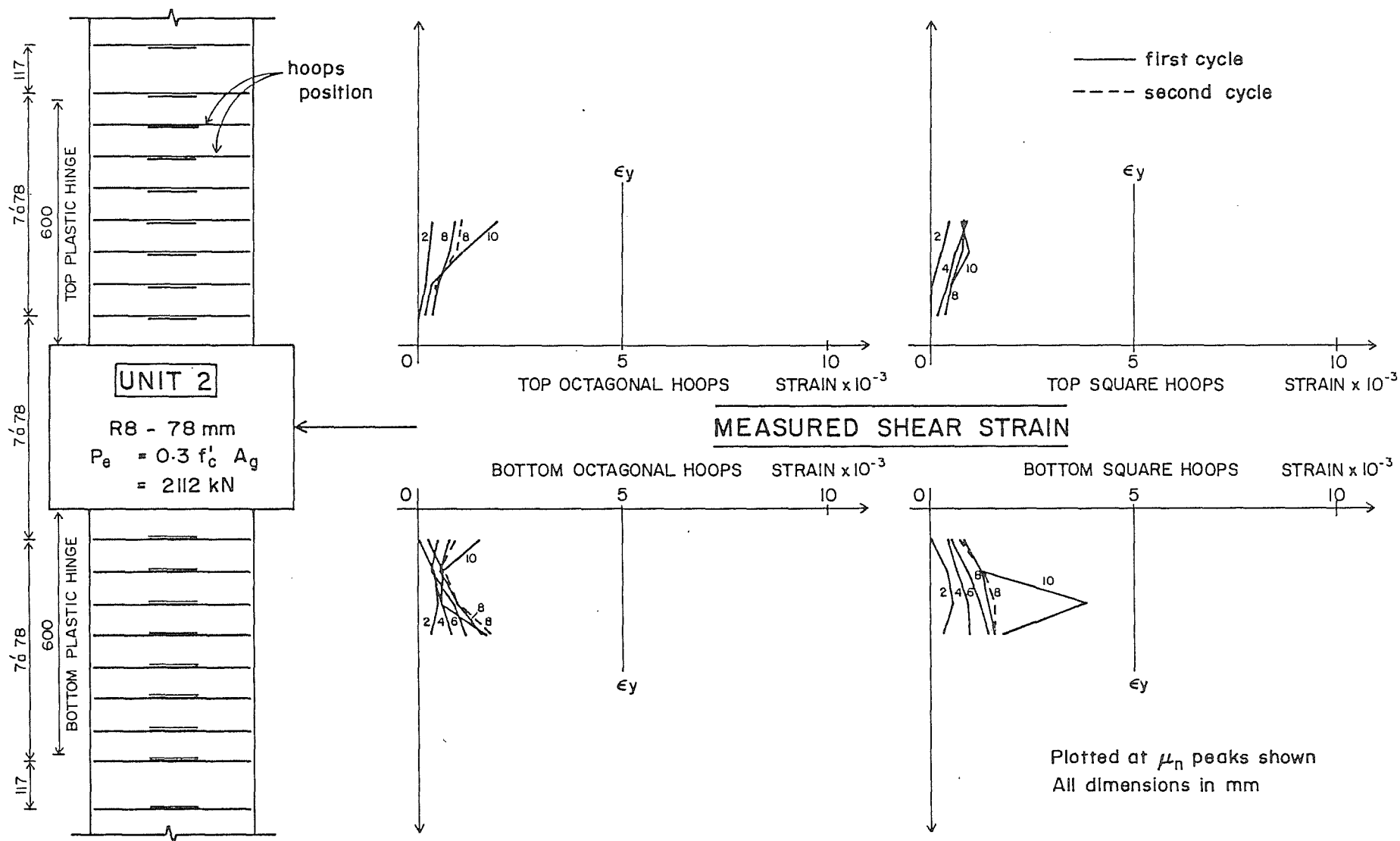


Fig. 7.38 : MEASURED STRAINS IN THE HOOPS DUE TO SHEAR AT THE POSITIVE LOADING PEAKS FOR COLUMN UNIT 2

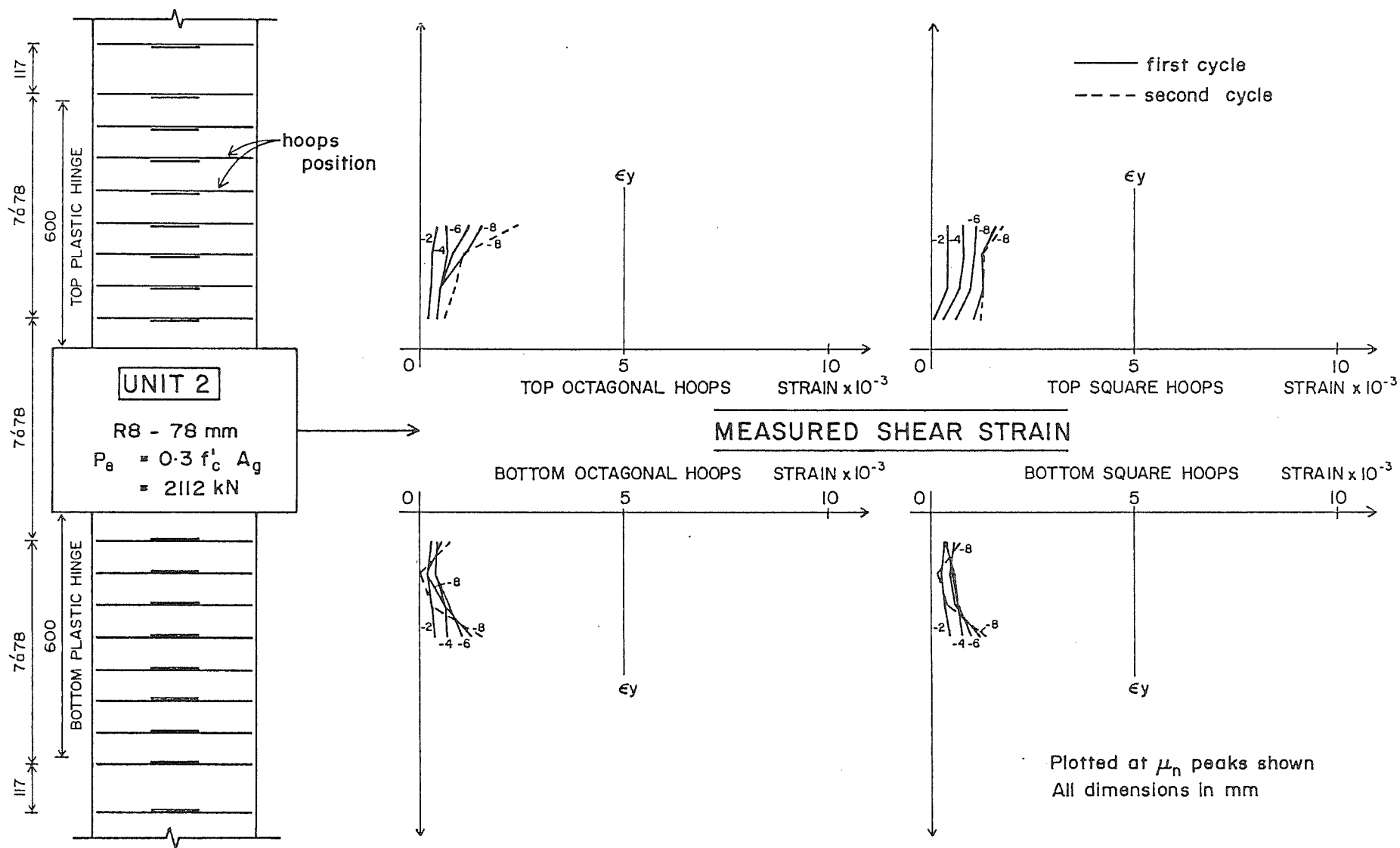


Fig. 7.39 : MEASURED STRAINS IN THE HOOPS DUE TO SHEAR AT THE NEGATIVE LOADING PEAKS FOR COLUMN UNIT 2

7.5 THE PERFORMANCE OF COLUMN UNIT 3

Unit 3 properties:

Axial load levels $P_e = 0.3 f'_c A_g$

Concrete compressive strength $f'_c = 44 \text{ MPa}$

Transverse hoops in the potential plastic hinge regions = R7 - 91 mm

Yield strength of the transverse reinforcing steel $f_y = 364 \text{ MPa}$

Total effective area of the transverse hoops A_{sh}
 = 30.4% of the current code value, Eq. 4.4 or
 45.6% of the proposed modified code value, Eq. 4.9

Lateral load at the ideal strength $H_i = 508 \text{ kN}$

(i) General Observations

Flexural cracks were first detected adjacent to the upper and lower faces of the central stub at about 60 percent of the ideal flexural strength of the column. Fig. 7.40 shows the extent of cracking after the completion of the initial elastic cycle which was taken up to ± 75 percent of the ideal strength.

At the first cycle of $\mu_n = 2$, the flexural cracks became more significant and the concrete in the compression zone started to split in the cover concrete. The tensile and splitting cracks were marked by the respective inclined and vertical lines. Cracking in the column after the completion of the load cycle of $\mu_n = 2$ is shown in Fig. 7.41.

The first sign of spalling of the cover concrete was observed over a distance of 75 mm from the top side of the central stub at the first cycle to a displacement ductility of μ_n of 4 when the concrete compressive strain was 0.008. At $\mu_n = -4$, the cover concrete immediately beneath the stub also exhibited signs of spalling.

At the second cycle of $\mu_n = 4$, the spalling of the cover concrete at the top plastic hinge extended over a distance of 300 mm. This significant spalling was followed by exposure of some longitudinal bars and transverse hoops as shown in Fig. 7.42. At this stage, it can be seen that plastic rotation was more concentrated at the top plastic hinge than at the bottom plastic hinge.

The longitudinal bars at the extreme compression fibre started to buckle during the first cycle of $\mu_n = 6$. The top plastic hinge rotation was quite significant at this cycle. Fig. 7.43 shows the unit at the first cycle of $\mu_n = -6$.

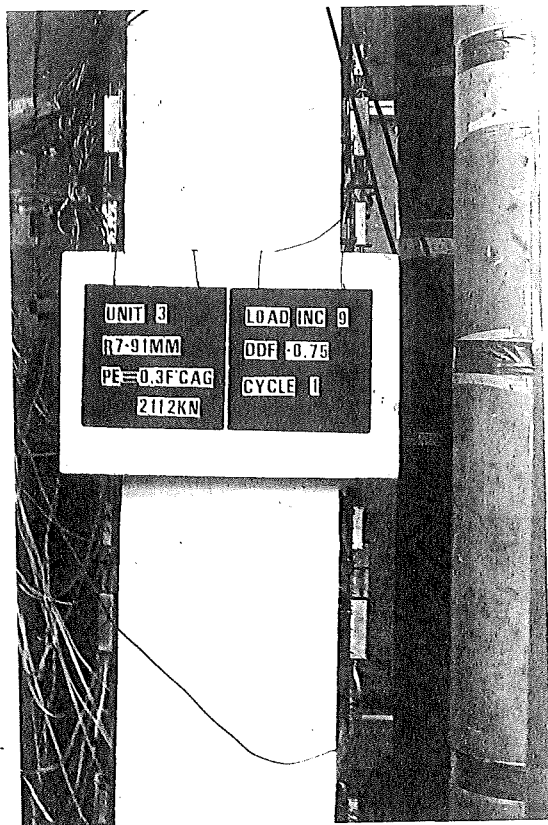


Fig. 7.40: UNIT 3, AFTER COMPLETION
OF THE ELASTIC CYCLE

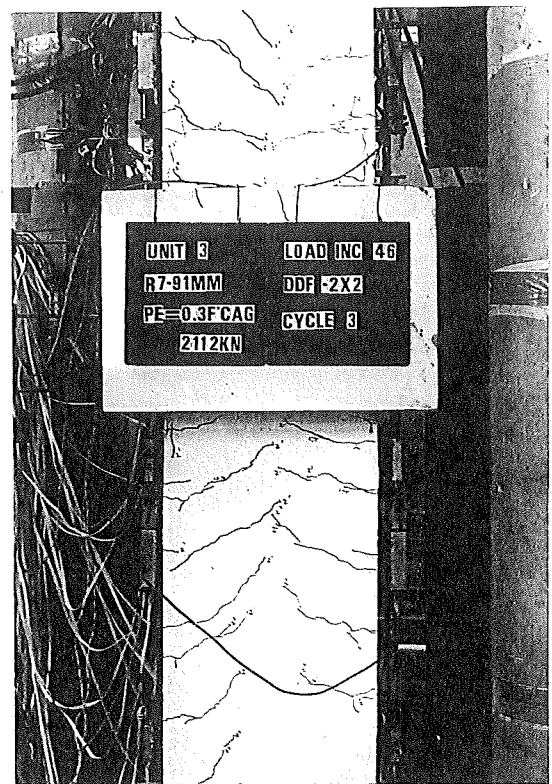


Fig. 7.41 : EXTENT OF CRACKING
AT $\mu_n = -2$



Fig. 7.42 : UNIT 3, AT THE SECOND
CYCLE OF $\mu_n = -4$

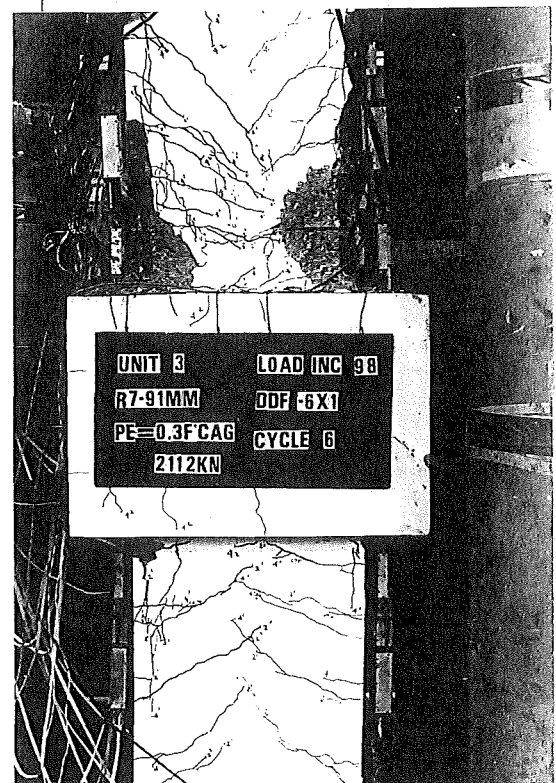


Fig. 7.43 : UNIT 3, AT THE FIRST
CYCLE OF $\mu_n = -6$



Fig. 7.44. : CONCENTRATION OF PLASTIC ROTATION AT THE TOP
HINGE AT $\mu_n = 6$

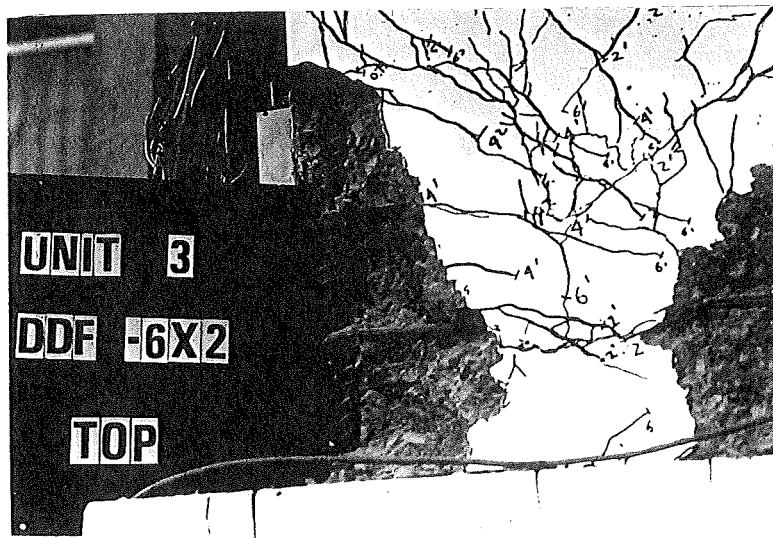


Fig. 7.45 : CLOSE UP VIEW OF THE TOP PLASTIC HINGE AT $\mu_n = -6$
(SECOND CYCLE)

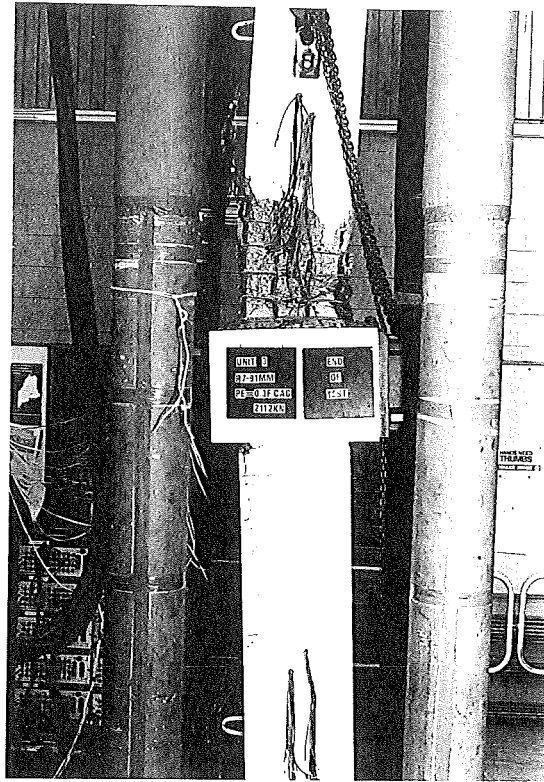


Fig. 7.46 : FRACTURE OF THE OCTAGONAL HOOP TERMINATED
THE TEST OF UNIT 3

Buckling of the longitudinal bars was more significant at the second cycle of $\mu_n = 6$. The concentration of the plastic hinge rotation at the top hinge resulted in severe damage at the top hinge, while the bottom hinge remained in a similar condition to the previous cycles. Fig. 7.44 illustrates the unit at this displacement ductility peak.

Fig. 7.45 shows a close up view of the top plastic hinge at the second cycle of $\mu_n = -6$. It can be seen that the corner longitudinal bar has buckled and that crushing of concrete has penetrated into the core. Strength degradation also occurred, although it was not greatly significant. The lateral load capacity at the peak of this cycle was 97 percent of the theoretical ideal strength (see Fig. 7.47).

In the next loading cycle, degradation of the column strength occurred rapidly. The anchorage bends at the ends of transverse hoops around the longitudinal bars opened up and fracture of some octagonal hoops occurred, resulting in buckling of longitudinal bars. The column collapsed thus terminating the test. The axial shortening of the column at the end of testing was 9.9 mm.

Fig. 7.46 shows the unit at the end of the testing and a close-up view of the hoop fracture.

It can be seen from Fig. 7.46 that by the end of testing severe damage had occurred at the top plastic hinge, but not at the bottom plastic hinge. The reason was that once a plastic hinge had developed, either above or below the stub, inelastic strains concentrated at the plastic hinge which formed first. In this case, the plastic rotation was concentrated at the top hinge.

(ii) Hysteretic Performance

Figs. 7.47 to 7.49 show the experimental lateral load-displacement graph and the lateral load-top column curvature and bottom column curvature graphs, respectively. It can be seen that in the second cycle to the similar displacement ductility factor some degradation of strength occurred. This strength degradation was most significant when $\mu_n = 6$.

The maximum lateral load H_{\max} occurred at the first cycle of $\mu_n = 2$ and it was 560 kN which resulted in a flexural overstrength factor M_{\max}/M_i of 1.18.

Although a significant strength degradation occurred in the second cycle of $\mu_n = \pm 6$, the maximum lateral load reached was still 90 percent of the theoretical ideal strength. However, in the third cycle of $\mu_n = 6$,

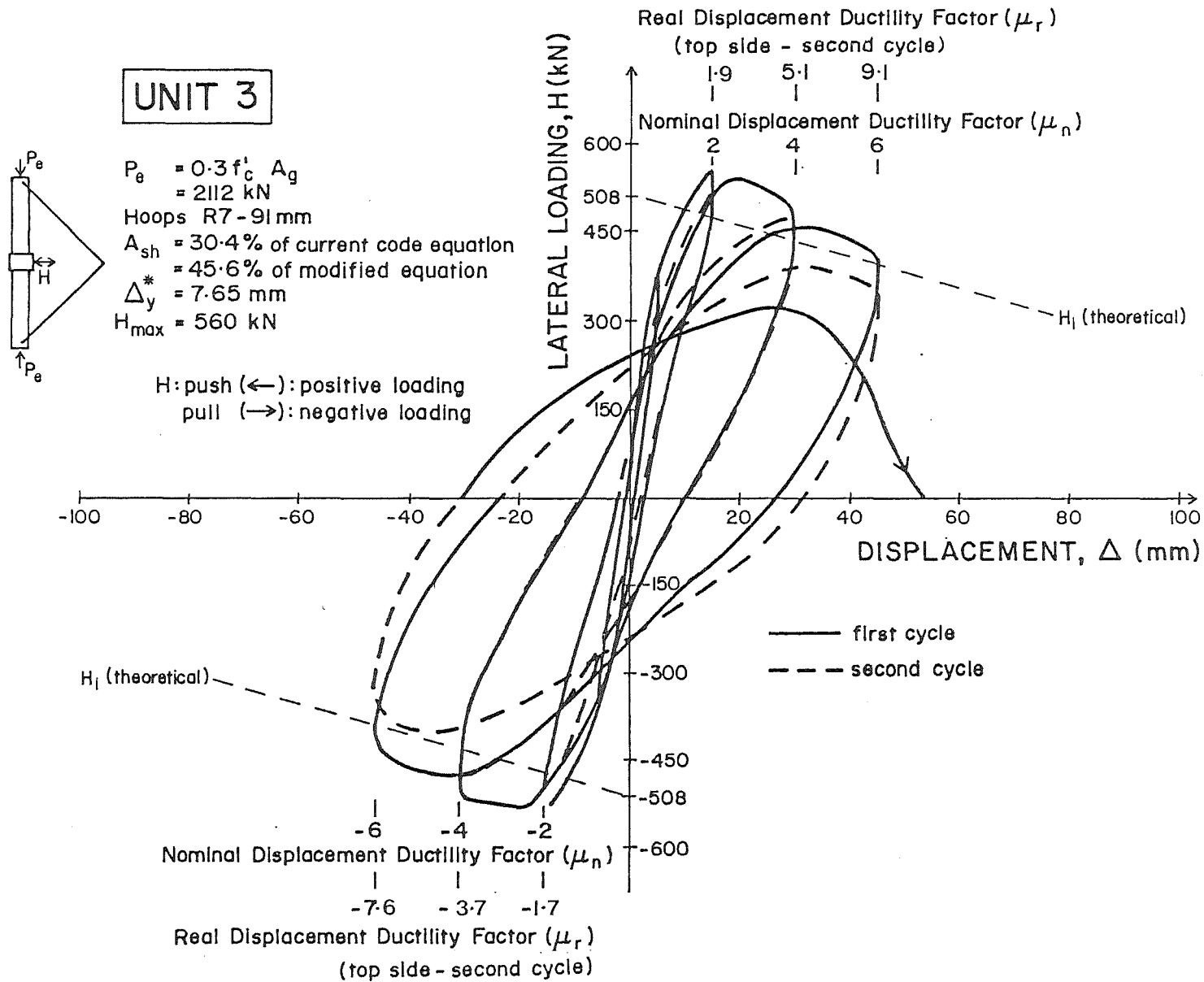


Fig. 7.47 : EXPERIMENTAL LATERAL LOAD-DISPLACEMENT HYSTERESIS LOOPS FOR COLUMN UNIT 3

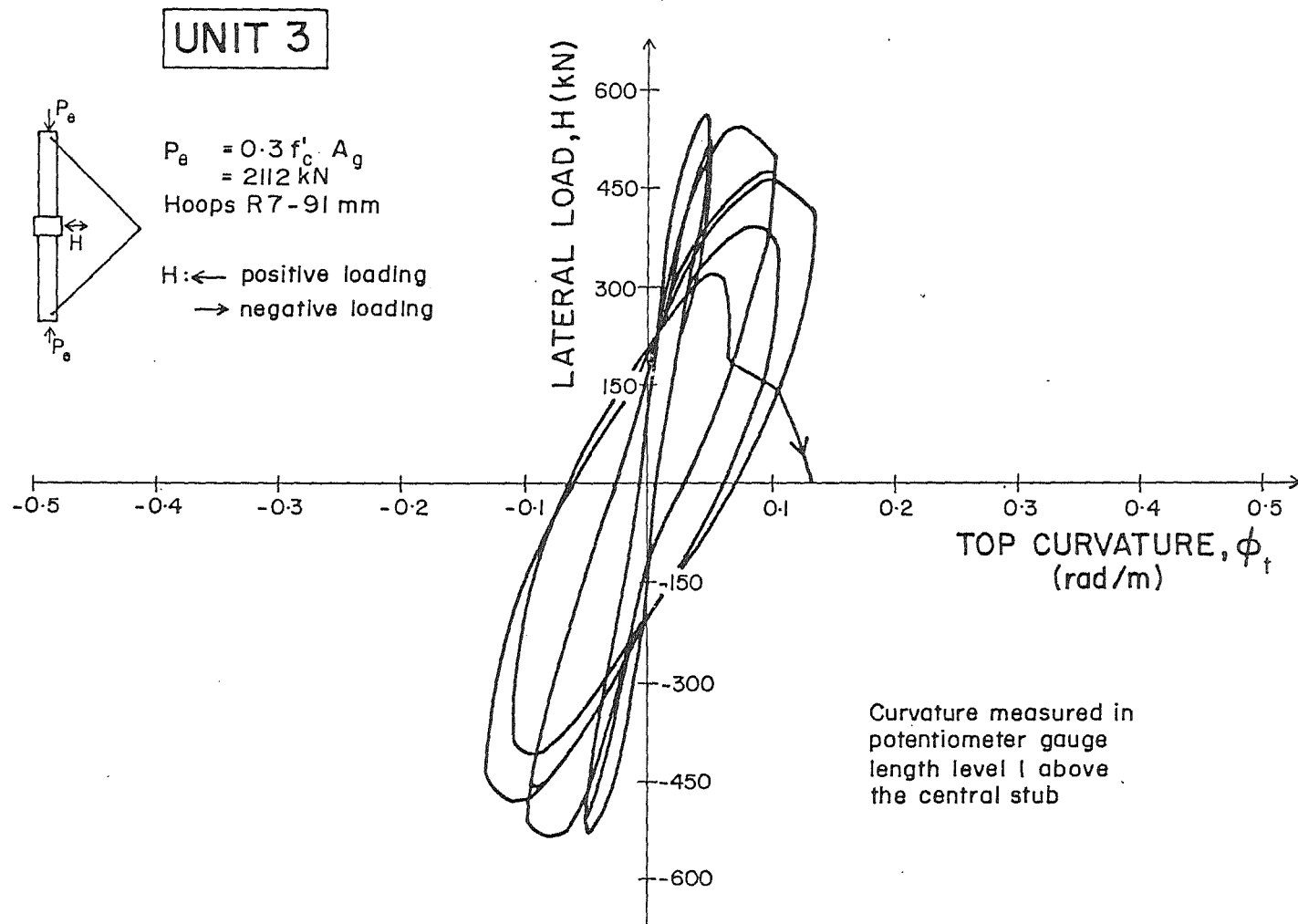


Fig. 7.48 : EXPERIMENTAL LATERAL LOAD-TOP COLUMN CURVATURE HYSTERESIS LOOPS FOR COLUMN UNIT 3

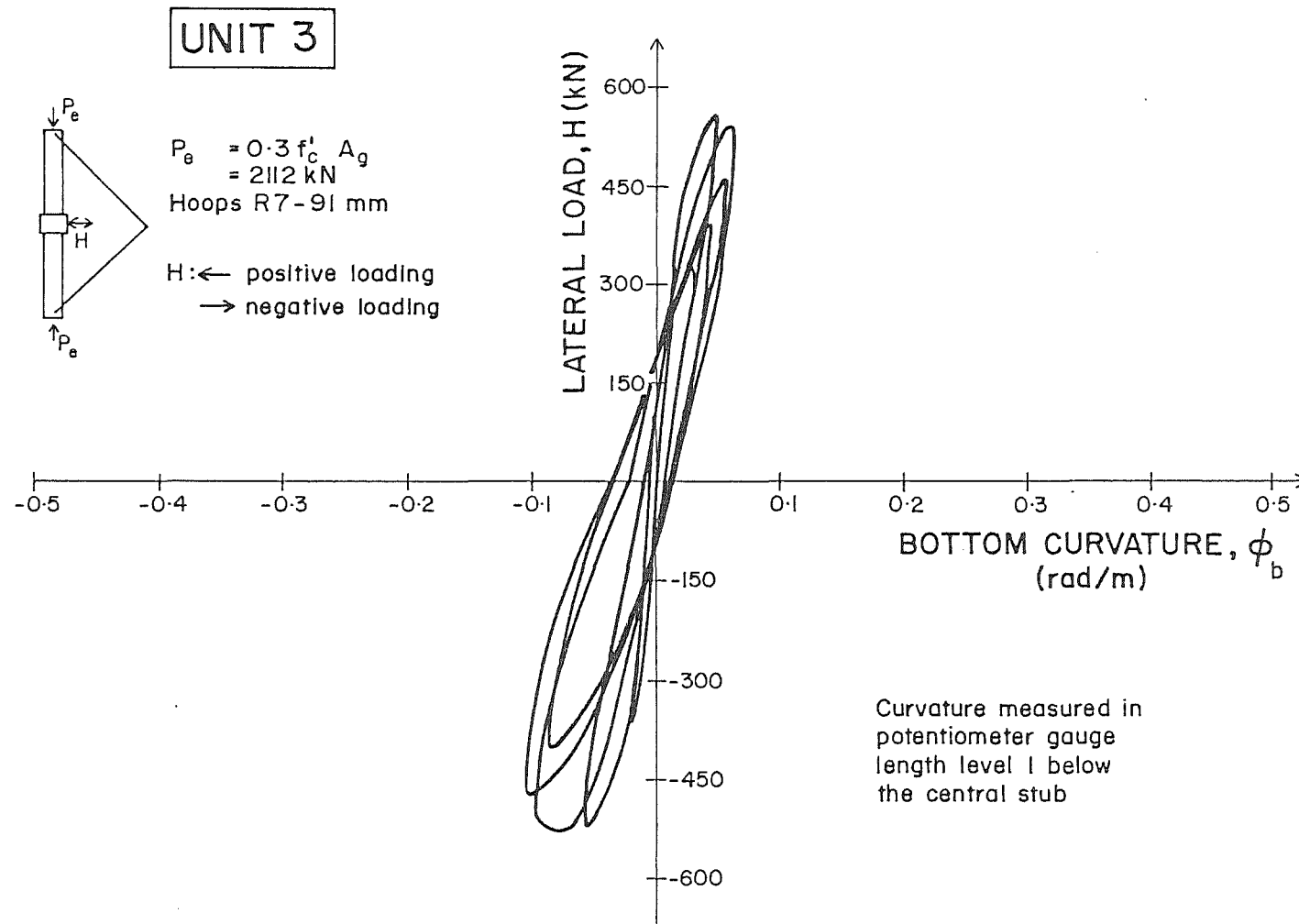


Fig. 7.49 : EXPERIMENTAL LATERAL LOAD-BOTTOM COLUMN CURVATURE HYSTERESIS LOOPS FOR COLUMN UNIT 3

the maximum lateral load reached was only 34 percent of the theoretical ideal strength and then this load had dropped rapidly to zero by the end of the load cycle.

Fig. 7.47 shows that the maximum displacement ductility factor which could be achieved by the column was $\mu_n = 6$, or $\mu_r = 9.1$ if the rotation θ of the central stub was taken into account. The maximum lateral displacement $\Delta + \theta \ell'$ was 68 mm, giving a maximum measured drift of 3.8 percent.

The plastic rotation concentrated above the central stub rather than below, as can be surmised from the load-curvature hysteresis loops shown in Figs. 7.48 and 7.49.

(iii) Curvature Distribution, Curvature Ductility and Equivalent Plastic Hinge Length

Fig. 7.50 illustrates the measured curvature profiles of Unit 3 at the positive and negative displacement ductility peaks of $\mu_n = 2$ and 6.

Again, the concentration of inelastic deformations at the top plastic hinge is evident. The maximum experimental curvature was taken as the curvature at the top plastic hinge at the second cycle of $\mu_n = 6$ when the measured flexural strength had reduced to not less than 80 percent of the theoretical ideal strength. The maximum experimental curvatures at the first and second potentiometer levels were 0.1280 and 0.1428 rad/m, respectively. The measured yield curvature was 8.0×10^{-3} rad/m. Thus the available curvature ductility factors ϕ_u/ϕ_y of 16.0 and 17.8 at the first and second potentiometer levels, respectively.

The equivalent plastic hinge length ℓ_p was 0.44h (176 mm) if the curvature at the first potentiometer level is taken as the maximum curvature and was 0.38h (152 mm) if the curvature at the second potentiometer level is considered as the maximum. The average plastic hinge length was then 0.41h or 164 mm.

(iv) Measured Strain Profiles

The profiles of the longitudinal concrete compressive strains at the extreme fibre of the core concrete and the transverse strains in the hoops measuring both confinement and tensile stress in the tension

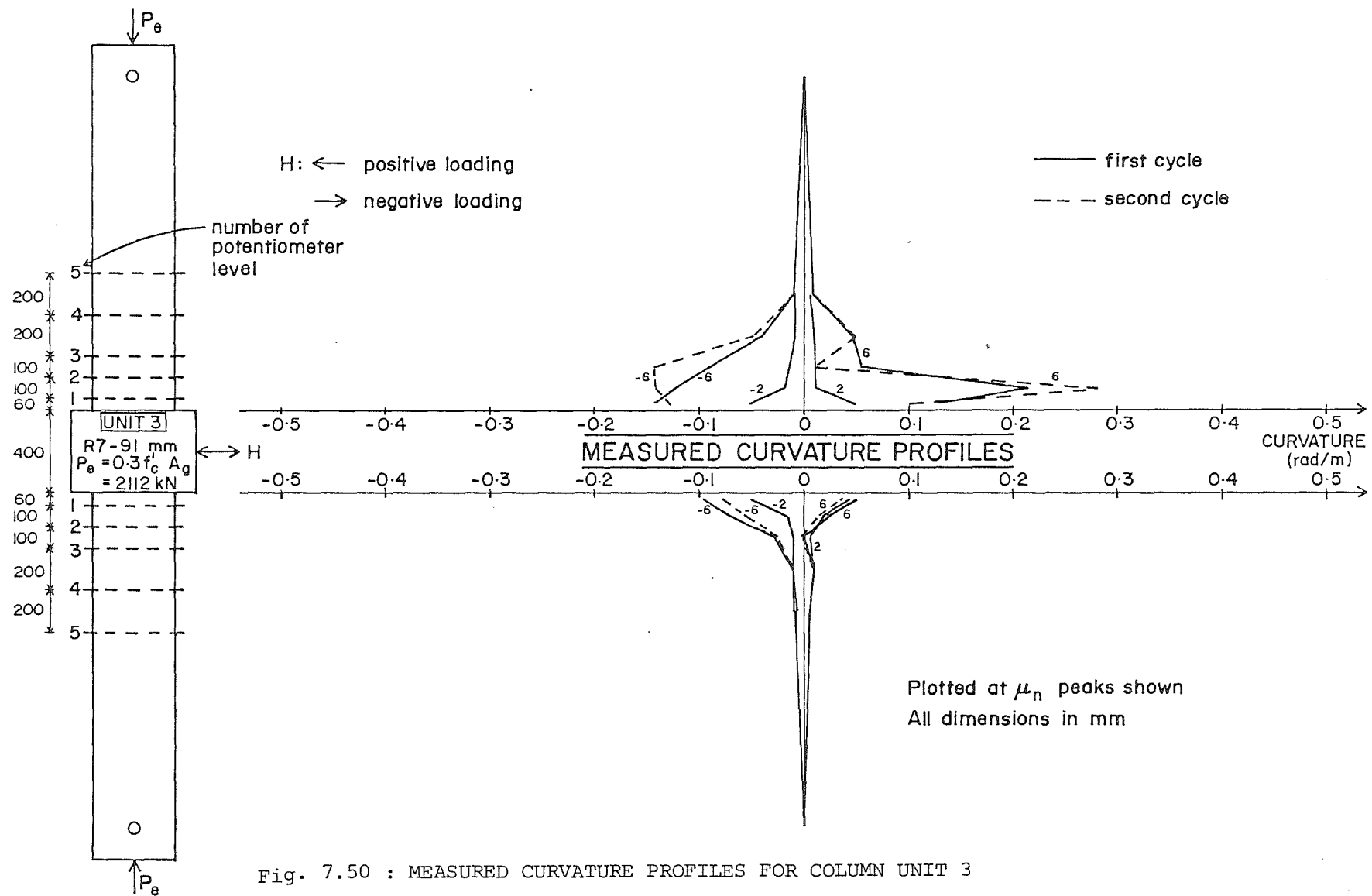


Fig. 7.50 : MEASURED CURVATURE PROFILES FOR COLUMN UNIT 3

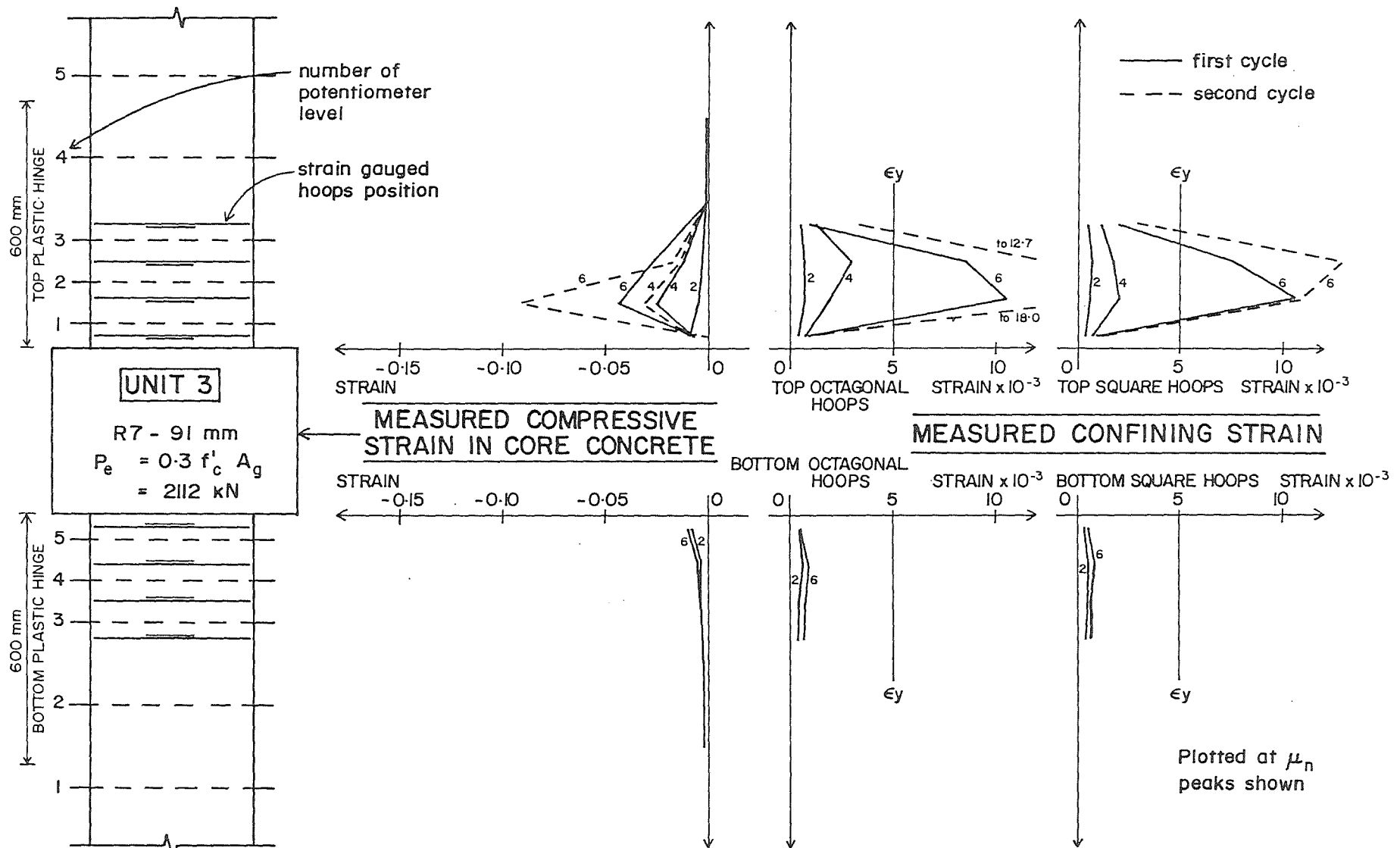


Fig. 7.51 : MEASURED COMPRESSIVE STRAINS IN THE CORE CONCRETE AND MEASURED STRAINS IN THE HOOPS DUE TO CONFINEMENT AT THE POSITIVE LOADING PEAKS FOR COLUMN UNIT 3

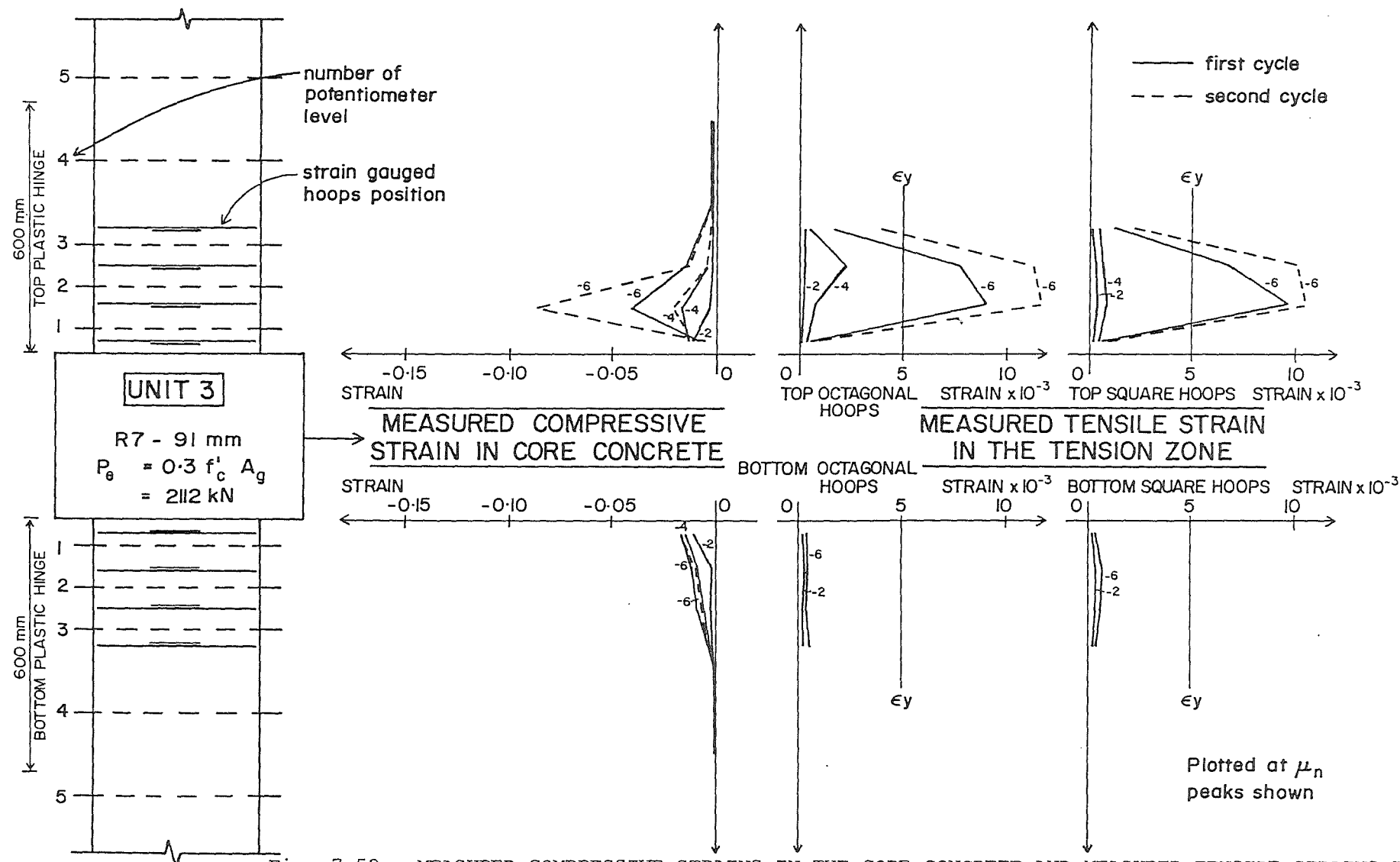


Fig. 7.52 : MEASURED COMPRESSIVE STRAINS IN THE CORE CONCRETE AND MEASURED TENSILE STRAINS IN THE HOOPS IN THE TENSION ZONE AT THE NEGATIVE LOADING PEAKS FOR COLUMN UNIT 3

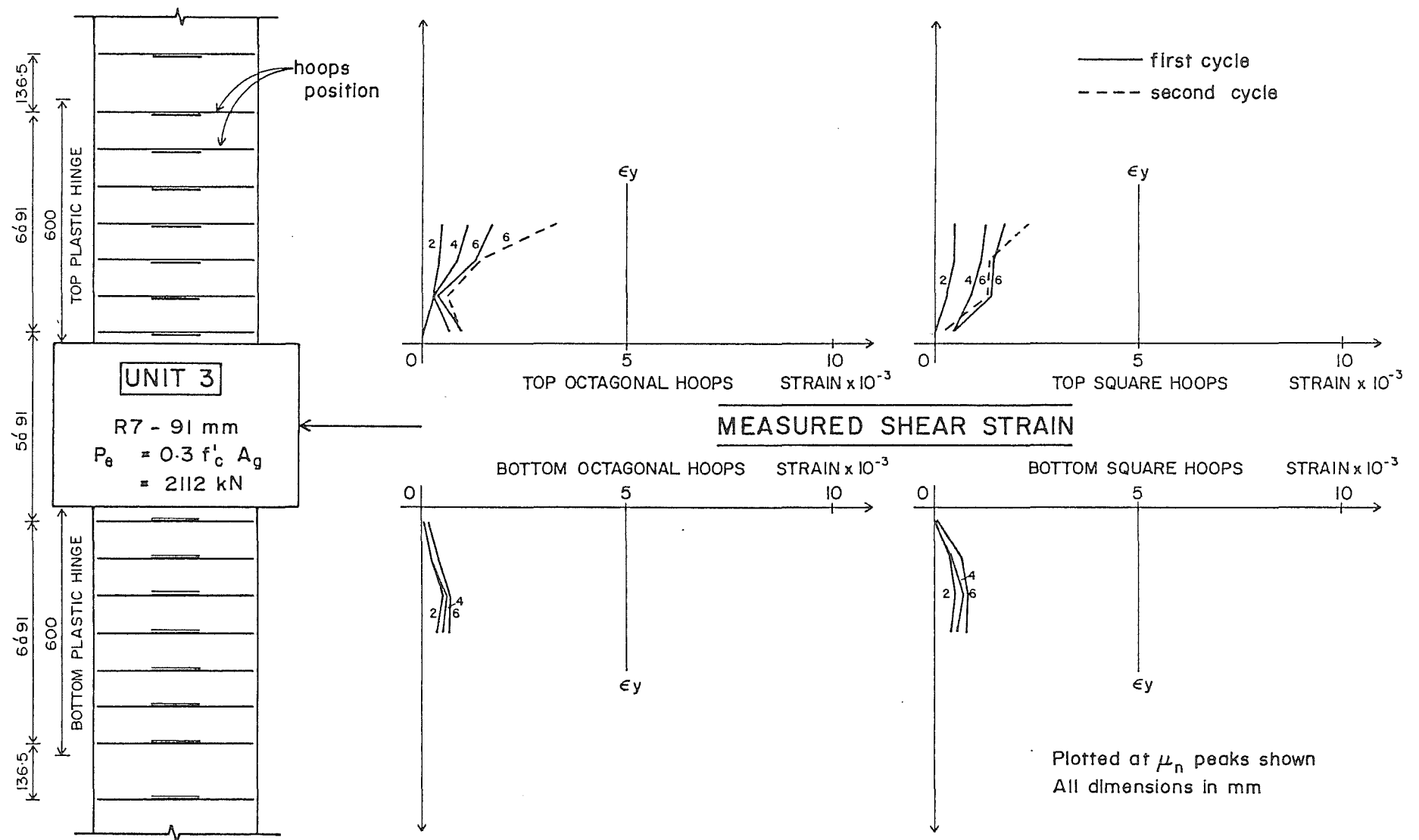


Fig. 7.53 : MEASURED STRAINS IN THE HOOPS DUE TO SHEAR AT THE POSITIVE LOADING PEAKS FOR COLUMN UNIT 3

zone are shown in Figs. 7.51 and 7.52, respectively. The profiles at the top plastic hinge were plotted at the displacement ductility peaks μ_n of ± 2 , ± 4 and ± 6 , while only at $\mu_n = \pm 2$ and ± 6 for the bottom plastic hinge.

The maximum concrete compressive strain at the top plastic hinge was 0.090, calculated at the second potentiometer level at the second cycle of $\mu_n = 6$ when the measured flexural strength had reduced to not less than 80% of the ideal flexural strength.

The profiles of measured hoop strains due to confinement also indicates the larger plastic rotation at the top hinge. Yielding of these transverse hoops did occur at displacement ductility factor μ_n greater than 4. However, confinement at that μ_n value was still adequately provided by the yielding hoops. First octagonal hoop fracture occurred at the third cycle of $\mu_n = 6$. The integrity of the core concrete was not maintained after the hoop fractured, resulting in loss of confinement and to a rapid deterioration in the lateral load strength of the column.

The hoop before fracture provided effective confinement although the actual spacing of the hoops (0.23h) was greater than the maximum (0.2h) permitted by the code⁽²⁾.

Figs. 7.53 and 7.54 illustrate the measured hoop strains due to shear at the $\mu_n =$ positive and negative displacement ductility peaks of 2, 4 and 6. As with Unit 2, yielding of transverse hoops due to shear did not occur during the test of this column.

7.6 THE PERFORMANCE OF COLUMN UNIT 4

Unit 4 properties:

Axial load levels $P_e = 0.3 f'_c A_g$

Concrete compressive strength $f'_c = 40$ MPa

Transverse hoops in the potential plastic hinge regions = R6 - 94 mm

Yield strength of the transverse reinforcing steel $f_{yh} = 255$ MPa

Total effective area of the transverse hoops A_{sh}

= 16.7% of the current code value, Eq. 4.4, or

25.0% of the proposed modified code value, Eq. 4.9

Lateral load at the ideal strength $H_i = 480$ kN

(i) General Observations

The initial elastic loading cycle was taken up to ± 75 percent

of the ideal flexural strength of the column. The first flexural cracks appeared when the lateral load was at about 60 percent of the ideal capacity, above and below the central stub. Fig. 7.55 shows the extent of cracking after the completion of the elastic loading cycle.

As mentioned in Section 6.3, the next cycle used for Unit 4 was $\mu_n = \pm 1$. The existing cracks widened at this stage. Not much additional information could be detected at the second cycle of this displacement ductility peak. Fig. 7.56 illustrates the unit after the completion cycle of $\mu_n = 1$.

The spalling of cover concrete was first observed at the bottom plastic hinge region over a distance of 50 mm beneath the central stub during the first cycle of $\mu_n = -2$. The measured compressive spalling strain was 0.012. At the second cycle of $\mu_n = -2$, the splitting cracks occurred at the top plastic hinge as shown in Fig. 7.57.

At the first cycle of $\mu_n = 3$, the spalling of the cover concrete was more significant, and the corner longitudinal bars and the transverse hoop became visible. Up to this load stage the plastic hinging occurred symmetrically at both hinges. Fig. 7.58 illustrates the unit at the second cycle of $\mu_n = -3$. At zero lateral load, the measured axial shortening of the column was 1.8 mm.

The spalling of the cover concrete extended up to 200 mm at the bottom plastic hinge at the first cycle of $\mu_n = 4$. The unit at the second cycle of this displacement ductility peak is shown in Fig. 7.59. At $\mu_n = -4$, crushing of the concrete commenced to penetrate into the core of the column but the flexural strength of the column was still 5 percent in excess of the theoretical ultimate strength (see Fig. 7.64). Also, buckling of the longitudinal bars had not yet occurred. Fig. 7.60 shows a close up view of the bottom plastic hinge at the second cycle of $\mu_n = -4$.

At the first cycle of $\mu_n = 5$, the longitudinal bars beneath the stub started to buckle, and the plastic rotation was seen to be concentrating at the bottom plastic hinge. The crushing of the core concrete was now more significant as illustrated in Fig. 7.61. However, the lateral load capacity was still maintained (see Fig. 7.64).

The next loading run to $\mu_n = -5$ resulted in the opening up of the anchorage of the hoop ends, followed by buckling of the longitudinal bars in the shape of sine curves. No more lateral load could be carried and the test was terminated. The axial shortening of the column at the end of testing was 4.7 mm. Fig. 7.62 illustrates the unit after the test was

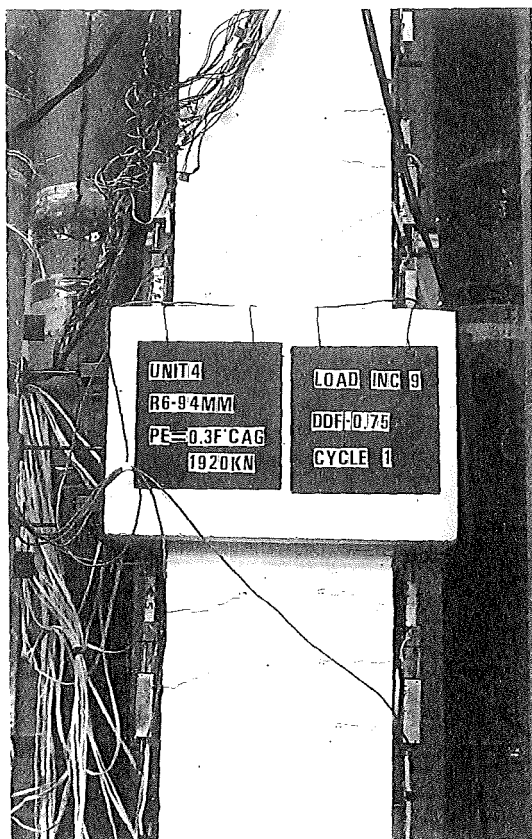


Fig. 7.55 : UNIT 4 AFTER
COMPLETION OF THE
ELASTIC CYCLE



Fig. 7.56 : EXTENT OF CRACKING AT
THE SECOND CYCLE OF $\mu_n = -1$



Fig. 7.57 : UNIT 4 AT THE SECOND
CYCLE OF $\mu_n = -2$

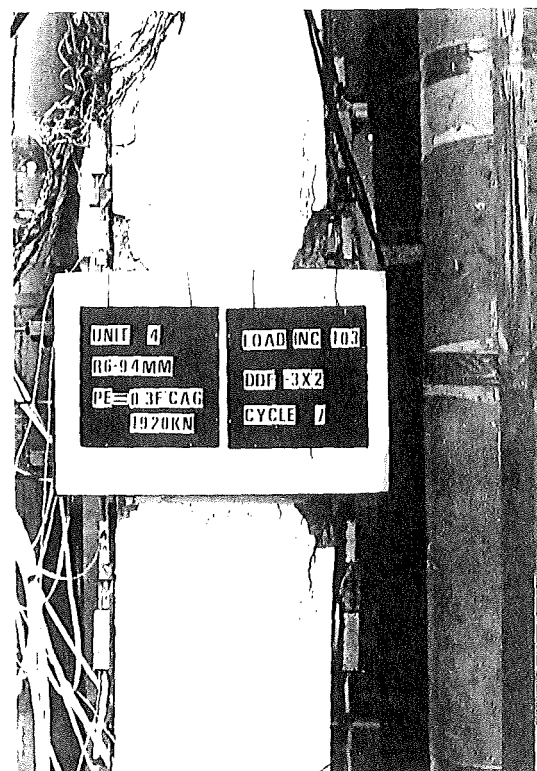


Fig. 7.58 : CRACKING AND SPALLING OF
THE UNIT AT THE SECOND
CYCLE OF $\mu_n = -2$



Fig. 7.59 : UNIT 4 AT THE SECOND CYCLE OF $\mu_n = 4$

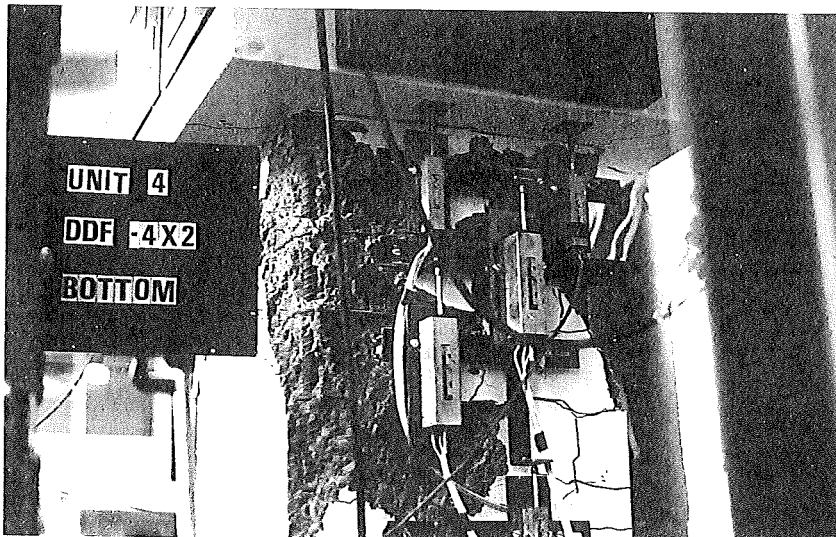


Fig. 7.60 : BOTTOM HINGE AT THE SECOND CYCLE OF $\mu_n = -4$

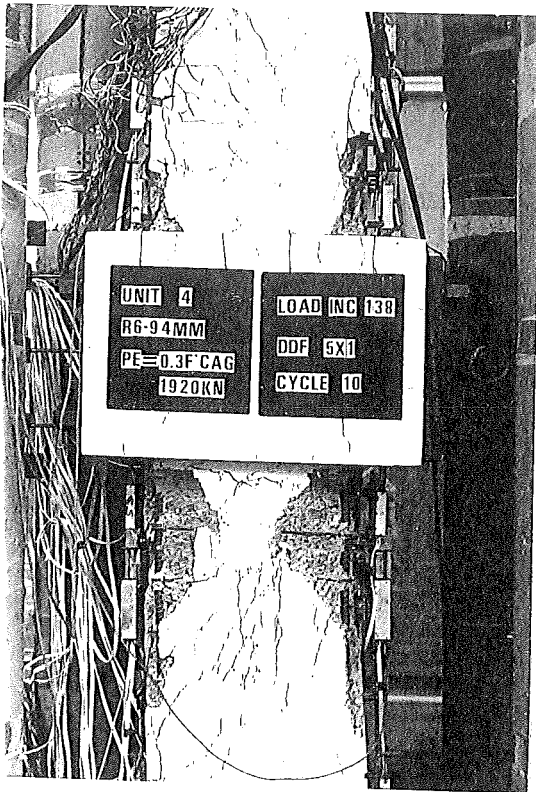


Fig. 7.61 : AT THE FIRST CYCLE OF
 $\mu_n = 5$

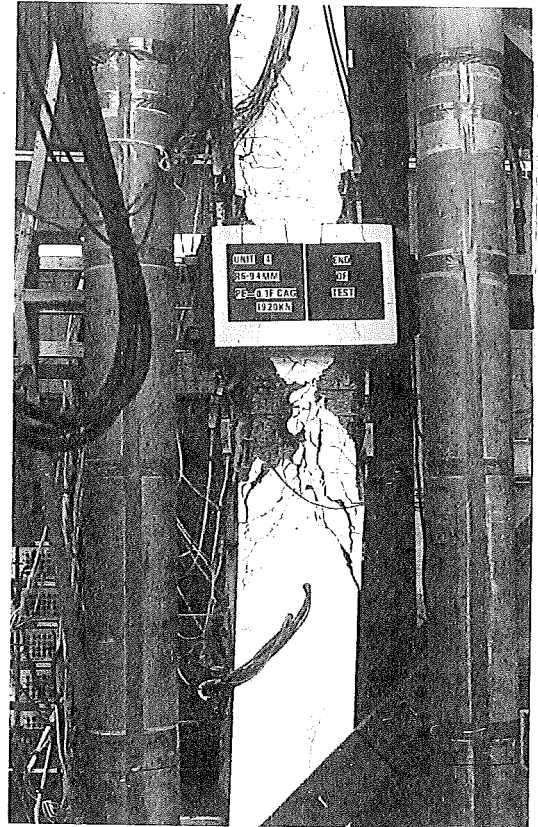


Fig. 7.62 : UNIT 4, WHEN THE TEST
 WAS TERMINATED



Fig. 7.63 : BUCKLING OF THE LONGITUDINAL BARS AT THE BOTTOM
 HINGE TERMINATED THE TEST

ended. A close up view of the bottom hinge where the damage concentrated is shown in Fig. 7.63.

A nominal displacement ductility factor $\mu_n = 5$ was reached in one loading run, although the amount of transverse reinforcement was 17 percent of that recommended by the code⁽²⁾. This indicated that a small quantity of transverse hoops is able to confine the concrete and to act as anti-buckling ties at moderate displacement ductility levels, providing that the spacing of the hoops does not exceed $6d_b$ and that the hoops are anchored well around the longitudinal bars.

(ii) Hysteretic Performance

The lateral load-displacement graph, the lateral load-top column curvature and the lateral load-bottom column curvature graphs are shown in Figs. 7.64 to 7.66, respectively. It can be seen that the maximum lateral load reached during the test was 523 kN, and occurred at the positive displacement peak of $\mu_n = 2$, resulting in a flexural over-strength factor M_{max}/M_i of 1.17.

At the first cycle of the displacement ductility factor μ_n of 5, or the real displacement ductility factor μ_r of 7.7, the theoretical ultimate load was just reached. However, a nominal displacement ductility factor μ_n of -5 was never achieved, owing to the failure of the hoop anchorages, followed by buckling of the longitudinal bars.

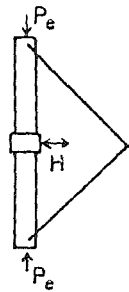
The maximum lateral displacement $\Delta + \theta l'$, measured at $\mu_n = -4$ was found to be 46 mm, giving a maximum measured drift of 2.6%.

From Figs. 7.65 and 7.66 it is clear that up to $\mu_n = 3$, plastic hinge rotation took place symmetrically at both hinges as mentioned previously. Further excursions to higher displacement ductility factors led to a concentration of plastic rotation at the bottom hinge.

(iii) Curvature Distribution, Curvature Ductility and Equivalent Plastic Hinge Length

Fig. 7.67 illustrates the measured curvature profiles for Unit 4 at the displacement ductility peaks μ_n of ± 1 , ± 4 and 5. The large plastic rotation at the bottom plastic hinge during the last stage of the testing is also clearly shown in the figure. This was more pronounced at the second potentiometer levels. The maximum curvatures calculated at the first and second potentiometer levels were 0.0982 and 0.1185 rad/m, respectively. These curvatures were measured at the displacement peak at the second cycle of $\mu_n = -4$. Using the procedure

UNIT 4



$P_e = 0.3 f'_c A_g$
 $= 1920 \text{ kN}$
 Hoops R6 - 94 mm
 $A_{sh} = 16.7\% \text{ of current code equation}$
 $= 25.0\% \text{ of modified equation}$
 $\Delta_y^* = 8.20 \text{ mm}$
 $H_{max} = 523 \text{ kN}$

H: push (\leftarrow): positive loading
 pull (\rightarrow): negative loading

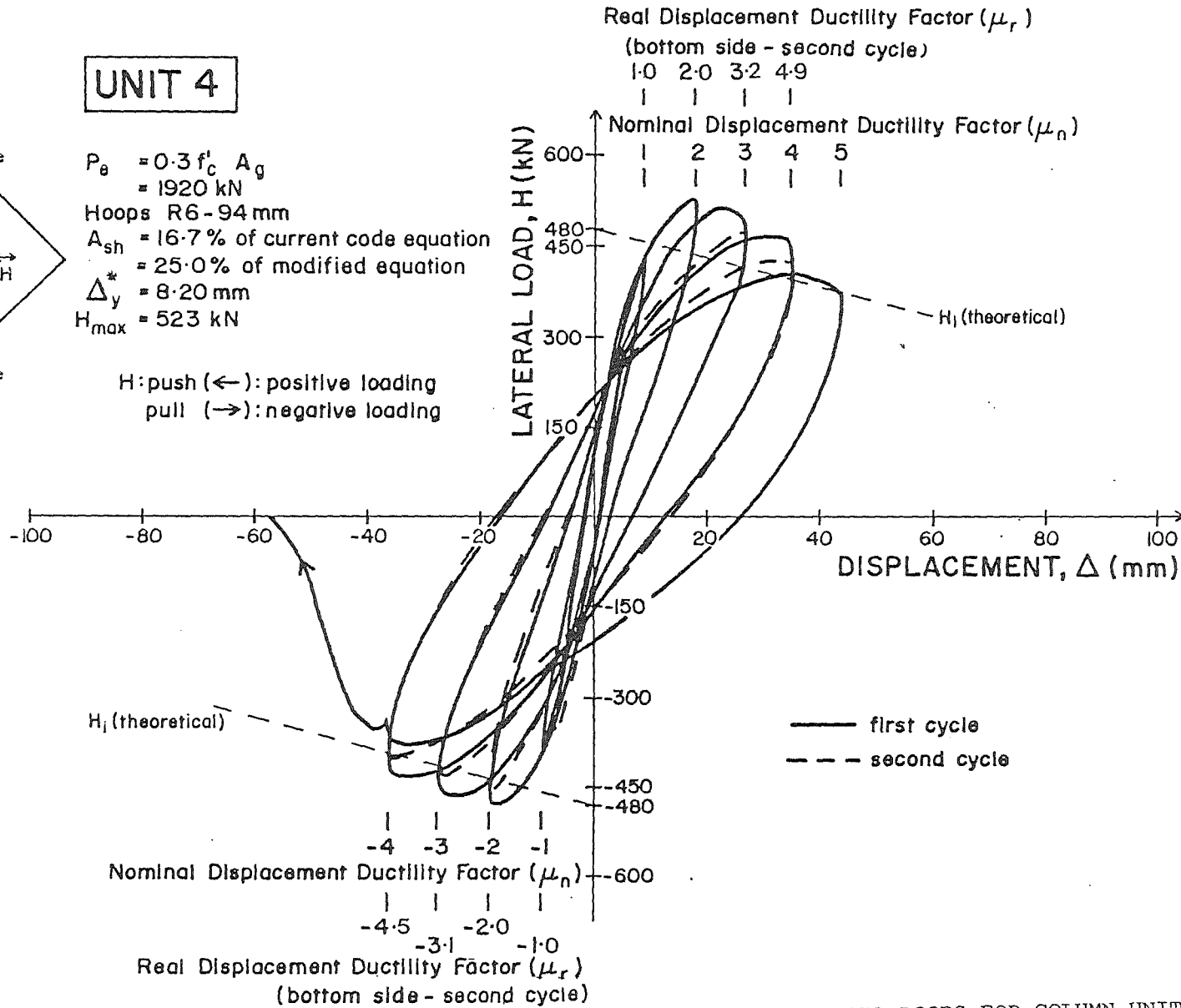


Fig. 7.64 : EXPERIMENTAL LATERAL LOAD-DISPLACEMENT HYSTERESIS LOOPS FOR COLUMN UNIT 4

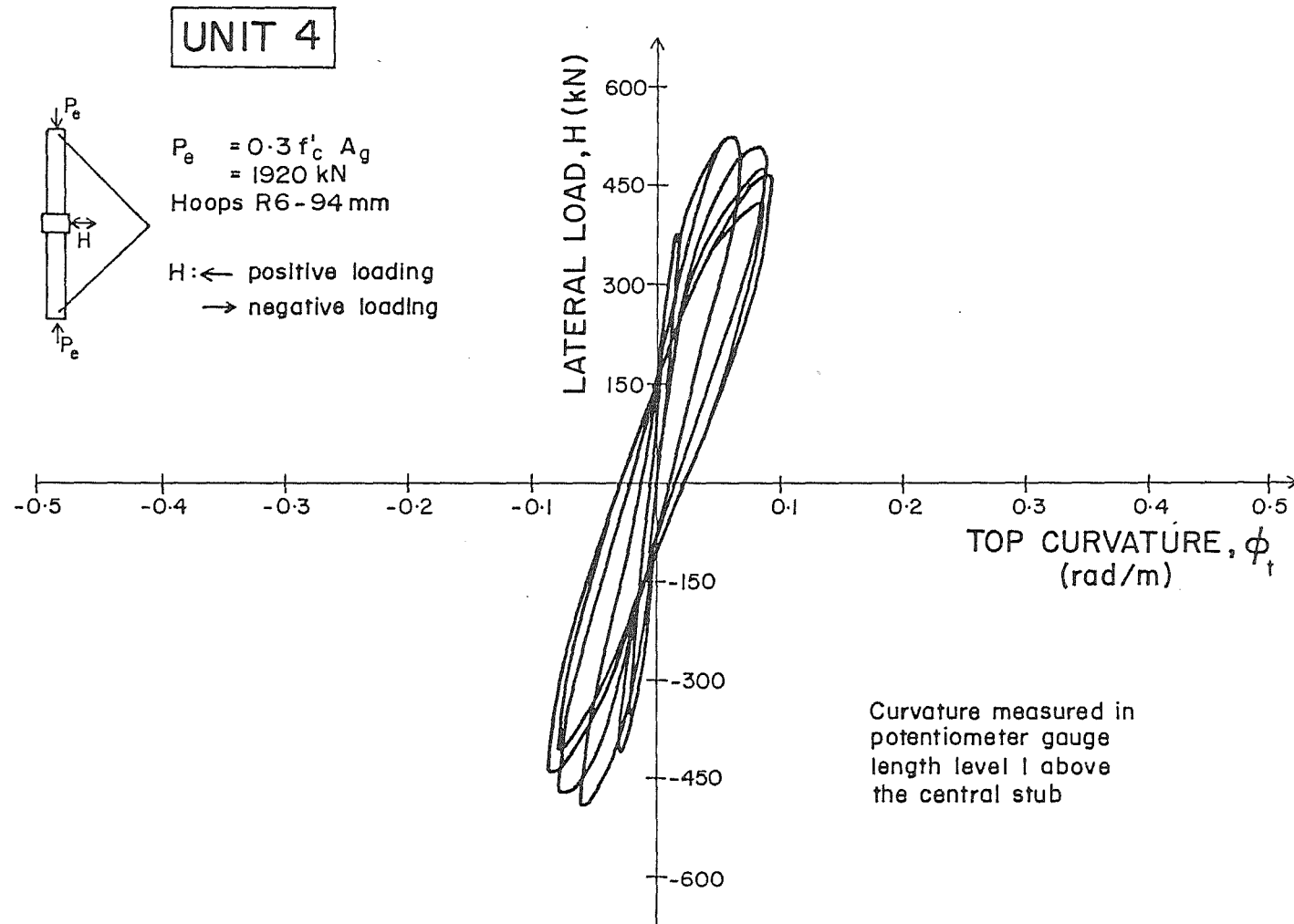


Fig. 7.65 : EXPERIMENTAL LATERAL LOAD-TOP COLUMN CURVATURE HYSTERESIS LOOPS FOR COLUMN UNIT 4

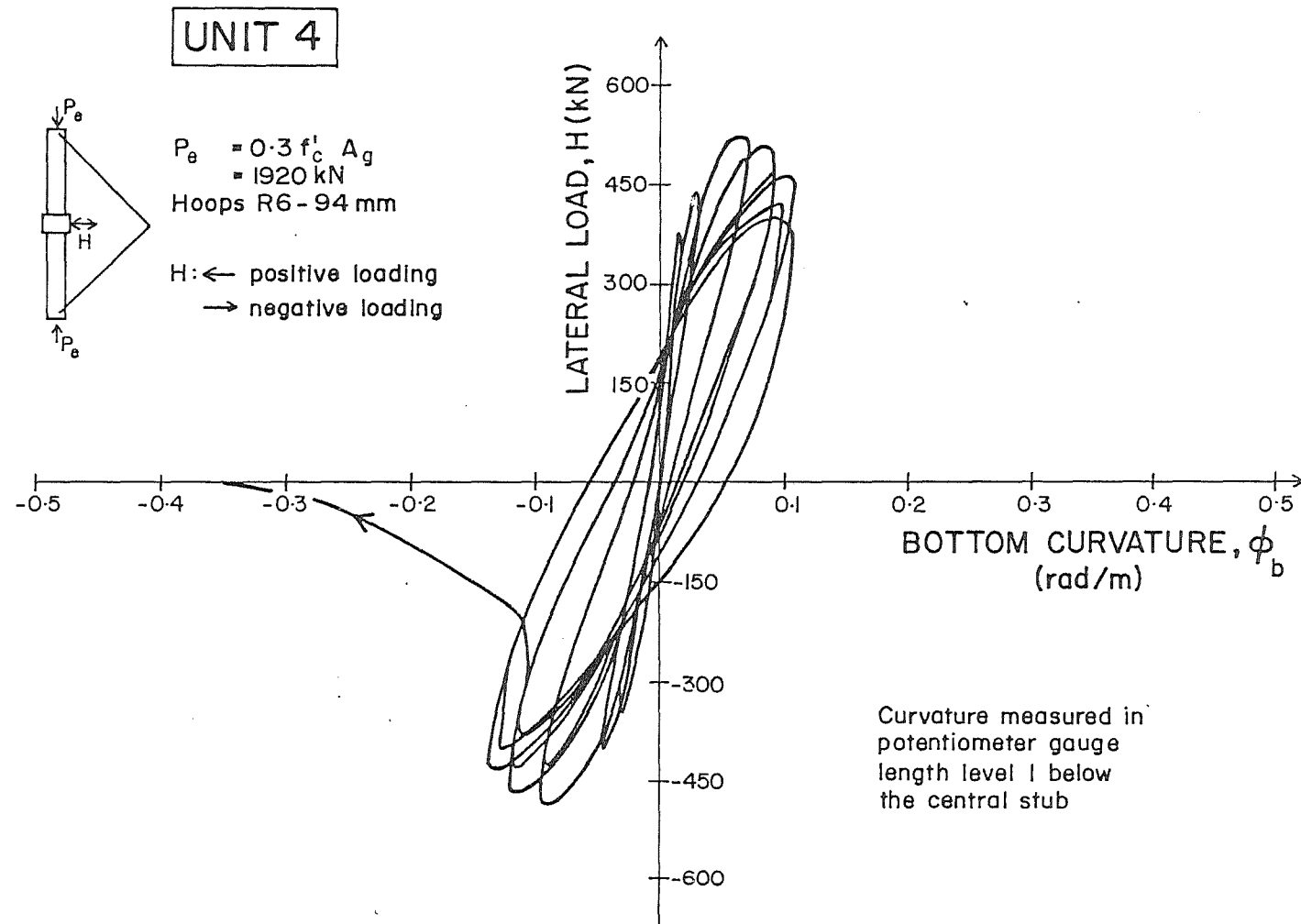


Fig. 7.66 : EXPERIMENTAL LATERAL LOAD-BOTTOM COLUMN CURVATURE HYSTERESIS LOOPS FOR COLUMN UNIT 4

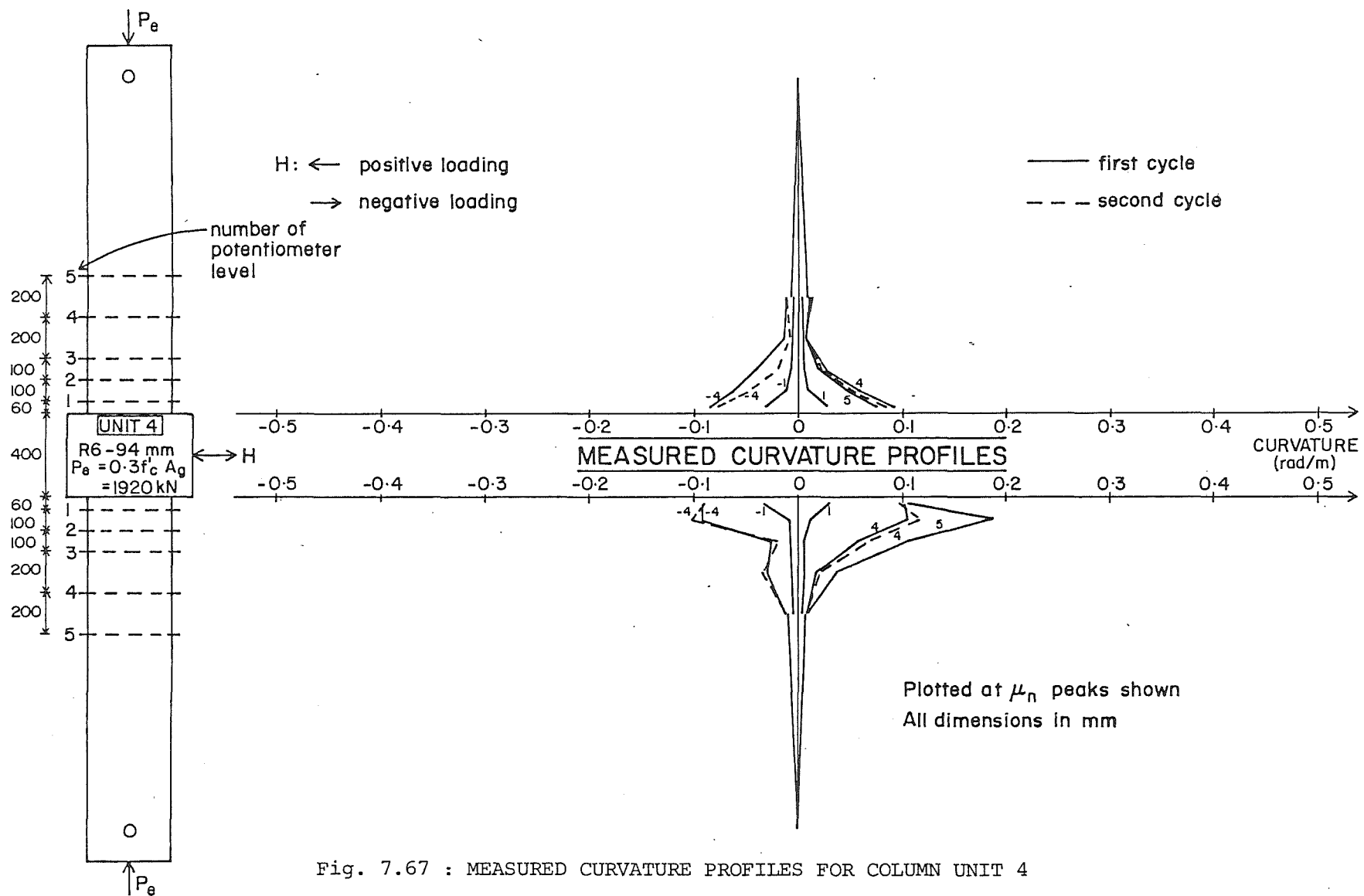


Fig. 7.67 : MEASURED CURVATURE PROFILES FOR COLUMN UNIT 4

described in Section 7.2 to calculate the experimental yield curvature, it was found that ϕ_y was 8.80×10^{-3} rad/m. Hence the available curvature ductility factors were 11.2 and 13.5 for the first and second potentiometer levels, respectively.

The equivalent plastic hinge length, where the inelastic deformations concentrated, was calculated from Eq. 7.7. Using the measured ultimate curvature at the first and second potentiometer levels the equivalent plastic hinge lengths were found to be $0.28h$ (112 mm) and $0.23h$ (92 mm), respectively, resulting in an average plastic hinge length $(\ell_p/h)_{av}$ of $0.26h$ or 104 mm.

(iv) Measured Strain Profiles

Figs. 7.68 and 7.69 show the measured concrete compressive strains in the core concrete and the measured strains due to confinement and the tensile strains in the tension zone in the hoops, for both directions of loading.

As mentioned previously, the spalling of the cover concrete was first observed when the concrete compressive strain was 0.012. The maximum concrete compressive strain reached was measured at the second potentiometer level located at the bottom plastic hinge and it was found to be 0.030. It should be noted that the concrete compressive strain at the second cycle of $\mu_n = -4$ was considered as the maximum strain.

Yielding of the transverse hoops did not occur at the top plastic hinge. However, as illustrated in Fig. 7.68, yielding of the square hoops occurred at the bottom plastic hinge at a displacement ductility factor higher than $\mu_n = 4$. The following features can be concluded. Firstly, the transverse hoops of R6 provided good confinement to the concrete, although the spacing of $0.24h$ was larger than the $0.2h$ permitted by the code⁽²⁾. Secondly, the yielding hoop at $\mu_n = 5$ was still able to prevent buckling of the longitudinal bars.

The measured strains in the octagonal and square hoops due to shear are shown in Figs. 7.70 and 7.71 for both directions of loading. The strains are plotted at the successive displacement ductility peaks μ_n of $\pm 1, \pm 2, \pm 3, \pm 4$ and 5. Yielding of transverse hoops due to shear did not occur, except for the octagonal hoop at the bottom plastic hinge (see Fig. 7.70) where the strain was slightly higher than the yield strain at $\mu_n = 5$. This indicated that the concrete shear resisting mechanisms made a large contribution in resisting shear (see Table 4.2 in Section 4.4).

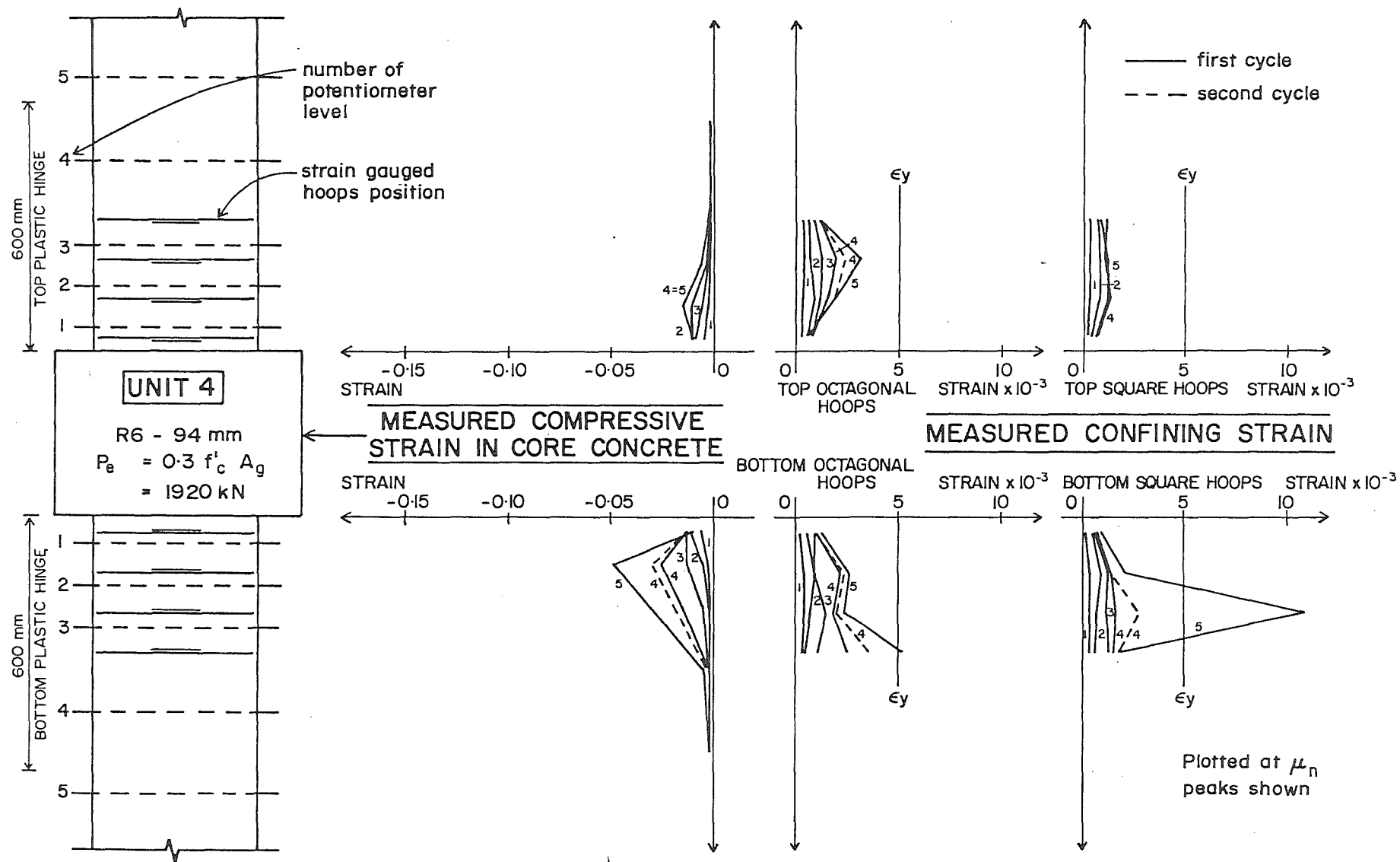


Fig. 7.68 : MEASURED COMPRESSIVE STRAINS IN THE CORE CONCRETE AND MEASURED STRAINS IN THE HOOPS DUE TO CONFINEMENT AT THE POSITIVE LOADING PEAKS FOR COLUMN UNIT 4

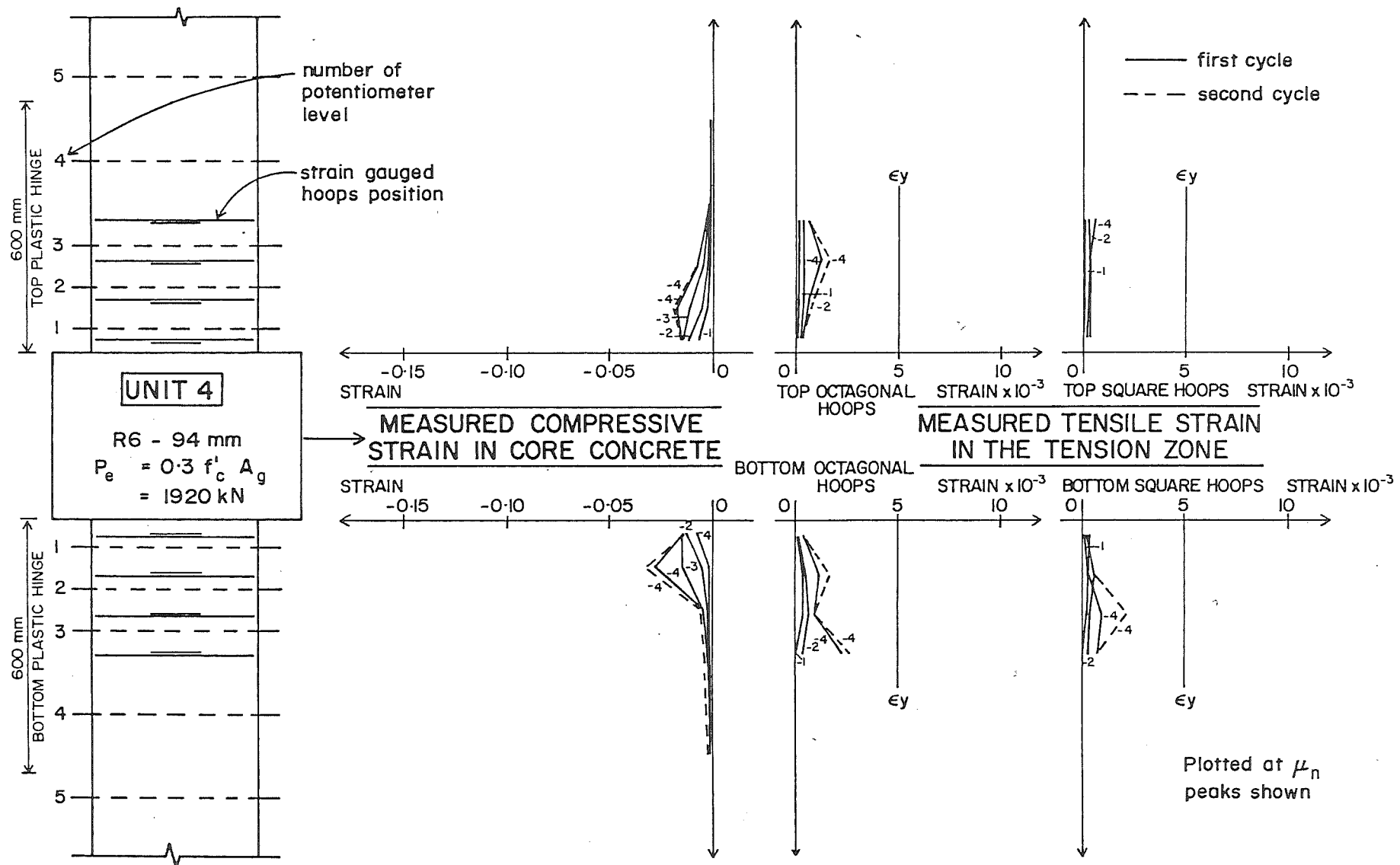


Fig. 7.69 : MEASURED COMPRESSIVE STRAINS IN THE CORE CONCRETE AND MEASURED TENSILE STRAINS IN THE HOOPS IN THE TENSION ZONE AT THE NEGATIVE LOADING PEAKS FOR COLUMN UNIT 4

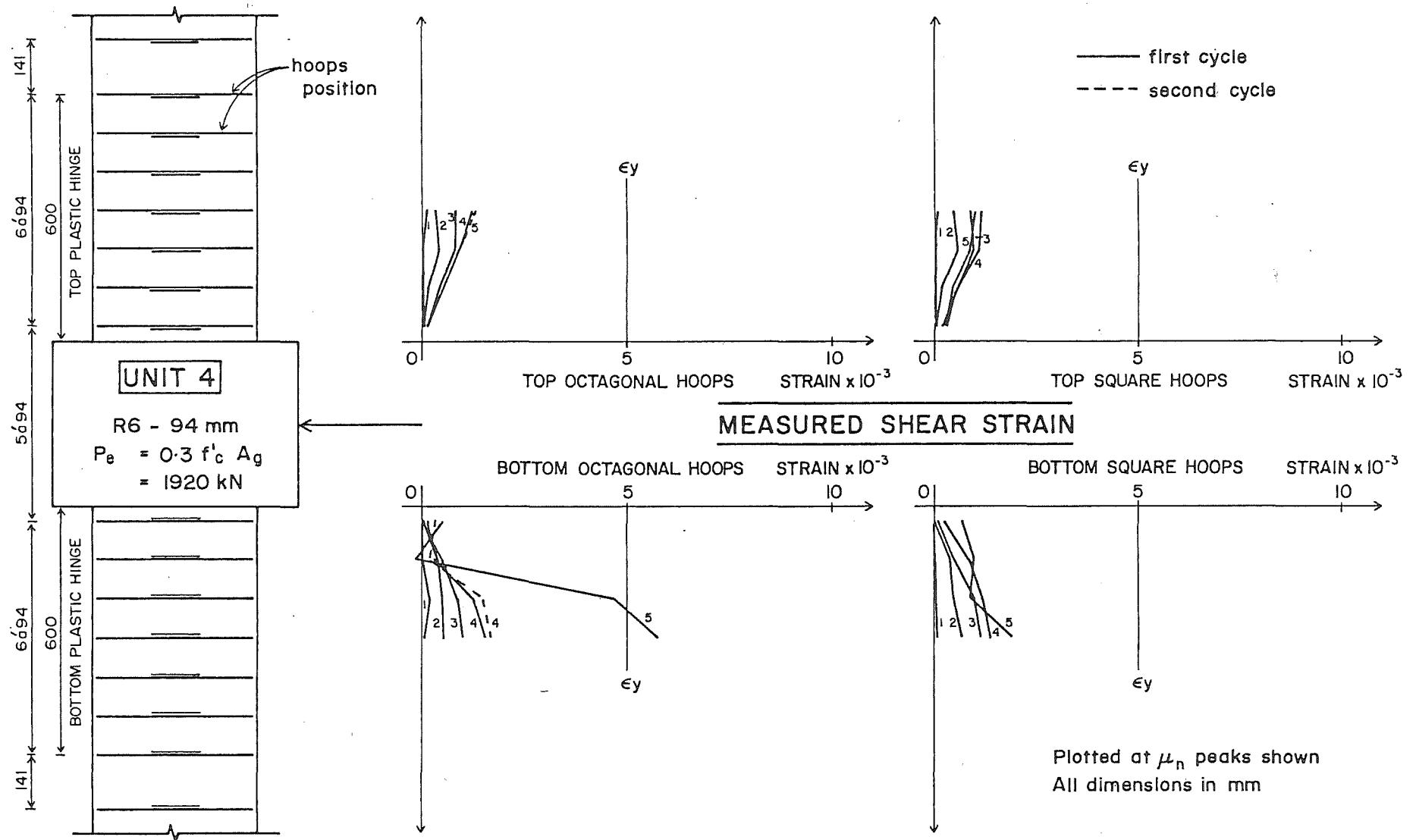


Fig. 7.70 : MEASURED STRAINS IN THE HOOPS DUE TO SHEAR AT THE POSITIVE LOADING PEAKS FOR COLUMN UNIT 4

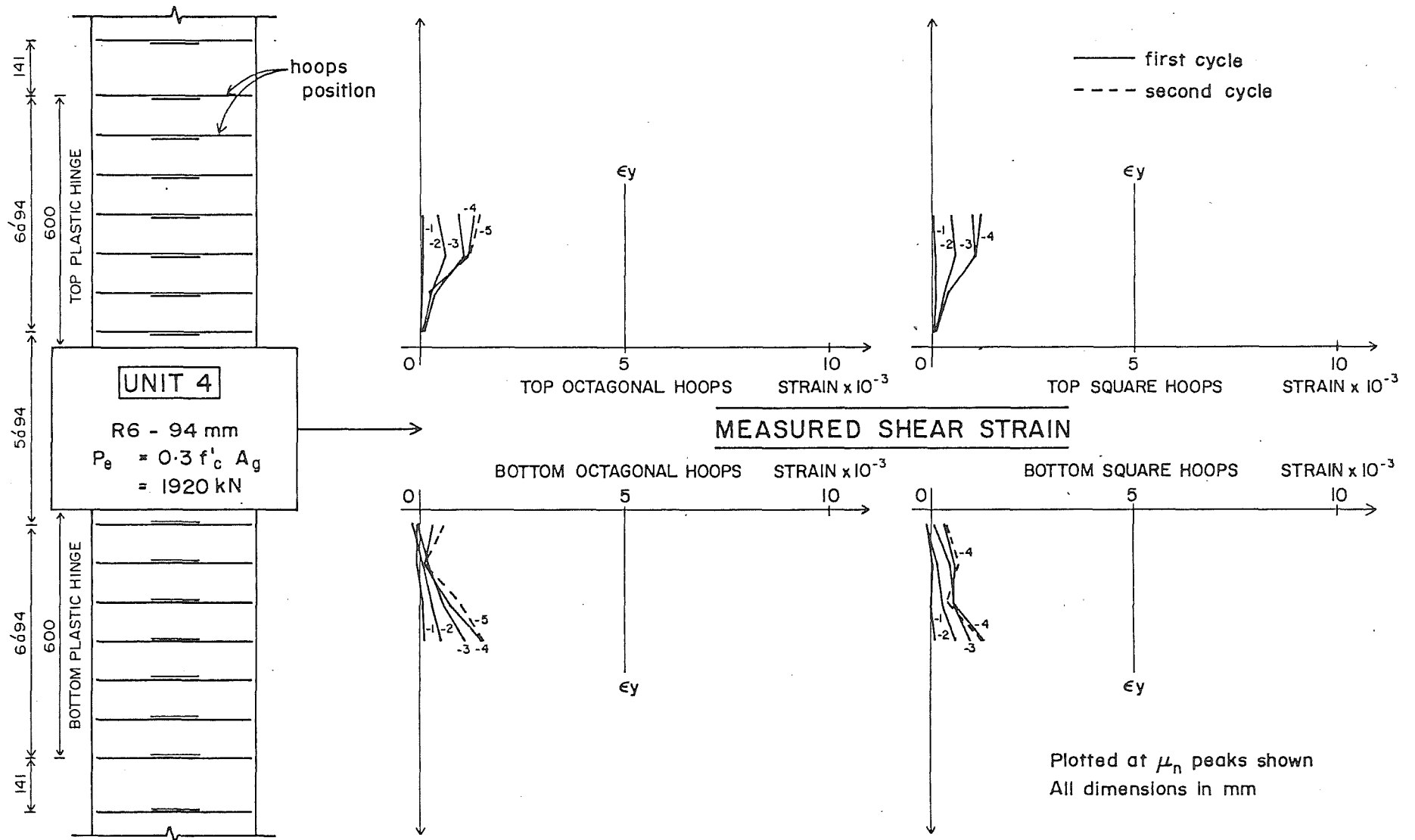


Fig. 7.71 : MEASURED STRAINS IN THE HOOPS DUE TO SHEAR AT THE NEGATIVE LOADING PEAKS FOR COLUMN UNIT 4

7.7 CONCLUDING REMARKS

The performance of the four column units observed during the tests may be summarized as follows:

- (1) Unit 1, which was subjected to the lower level of axial load of $0.1 f'_c A_g$ compared to the $0.3 f'_c A_g$ of Units 2, 3 and 4, exhibited some pinching in its hysteresis loops. Pinching of the hysteresis loops did not occur in the case of Units 2, 3 and 4. Also, there was a tendency for the flexural cracks in Unit 1 to grow faster and to open wider as the lateral load increased than those in the other units.
- (2) At the end of the tests, Units 1 and 2, which contained 43 and 46 percent of the code⁽²⁾ recommended quantity of transverse reinforcement respectively, exhibited ductile behaviour, longitudinal bars at the extreme tensile fibre eventually fractured. However for Unit 3, which contained 30 percent of the code recommended quantity of transverse reinforcement, there was fracture of an octagonal hoop at the end of testing. For Unit 4, which contained 17% of the code recommended quantity of transverse reinforcement, there was failure of the hoop anchorage at the longitudinal bars followed by buckling of the longitudinal bars.
- (3) A summary of the experimental results for the column units is listed in Table 7.1. Table 7.1a includes the maximum lateral load reached H_{max} which occurred at the first cycle of $\mu_n = 2$ for all units, the flexural overstrength factor M_{max}/M_i , the maximum nominal and real displacement ductility factors μ_n and μ_r , the maximum displacement Δ_{max} including the effect of stub rotation, and the corresponding maximum drift Δ_{max}/l' , the spalling strain of the cover concrete ϵ_{spall} , and the maximum compressive strain in the core concrete ϵ_{cmax} . Table 7.1b includes the yield displacement Δ_y , the yield curvature ϕ_y , the maximum ultimate curvature ϕ_u , the available curvature ductility factors ϕ_u/ϕ_y , and the equivalent plastic hinge lengths l_p . The measurements at both the first and the second levels of pairs of potentiometers were considered. It should be noted that the values of μ_n , μ_r , Δ_{max} , Δ_{max}/l' , ϵ_{cmax} , ϕ_u and ϕ_u/ϕ_y listed in Table 7.1 are taken as the values at the displacement ductility peak where the load carrying capacity of the column in the cycle of loading had reduced to not less than 80% of the theoretical ultimate capacity.

Table 7.1 : A SUMMARY OF THE EXPERIMENTAL RESULTS FOR
ALL COLUMN UNITS

Table 7.1a The Experimental Values of H_{\max} , M_{\max}/M_i , μ_n , μ_r ,
 Δ_{\max} , Δ_{\max}/ℓ' , ϵ_{spall} and ϵ_{cmax}

Unit	H_{\max}	$\frac{M_{\max}}{M_i}$	(a) μ_n	(a) μ_r	Δ_{\max} (mm)	$\frac{\Delta_{\max}}{\ell'}(\%)$	ϵ_{spall}	ϵ_{cmax}
1	402	1.11	8	8.5	91	5.1	0.013	0.050
2	562	1.20	8	11.9	118	6.6	0.013	0.110
3	560	1.18	6	9.1	68	3.8	0.008	0.090
4	523	1.17	4	4.9	46	2.6	0.012	0.030

(a) Greatest value reached in second cycle of loading when
measured lateral load had reduced to not less than 80%
of theoretical H_i

Table 7.1b The Experimental Values of Δ_y , ϕ_y , ϕ_u , ϕ_u/ϕ_y ,
 ℓ_p/h and $(\ell_p/h)_{\text{av}}$

Unit	Δ_y (mm)	ϕ_y (rad/m)	ϕ_{u1} (a) (rad/m)	ϕ_{u2} (b) (rad/m)	$\frac{\phi_{u1}}{\phi_y}$	$\frac{\phi_{u2}}{\phi_y}$	$\frac{\ell_{p1}}{h}$	$\frac{\ell_{p2}}{h}$	$\frac{\ell_p}{h}$ ($\frac{p}{h}$) _{av}
1	10.70	10.14×10^{-3}	0.2014	0.2426	19.9	23.9	0.29	0.23	0.26
2	9.92	11.10×10^{-3}	0.1981	0.3124	17.9	28.1	0.41	0.24	0.33
3	8.96	8.0×10^{-3}	0.1280	0.1428	16.0	17.8	0.44	0.38	0.41
4	9.40	8.80×10^{-3}	0.0982	0.1185	11.2	13.5	0.28	0.23	0.26

(a) Subscript 1 indicated the first potentiometer level

(b) Subscript 2 indicated the second potentiometer level

CHAPTER EIGHT

DISCUSSION OF THE EXPERIMENTAL RESULTS

8.1 INTRODUCTION

In this chapter a discussion of the experimental results from the four columns tested and a comparison of those results with the analytical investigation mentioned in Section 5.5., are given.

The behaviour of the columns is also compared with that of the columns tested by Ang et al⁽⁷⁾.

8.2 ASPECTS OF THE DISCUSSION AND COMPARISONS OF THE EXPERIMENTAL RESULTS WITH THE ANALYTICAL INVESTIGATIONS

8.2.1 General Behaviour

Units 1 and 2, with 43 to 46 percent of the NZS 3101:1982⁽²⁾ recommended quantity of transverse reinforcement, performed extremely well. A ductile failure was observed at the end of testing and a nominal displacement ductility factor of 8 during cyclic loading was achieved, indicating that the transverse hoops provided adequate confinement to the concrete, prevented premature buckling of the longitudinal bars, and sufficiently provided shear resistance.

Unit 3, with 30 percent of transverse reinforcement recommended by the code⁽²⁾, reached a nominal displacement ductility factor of 6 during cyclic loading. The test indicated that the transverse hoops effectively confined the concrete although the spacing of the hoops was $0.23h$ which was greater than the limit of $0.20h$ required by the code⁽²⁾.

Unit 4, with 17 percent of the code⁽²⁾ requirements of transverse reinforcement, performed satisfactorily up to a nominal displacement ductility factor of 4 during cyclic loading. This test indicated that a small quantity of hoops could give adequate restraint against buckling of the longitudinal bars, providing that the spacing of the hoops did not exceed $6d_b$ and that the bend of the hoops around the longitudinal bars anchored the hoops well.

8.2.2 Moment-Curvature Relationships

The experimental curvature ductility factors measured for each column unit were compared with the analytical monotonic^(21,18,22,3) and

cyclic moment-curvature^(3,24) relationships determined as described in Section 5.5. The experimental values of the curvature ductility factors plotted were the values measured at the peaks of the second loading cycles to that ductility factor at the first potentiometer level, either at the top or bottom plastic hinges where most of the plastic rotation concentrated. It should be noted that the measurements included the effects of yield penetration of longitudinal reinforcement into the stub at the mid-height of the columns.

Figs. 8.1 and 8.2 illustrate the moment-curvature comparisons for Unit 1. In Fig. 8.1 the theoretical predictions are from the monotonic moment-curvature analyses and in Fig. 8.2 the theoretical predictions are from the cyclic moment-curvature analysis. It is evident, the moment-curvature analyses predicted the measured moment very well.

The analytical monotonic and cyclic moment-curvature relationships for Unit 2 are compared with the experimental values in Figs. 8.3 and 8.4, respectively. Reasonably good agreement between the analytical and experimental results is indicated in the figures, but at higher curvature ductilities, the theoretical predictions led to a slight underestimate of the measured moments.

Figs. 8.5 to 8.8 show the analytical and experimental moment-curvature comparisons for Units 3 and 4. It is clear that the theoretical predictions underestimated the experimental moments at high curvature ductilities. This may be explained as follows. It can be seen from the analytical stress-strain curves for concrete confined as in these columns shown in Figs. 5.6 and 5.7 (see Section 5.3.3) that the concrete stresses reduced markedly at the higher strains. This resulted in quite steep falling branches in the moment-curvature curves. It is evident that the models used for the stress-strain behaviour of the concrete (i.e. Modified Kent-Park model and Mander et al model) predicted overly conservative concrete stresses at higher strains for Units 3 and 4 which had relatively small amounts of transverse reinforcement.

It should also be noted that in Figs. 8.1 to 8.8, owing to the effect of yield penetration which was already pronounced at the early stage of testing, the experimental results indicated larger values of curvature ductility factors than those predicted analytically.

8.2.3 Yield Curvature and Yield Displacement

Table 8.1 gives the values of the yield curvatures ϕ_y and the yield displacements Δ_y for all column units. The measured values

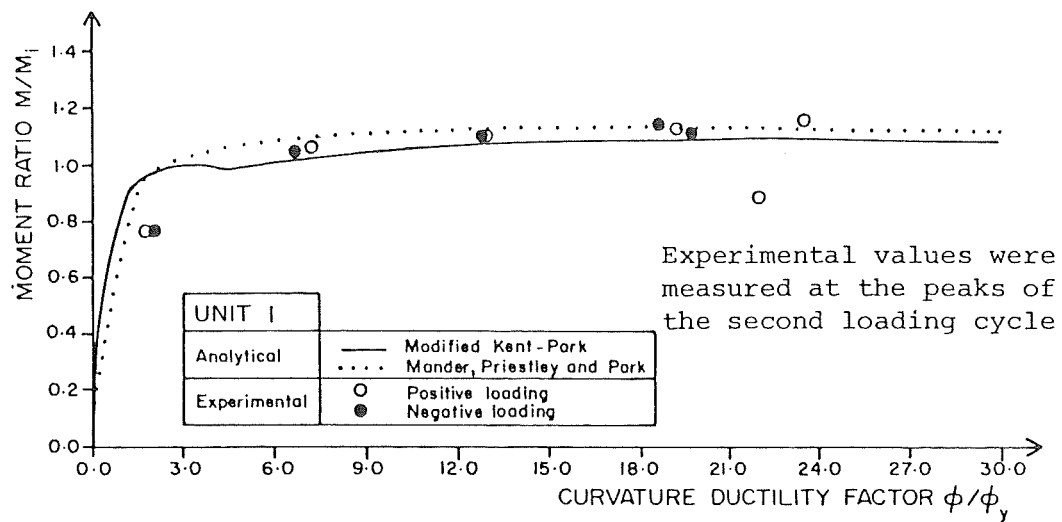


Fig. 8.1 : ANALYTICAL MONOTONIC MOMENT-CURVATURE CURVES AND MEASURED VALUES FOR UNIT 1

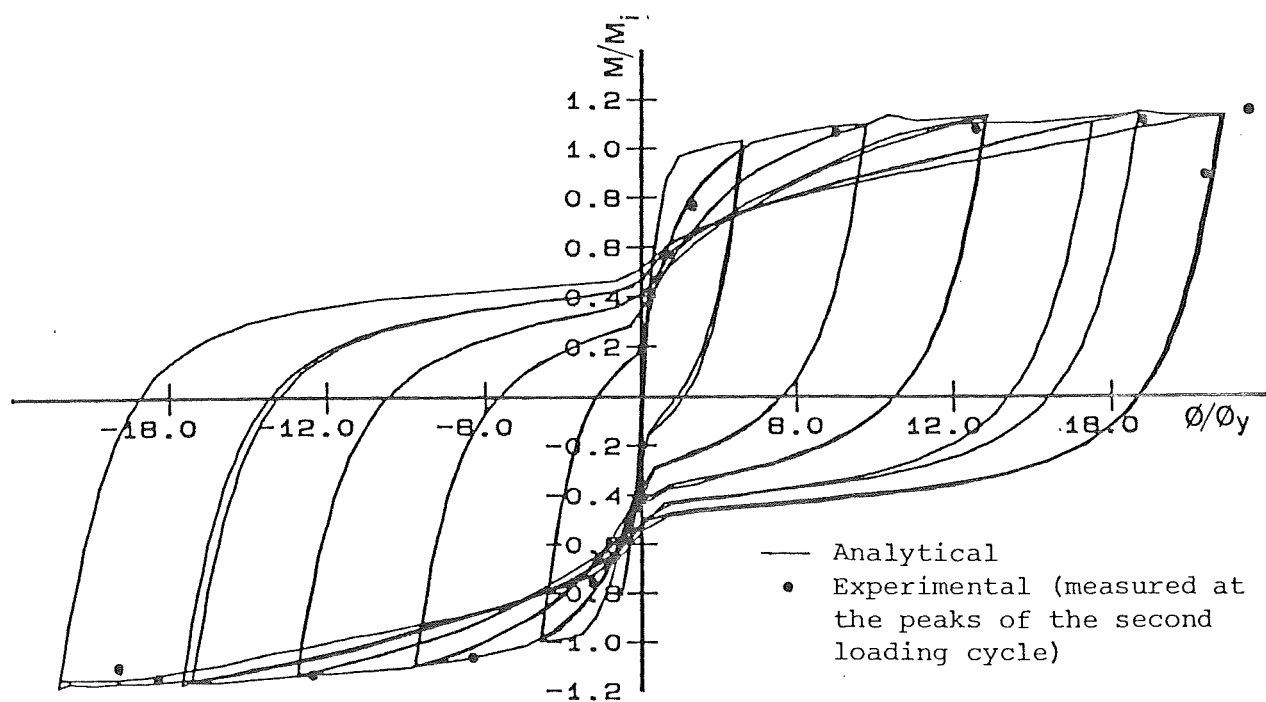


Fig. 8.2 : ANALYTICAL CYCLIC MOMENT-CURVATURE CURVE AND MEASURED VALUES FOR UNIT 1

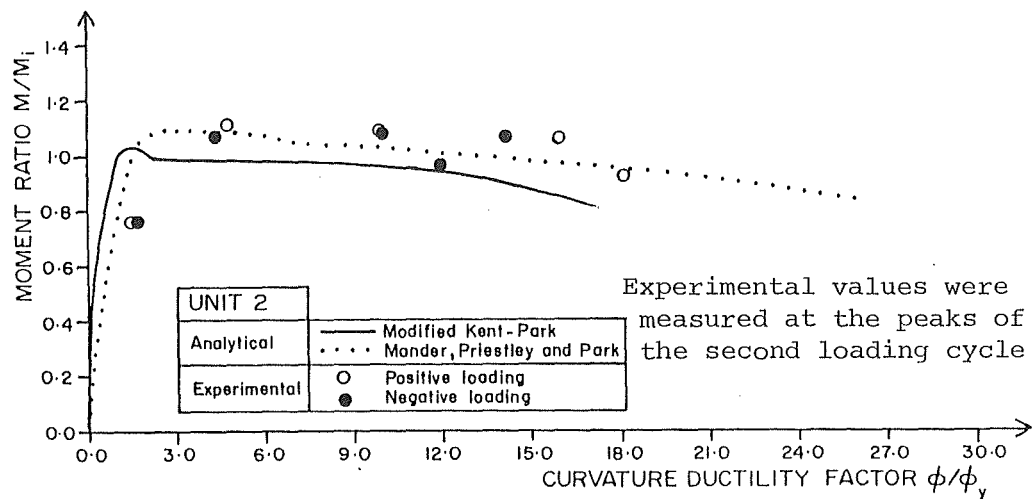


Fig. 8.3 : ANALYTICAL MONOTONIC MOMENT-CURVATURE CURVES AND MEASURED VALUES FOR UNIT 2

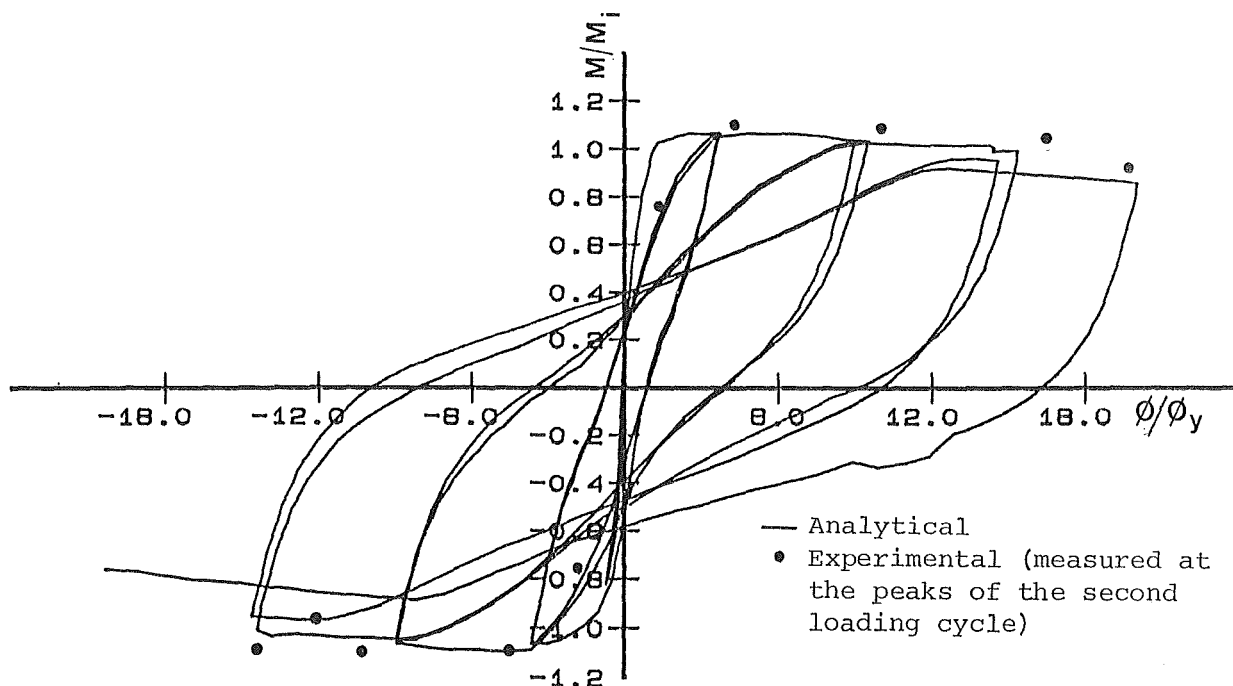


Fig. 8.4 : ANALYTICAL CYCLIC MOMENT-CURVATURE CURVE AND MEASURED VALUES FOR UNIT 2

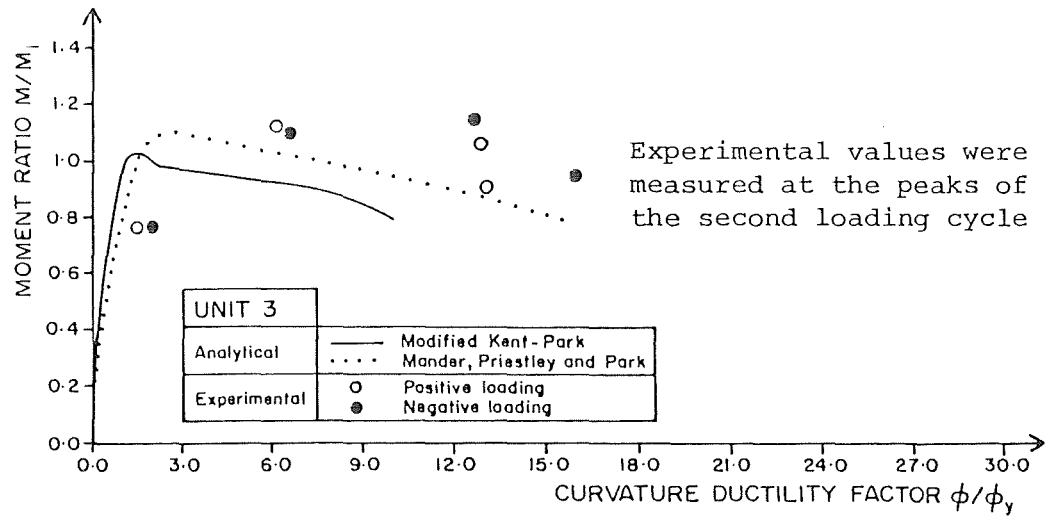


Fig. 8.5 : ANALYTICAL MONOTONIC MOMENT-CURVATURE CURVES AND MEASURED VALUES FOR UNIT 3

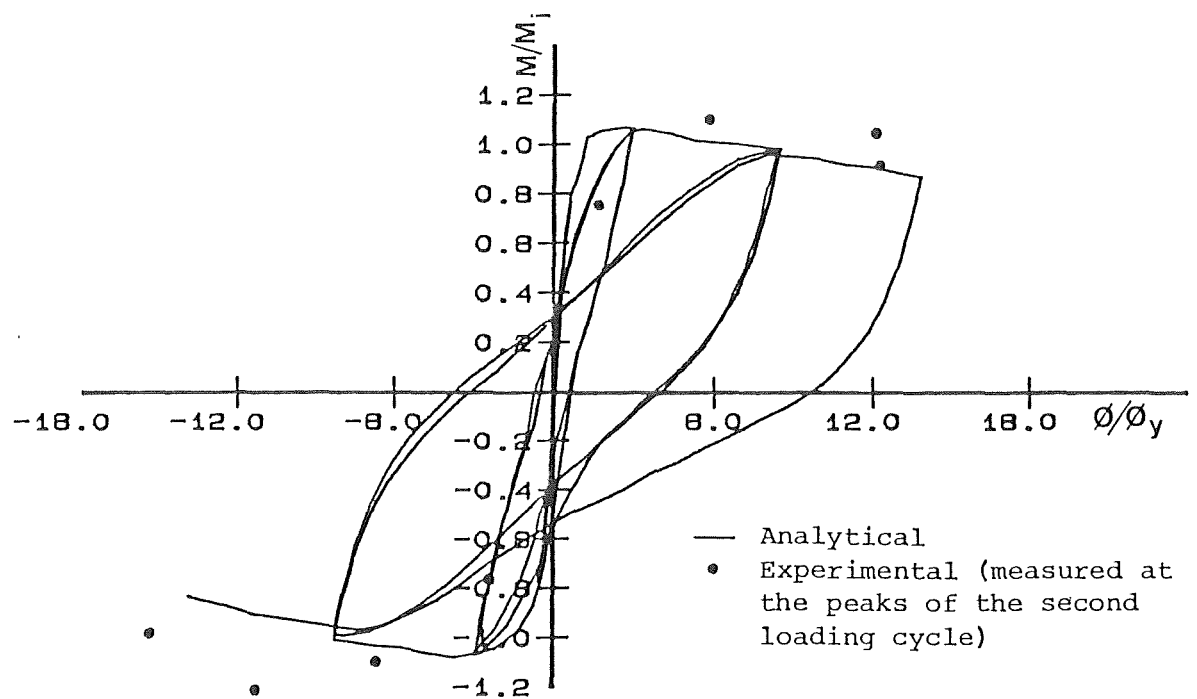


Fig. 8.6 : ANALYTICAL CYCLIC MOMENT-CURVATURE CURVE AND MEASURED VALUES FOR UNIT 3

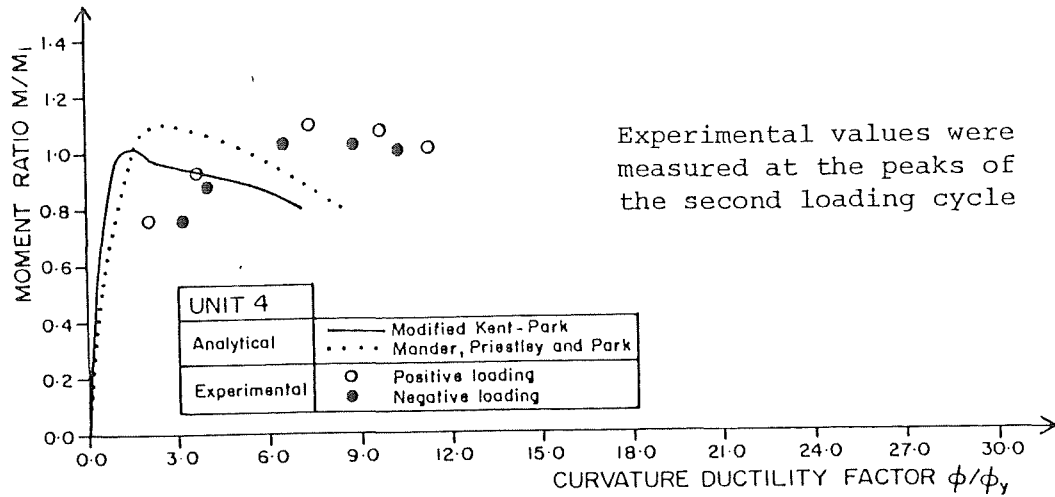


Fig. 8.7 : ANALYTICAL MONOTONIC MOMENT-CURVATURE CURVES AND MEASURED VALUES FOR UNIT 4

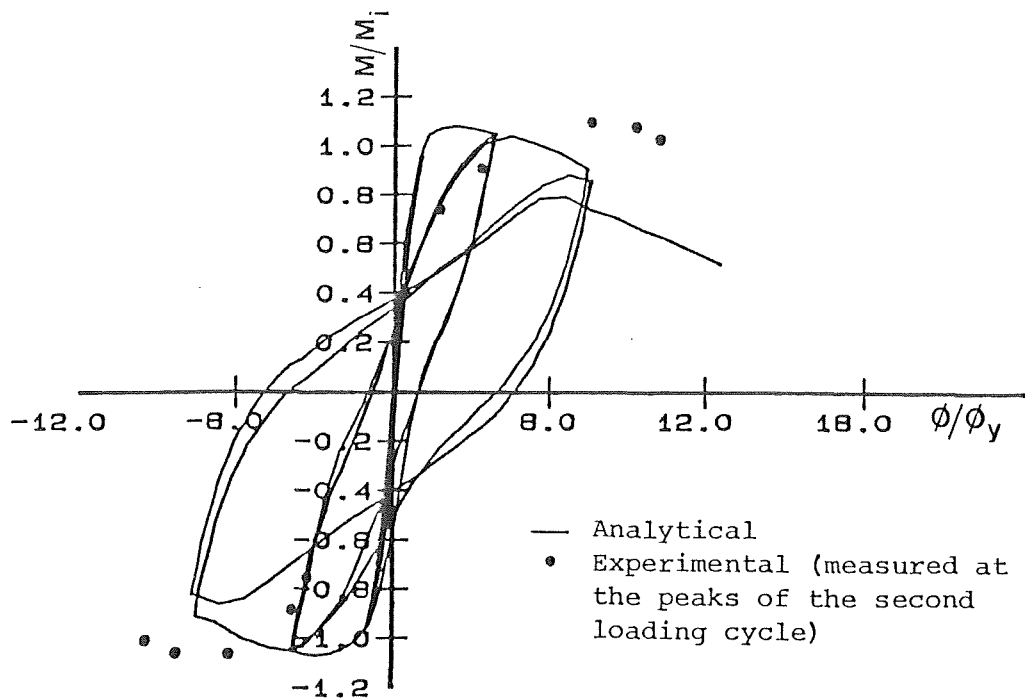


Fig. 8.8 : ANALYTICAL CYCLIC MOMENT-CURVATURE CURVE AND MEASURED VALUES FOR UNIT 4

Table 8.1 : YIELD CURVATURES AND YIELD DISPLACEMENTS FOR UNITS 1 TO 4

Unit	Experimental		Theoretical					
			Monotonic moment-curvature analyses				Cyclic moment-curvature analysis	
	ϕ_y	Δ_y	Kent and Park with modifications		Mander, Priestley and Park		ϕ_y	Δ_y
			ϕ_y	Δ_y	ϕ_y	Δ_y		
1	10.14×10^{-3}	10.70	11.1×10^{-3}	9.47	12.2×10^{-3}	10.41	10.16×10^{-3}	8.96
2	11.10×10^{-3}	9.92	10.1×10^{-3}	8.62	10.7×10^{-3}	9.13	10.00×10^{-3}	8.24
3	8.0×10^{-3}	8.96	11.1×10^{-3}	9.47	11.8×10^{-3}	10.07	10.42×10^{-3}	9.13
4	8.80×10^{-3}	9.40	11.2×10^{-3}	9.56	11.5×10^{-3}	9.81	10.14×10^{-3}	10.02

(a) ϕ_y in rad/m units

(b) Δ_y in mm units

obtained from the tests are compared with the theoretical values obtained using the procedure described in Section 5.6.

The yield displacement obtained from the monotonic moment-curvature analyses^(21,18,22,3) consisted of the flexural displacement which was calculated assuming an equivalent triangular distribution of the curvatures along the column. In the cyclic moment-curvature analysis⁽³⁾, the deformation due to shear was added to the flexural deformation in calculating the yield displacement. Both the uncracked and cracked section shear stiffness at first yield were assessed from which the shear displacements were estimated. Good agreement between the theoretical and experimental values is shown in Table 8.1.

8.2.4 Ultimate Curvature and Available Curvature Ductility Factor

As defined earlier, the measured ultimate curvatures for the columns tested were taken as the curvatures when the measured flexural strength of the columns had reduced to not less than 80% of the theoretical ideal strength in the second loading cycle to that displacement ductility factor. The measured ultimate curvatures ϕ_u and the available curvature ductility factors ϕ_u/ϕ_y , measured in the first and second potentiometer levels, were given in Table 7.1b, and for convenience are restated as Table 8.2. For comparison, the theoretical values of ϕ_u and ϕ_u/ϕ_y calculated from the monotonic^(21,18,22,3) and cyclic moment-curvature analyses⁽³⁾, and ϕ_u/ϕ_y obtained from the design charts for ductility⁽²⁴⁾ (see Appendix B.1), are listed as well.

It is clearly shown in Table 8.2 that the ultimate curvatures measured at the second potentiometer level were larger than those measured at the first level. This difference was due to the additional confining effect provided by the central stub in the regions of the column immediately above and below the stub.

Unit 1 reached the largest measured value of ϕ_u . This column had the lowest level of axial load and hence only a small proportion of the flexural strength is carried by the concrete. Thus the flexural capacity was well-maintained at high curvatures.

In general the measured ultimate curvatures in Units 2, 3 and 4 were less than that in Unit 1. This would be because the available curvature ductility of a column decreases as the applied axial load level increases and because the quantities of confining steel were less than the code recommended amounts.

Table 8.2 : ULTIMATE CURVATURES AND AVAILABLE CURVATURE DUCTILITY FACTORS FOR UNITS 1 TO 4

Unit	Experimental				Theoretical						
	Measured at the first potentiometer level		Measured at the second potentiometer level		Monotonic moment-curvature analyses				Cyclic moment-curvature analysis		Design charts for ductility
	ϕ_u	ϕ_u/ϕ_y	ϕ_u	ϕ_u/ϕ_y	Kent and Park with modifications		Mander, Priestley and Park		ϕ_u	ϕ_u/ϕ_y	ϕ_u/ϕ_y
					ϕ_u	ϕ_u/ϕ_y	ϕ_u	ϕ_u/ϕ_y			
1	0.2014	19.9	0.2426	23.9	> 0.3	> 30	> 0.3	> 30	> 0.3	> 30	No apparent limits
2	0.1981	17.9	0.3124	28.1	0.1858	16.7	0.2996	24.5	0.2013	20.1	20.8
3	0.1280	16.0	0.1428	17.8	0.1034	9.3	0.1483	12.6	0.1411	13.9	10.7
4	0.0982	11.2	0.1185	13.5	0.0771	6.9	0.0778	6.8	0.0776	7.7	4.0

(a) ϕ_u in rad/m units.

It is well known that the presence of closely spaced transverse reinforcement in a column results in a substantial increase in both the strength and the ductility of the column. Therefore, the lowest values of the maximum curvature and the available curvature ductility were observed in Unit 4 which contained the least amount of transverse hoops.

The theoretical ultimate curvature can be defined as the smallest of the following limiting curvatures⁽⁶⁾:

- when the flexural capacity dropped to 80 percent of the ideal flexural strength,
- when the first transverse hoops fractured,
- when the longitudinal bars reached the fracture strain.

For Unit 1, none of these limitations governed, therefore no apparent limits existed to define the theoretical ultimate curvature. For Units 2 to 4, the first limitation governed the magnitude of the theoretical ultimate curvatures. These theoretical ultimate curvatures ϕ_u are shown in Table 8.2 for Units 1 to 4.

For Unit 2, reasonably good agreement was achieved between the theoretical prediction for ϕ_u and the experimental results, although the monotonic moment-curvature analysis using the Modified Kent-Park stress-strain curve for concrete underestimated the experimental results.

For Units 3 and 4, which contained small quantities of transverse reinforcement, the theoretical predictions for ϕ_u indicated overly conservative values for these values and the available curvature ductility factors.

8.2.5 Flexural Overstrength Factor

The actual flexural overstrength factors M_{\max}/M_i obtained from the tests were 1.11, 1.20, 1.18 and 1.17 for Units 1, 2, 3 and 4, respectively, where M_{\max} is the maximum measured moment capacity and M_i is the theoretical (ideal) flexural strength based on the measured yield strength neglecting strain hardening and the measured concrete compressive strength neglecting the effect of confinement.

For the columns tested, the moment enhancement was mostly due to the increase in concrete compressive strength due to confinement and the additional steel strength due to strain hardening. Obviously, Unit 2 which contained the largest amount of the confining steel reached the highest flexural overstrength factor.

In the case of Unit 1, which had the lowest axial load level, the smallest flexural enhancement was achieved, since the flexural strength of the column was less dependent on the contribution of the compressed concrete. Thus, the effect of the confining steel to enhance the concrete strength was insignificant and could be ignored.

The actual flexural overstrength factors are compared in Fig. 8.9 with the empirical expressions for the flexural overstrength factor developed by Ang et al^(25,6) given by

$$\text{For } \frac{P_e}{\phi f'_c A_g} < 0.1 : \frac{M_{\max}}{M_i} = 1.13 \quad (8.1a)$$

$$\text{For } \frac{P_e}{\phi f'_c A_g} \geq 0.1 : \frac{M_{\max}}{M_i} = 1.13 + 2.35 \left(\frac{P_e}{\phi f'_c A_g} - 0.1 \right)^2 \quad (8.1b)$$

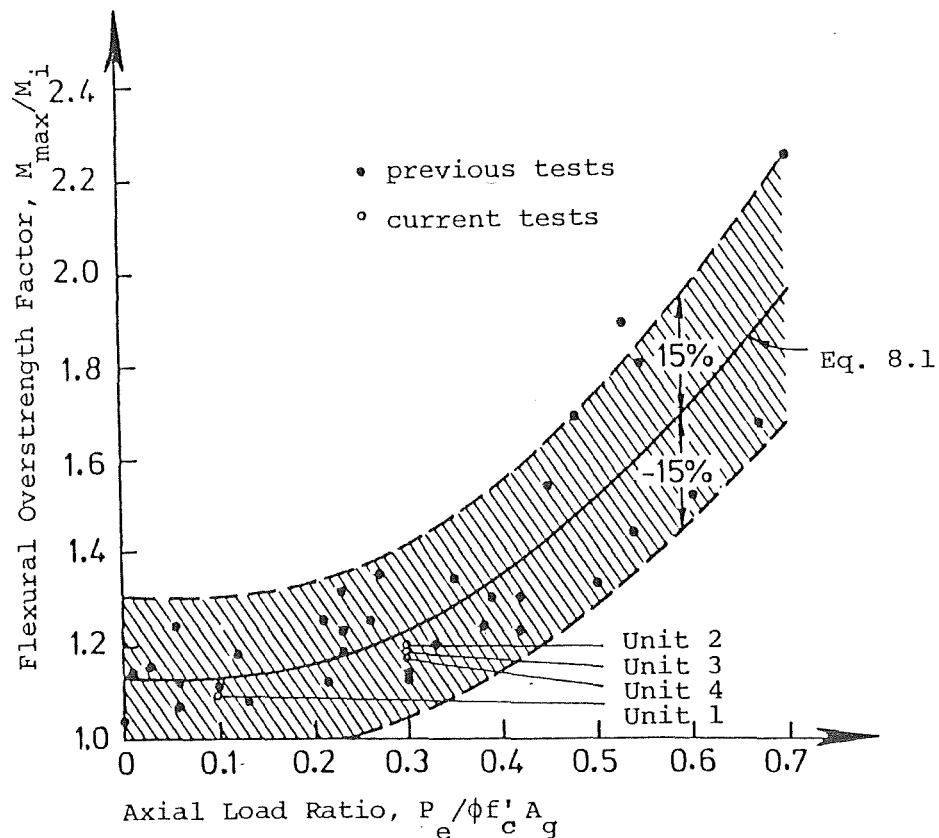


Fig. 8.9 : RELATIONSHIP BETWEEN FLEXURAL OVERSTRENGTH FACTOR AND AXIAL LOAD LEVELS, DEVELOPED BY ANG^(25,6)

Table 8.3 : IDEAL FLEXURAL STRENGTHS AND FLEXURAL OVERSTRENGTH FACTORS FOR UNITS 1 TO 4

Unit	Code approach ideal flexural strength M_i (kNm)	Flexural Overstrength Factor M_{max}/M_i					
		Actual (b) $\frac{M_{max}}{M_i}$	Using empirical expression Eq. 8.1	Using moment-curvature analyses to obtain M_{max} (c)			
				Monotonic moment-curvature		Cyclic moment- curvature	Design charts for flexural strength
				Kent and Park with modifi- cations	Mander, Priestley and Park		
1	302	1.11	1.13	1.09	1.09	1.03	1.10
2	405	1.20	1.22	1.04	1.05	1.07	1.10
3	406	1.18	1.22	1.03	1.06	1.07	1.10
4	383	1.17	1.22	1.02	1.06	1.08	1.10

(a) M_i calculated using measured f_y and f'_c and using code approach⁽²⁾

(b) M_{max} is maximum moment capacity measured in tests

(c) Calculated using as M_{max} the maximum theoretical moment obtained by those analyses.

The flexural overstrength factor given by Eq. 8.1 was found to be 1.13 for Unit 1 and 1.22 for Units 2, 3 and 4. Very good agreement with the actual flexural overstrength factors was achieved for Units 1 and 2 and reasonable agreement for Units 3 and 4. However, it should be noted that Eq. 8.1 was derived empirically for columns which contained close to the code recommended quantity of confining reinforcement and that Units 3 and 4 contained significantly less than the code quantity. Nevertheless, as with the previous tests, the measured flexural overstrength factors for all units tested fall within 15 percent of Eq. 8.1 (see Fig. 8.9).

Table 8.3 summarizes the ideal flexural strength M_i calculated using the concrete design code NZS 3101:1982⁽²⁾ approach, the actual (measured) flexural overstrength factor, and the flexural overstrength factor predicted from the empirical expression Eq. 8.1, for all test units.

For comparison, the theoretical flexural overstrength factors calculated using as M_{\max} the maximum theoretical moments obtained from the monotonic^(21,18,22,3) and cyclic moment-curvature⁽¹³⁾ analyses, and those obtained from the design charts for flexural strength⁽²⁴⁾, (see Appendix B.2), are also listed in Table 8.3. Clearly, the moment-curvature analyses predicted smaller overstrength factors than those measured in the tests.

8.2.6 Lateral Load-Displacement Hysteresis Loops

The theoretical lateral load-displacement hysteresis loops obtained from the cyclic moment-curvature analysis⁽³⁾ using the computer program COLUMN are compared with the experimental results in Figs. 8.10 to 8.17. Shown on the hysteresis loops are sloping dashed lines representing the theoretical ideal column flexural strengths M_i calculated for the measured f_y and f'_c values using the code approach.

Figs. 8.10 and 8.11 compare the experimental and analytical lateral load-displacement hysteresis loops for Unit 1. The general shape of the experimental hysteresis loops was predicted satisfactorily. However, some minor discrepancies are evident, i.e. larger displacements were predicted at the zero lateral loads than those observed during testing. The analytical model was not able to predict the significant strength degradation observed during the last stage of the testing.

The experimental and analytical lateral load-displacement hysteresis loops for Unit 2 are illustrated in Figs. 8.12 and 8.13, respectively. The general shape of the experimental hysteresis loops was predicted satisfactorily up to moderate displacement levels of $\mu_n = \pm 4$, but at

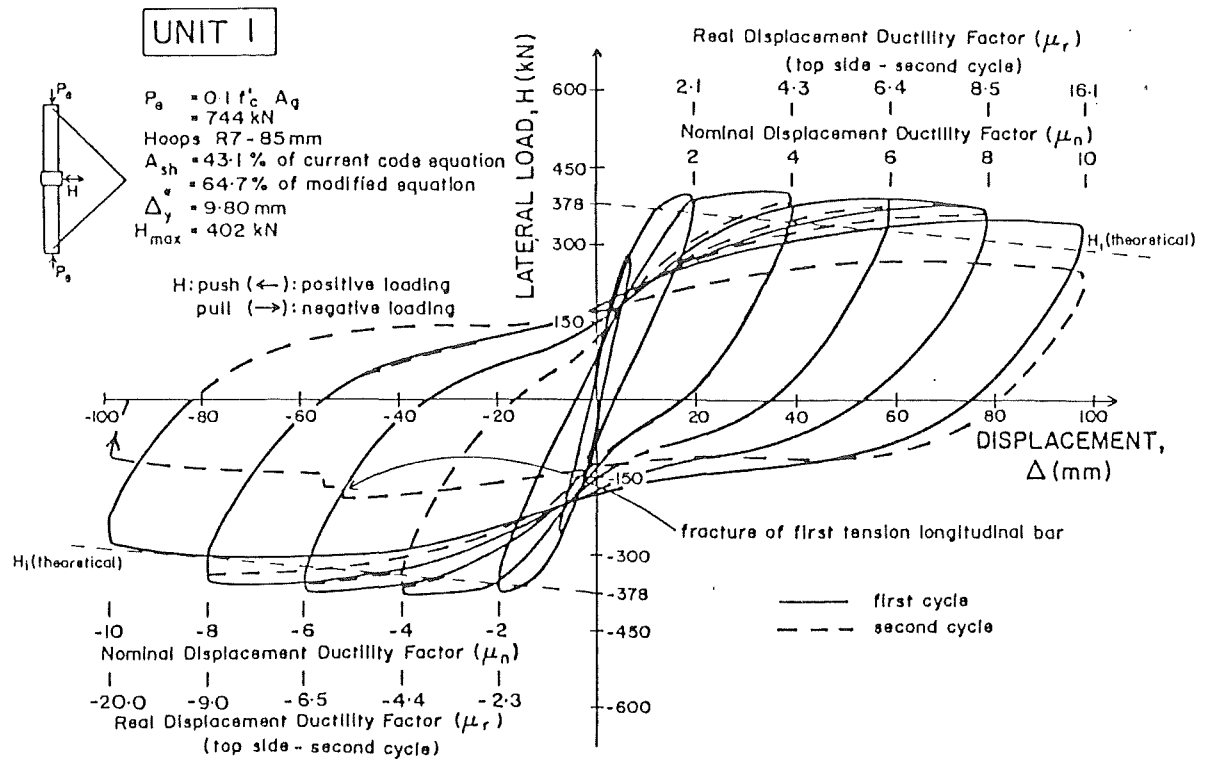


Fig. 8.10: EXPERIMENTAL LATERAL LOAD-DISPLACEMENT HYSTERESIS LOOPS FOR UNIT 1

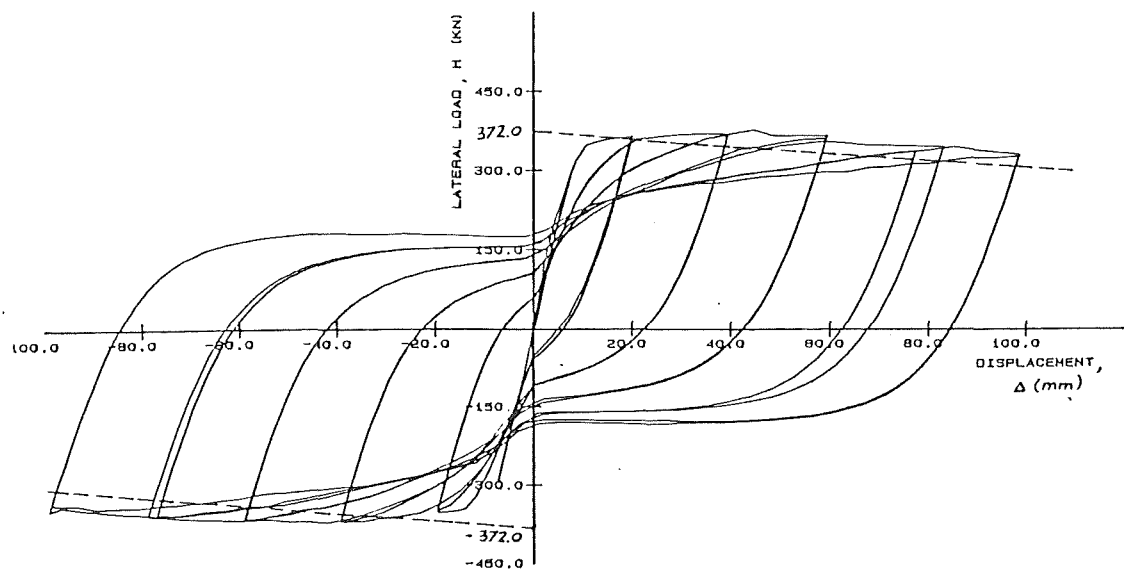


Fig. 8.11 : ANALYTICAL LATERAL LOAD-DISPLACEMENT HYSTERESIS LOOPS FOR UNIT 1

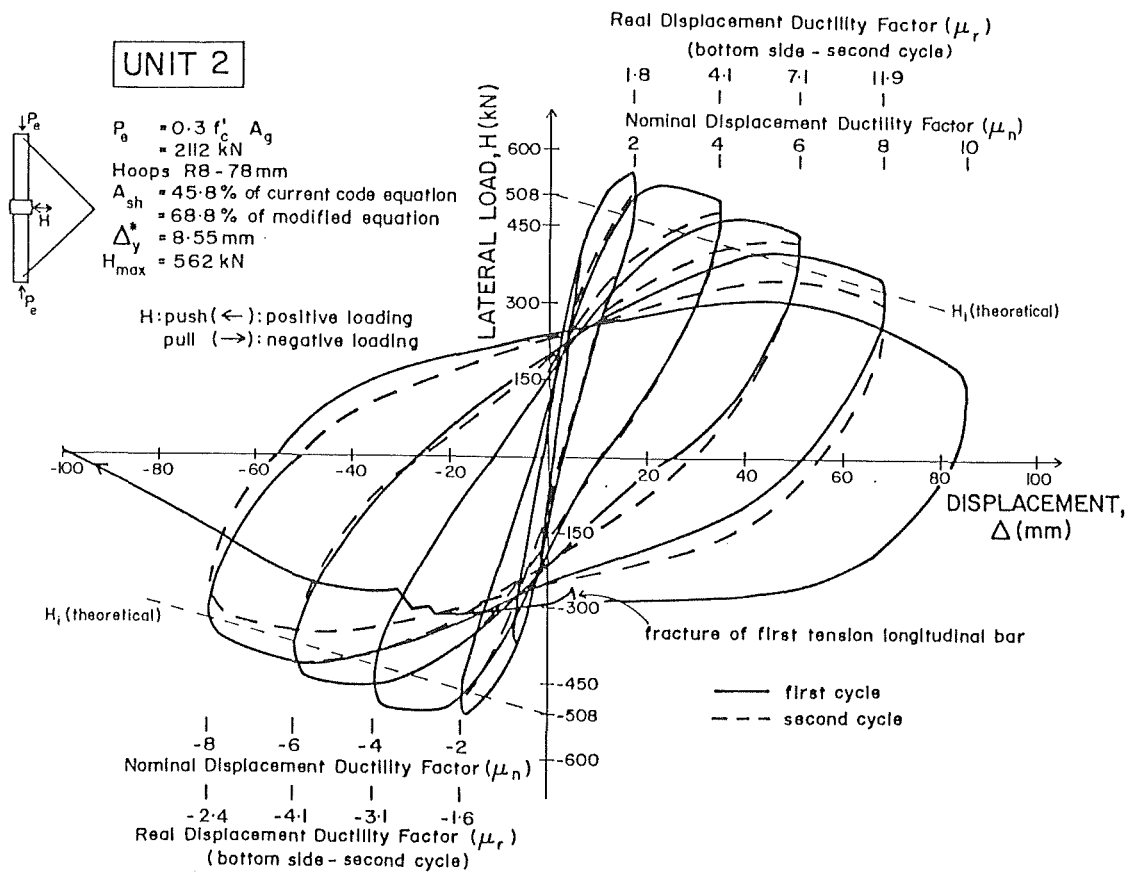


Fig. 8.12 : EXPERIMENTAL LATERAL LOAD-DISPLACEMENT HYSTERESIS LOOPS FOR UNIT 2

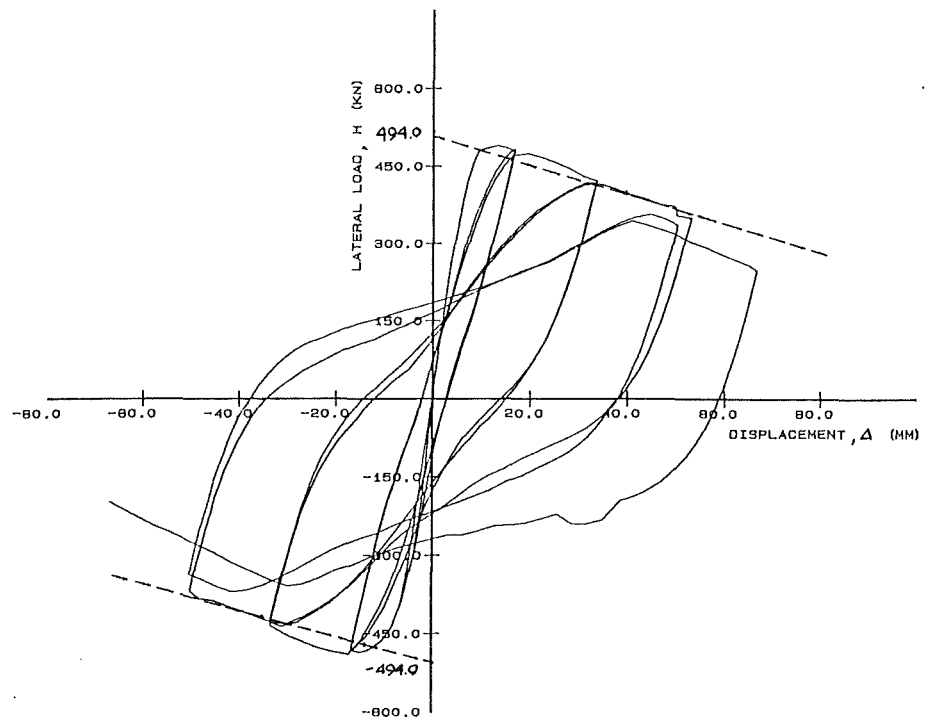


Fig. 8.13 : ANALYTICAL LATERAL LOAD-DISPLACEMENT HYSTERESIS LOOPS FOR UNIT 2

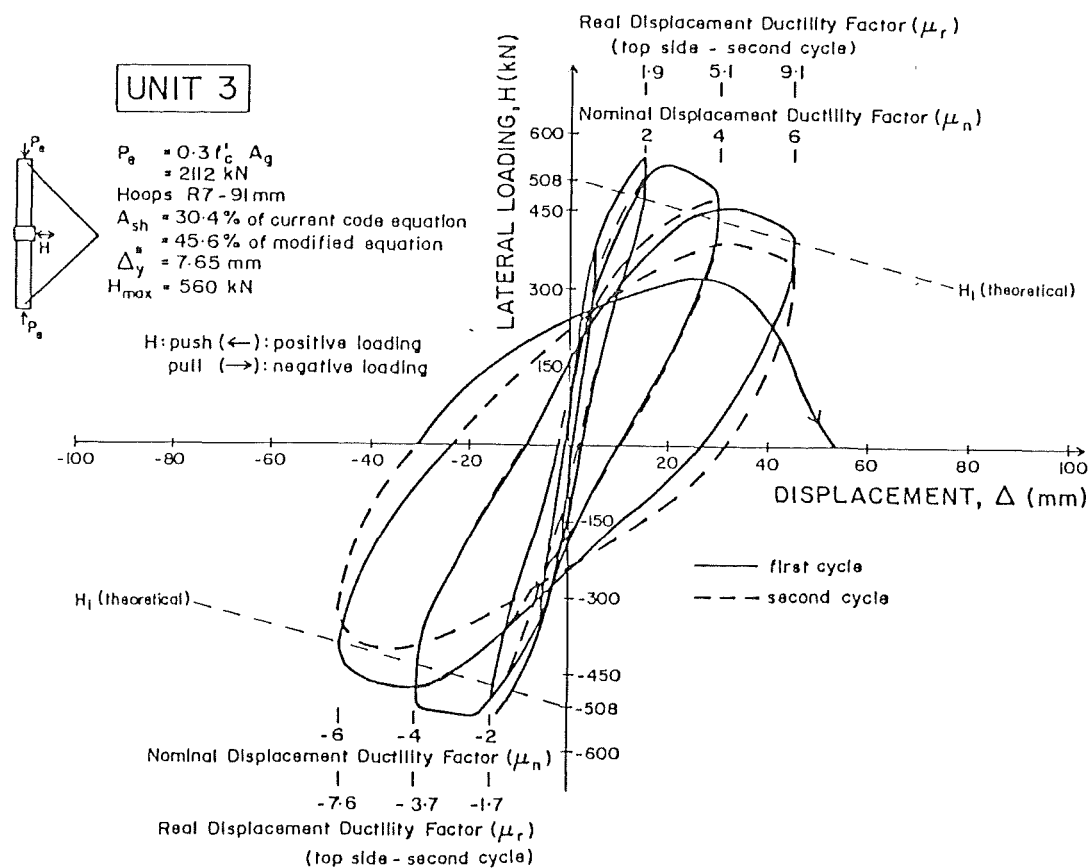


Fig. 8.14 : EXPERIMENTAL LATERAL LOAD-DISPLACEMENT HYSTERESIS LOOPS FOR UNIT 3

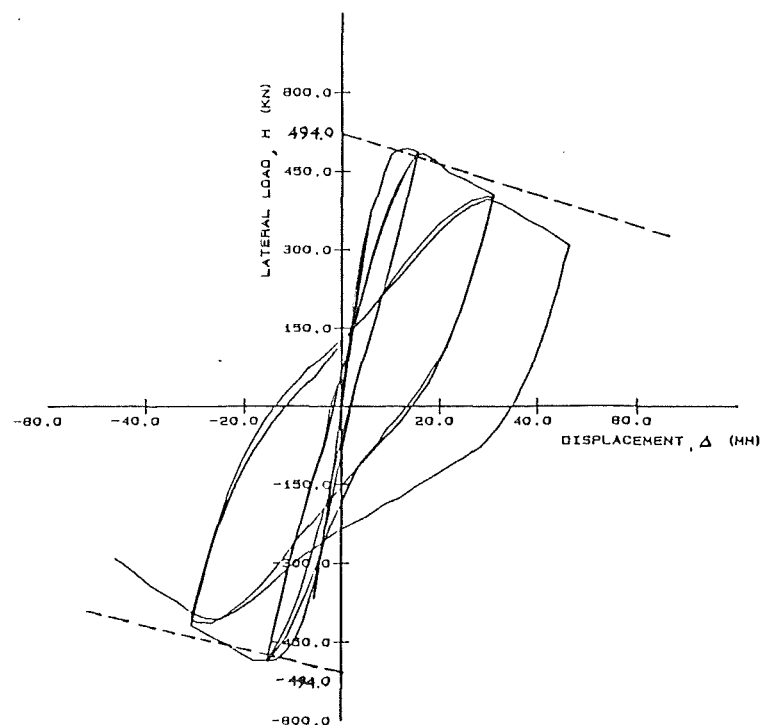


Fig. 8.15 : ANALYTICAL LATERAL LOAD-DISPLACEMENT HYSTERESIS LOOPS FOR UNIT 3

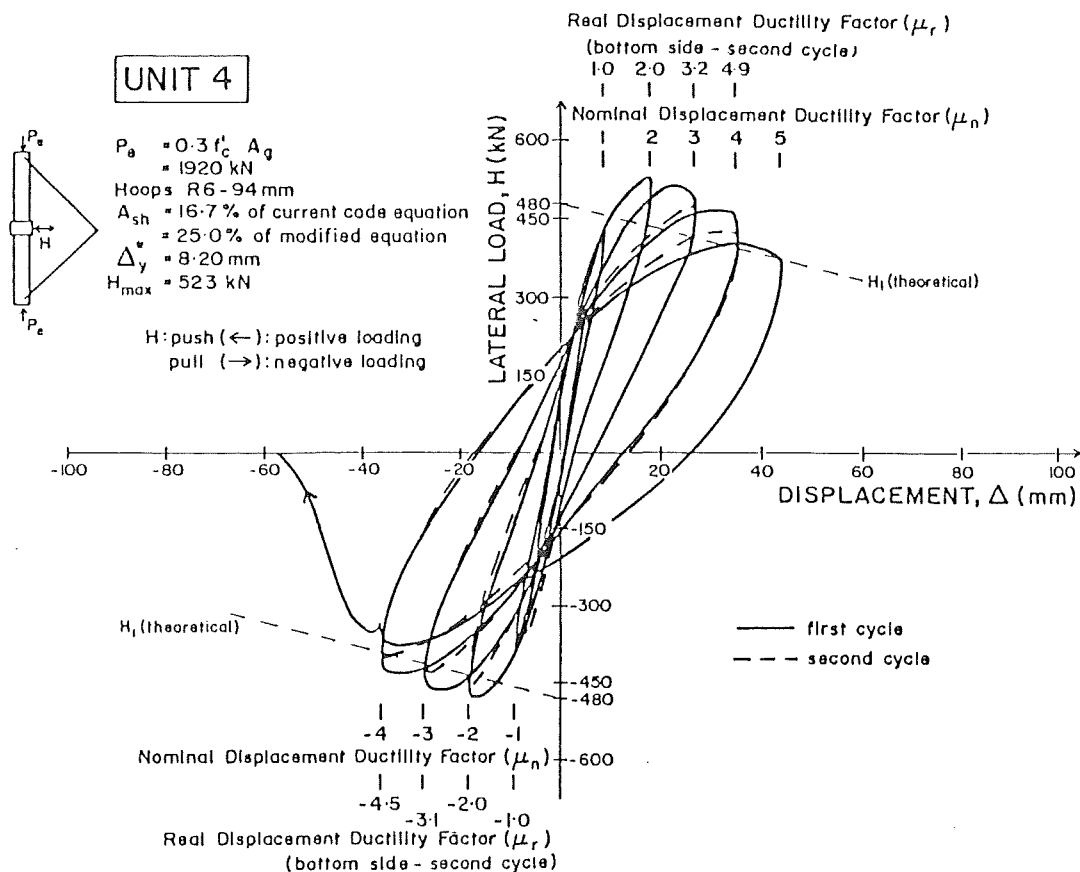


Fig. 8.16 : EXPERIMENTAL LATERAL LOAD-DISPLACEMENT HYSTERESIS LOOPS FOR UNIT 4

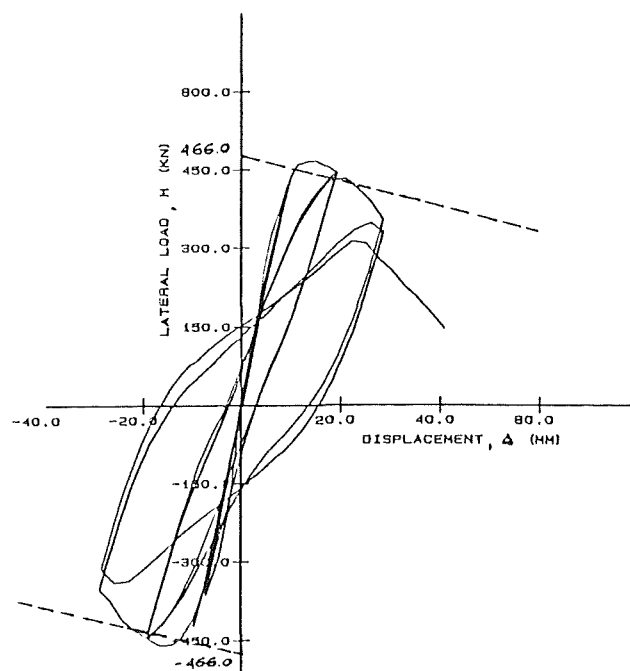


Fig. 8.17 : ANALYTICAL LATERAL LOAD-DISPLACEMENT HYSTERESIS LOOPS FOR UNIT 4

higher displacement levels the predicted strength degradation occurred more rapidly than that was observed. An attempt to reach higher displacements than those shown in Fig. 8.13, led to an unsatisfactory convergence test.

Figs. 8.14 and 8.15 show the experimental and analytical lateral load-displacement hysteresis loops for Unit 3. As with Unit 2 good agreement between the analytical and experimental results was achieved at lower displacement. Beyond a displacement ductility factor of $\mu_n = \pm 2$ the predicted strength degradation occurred more rapidly than observed.

The comparison between the experimental and analytical lateral load-displacement hysteresis loops for Unit 4 are presented in Figs. 8.16 and 8.17. Again reasonably good agreement is indicated up to $\mu_n = \pm 2$, and the strength degradation predicted at higher displacements was greater than observed.

The theoretical lateral load capacity calculated from the computer program COLUMN used for the cyclic moment-curvature analysis was slightly smaller than that used in the calculation of M_1 shown as sloping dashed lines in the Figs. 8.10 to 8.17, because the program deducted the area of steel in compression when calculating the area of compressed concrete.

From the above comparisons it is evident that the theoretical lateral load-deflection hysteresis loops, predicted by the computer program COLUMN, were conservative at high displacements for the columns of this test series which contained lesser amounts of transverse reinforcement than recommended in the code⁽²⁾.

8.2.7 Available Displacement Ductility Factor

Mander et al⁽³⁾ have suggested that the available displacement ductility factor for columns containing less than the quantity of confining steel recommended by the code⁽²⁾ can be expressed by the following empirical relationship

$$\mu = 2 + 6 \frac{A_{sh}(\text{provided})}{A_{sh}(\text{code})} \quad (8.2)$$

where $A_{sh}(\text{provided})$ is the area of hoops provided in the column and $A_{sh}(\text{code})$ is the area recommended by the code.

Ang et al⁽²⁵⁾ have derived the relationship shown in Fig. 8.18 between the ratio of the amount of transverse reinforcement provided in a column to the code⁽²⁾ requirement, $\rho_s/\rho_{s\text{ code}}$, the available displacement ductility factor μ , and the M/VD ratio where M = maximum column moment,

V = column shear and D = column diameter.

The measured available displacement ductility factors for Units 1 to 4 are compared with the theoretical prediction developed by Ang et al^(25,6) and the empirical expression Eq. 8.2 proposed by Mander et al⁽³⁾ in Table 8.4.

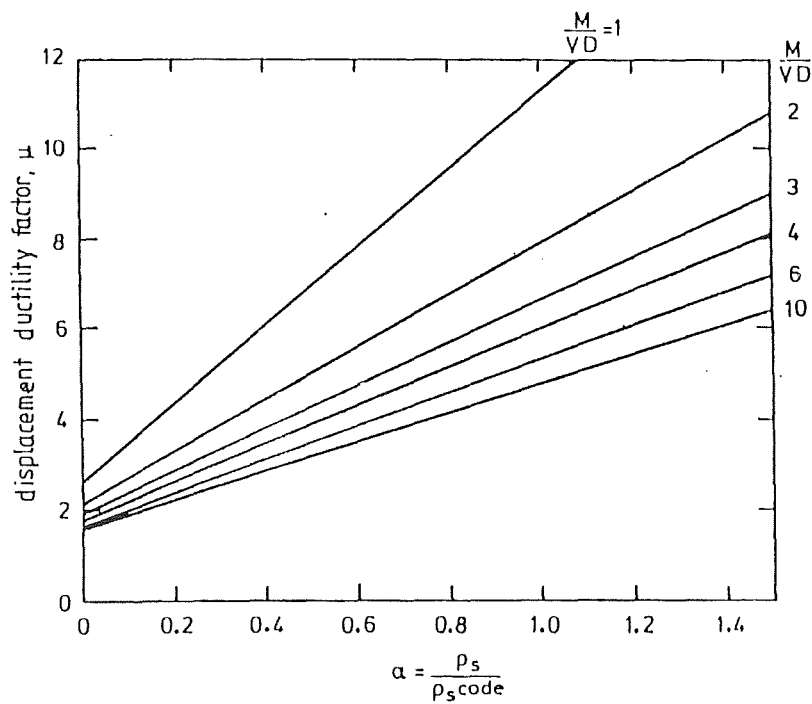


Fig. 8.18 : RELATIONSHIP BETWEEN THE AMOUNT OF TRANSVERSE REINFORCEMENT AND THE DISPLACEMENT DUCTILITY FACTOR DEVELOPED BY ANG ET AL^(25,6)

Table 8.4 : AVAILABLE DISPLACEMENT DUCTILITY FACTORS FOR UNITS 1 TO 4

Unit	$\alpha = \frac{\rho_s}{\rho_{s \text{ code}}}$	Displacement ductility factor			
		Experimental		Theoretical	
		Nominal	Real	Mander et al Eq.8.2	Ang et al Fig. 8.18
1	0.431	8	8.5	4.7	3.7
2	0.458	8	11.9	4.8	3.8
3	0.304	6	9.1	3.8	3.2
4	0.167	4	4.9	3.0	2.5

Note: For all units $M/VD = 4.0$.

It can be seen that both of the theoretical predictions are overly conservative. Ang et al⁽²⁵⁾ derived the relationship given in Fig. 8.18 by conservatively assuming that a displacement ductility factor of 6 is achieved for a column with an aspect ratio of $M/VD = 4$ containing the transverse reinforcement recommended by the code⁽²⁾. Also, an ultimate compression strain of 0.004 for unconfined concrete was assumed. The empirical equation proposed by Mander et al⁽³⁾ simply assumed that the available displacement ductility factor varies linearly between 8 for columns designed in accordance with the code⁽²⁾ provisions and 2 if the column is unconfined.

It should be noted that the experimental displacement ductility factors shown in Table 8.4 are taken as those values found in the column tests when the flexural capacity reduced to not less than 80% of the theoretical ideal strength calculated using the measured f_y and f'_c values and taking the $P-\Delta$ effect into account.

8.2.8 Maximum Displacement and Maximum Drift

The measured maximum displacements in Units 1 to 4 when the flexural strength of the columns had reduced to not less than 80% of the theoretical ideal strength were 91, 118, 68 and 46 mm, resulting in the maximum drifts of 5.1, 6.6, 3.8 and 2.6 percent, respectively.

The New Zealand loading code, NZS 4203:1984⁽¹⁾ recommends a maximum drift of 1.2% at a displacement ductility factor of 4. Clearly, the maximum drifts achieved in the column tests were much larger than the code⁽¹⁾ limitations, indicating that the actual plastic rotations required in the columns would be less than that occurring during the testing.

8.2.9 Equivalent Plastic Hinge Length

In a reinforced concrete column the equivalent plastic hinge length ℓ_p over which the plastic rotations mostly occur, is affected by the spread of plasticity along the member due to the moment gradient and yield penetration along the longitudinal bars. According to Priestley and Park⁽⁶⁾ the predicted equivalent plastic hinge length can be found from the expression

$$\ell_p = 0.08 + 6 d_b \quad (8.3)$$

where ℓ is the length from the section of maximum moment to the point of contraflexure and d_b is the diameter of the longitudinal reinforcement. Table 8.5 compares the average experimental values of the non-dimensional equivalent plastic hinge length $(\ell_p/h)_{av}$ found for columns Units 1 to 4 with the values predicted by Eq. 8.3. It can be seen that good agreement was found for Units 2 and 3. For Units 1 and 4, the equivalent plastic hinge length predicted by Eq. 8.3 was conservative.

Table 8.5 : EQUIVALENT PLASTIC HINGE LENGTHS FOR UNITS 1 TO 4

Unit	Equivalent plastic hinge length ℓ_p/h	
	Experimental Eq. 7.7	Predicted Eq. 8.3
1	0.26	0.56
2	0.33	0.56
3	0.41	0.56
4	0.26	0.56

8.2.10 Spalling Strain and Maximum Compressive Strain

The concrete compressive strain ϵ_{spall} when spalling of the cover concrete commenced were 0.013, 0.013, 0.008 and 0.012 for Units 1 to 4, respectively.

It is known that the spalling strain is mostly affected by the strength of the concrete, the quantity of transverse reinforcement present, and the levels of axial load applied to the column. The higher the concrete strength and the closer the spacing of the transverse hoops, the sooner the spalling of the concrete commences. Unit 4 which had a lower concrete strength and contained the least transverse reinforcement gave a high spalling strain. Although Unit 1 had the largest concrete

compressive strength, a higher spalling strain was measured. This resulted from the lower axial load applied which delayed the spalling of the cover concrete.

The quantity of transverse hoops provided in Unit 2 was larger than that in Unit 3, but Unit 2 indicated a higher spalling strain. This discrepancy indicates how difficult it is to make precise predictions of the spalling strain. However, the minimum spalling strain measured was 0.008, which is well in excess of the value 0.003 generally used as the extreme fibre strain in flexural strength calculations, and also in excess of 0.004 often assumed in many moment-curvature analyses.

The measured maximum compressive strain ϵ_{cmax} at the edge of the confined concrete core is compared in Table 8.6 with the predicted maximum strains proposed by Scott, Park and Priestley⁽²²⁾ as

$$\epsilon_{cmax} = 0.004 + 0.9 \rho_s \left(\frac{f_{yh}}{300} \right) \quad (8.4)$$

and by Mander. Priestly and Park⁽³⁾ as

$$\epsilon_{cmax} = \epsilon_{spall} + 0.04 (K - 1) \quad (8.5)$$

where $K = f'_{cc}/f'_c$, f_{yh} = yield strength of transverse reinforcement, ρ_s = ratio of volume of transverse reinforcement to volume of concrete core, f'_c = concrete compressive cylinder strength, and f'_{cc} = confined concrete compressive strength (see Eq. 5.17).

Table 8.6 : MAXIMUM COMPRESSIVE STRAINS FOR UNITS 1 TO 4

Unit	ρ_s	K	Measured ϵ_{cmax}	Predicted ϵ_{cmax}		$(\epsilon_{cmax})_{measured}$	
						$(\epsilon_{cmax})_{predicted}$	
				Scott, Park & Priestley Eq. 8.4	Mander, Priestley and Park Eq. 8.5	Eq. 8.4	Eq. 8.5
1	0.0086	1.10	0.050	0.013	0.017	3.1	2.9
2	0.0122	1.15	0.110	0.017	0.019	6.5	5.8
3	0.0080	1.14	0.090	0.013	0.014	6.9	6.4
4	0.0057	1.10	0.030	0.008	0.016	3.8	1.9

Clearly, the ϵ_{cmax} values measured in the tests are much greater than those predicted by Eqs. 8.4 and 8.5. This is mainly because the predictions ignore the enhancement of the strain capacity due to the presence of a strain gradient in the sections of the columns. Moreover, Eq. 8.4 assumed that the spalling strain is 0.004 which was shown to be a

very conservative assumption.

8.3 COMPARISON OF THE PERFORMANCE OF UNITS 1 AND 2 WITH THE COLUMN UNITS TESTED BY ANG ET AL

As mentioned in Section 2.2.2, the overall dimensions and the longitudinal reinforcement provided in the columns tested in this experimental programme were similar to the square columns (i.e. Units SQ3 and SQ4) tested by Ang et al⁽⁷⁾. It is of interest therefore, to compare the performance of Units 1 and 2, which indicated a ductile behaviour during the testing, with that of Units SQ3 and SQ4 tested by Ang et al⁽⁷⁾.

Table 8.7 summarizes the details of the units mentioned above. It can be seen that the quantities of transverse reinforcement in Units SQ3 and SQ4 were about three times of those in Units 1 and 2. The concrete compressive strength of the Units SQ3 and SQ4 were much lower than that of Units 1 and 2.

Table 8.7 : DETAILS OF UNITS 1, 2 AND UNITS SQ3, SQ4

Unit	(a) f'_c (MPa)	$\frac{P_e}{\phi f'_c A_g}$	Longitudinal reinforcement			Transverse reinforcement			
			Dia-meter (mm)	ρ_t	f_y (MPa)	Dia-meter (mm)	f_{yh} (MPa)	Spacing ^(b) (mm)	% of current code ^(c) equation
1	46.5	0.1	HD 16	0.0162	446	R7	364	85	43.1
2	44.0	0.3	HD 16	0.0162	446	R8	360	78	45.8
SQ3	23.6	0.38	HD 16	0.0151	427	R12	320	100	147.7
SQ4	25.0	0.21	HD 16	0.0151	427	R10	280	90	121.7

(a) f'_c measured at the day of testing

(b) spacing of transverse reinforcement in potential plastic hinge regions

$$(c) A_{sh} = 0.12 s_h h'' \frac{f_c}{f_{yh}} \left(0.5 + 1.25 \frac{P_e}{\phi f'_c A_g} \right)$$

The experimental lateral load-displacement hysteresis loops for Units SQ3 and SQ4 are shown in Figs. 8.19 and 8.20 respectively. Compared with the hysteresis loops of Unit 2 in Fig. 8.12, the performance of Unit SQ3 shown in Fig. 8.18 was more satisfactory. As can be seen in Fig. 8.19, up to a nominal displacement ductility μ_n of 10, the

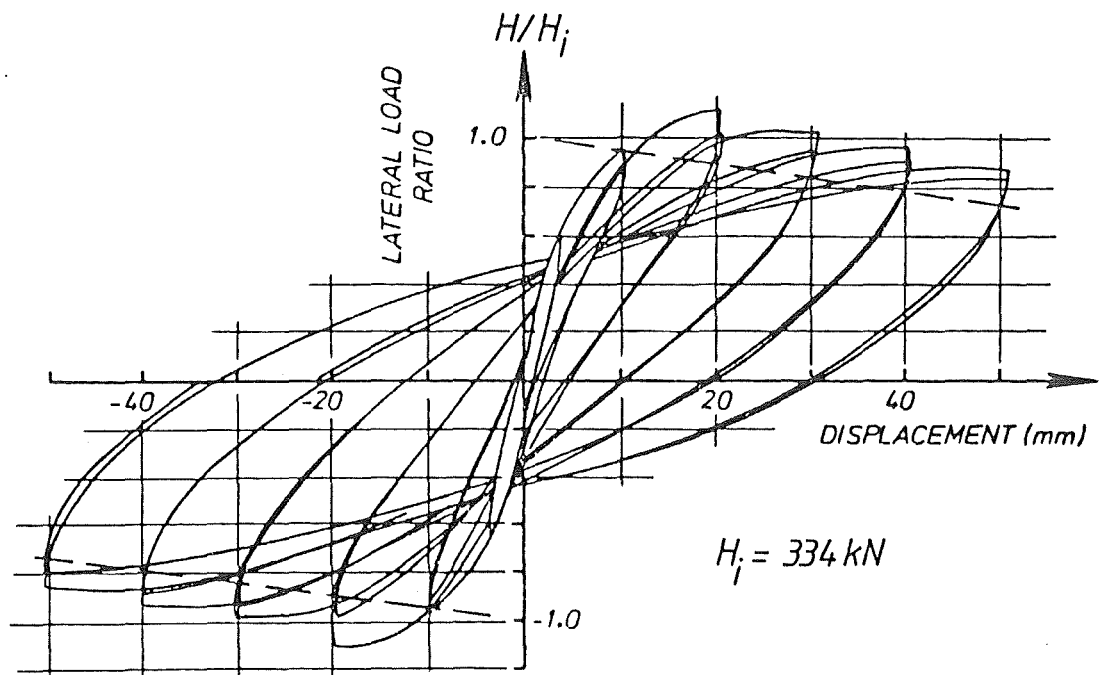


Fig. 8.19 : EXPERIMENTAL LATERAL LOAD-DISPLACEMENT HYSTERESIS
LOOPS FOR UNIT SQ3 TESTED BY ANG ET AL ⁽⁷⁾

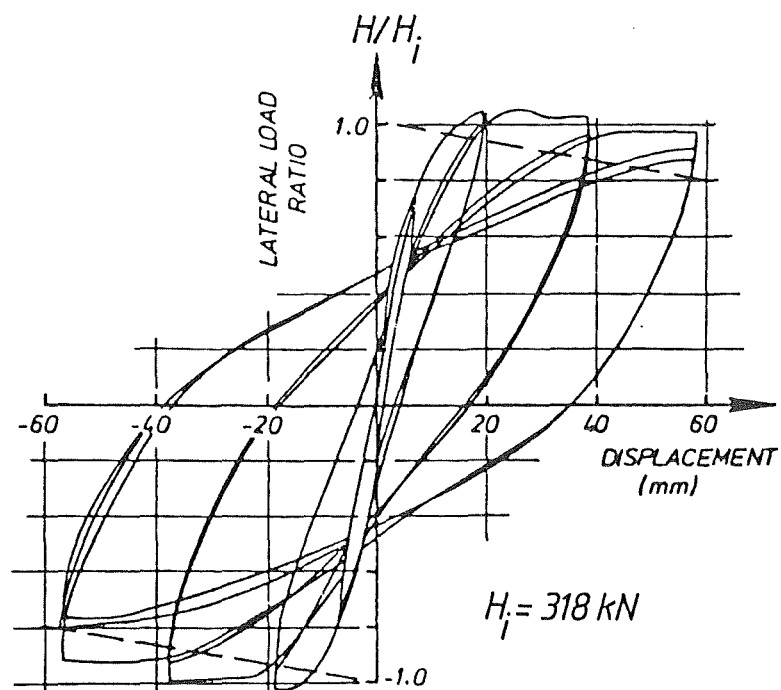


Fig. 8.20 : EXPERIMENTAL LATERAL LOAD-DISPLACEMENT HYSTERESIS
LOOPS FOR UNIT SQ4 TESTED BY ANG ET AL ⁽⁷⁾

Flexural strength of Unit SQ3 was still well in excess of the theoretical ideal column strength. Comparing the performance of Units SQ4 and Unit 1, shown in Figs. 8.20 and 8.10, a reasonably good agreement was shown up to $\mu_n = 6$ although some pinching of the hysteresis loops was pronounced in Unit 1 which was subjected to a lower level of axial load.

Table 8.8 summarizes the experimental values of Δ_y , ϕ_u/ϕ_y , ℓ_p/h , ϵ_{spall} and ϵ_{cmax} for Units 1, 2, SQ3 and SQ4.

Table 8.8 : EXPERIMENTAL VALUES OF Δ_y , ϕ_u/ϕ_y , ℓ_p/h , ϵ_{spall} AND ϵ_{cmax} FOR UNITS 1, 2, SQ3 AND SQ 4

Unit	Δ_y	$\frac{\phi_u}{\phi_y}$	$\frac{\ell_p}{h}$	ϵ_{spall}	ϵ_{cmax}
1	10.7	(a) 20	0.26	0.013	0.050
2	9.9	(a) 18	0.33	0.013	0.110
SQ3	6.6	10	0.74	0.005	0.023
SQ4	9.3	11	0.55	0.008	0.036

(a) Measured at the first potentiometer level.

It should be noted that the values of ϕ_u/ϕ_y and ϵ_{cmax} for Units SQ3 and SQ4 were measured when the tests were terminated at μ_n values of 10 and 6, respectively. The μ_n values applied to Units 1 and 2 were larger and this explains why the ϕ_u/ϕ_y and ϵ_{cmax} values for Units 1 and 2 are greater than for Units SQ3 and SQ4 in Table 8.8.

The equivalent plastic hinge lengths ℓ_p/h for Units SQ3 and SQ4 shown in Table 8.8 are reasonably close to the predicted value of 0.56 given by Eq. 8.3. The spalling strains measured for Units SQ3 and SQ4 were less than those for Units 1 and 2, probably due to the greater quantity of confining steel present in Units SQ3 and SQ4.

8.4 CONCLUDING REMARKS

From the discussion of the experimental and analytical results, the following conclusions can be reached:

- (1) Units 1 and 2, with 43 and 46 percent of the NZS 3101:1982⁽²⁾ recommended quantity of transverse reinforcement, respectively, were

capable of maintaining very stable lateral load-displacement hysteresis loops up to displacement ductility factors of 8. Units 3 and 4 which contained 30 and 17 percent of the code recommended quantity of transverse reinforcement respectively, performed satisfactorily up to displacement ductility factors of 6 and 4 respectively.

(2) The minimum value of the spalling strain observed was 0.008, which indicated the conservative nature of the extreme fibre concrete compressive strain use in many flexural strength calculations (0.003) and in many moment-curvature analyses (0.004).

(3) In general, reasonably good agreement was found between the analytical cyclic moment-curvature predictions and the experimental results for Units 1 and 2. The analytical predictions were found to be overly conservative for Units 3 and 4 at high curvatures.

(4) Compared with the performance of Units SQ3 and SQ4, which contained approximately three times the quantities of transverse reinforcement present in Units 1 and 2, an acceptable performance was exhibited by Units 2 and 1.

CHAPTER NINE

ANALYTICAL INVESTIGATION OF RECTANGULAR COLUMNS
WITH THE PROPOSED MODIFIED CODE QUANTITY OF
TRANSVERSE REINFORCEMENT FOR CONFINEMENT

9.1 INTRODUCTION

Results from the columns tested indicated that square columns with 65 and 69 percent of the proposed modified code quantity of transverse confining reinforcement given by Eq. 4.9, were capable of reaching a displacement ductility factor of at least 8 and an available curvature ductility of about 20.

In this chapter, the applicability of the proposed modified expression, Eq. 4.9, is investigated analytically for rectangular columns. A comparison is made between the analytical moment-curvature response obtained from rectangular columns containing transverse reinforcement as given by the proposed Eq. 4.9 and from circular columns containing spiral steel as given by the code expression (Eq. 4.2).

9.2 MOMENT-CURVATURE ANALYSES FOR RECTANGULAR COLUMNS WITH THE
 QUANTITY OF TRANSVERSE REINFORCEMENT AS GIVEN BY THE MODIFIED
 EQUATION

9.2.1 General Description

The use of Eq. 4.9 is applied to rectangular columns of 600 x 400 mm cross section, subjected to uniaxial bending about the weak axis and different levels of axial load, namely $0.1 f'_c A_g$, $0.3 f'_c A_g$, $0.5 f'_c A_g$ and $0.7 f'_c A_g$ or $0.7 P_o$ whichever is greater, where f'_c is concrete compressive strength, A_g is gross area of column cross section and P_o is ideal axial load compressive strength of column when the load is applied with zero eccentricity.

In this analytical investigation, $f'_c = 30$ MPa, $f_y = 380$ MPa and $f_{yh} = 275$ MPa were assumed. As mentioned in Section 2.2.4, for Eq. 4.9 to be critical, the cover to hoops has to be such that $\frac{A_g}{A_c} < 1.267$ where A_c is area of concrete core of section measured to the outside of peripheral hoop. In the rectangular columns investigated, the cover to the hoops used was 20 mm.

With the bending in the weak axis direction, the modified equation can be rewritten as follows

$$A_{sh} = 0.08 s_h b'' \frac{f'_c}{f_{yh}} \left(0.5 + 1.25 \frac{P_e}{f'_c A_g} \right) \quad (9.1)$$

where $b'' = h''$ in Eq. 4.9.

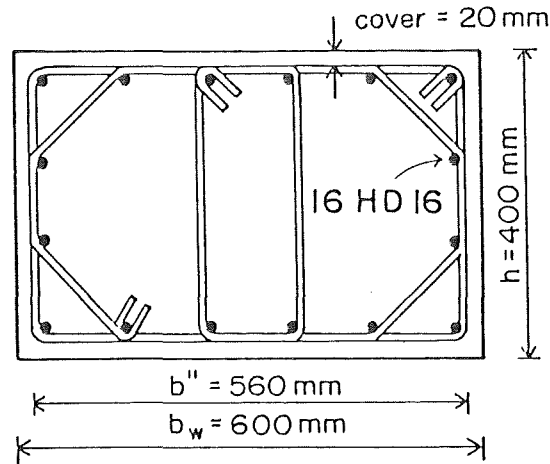


Fig. 9.1 : CROSS SECTION OF RECTANGULAR COLUMNS

The sets of overlapping rectangular and octagonal hoops shown in Fig. 9.1 were used as transverse reinforcement. With this hoop arrangement, the amount of transverse reinforcement in the columns as given by Eq. 9.1 is listed in Table 9.1.

Table 9.1 : AMOUNT OF TRANSVERSE REINFORCEMENT IN THE RECTANGULAR COLUMNS

Unit	Axial load levels		Transverse reinforcement	
	P_e	P_e (kN)	diameter (mm)	spacing (a) s_h (mm)
RECT1	$0.1f'_c A_g$	720	R8	89
RECT2	$0.3f'_c A_g$	2160	R8	63
RECT3	$0.5f'_c A_g$	3600	R10	77
RECT4	$0.7 P_o$	5082	R12	90

(a) spacing of transverse reinforcement in potential plastic hinge regions

(Note: all are less than $6d_b = 6 \times 16 = 96$ mm).

(b) $0.7 P_o$ (= 5082 kN) is greater than $0.7f'_c A_g$ (= 5040 kN)

(c) $\phi = 1$ is assumed in all calculations.

9.2.2 Analytical Moment-Curvature Relationships

Figs. 9.2 to 9.5 show the analytical monotonic moment curvature relationships for the rectangular columns obtained for bending about the weak axis. The analytical cyclic moment-curvature hysteresis loops for the rectangular columns are shown later in Section 9.3. The analytical curves were derived using either the Modified Kent-Park model or the Mander, Priestley and Park model for the stress-strain behaviour of the compressed concrete.

The available curvature ductility factors obtained from the above monotonic and the cyclic moment-curvature analyses^(21,18,22,3), and the design charts for ductility⁽²⁴⁾, are compared in Table 9.2. The ultimate curvature obtained from the monotonic and cyclic moment-curvature analyses was defined as in Section 8.2.4.

Table 9.2 : AVAILABLE CURVATURE DUCTILITY FACTORS FOR
RECTANGULAR COLUMNS

Unit	Available curvature ductility factors ϕ_u/ϕ_y			
	Monotonic moment-curvature		Cyclic moment curvature	Design charts for ductility
	Kent and Park with modification	Mander, Priestley and Park		
RECT 1	> 30	> 30	> 30	No apparent limits
RECT 2	28.5	29.3	> 25	30
RECT 3	14.3	17.2	16.5	18.3
RECT 4	6.0	10.9	12.4	12.3

According to the commentary of the New Zealand concrete design code NZS 3101:1982⁽²⁾ the use of the amount of transverse reinforcement given by Eqs. 4.1 to 4.4 (see Section 4.2.1) in a column will lead to an available curvature ductility factor of up to 18. As can be seen from Table 9.2, the modified equation satisfied this code statement for columns with low to moderate axial load levels (0.1 to $0.3f'_c A_g$). For an axial load level of $0.5f'_c A_g$, the available curvature ductility factors ϕ_u/ϕ_y obtained from the design charts for ductility⁽²⁴⁾ also satisfy this code statement. The ϕ_u/ϕ_y calculated from the moment-curvature analyses are slightly less than 18. For heavily loaded columns ($P_e = 0.7f'_c A_g$ or $0.7P_o$) the use of the modified equation would lead to a curvature ductility factor of significantly

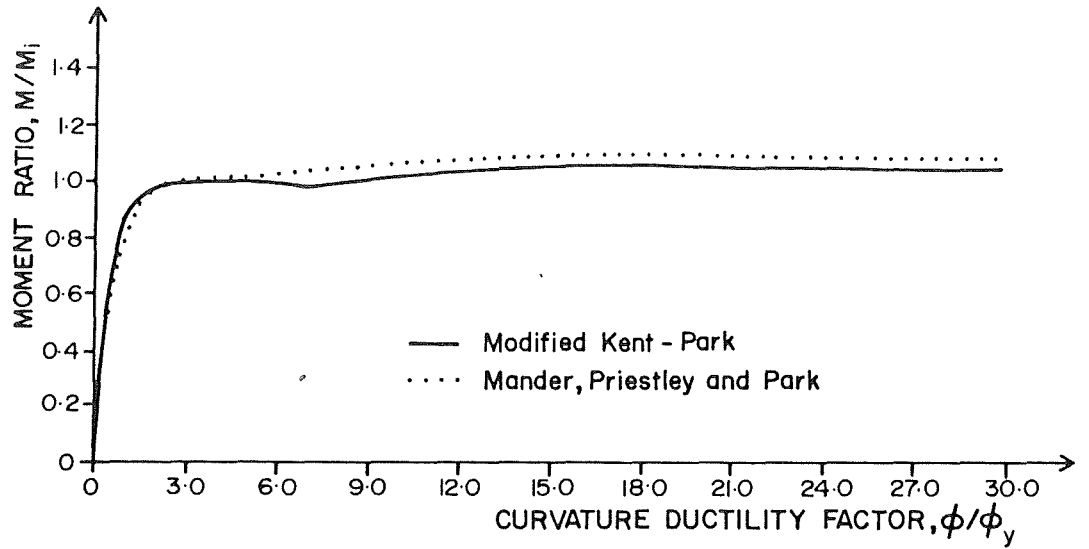


Fig. 9.2 : MONOTONIC MOMENT-CURVATURE CURVES FOR RECTANGULAR
COLUMN RECT 1

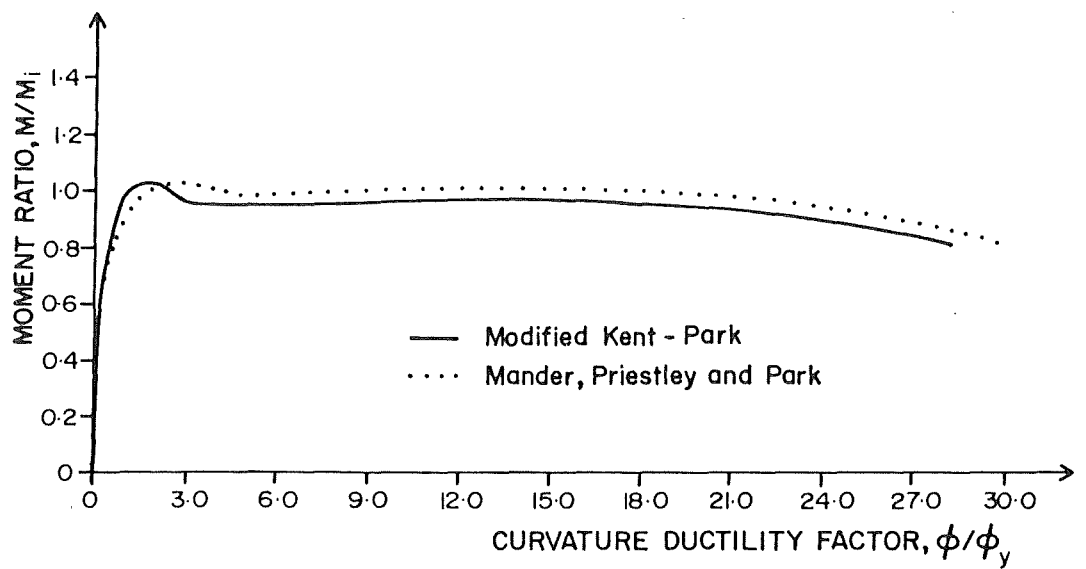


Fig. 9.3 : MONOTONIC MOMENT CURVATURE CURVES FOR RECTANGULAR
COLUMN RECT 2

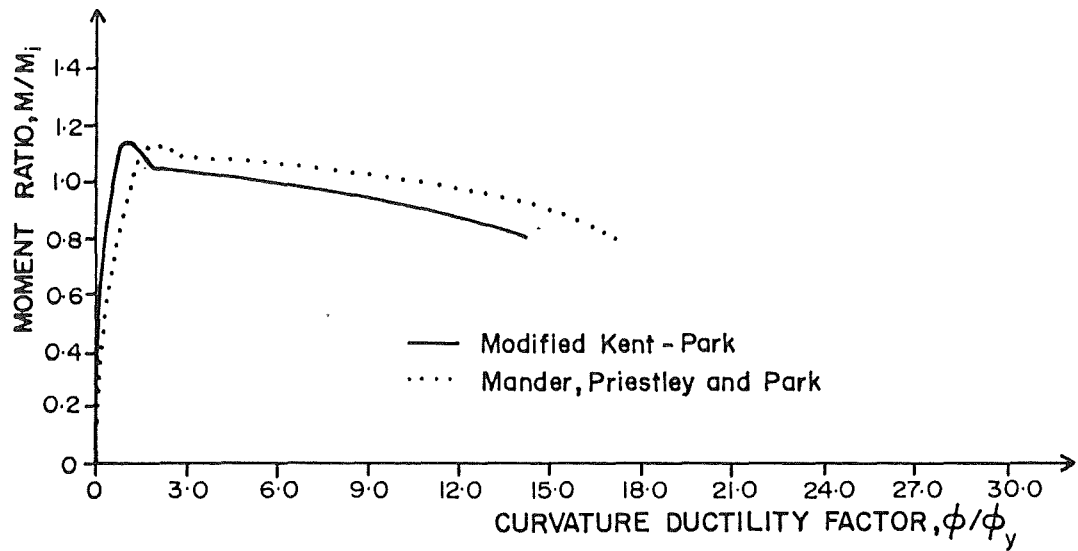


Fig. 9.4 : MONOTONIC MOMENT CURVATURE CURVES FOR RECTANGULAR
COLUMN RECT 3

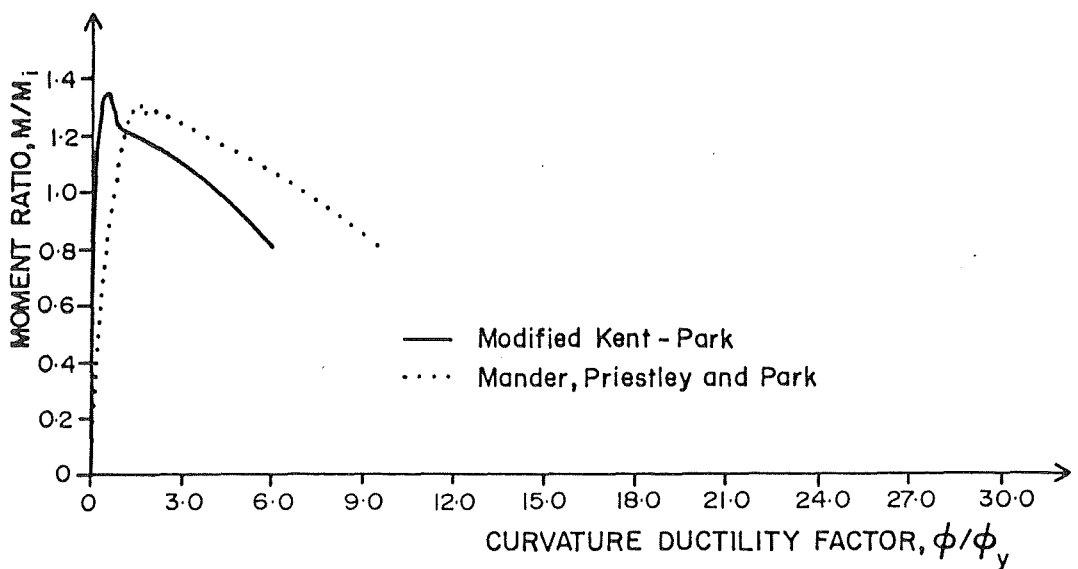


Fig. 9.5 : MONOTONIC MOMENT CURVATURE CURVES FOR RECTANGULAR
COLUMN RECT 4

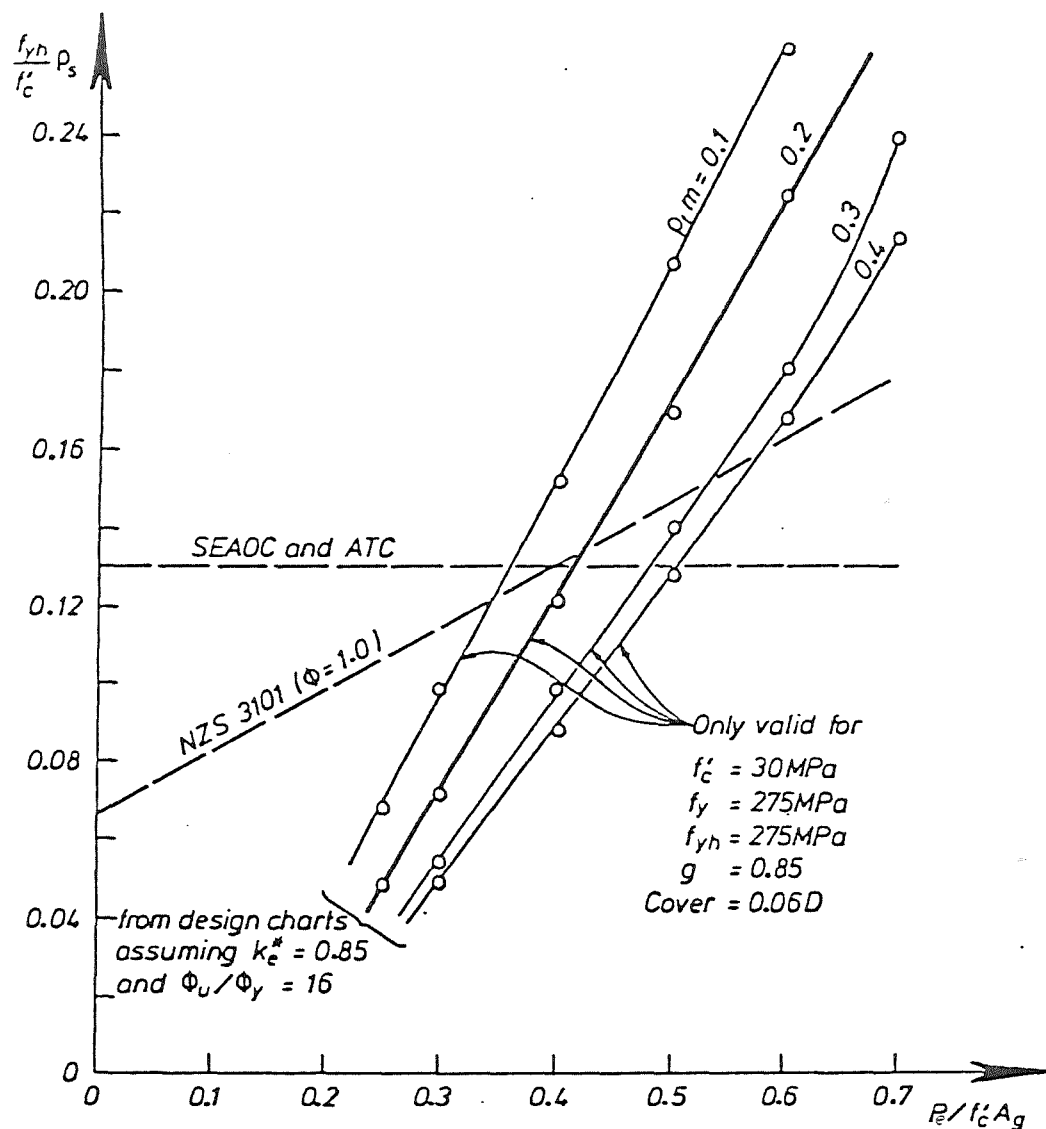


Fig. 9.6 : REQUIRED AMOUNT OF CONFINING STEEL IN THE PLASTIC HINGE REGION OF CIRCULAR COLUMNS DETERMINED BY ZAHN⁽²⁴⁾ AND A COMPARISON WITH THE NZS 3101:1982⁽²⁾ AND SEAOC⁽¹⁴⁾ REQUIREMENTS

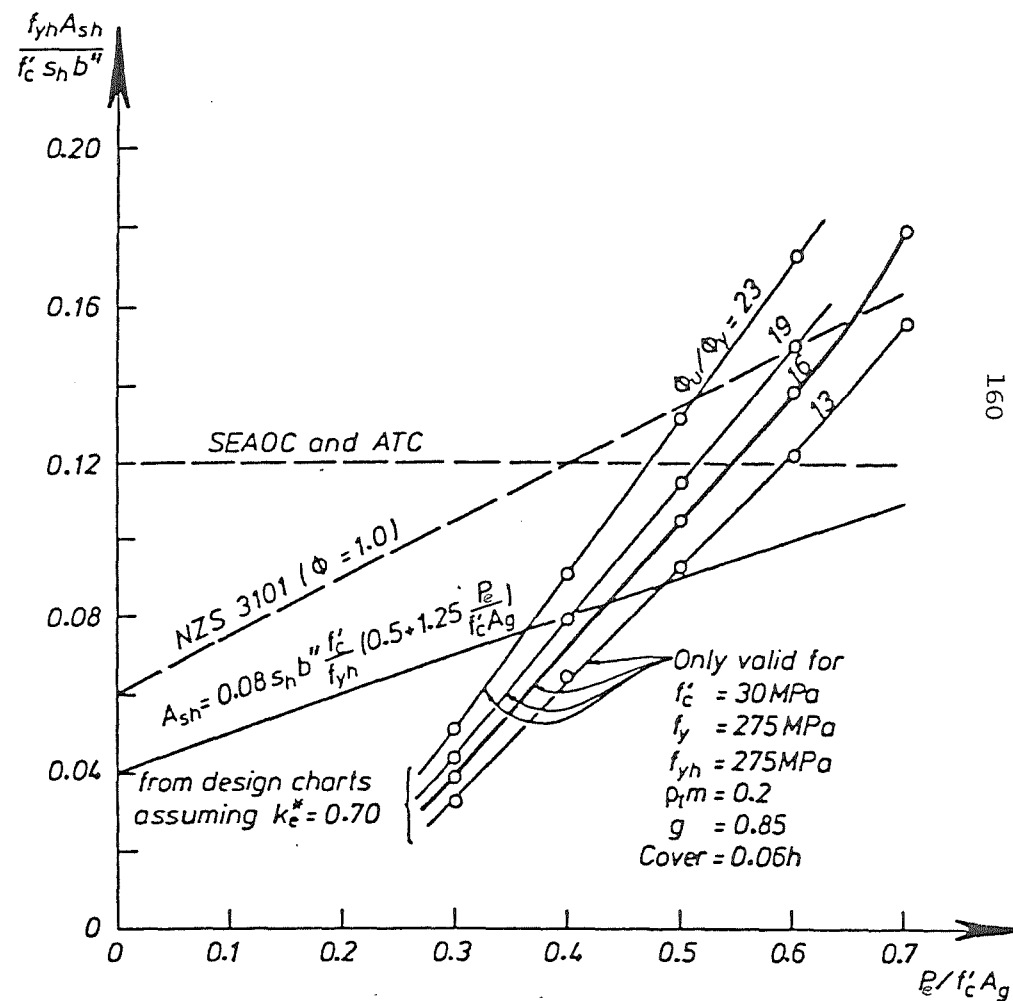


Fig. 9.7 : REQUIRED AMOUNT OF CONFINING STEEL IN THE PLASTIC HINGE REGION OF THE RECTANGULAR COLUMN INVESTIGATED BY ZAHN⁽²⁴⁾ AND A COMPARISON WITH THE NZS 3101:1982⁽²⁾ AND SEAOC⁽¹⁴⁾ REQUIREMENTS

less than 18. However, as has been concluded by Zahn⁽²⁴⁾, the code recommended quantity of transverse reinforcement may also be unconservative for heavily loaded columns, particularly for a small value of mechanical reinforcing ratio $\rho_t m$, where ρ_t = longitudinal steel ratio (A_{st}/A_g) and $m = f_y/0.85f'_c$ (see Figs. 9.6 and 9.7). Therefore, a more appropriate equation for the amount of transverse reinforcement which is more dependent on the levels of axial load than that recommended in the code⁽²⁾ needs to be established. A possible modification would be to use a bi-linear relation for the influence of axial load. That is Eq. 4.9 could be used for low to moderate axial load levels and a more conservative equation for heavily loaded columns (e.g. the curve for $\phi_u/\phi_y = 19$ in Fig. 9.7).

9.3 COMPARISON OF THE ANALYTICAL CYCLIC MOMENT-CURVATURE HYSTERESIS LOOPS AND THE AVAILABLE CURVATURE DUCTILITY FACTORS FOR RECTANGULAR COLUMNS CONTAINING THE PROPOSED MODIFIED CODE VALUE OF TRANSVERSE REINFORCEMENT WITH CIRCULAR COLUMNS CONTAINING THE CODE RECOMMENDED QUANTITY OF SPIRAL CONFINING STEEL

The available curvature ductility factors obtained from the cyclic moment curvature analysis⁽¹⁾ and the design charts for ductility⁽²⁴⁾, for the rectangular columns investigated in Section 9.2 need to be compared to those for circular columns containing the quantities of spiral or circular hoop reinforcement given by Eq. 4.2 (given below as Eq. 9.2) in order to check whether similar ductilities are available.

$$\rho_s = 0.12 \frac{f'_c}{f_{yh}} \left(0.5 + 1.25 \frac{P_e}{\phi f'_c A_g} \right) \quad (9.2)$$

The circular columns were subjected to the same levels of axial load P_e and had the same ideal flexural strength M_i as the rectangular columns. Table 9.3 shows the details of the circular columns. The circular columns had an overall diameter D of 525 mm. For comparison, the details of the rectangular columns and the ideal flexural strength M_i for both columns are listed in Table 9.3 as well.

Figs. 9.8 to 9.15 compare the cyclic moment-curvature hysteresis loops for the rectangular column units RECT 1 to RECT 4 and the circular column units CIRC 1 to CIRC 4. As is evident from Figs. 9.8 and 9.9, the moment-curvature hysteresis loops for Units RECT 1 and CIRC 1 are extremely identical. Figs. 9.10 and 9.11 illustrate the moment-curvature hysteresis loops for Units RECT 2 and CIRC 2. Good agreement is shown, although a slightly greater curvature ductility factor was achieved by Unit RECT 2, indicating that the arrangement of transverse

Table 9.3 : DETAILS OF RECTANGULAR AND CIRCULAR COLUMNS

Unit	Axial load levels		Longitudinal reinforcement		Transverse reinforcement		Ideal flexural strength M_i (kNm)
	P_e	P_e (kN)	Quantity	ρ_t m	Diameter (mm)	Spacing ^(a) s_h (mm)	
RECT 1	$0.1f'_c A_g$	720	16 HD 16	0.20	R8	89	318
CIRC 1	$0.11f'_c A_g$	720	13 HD 16	0.18	R8	50	319
RECT 2	$0.3f'_c A_g$	2160	16 HD 16	0.20	R8	63	437
CIRC 2	$0.33f'_c A_g$	2160	14 HD 16	0.19	R10	54	438
RECT 3	$0.5f'_c A_g$	3600	16 HD 16	0.20	R10	77	423
CIRC 3	$0.55f'_c A_g$	3600	16 HD 16	0.22	R12	60	421
RECT 4	$0.70 P_o$	5082	16 HD 16	0.20	R12	90	315
CIRC 4	$0.74 P_o^{(b)}$	5082	19 HD 16	0.26	R12	48	311

(a) Spacing of transverse reinforcement in the potential plastic hinge regions.

(b) The axial load level is greater than the upper limit recommended in the code⁽²⁾.

(c) Cover to hoops and spirals of 20 mm is used.

(d) $\phi = 1$ is assumed in all calculations.

NOTE: Transverse reinforcement is designed according to Eq. 9.1 for the rectangular columns and to Eq. 9.2 for the circular columns.

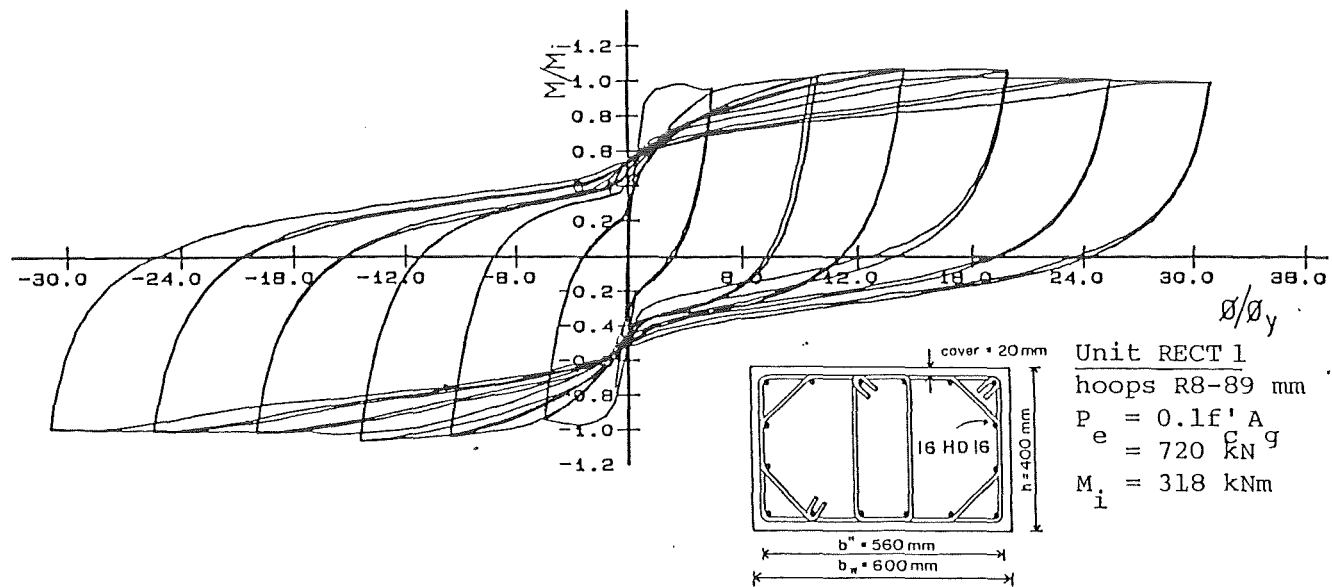


Fig. 9.8 : CYCLIC MOMENT-CURVATURE HYSTERESIS LOOPS FOR RECTANGULAR COLUMN RECT 1

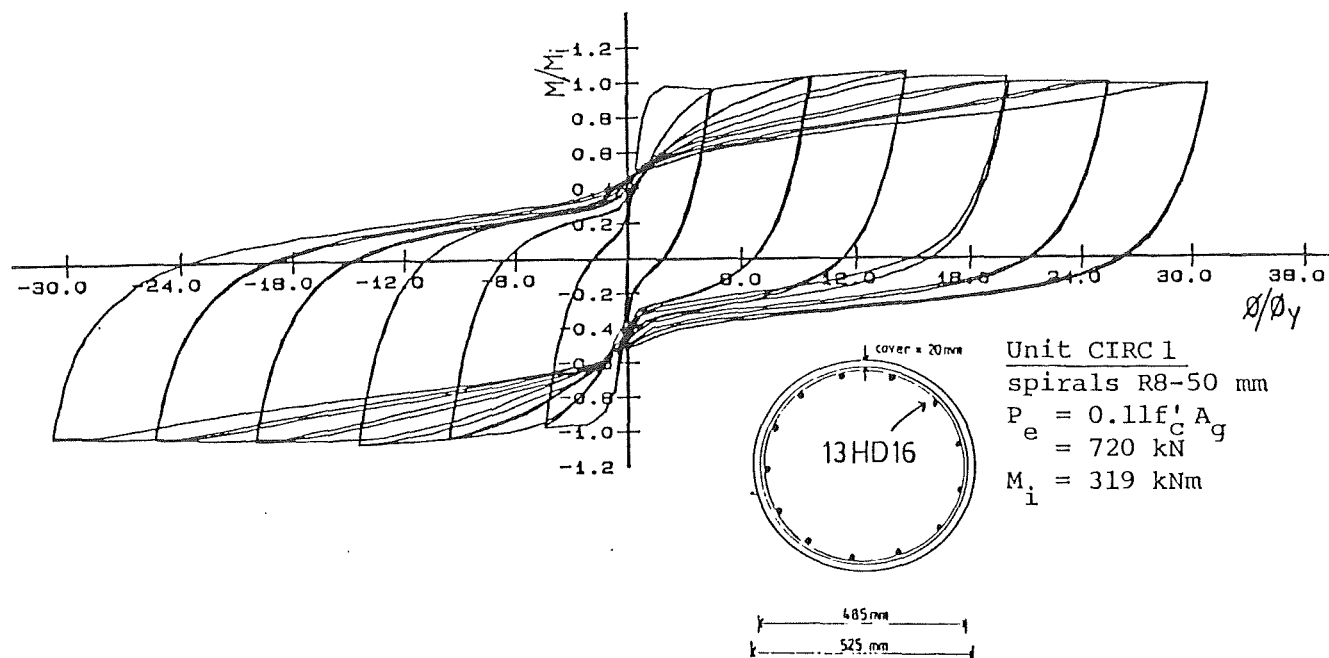


Fig. 9.9 : CYCLIC MOMENT-CURVATURE HYSTERESIS LOOPS FOR CIRCULAR COLUMN CIRC 1

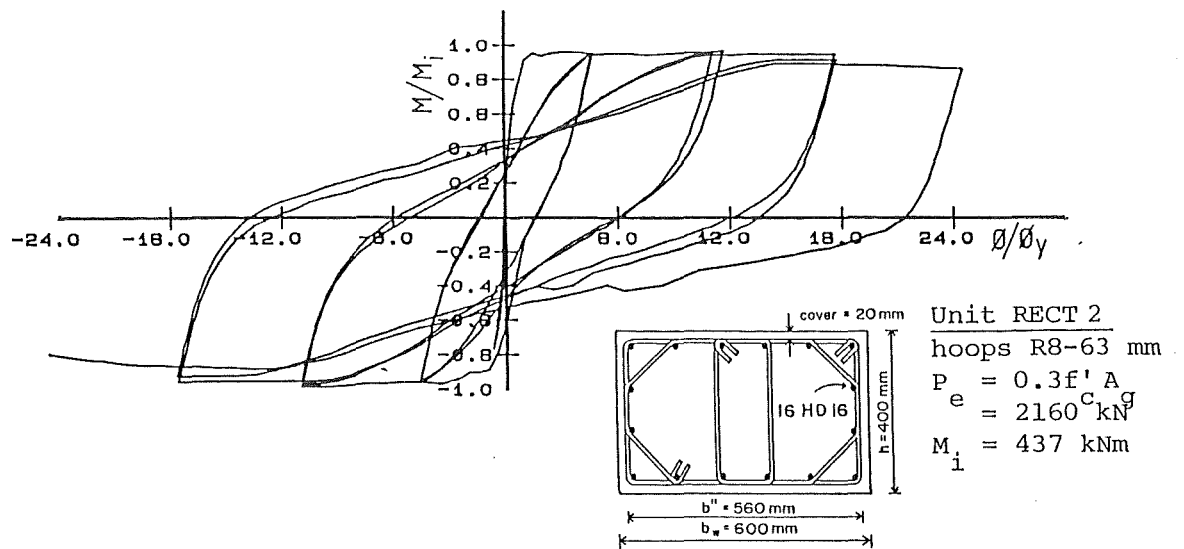


Fig. 9.10 : CYCLIC MOMENT-CURVATURE HYSTERESIS LOOPS FOR RECTANGULAR COLUMN RECT 2

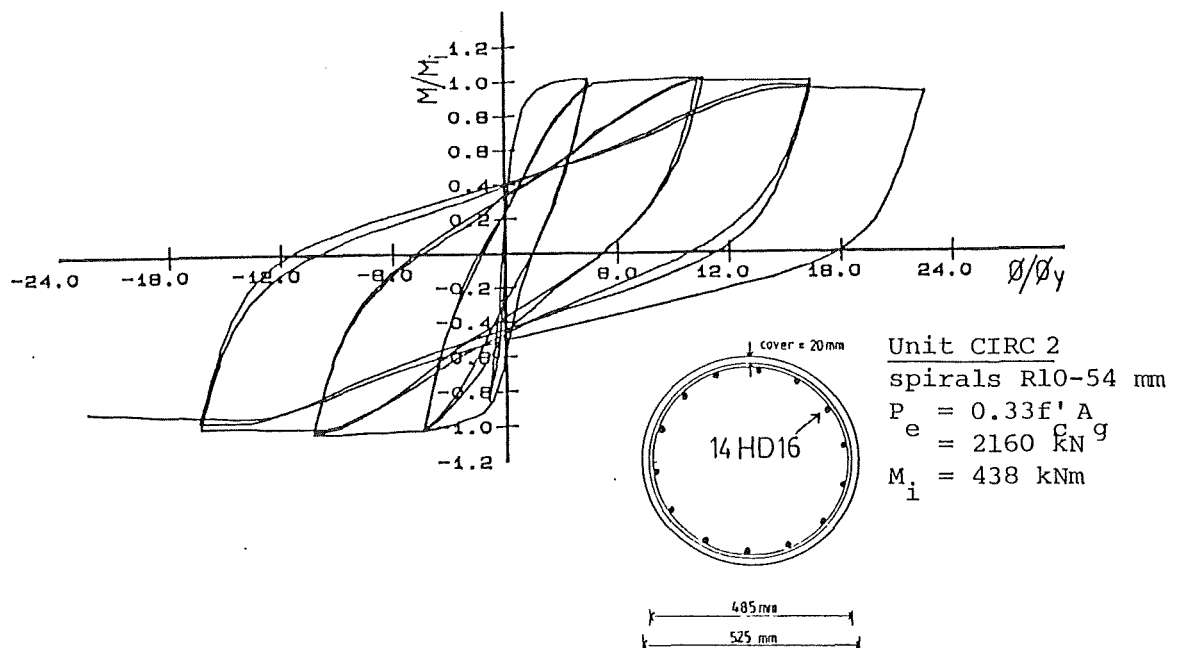


Fig. 9.11 : CYCLIC MOMENT-CURVATURE HYSTERESIS LOOPS FOR CIRCULAR COLUMN CIRC 2

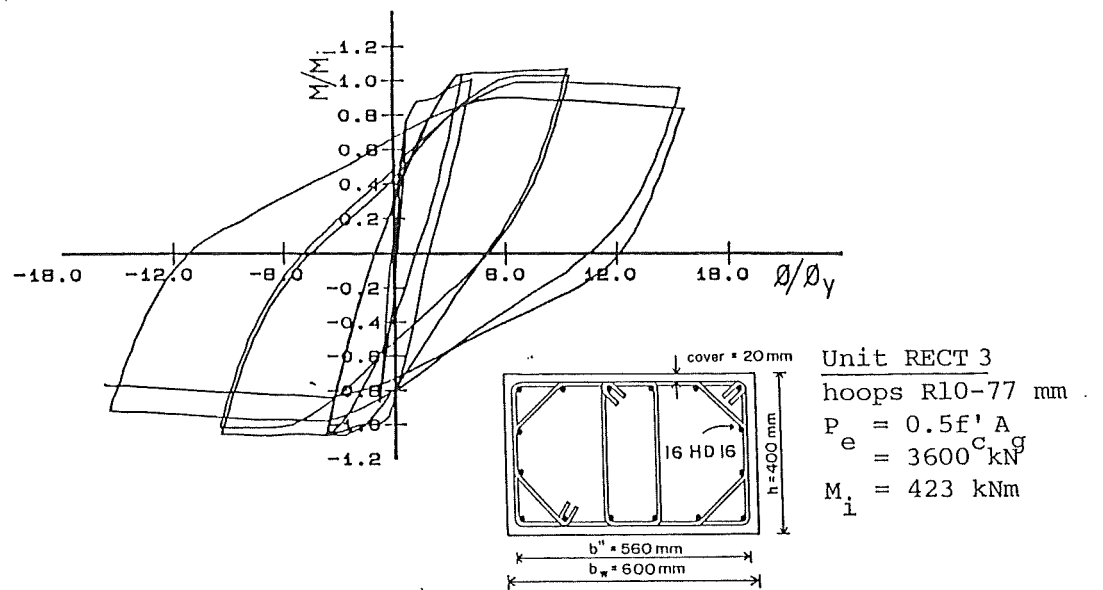


Fig. 9.12 : CYCLIC MOMENT-CURVATURE HYSTERESIS LOOPS FOR RECTANGULAR COLUMN RECT 3

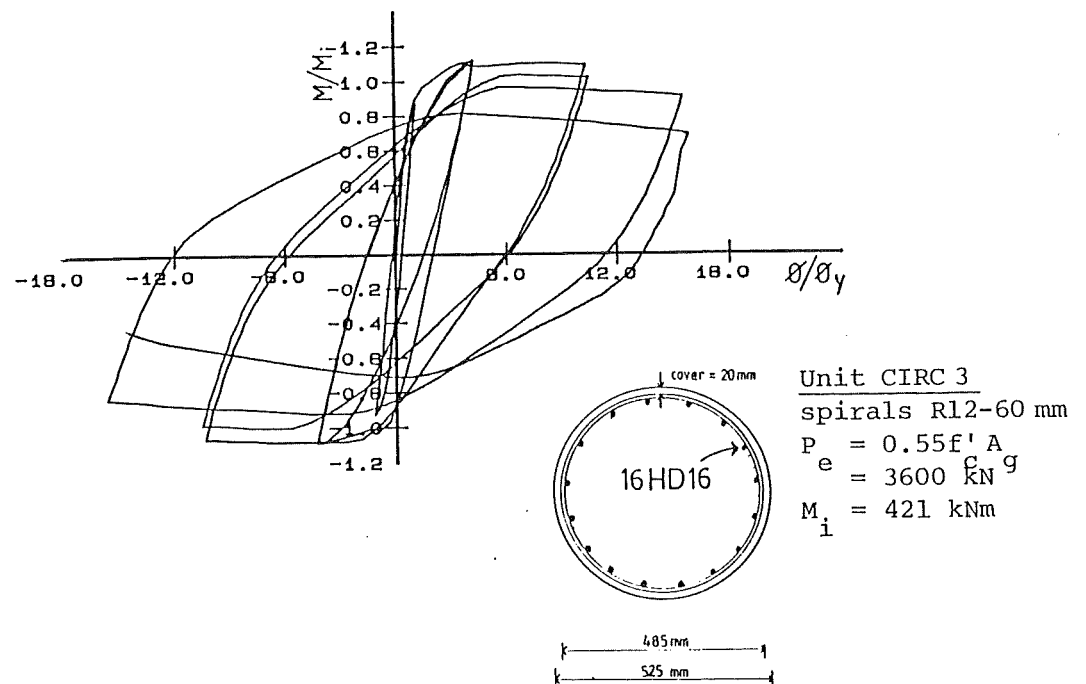


Fig. 9.13 : CYCLIC MOMENT-CURVATURE HYSTERESIS LOOPS FOR CIRCULAR COLUMN CIRC 3

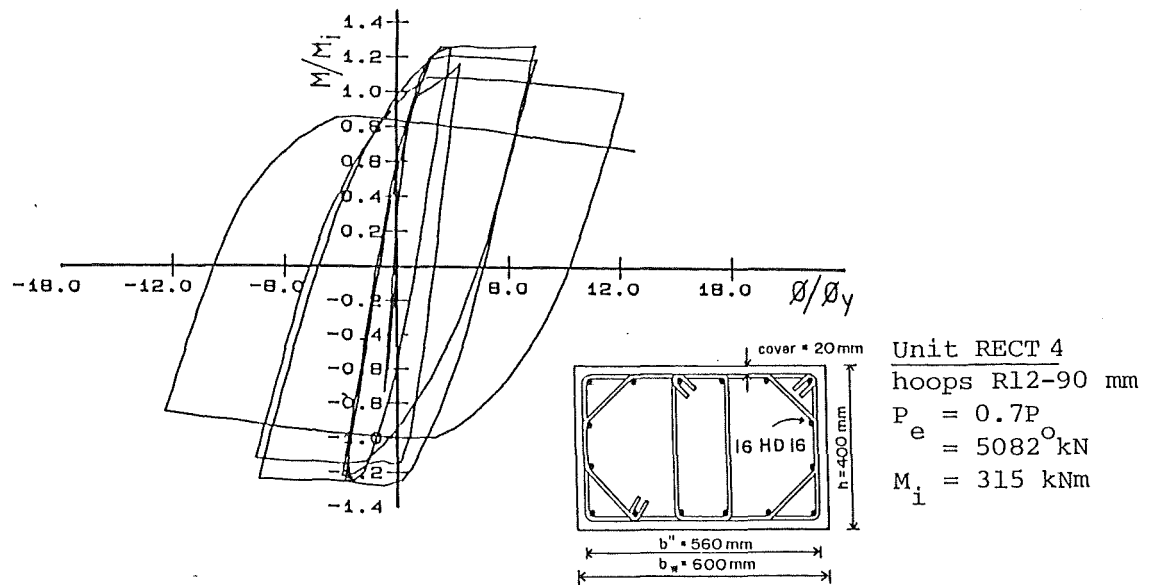


Fig. 9.14 : CYCLIC MOMENT-CURVATURE HYSTERESIS LOOPS FOR RECTANGULAR COLUMN RECT 4

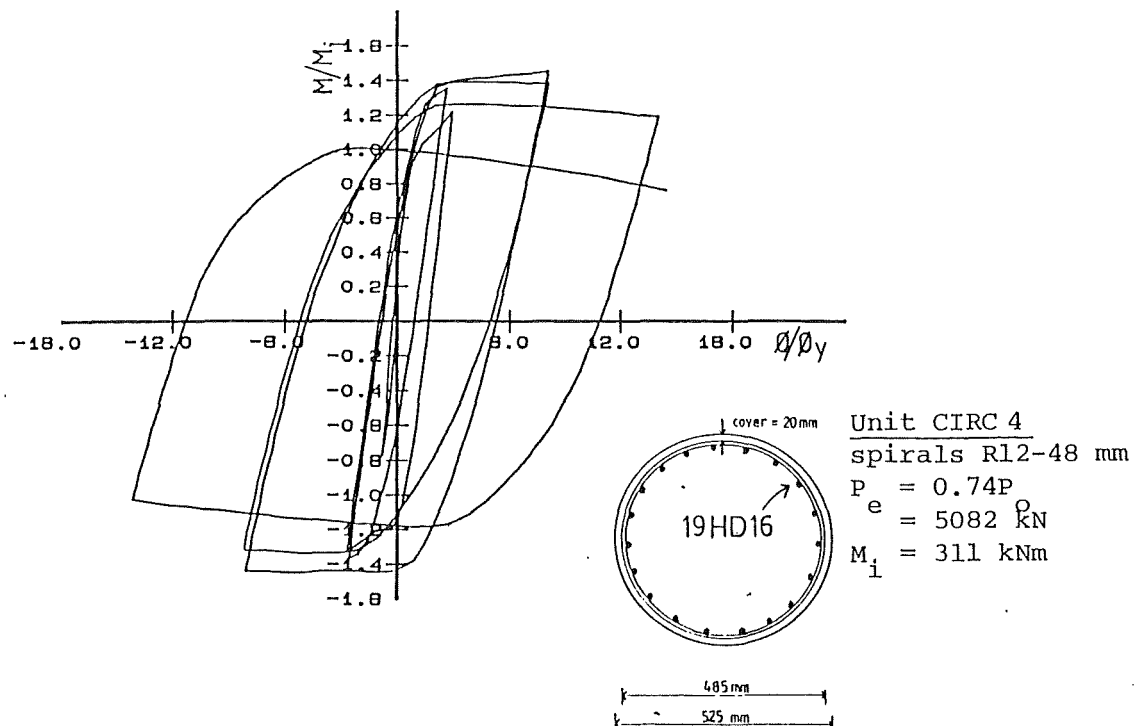


Fig. 9.15 : CYCLIC MOMENT-CURVATURE HYSTERESIS LOOPS FOR CIRCULAR COLUMN CIRC 4

hoops in the rectangular columns as shown in Fig. 9.1 provided as good confinement as that provided by the spirals in the circular columns. As illustrated in Figs. 9.12 and 9.13, reasonably good agreement is achieved between the moment-curvature hysteresis loops of Units RECT 3 and CIRC 3. However, more stable hysteresis loops are shown by Unit RECT 3. Figs. 9.14 and 9.15 show the moment-curvature hysteresis loops for Units RECT 4 and CIRC 4. Again, the hysteresis loops are quite identical.

The available curvature ductility factors ϕ_u/ϕ_y for the circular columns obtained from the cyclic moment-curvature analysis⁽³⁾ and the design charts for ductility⁽²⁴⁾ are compared with those for the rectangular columns in Table 9.4.

Table 9.4 : AVAILABLE CURVATURE DUCTILITY FACTORS FOR RECTANGULAR AND CIRCULAR COLUMNS

Unit	Available curvature ductility factors ϕ_u/ϕ_y	
	Cyclic moment-curvature analysis	Design charts for Ductility
RECT 1	>30	no apparent limits
CIRC 1	>30	no apparent limits
RECT 2	>25	>30
CIRC 2	>23	>30
RECT 3	16.5	18.3
CIRC 3	16.0	17.9
RECT 4	12.4	12.3
CIRC 4	13.8	11.5

It is evident from Figs. 9.8 to 9.15 and Table 9.4 that the modified code value for the transverse hoops in rectangular columns, Eq. 9.1, and the current code value for spirals or circular hoops in circular columns, Eq. 9.2, resulted in similar moment-curvature hysteresis loops and also similar values for ϕ_u/ϕ_y for columns with the same levels of axial load P_e and with the same ideal flexural strength M_i .

9.4 CONCLUDING REMARKS

The use of the proposed modified expression, Eq. 9.1, for rectangular columns resulted in the following conclusions.

(1) As with the code⁽²⁾ equations, the modified equation is conservative for columns with low to moderate axial load levels but may be unconservative for heavily loaded columns.

(2) The analytical cyclic moment-curvature hysteresis loops and the available curvature ductility factors for rectangular columns containing transverse reinforcement as given by the modified equation are approximately similar to those for circular columns with the code recommended quantity of circular transverse reinforcement, indicated that the proposed modified equation can satisfactorily replace the current code⁽²⁾ equation for determining the lower limiting value for the effective area of hoop sets A_{sh} in the potential plastic hinge regions of rectangular columns in seismic design.

CHAPTER TEN

CONCLUSIONS AND RECOMMENDATIONS

10.1 CONCLUSIONS

The conclusions reached during this study may be summarized as follows:

(1) A very good performance was shown by the reinforced concrete columns with square cross section tested during constant axial compression load and reversible lateral loading, which simulated seismic loading. Units 1 and 2, with 43 and 46 percent of the New Zealand code⁽²⁾ recommended quantity of transverse reinforcement, achieved displacement ductility factors of at least 8 without significant strength degradation. Longitudinal bars at the extreme tension fibre eventually fractured. Unit 3, with 30 percent of the New Zealand code⁽²⁾ recommended quantity of transverse reinforcement was capable of reaching a displacement ductility factor of 6. Fracture of an octagonal hoop was observed at the end of testing. Unit 4 with 17 percent of the New Zealand code⁽²⁾ recommended quantity of transverse reinforcement reached a displacement ductility factor of 4, and indicated failure of the hoop anchorage at longitudinal bars followed by buckling of the bars.

(2) It was observed during the testing that the minimum spalling strain of the cover concrete was 0.008. Therefore the use of the extreme fibre concrete compressive strain of 0.003 in flexural strength calculations and of 0.004 as the spalling strain in many moment-curvature analyses are inevitably conservative. A value of 0.006 could be used in the calculations and the analyses.

(3) It was observed during the previous and present experimental work that it is more appropriate to measure the dimensions of the core concrete to the centreline of the peripheral hoop. However, the code⁽²⁾ definition, which measures the core to the outside of the peripheral hoop, is preferred for simplicity in design.

(4) The test results from Unit 1, which had an axial load level of $0.1f_c' A_g$ indicated that the concrete shear resisting mechanisms made a contribution to resisting shear even after significant cyclic loading in the elastic range. Therefore, the assumption of zero shear stress carried by concrete for columns with low axial load, which is recommended by the New Zealand code⁽²⁾, is overly conservative.

(5) The columns tested with centre-to-centre spacing of hoop sets of up to $0.24h$ led to satisfactory performance. It is proposed that the code⁽²⁾ limitations for the centre-to-centre spacing of hoop sets can be expressed as one-quarter of the least lateral dimension of the cross section, or six times the diameter of the longitudinal bar to be restrained, or 200 mm, whichever is smaller.

(6) The analytical approaches, namely the monotonic and cyclic moment-curvature analyses, and the design charts for flexural strength and ductility, predicted the performance of Units 1 and 2 reasonably well. However, the analytical predictions were found to be overly conservative for Units 3 and 4.

(7) It was demonstrated that the analytical cyclic moment-curvature hysteresis loops and the available curvature ductility factors for rectangular columns containing transverse reinforcement as given by a proposed modified equation are approximately similar to those for circular columns with the code⁽²⁾ recommended quantity of circular transverse reinforcement. Therefore, this proposed modified equation for confining reinforcement in rectangular columns could satisfactorily replace the New Zealand code⁽²⁾ equation for determining the lower limiting value for the effective area of hoop sets, A_{sh} . On this basis, the requirements for the total effective area of transverse hoops in each principal direction in the potential plastic hinge regions of rectangular columns in seismic design, can be expressed by the following equations:

$$A_{sh} = 0.3 s_h h'' \left(\frac{A_g}{A_c} - 1 \right) \frac{f'_c}{f_{yh}} \left(0.5 + 1.25 \frac{P_e}{\phi f'_c A_g} \right)$$

or

$$A_{sh} = 0.08 s_h h'' \frac{f'_c}{f_{yh}} \left(0.5 + 1.25 \frac{P_e}{\phi f'_c A_g} \right)$$

whichever is greater.

10.2 RECOMMENDATIONS FOR FUTURE RESEARCH

It has been demonstrated that the existing analytical approaches result in good predictions of the performance of columns designed in accordance with the New Zealand code⁽²⁾ requirements for full ductility, but not for columns of limited ductility which contain substantially less transverse reinforcement than the code⁽²⁾ recommended quantity. Theoretical and experimental studies to assess the performance of reinforced concrete columns and frames of limited ductility are needed. This includes a derivation of design provisions for shear and confinement for

beams, columns and beam column joints for frames expected to act in a limited ductile manner.

It was shown that the code⁽²⁾ equations for confining reinforcement in the potential plastic hinge regions of both rectangular and circular columns in seismic design, may be unconservative for heavily loaded columns. Therefore, a more appropriate equation which is more dependent on the levels of axial load than that recommended in the code⁽²⁾ needs to be established. A possible modification would be to use a bi-linear relation for the influence of axial load. That is, the proposed modified equation could be used for low to moderate axial load levels and a more conservative equation for heavily loaded columns.

REFERENCES

1. "Code of Practice for General Structural Design and Design Loadings for Buildings, NZS 4203:1984", Standards Association of New Zealand, Wellington, December 1984.
2. "Code of Practice for the Design of Concrete Structures, NZS 3101:1982" (Code is Part 1 and Commentary is Part 2), Standards Association of New Zealand, Wellington, July 1982.
3. MANDER, J.B., PRIESTLEY, M.J.N. and PARK, R., "Seismic Design of Bridge Piers", Research Report 84-2, Department of Civil Engineering, University of Canterbury, Christchurch, February 1984, 483 pp.
4. PAM, H.J. and PARK, R., "Ductility of Prestressed Concrete Piles Subjected to Simulated Seismic Loading", Research Report 84-4. Department of Civil Engineering, University of Canterbury, Christchurch, February 1984, 169 pp.
5. "Applications of New Zealand Standard Code of Practice for the Design of Concrete Structures NZS 3101:1982", Technical Report No. 2, New Zealand Concrete Society, Wellington, August 1983.
6. PRIESTLEY, M.J.N. and PARK, R., "Strength and Ductility of Bridge Substructures", Bulletin No. 71, Road Research Unit, National Roads Board, Wellington, New Zealand, November 1984, 113 pp.
7. ANG, B.G., PRIESTLEY, M.J.N. and PARK, R., "Ductility of Reinforced Concrete Bridge Piers Under Seismic Loading", Research Report 81-3, Department of Civil Engineering, University of Canterbury, February 1981, 109 pp.
8. PARK, R., "Aseismic Design of Reinforced Concrete Bridge Columns and Piers", Lecture Notes for a session of a seminar on the Seismic Design and Analysis of Bridges, University, Berkeley, April 1984.
9. "Specification for Concrete Construction, NZS 3109:1980", Standards Association of New Zealand, Wellington, December 1980.
10. "Methods for Tensile Testing of Metals, BS 18:1971, Part 2: Steel (General)", British Standards Institution, London, July 1971.
11. "Annual Book of ASTM Standards, ASTM 1973, Part 4", American Society for Testing and Materials, Philadelphia, 1973.
12. PARK, R. and PAULAY, T., "Reinforced Concrete Structures", John Wiley and Sons, New York, 1975, 769 pp.

13. "Specification for Methods of Test for Concrete, NZS 3112:1980, Part 2 : Test Relating to the Determination of Strength of Concrete", Standards Association of New Zealand, Wellington, December 1980.
14. "Recommended Lateral Force Requirements and Commentary", Structural Engineers Association of California, San Francisco, 1980.
15. PARK, R. and LESLIE, P.D., "Curvature Ductility of Circular Reinforced Concrete Columns Confined by the ACI Spiral", 6th Australasian Conference on the Mechanics of Structures and Materials, Vol. 1, Christchurch, August 1977, pp. 342-349.
16. PARK, R. and NORTON, J.A., "Effects of Confining Reinforcement on the Flexural Ductility of Rectangular Reinforced Concrete Columns with High Strength Steel", Symposium on Design and Safety of Reinforced Concrete Compression Members, Reports of Working Commissions, Vol. 16, International Association for Bridge and Structural Engineering, Quebec, 1974, pp.267-275.
17. PARK, R., and SAMPSON, R.A., "Ductility of Reinforced Concrete Column Sections in Seismic Design", Journal of American Concrete Institute, Vol. 69, No. 9, September 1972, pp.543-551.
18. PARK, R., PRIESTLEY, M.J.N. and GILL, W.G., "Ductility of Square-Confined Concrete Columns", Journal of the Structural Division, Proceedings of American Society of Civil Engineers, Vol. 108, No. ST 4, April 1982, pp.929-950.
19. PRIESTLEY, M.J.N., PARK, R. and POTANGAROA, R.T., "Ductility of Spirally-Confined Concrete Columns", Journal of the Structural Division, Proceedings of American Society of Civil Engineers, Vol. 107, No. ST 1, January 1981, pp.181-202.
20. "Building Code Requirements for Reinforced Concrete ACI 318-83", American Concrete Institute, Detroit, November 1983, 111 pp.
21. KENT, D.C. and PARK, R., "Flexural Members with Confined Concrete", Journal of the Structural Division, Proceedings of American Society of Civil Engineers, Vol. 97, No. ST 7, July 1971, pp.1969-1990.
22. SCOTT, B.D., PARK, R. and PRIESTLEY, M.J.N., "Stress-strain Behaviour of Concrete Confined by Overlapping Hoops at Low and High Strain Rates", Journal of American Concrete Institute, Proc. V.79, No. 1, Jan-Feb. 1982, pp.13-27.

23. POPOVICS, S., "A Numerical Approach to the Complete Stress-Strain Curves of Concrete", Cement and Concrete Research, Vol. 3, No. 5, September 1973, pp.583-599.
24. ZAHN, F., "Design of Reinforced Concrete Bridge Columns for Strength and Ductility", Ph.D. Thesis, Department of Civil Engineering, University of Canterbury, Christchurch, 1985.
25. ANG, B.G., PRIESTLEY, M.J.N. and PAULAY, T., "Seismic Shear Strength of Circular Bridge Piers", Research Report 85-5, Department of Civil Engineering, University of Canterbury, Christchurch, July 1985, 407 pp.

APPENDIX A

COMPUTER PROGRAMS

A.1 GENERAL

As outlined earlier in Section 5.5.1, three computer programs were written to carry out the analytical investigation of the column units. They are as follows:

- (i) SSConcrete to plot the stress-strain curves for concrete given by the Modified Kent-Park model^(21,18,22) and the model of Mander, Priestley and Park⁽³⁾.
- (ii) SSSteel to plot the stress-strain curve for longitudinal reinforcing steel given by the model of Mander, Priestley and Park⁽³⁾.
- (iii) MMPHI to determine the analytical monotonic moment-curvature relationship for a rectangular reinforced concrete column.

A.2 UNITS

The units used in the programs are as follows:

Length	: mm
Stress	: MPa
Force	: kN
Moment	: kNm
Curvature	: rad/m
Strain	: dimensionless

A.3 SOURCE LISTING OF SSConcrete

```

$ RESET FREE                                00000100
$ RESET LIST                                00000200
$ SET AUTOBIND                              00000300
$ BIND = FROM PLOTA/=                      00000400
C *****                                00000500
C PROGRAM SSConcrete                        00000600
C BY SOESIANAWATI, NOVEMBER 1985          00000700
C *****                                00000800
C                                           00000900
C                                           00001000
C PROGRAM TO PLOT STRESS-STRAIN CURVES FOR 00001100
C CONFINED AND UNCONFINED CONCRETE GIVEN BY 00001200
C THE MODIFIED KENT-PARK MODEL AND          00001300
C THE MODEL OF MANDER, PRIESTLEY AND PARK   00001400
C                                           00001500
C -----                                00001600
C NOTATION                                00001700
C -----                                00001800
C                                           00001900
C BCORKP = WIDTH OF CORE CONCRETE MEASURED TO THE OUTSIDE 00002000
C OF PERIMETER HOOP                                00002100
C BCOREM = WIDTH OF CORE CONCRETE MEASURED TO THE CENTRELINE 00002200
C OF PERIMETER HOOP                                00002300
C CK = ENHANCEMENT OF CONCRETE STRENGTH DUE TO CONFINEMENT 00002400
C CKE = CONFINEMENT EFFECTIVENESS COEFFICIENT 00002500
C DCS = DIAMETER OF CONFINING STEEL           00002600
C DS = DIAMETER OF LONGITUDINAL BARS          00002700
C ECM = MODULUS OF ELASTICITY OF CONCRETE, IN THE MANDER MODEL 00002800
C = 5000*SQRT(FPCO)                                00002900
C EPSC(M) = CONCRETE COMPRESSIVE STRAIN        00003000
C EPSCC = STRAIN AT MAXIMUM CONFINED CONCRETE STRESS FPCC 00003100
C EPSCO = STRAIN AT MAXIMUM UNCONFINED CONCRETE STRESS FPCO 00003200
C EPSCPL = SPALLING STRAIN                     00003300
C EPSCMX = MAXIMUM CONCRETE STRAIN              00003400
C ESEC = FPCC/EPSCC IN POPOVIC'S EQUATION (IN THE MANDER 00003500
C MODEL)                                           00003600
C FCKP(M) = CONFINED CONCRETE COMPRESSIVE STRESS BASED ON THE 00003700
C MODIFIED KENT-PARK MODEL                        00003800
C FCM(M) = CONFINED CONCRETE COMPRESSIVE STRESS BASED ON THE 00003900
C MANDER MODEL                                    00004000
C FPC = CONCRETE COMPRESSIVE STRENGTH           00004100
C FPC28 = CONCRETE COMPRESSIVE STRENGTH AT 28 DAYS 00004200
C FPCC = PEAK OR MAXIMUM STRENGTH OF CONFINED CONCRETE 00004300
C FPCO = MAXIMUM STRENGTH OF UNCONFINED CONCRETE 00004400
C FPL = EFFECTIVE CONFINING STRESS ACTING ON CONCRETE 00004500
C FUKP(M) = UNCONFINED CONCRETE COMPRESSIVE STRESS BASED ON THE 00004600
C KENT-PARK MODEL                                00004700
C FUM(M) = UNCONFINED CONCRETE COMPRESSIVE STRESS BASED ON THE 00004800
C MANDER MODEL                                    00004900
C FYH = YIELD STRENGTH OF CONFINING STEEL       00005000
C HCORKP = DEPTH OF CONCRETE CORE MEASURED TO THE OUTSIDE 00005100
C OF PERIMETER HOOP                                00005200
C HCOREM = DEPTH OF CONCRETE CORE MEASURED TO THE CENTRELINE 00005300
C OF PERIMETER HOOP                                00005400
C M = NUMBER OF STRAIN CALCULATED, CONFINED      00005500
C N = NUMBER OF STRAIN CALCULATED, UNCONFINED    00005600
C NB = NUMBER OF LONGITUDINAL BARS SUPPORTED     00005700
C IN THE CORNERS OF THE BENT TRANSVERSE HOOPS    00005800
C IN WHICH ARCHING ACTION DEVELOPS               00005900
C NBARS = NUMBER OF LONGITUDINAL BARS            00006000
C RHOC = VOLUMETRIC RATIO OF THE LONGITUDINAL BARS IN THE 00006100
C CONFINED CORE CONCRETE, MEASURED TO THE CENTRELINE 00006200
C OF PERIMETER HOOP                                00006300
C RHOSKP = VOLUMETRIC RATIO OF CONFINING STEEL IN THE 00006400
C CONFINED CORE CONCRETE, MEASURED TO THE OUTSIDE 00006500
C OF PERIMETER HOOP                                00006600
C RHOSM = VOLUMETRIC RATIO OF CONFINING STEEL IN THE 00006700
C CONFINED CORE CONCRETE, MEASURED TO THE CENTRELINE 00006800
C OF PERIMETER HOOP                                00006900
C RM = ECM/(ECM-ESEC) IN POPOVIC'S EQUATION (IN THE MANDER 00007000
C MODEL)                                           00007100
C SCS = CENTRE-TO-CENTRE SPACING OF HOOP SETS    00007200
C SCSC = CLEAR SPACING BETWEEN HOOP BARS IN WHICH ARCHING 00007300
C ACTION DEVELOPS                                00007400

```

[illegible]

```

C
C -----
C CALCULATION OF STRESSES
C FOR CONFINED, MODIFIED KENT-PARK MODEL
C -----
M = 0
STRAIN = 0.0
200 M = M+1
EPSC(M) = STRAIN+0.0002
STRAIN = EPSC(M)
IF(EPSC(M) .GT. EPSCMX) GO TO 250
IF(EPSC(M) .LE. 0.002*CK) GO TO 210
C
C FALLING BRANCH
C
FCKP(M) = CK*FPC*(1.0-ZM*(EPSC(M)-0.002*CK))
FCMIN = 0.2*CK*FPC
IF(FCKP(M) .LE. FCMIN) FCKP(M)=FCMIN
GO TO 200
C
C ASCENDING BRANCH
C
210 FCKP(M) = CK*FPC*(2.0*EPSC(M)/0.002/CK- (EPSC(M)/0.002/CK)**2)
GO TO 200
250 MCKP = M-1
C
C =====
C STRESS-STRAIN RELATIONSHIP FOR CONCRETE
C GIVEN BY THE MODEL OF MANDER, PRIESTLEY AND PARK
C =====
C
C STRESS-STRAIN PARAMETERS
C
SCSCL = SCS-DCS
SIGMA = 0.0
DO 10 I = 1,NB
  READ(5,/)SS(I)
  WCL(I) = SS(I)-DS
  SIGMA = SIGMA+WCL(I)**2
10 CONTINUE
RHOSM = (3.414*0.7854*DCS**2)/(SCS*HCOREM)
RHOCC = (NBARS*0.7854*DS**2)/(BCOREM*HCOREM)
CKE = (1.0-SIGMA/6.0/HCOREM**2)*((1.0-0.5*SCSCL/HCOREM)**2)/
* (1.0-RHOCC)
FPL = CKE*RHOSM*FYH
FPCO = (T/(2.5+0.93*T))*FPC28
FPCC = FPCO*(-1.254+2.254*(SQRT(1.0+7.94*FPL/FPCO))-2.0*FPL/FPCO)
EPSCO = 0.002*(4.0+0.85*T)/(2.5+0.93*T)
EPSCC = EPSCO*(1.0+5.0*(FPCC/FPCO-1.0))
SRATIO = FPCC/FPC
ECM = 5000.0*SQRT(FPCO)
ESEC = FPCC/EPSCC
RM = ECM/(ECM-ESEC)
ESECU = FPCO/EPSCO
RMU = ECM/(ECM-ESECU)
WRITE(6,2000) T,RHOSM,RHOCC,CKE,FPL,FPCO,FPCC,EPSCO,EPSCC,
* SRATIO,ECM
C
C -----
C CALCULATION OF STRESSES
C FOR UNCONFINED
C -----
N = 0
STRAIN = 0.0
300 N = N+1
EPSC(N) = STRAIN+0.0002
STRAIN = EPSC(N)
IF(EPSC(N) .GT. EPSCPL) GO TO 350
FUM(N) = FPCO*(EPSC(N)/EPSCO)*RMU/(RMU-1.0+(EPSC(N)/EPSCO)**RMU)
GO TO 300
350 NUM = N-1

```

```

C -----
C CALCULATION OF STRESSES
C FOR CONFINED
C -----
C
M      = 0
STRAIN = 0.0
400 M    = M+1
      EPSC(M) = STRAIN+0.0002
      STRAIN  = EPSC(M)
      IF(EPSC(M) .GT. EPSCMX) GO TO 450
      FCM(M)  = FPCC*(EPSC(M)/EPSCC)*RM/(RM-1.0+(EPSC(M)/EPSCC)**RM)
      GO TO 400
450 MCM = M-1
C
      WRITE(6,3000)
      WRITE(6,3100)
      WRITE(6,3200) (EPSC(I),FUKP(I),FUM(I),I=1,N)
      WRITE(6,3300)
      WRITE(6,3400)
      WRITE(6,3500) (EPSC(I),FCKP(I),FCM(I),I=1,M)
C
C -----
C PLOTTING
C -----
C
      READ(5,4000) GNAME
      READ(5,4000) XNAME
      READ(5,4000) YNAME
      READ(5,4000) FUNCKP
      READ(5,4000) FCONKP
      READ(5,4000) FUNCM
      READ(5,4000) FCONM
      CALL AINIT(5000)
      CALL AORIG(150,200)
      CALL ABOX(0,0,10,6,80,80,2)
      CALL ASCALE(55,-16,80,0,0.004,0.004,10,1,2,FMX,5)
      CALL ASCALE(-37,-5,0,80,0.0,10,0,7,1,2,FMY,3)
      CALL ALAB(125,-100,GNAME,60,1,2)
      CALL ALAB(650,-50,XNAME,20,1,2)
      CALL ALAB(-65,300,YNAME,20,1,4)
      CALL ALAB(500,450,FUNCKP,60,1,2)
      CALL ALAB(500,400,FCONKP,60,1,2)
      CALL ALAB(500,350,FUNCM,60,1,2)
      CALL ALAB(500,300,FCONM,60,1,2)
      CALL ALINED(EPSC,FUKP,NUKP,0.0,0.0,0.005,12.5,3,3)
      CALL ALINE(EPSC,FCKP,MCKP,0.0,0.0,0.005,12.5)
      CALL ALINED(EPSC,FUM,NUM,0.0,0.0,0.005,12.5,12,12)
      CALL ALINEC(EPSC,FCM,MCM,0.0,0.0,0.005,12.5,CHAR,3,3,1,2)
      CALL AEND
      STOP
1000 FORMAT(1H1,21X,
*56HSTRESS-STRAIN PARAMETERS IN THE MODIFIED KENT-PARK MODEL,/
*22X,56(1H-))///
*22X,45HCONCRETE STRAIN AT 50U.....= ,F7.5//
*22X,45HVOLUMETRIC RATIO OF CONFINING STEEL.....= ,F7.5//
*22X,45HCONCRETE STRAIN AT 50H.....= ,F7.5//
*22X,45HENHANCEMENT OF CONCRETE STRENGTH.....= ,F7.5//
*22X,45HPEAK STRENGTH OF CONFINED CONCRETE.....= ,F7.3,1X,
*3HMPA//
*22X,45HSTRAIN AT PEAK STRENGTH OF CONFINED.....= ,F7.5//
*22X,45HSLOPE OF FALLING BRANCH FOR UNCONFINED.....= ,F7.2//
*22X,45HSLOPE OF FALLING BRANCH FOR CONFINED.....= ,F7.2////////)
2000 FORMAT(22X,44HSTRESS-STRAIN PARAMETERS IN THE MANDER MODEL,/
*22X,44(1H-))///
*22X,45HAGE OF CONCRETE.....= ,I7,1X,
*4HDAYS//
*22X,45HVOLUMETRIC RATIO OF CONFINING STEEL.....= ,F7.5//
*22X,45HVOLUMETRIC RATIO OF LONGITUDINAL STEEL.....= ,F7.5//
*22X,45HCONFINEMENT EFFECTIVENESS COEFFICIENT.....= ,F7.5//
*22X,45HEFFECTIVE CONFINING STRESS.....= ,F7.3,1X,
*3HMPA//
*22X,45HPEAK STRENGTH OF UNCONFINED CONCRETE.....= ,F7.3,1X,

```

```

*3HMPA//
*22X,45HPEAK STRENGTH OF CONFINED CONCRETE.....= ,F7.3,1X,
*3HMPA//
*22X,45HSTRAIN AT PEAK STRENGTH OF UNCONFINED.....= ,F7.5//
*22X,45HSTRAIN AT PEAK STRENGTH OF CONFINED.....= ,F7.5//
*22X,45HENHANCEMENT OF CONCRETE STRENGTH.....= ,F7.5//
*22X,45HMODULUS OF ELASTICITY OF CONCRETE.....= ,F7.1,1X,
*3HMPA//)
3000 FORMAT(1H1,132(1H*)//47X,37HSTRESS-STRAIN FOR UNCONFINED CONCRETE/
*1H0,132(1H*)//)
3100 FORMAT(12X,6HSTRAIN,20X,30HSTRESS IN MPA, KENT-PARK MODEL,20X,
*27HSTRESS IN MPA, MANDER MODEL//)
3200 FORMAT(12X,F6.4,31X,F5.2,44X,F5.2)
3300 FORMAT(1H1,132(1H*)//48X,35HSTRESS-STRAIN FOR CONFINED CONCRETE/
*1H0,132(1H*)//)
3400 FORMAT(12X,6HSTRAIN,17X,35HSTRESS IN MPA, MOD. KENT-PARK MODEL,
*18X,27HSTRESS IN MPA, MANDER MODEL//)
3500 FORMAT(12X,F6.4,31X,F5.2,44X,F5.2)
4000 FORMAT(10A6)
END

```

00029700
00029800
00029900
00030000
00030100
00030200
00030300
00030400
00030500
00030600
00030700
00030800
00030900
00031000
00031100
00031200
00031300
00031400
00031500
00031600
00031700

A.4 SOURCE LISTING OF SSSTEEL

```

$ RESET FREE                                00000100
$ RESET LIST                                00000200
$ SET AUTOBIND                              00000300
$ BIND = FROM PLOTA/=                      00000400
C                                           00000500
C *****                                00000600
C PROGRAM SSSTEEL                          00000700
C BY SOESIANAWATI, NOVEMBER 1985          00000800
C *****                                00000900
C                                           00001000
C PROGRAM TO PLOT STRESS-STRAIN CURVE FOR LONGITUDINAL REINFORCING 00001100
C STEEL GIVEN BY THE MODEL OF MANDER, PRIESTLEY AND PARK 00001200
C                                           00001300
C -----                                00001400
C NOTATION                                00001500
C -----                                00001600
C                                           00001700
C EPSS(M) = STRAIN IN STEEL                00001800
C EPSSH = STEEL STRAIN AT THE COMMENCEMENT OF STRAIN-HARDENING 00001900
C EPSSU = ULTIMATE STEEL STRAIN            00002000
C EPSSY = STEEL STRAIN AT FIRST YIELD      00002100
C ES = MODULUS OF ELASTICITY OF STEEL     00002200
C ESH = STRAIN-HARDENING MODULUS OF STEEL 00002300
C FS(M) = STRESS IN STEEL                 00002400
C FSU = ULTIMATE TENSILE STRENGTH OF STEEL 00002500
C FY = YIELD STRENGTH OF STEEL            00002600
C M = NUMBER OF STRAIN CALCULATED          00002700
C P = STRAIN HARDENING POWER              00002800
C FMX = FORMAT FOR STRAIN SCALE ON THE PLOT 00002900
C FMY = FORMAT FOR STRESS SCALE ON THE PLOT 00003000
C GNAME = GRAPH OPTION                    00003100
C XNAME = LABEL TO BE GIVEN TO X AXIS     00003200
C YNAME = LABEL TO BE GIVEN TO Y AXIS     00003300
C                                           00003400
C                                           00003500
C                                           00003600
C REAL FMX(1) / 'F4.2' / , FMY(1) / 'F4.0' / 00003700
C DIMENSION GNAME(10), XNAME(10), YNAME(10), EPSS(600), FS(600) 00003800
C                                           00003900
C READ(5,/) FY,FSU,ES,ESH,EPSSH,EPSSU     00004000
C EPSSY = FY/ES                            00004100
C                                           00004200
C WRITE(6,250) FY,EPSSY,FSU,EPSSU,ES,ESH,EPSSH 00004300
C WRITE(6,260)                             00004400
C WRITE(6,270)                             00004500
C P = ESH*(EPSSU-EPSSH)/(FSU-FY)           00004600
C M = 0                                    00004700
C STRAIN = 0.0                             00004800
210 M = M+1                                00004900
C EPSS(M) = STRAIN+0.0002                  00005000
C STRAIN = EPSS(M)                        00005100
C RATIO = (EPSSU-EPSS(M))/(EPSSU-EPSSH)    00005200
C IF(RATIO .LT. 1.0) GO TO 230             00005300
C IF((EPSS(M)-EPSSY) .GT. 0.0) GO TO 220  00005400
C                                           00005500
C -----                                00005600
C ELASTIC BRANCH                          00005700
C -----                                00005800
C                                           00005900
C FS(M) = EPSS(M)*ES                      00006000
C GO TO 210                               00006100
C                                           00006200
C -----                                00006300
C YIELD PLATEAU                           00006400
C -----                                00006500
C                                           00006600
220 FS(M) = FY                            00006700
C GO TO 210                               00006800
C                                           00006900
C -----                                00007000
C HARDENED SKELETON BRANCH                00007100
C -----                                00007200
C                                           00007300
230 IF(EPSS(M) .GT. EPSSU) GO TO 240      00007400
C FS(M) = FSU-(FSU-FY)*(RATIO)**P          00007500
C GO TO 210                               00007600
240 WRITE(6,280) (EPSS(I),FS(I),I=1,M)    00007700
C MS = M-1                               00007800

```

```

C          00007900
C          -----
C          PLOTTING
C          -----
          READ(5,300) GNAME          00008400
          READ(5,300) XNAME          00008500
          READ(5,300) YNAME          00008600
          CALL AINIT(5000)           00008700
          CALL AORIG(150,200)         00008800
          CALL ABOX(0,0,10,8,80,50,2) 00008900
          CALL ASCALE(60,-16,80,0,0.01,0.01,10,1,2,FMX,4) 00009000
          CALL ASCALE(-45,-5,0,50,0.0,100.,9,1,2,FMY,4) 00009100
          CALL ALAB(125,-100,GNAME,60,1,2) 00009200
          CALL ALAB(650,-50,XNAME,20,1,2) 00009300
          CALL ALAB(-75,225,YNAME,20,1,4) 00009400
          CALL ALINE(EPSS,FS,MS,0.0,0.0,0.0125,200.0) 00009500
          CALL AEND                    00009600
          STOP                         00009700
250 FORMAT(1H1,21X,30HLONGITUDINAL REINFORCING STEEL,/22X,30(1H-))/// 00009800
      *22X,35HYIELD STRENGTH.....= ,F7.1,1X,3HMPA// 00009900
      *22X,35HYIELD STRAIN.....= ,F7.5// 00010000
      *22X,35HULTIMATE TENSILE STRENGTH.....= ,F7.1,1X,3HMPA// 00010100
      *22X,35HULTIMATE STRAIN.....= ,F7.5// 00010200
      *22X,35HMODULUS OF ELASTICITY.....= ,F7.0,1X,3HMPA// 00010300
      *22X,35HSTRAIN HARDENING MODULUS.....= ,F7.0,1X,3HMPA// 00010400
      *22X,35HSTRAIN-HARDENING STRAIN.....= ,F7.5/// 00010500
260 FORMAT(1H1,132(1H*)//35X, 00010600
      *62HSTRESS-STRAIN GIVEN BY THE MODEL OF MANDER, PRIESTLEY AND PARK/00010700
      *1H0,132(1H*)//) 00010800
270 FORMAT(3X,5(20HSTRAIN STRESS (MPA),4X)//) 00010900
280 FORMAT(5(3X,F6.4,4X,F5.1,6X)) 00011000
300 FORMAT(10A6) 00011100
      END 00011200

```


A.5 COMPUTER PROGRAM MMPHI

A.5.1 Description

In this program, two models for concrete were adopted, namely the Modified Kent-Park^(21,18,22) and Mander et al⁽³⁾ models. For longitudinal reinforcing steel, the model proposed by Mander, Priestley and Park⁽³⁾ was used.

The bisection iterative technique was used to determine the neutral axis depth c which for the concrete strain at the extreme compression fibre ϵ_{cm} satisfies the force equilibrium equation (Eq. 5.1 in Section 5.2).

The ideal flexural column strength M_i calculated is based on the code⁽²⁾ approach. The yield curvature ϕ_y is defined as in Section 5.6. The next step is to compute the moment M from Eq. 5.2 and the curvature ϕ corresponding to the value of ϵ_{cm} .

By carrying out the calculation for M and ϕ for a range of ϵ_{cm} values, the monotonic moment-curvature curves can be plotted.

To terminate the program, two limitations were made, i.e. when the flexural strength of the column dropped to 80 percent of the ideal column strength or when the curvature ductility factor reached a certain value defined by the user.

A.5.2 Data Deck

The reinforced concrete column and the monotonic moment-curvature analysis are defined by the following sequence of free format data cards.

1. Job Title

Field	Parameter	Description	Format
1	TITLE	Alphanumeric description of job	80A1

2. Dimensions of Cross Section

Field	Parameter	Description	Format
1	BSEC	Width of section, b (mm)	F
2	HSEC	Overall depth of section, h (mm)	F

3. Concrete Properties

Field	Parameter	Description	Format
1	T	Age of concrete, t (days)	I
2	FPC	Concrete compressive strength, f'_c (MPa)	F
3	FPC28	Concrete compressive strength at 28 days, $(f'_c)_{28d}$ (MPa)	F
4	FPT	Concrete tensile strength, f'_t (MPa)	F
5	EPSPL	Spalling strain of concrete, ϵ_{spall}	F

4. Longitudinal Reinforcing Steel Properties

Field	Parameter	Description	Format
1	DS	Diameter of bars, d_b (mm)	F
2	FY	Yield strength of steel, f_y (MPa)	F
3	FSU	Ultimate strength of steel, f_{su} (MPa)	F
4	ES	Modulus of elasticity of steel, E_s (MPa)	F
5	ESH	Strain hardening modulus of steel, E_{sh} (MPa)	F
6	EPSSH	Strain hardening strain of steel, ϵ_{sh}	F
7	EPSSU	Ultimate strain of steel, ϵ_{su}	F

5. Transverse Reinforcing Steel Properties

Field	Parameter	Description	Format
1	DCS	Diameter of hoops (mm)	F
2	SCS	Centre-to-centre spacing of hoops, s_h (mm)	F
3	FYH	Yield strength of hoops, f_{yh} (MPa)	F
4	TLENGT	Total length of hoops (mm)	F

6. Dimensions of Core Concrete

Field	Parameter	Description	Format
1	BCORKP	Width of core concrete, measured to the outside of perimeter hoops (mm)	F
2	HCORKP	Depth of core concrete, measured to the outside of perimeter hoop (mm)	F
3	BCOREM	Width of core concrete, measured to the centreline of perimeter hoop (mm)	F
4	HCOREM	Depth of core concrete, measured to the centreline of perimeter hoop (mm)	F

7. Program Control Parameters

Field	Parameter	Description	Format
1	NSEC	Number of sub-sections	I
2	NE	Number of strips to be used	I
3	NSTEEL	Number of levels of reinforcing bars	I

8. Concrete Sub-section Dimensions

Field	Parameter	Description	Format
1	K	Sub-section number	I
2	YISEC	Starting ordinate of sub-section (mm)	F
3	YJSEC	Finishing ordinate of sub-section (mm)	F
4	BSECOP	Total width of cover, measured from the face of concrete to the outside of hoops (mm)	F
5	BSECOM	Total width of cover, measured from the face of concrete to the centreline of hoops (mm)	F

9. Longitudinal Reinforcing Steel Levels

Field	Parameter	Description	Format
1	KS	Steel level number	I
2	NBARS	Number of bars in level	I
3	YS	Ordinate position of steel level (mm)	F

10. Axial Loading

Field	Parameter	Description	Format
1	RATIO	Ratio of axial load levels $\frac{P_e}{\phi f'_c A_g}$	F

11. Neutral Axis Depth and Ultimate Curvature Ductility Factor

Field	Parameter	Description	Format
1	C	Initial estimation of neutral axis depth, c (mm)	F
2	CDFMAX	Maximum curvature ductility factor for terminating the program	F

12. Section Type

Field	Parameter	Description	Format
1	ITYPE	Section type set 1 for square section or set 2 for rectangular section	I

If ITYPE = 2 then skip cards Nos. 13 and 14.

13. Number of Longitudinal Bars

Field	Parameter	Description	Format
1	NB	Number of longitudinal bars supported in the corners of the bent transverse hoops in which arching action develops	I

14. Transverse Spacing Between Longitudinal Bars (One card needed for
each spacing)

Field	Parameter	Description	Format
1	I	Number of spacings between longitudinal bars	I
2	SS	Transverse spacing between longitudinal bars, in which arching action of concrete develops	F

15. Confined Concrete Strength

If ITYPE = 1 then skip this card

Field	Parameter	Description	Format
1	FPCC	Confined concrete compressive strength, f'_{cc} (MPa)	F

Plotting Cards : Moment-Curvature Plot

16. Graph Title

Field	Parameter	Description	Format
1	GNAME	Alphanumeric caption for graph	10A6

17. X-axis Label

Field	Parameter	Description	Format
1	XNAME	Label to be given to x-axis on graph	10A6

18. Y-axis Label

Field	Parameter	Description	Format
1	YNAME	Label to be given to y-axis on graph	10A6

A.5.3 Source Listing

A source listing of the computer program MMPHI is as follows:

```

$ RESET FREE                                00000100
$ RESET LIST                                00000200
$ SET AUTOBIND                              00000300
$ BIND = FROM PLOTA/=                      00000400
C                                           00000500
C *****                                00000600
C PROGRAM MMPHI                            00000700
C BY SOESIANAWATI, DECEMBER 1985          00000800
C *****                                00000900
C                                           00001000
C PROGRAM TO DETERMINE THE ANALYTICAL MONOTONIC 00001100
C MOMENT-CURVATURE RELATIONSHIP FOR A RECTANGULAR COLUMN 00001200
C SUBJECTED TO COMBINED FLEXURE AND AXIAL LOAD 00001300
C                                           00001400
C REFERENCES                                00001500
C -----                                00001600
C 1. CLARKE,B.J. AND BROUGHTON,R.L., RELIABLE COMPUTER PROGRAMMING, 00001700
C INCLUDING WORKBOOK CHAPTERS FOR FORTRAN, 1983 EDITION 00001800
C 2. MANDER,J.B., COLUMN ANALYSIS PROGRAM 'COLUMN', 1983 00001900
C 3. PAM,H.J., MOMENT CURVATURE OF OCTAGONAL PILE 'MOMCURV', 1984 00002000
C                                           00002100
C                                           00002200
C =====                                00002300
C NOTATION FOR INPUT DATA                 00002400
C =====                                00002500
C                                           00002600
C JOB TITLE                                00002700
C -----                                00002800
C TITLE = ALPHANUMERIC DESCRIPTION OF JOB 00002900
C                                           00003000
C DIMENSIONS OF CROSS SECTION              00003100
C -----                                00003200
C BSEC = WIDTH OF SECTION (MM)             00003300
C HSEC = OVERALL DEPTH OF SECTION (MM)      00003400
C                                           00003500
C CONCRETE PROPERTIES                      00003600
C -----                                00003700
C T = AGE OF CONCRETE (DAYS)               00003800
C FPC = CONCRETE COMPRESSIVE STRENGTH (MPA) 00003900
C FPC28 = CONCRETE COMPRESSIVE STRENGTH AT 28 DAYS (MPA) 00004000
C FPT = CONCRETE TENSILE STRENGTH (MPA)    00004100
C EPSPL = SPALLING STRAIN OF CONCRETE      00004200
C                                           00004300
C LONGITUDINAL REINFORCING STEEL PROPERTIES 00004400
C -----                                00004500
C DS = DIAMETER OF BARS (MM)               00004600
C FY = YIELD STRENGTH OF STEEL (MPA)        00004700
C FSU = ULTIMATE STRENGTH OF STEEL (MPA)    00004800
C ES = MODULUS OF ELASTICITY OF STEEL (MPA) 00004900
C ESH = STRAIN-HARDENING MODULUS OF STEEL (MPA) 00005000
C EPSSH = STRAIN-HARDENING STRAIN OF STEEL 00005100
C EPSSU = ULTIMATE STRAIN OF STEEL          00005200
C                                           00005300
C TRANSVERSE REINFORCING STEEL PROPERTIES 00005400
C -----                                00005500
C DCS = DIAMETER OF HOOPS (MM)             00005600
C SCS = CENTRE-TO-CENTRE SPACING OF HOOPS (MM) 00005700
C FYH = YIELD STRENGTH OF HOOPS (MPA)       00005800
C TLENGT = TOTAL LENGTH OF HOOPS (MM)       00005900
C                                           00006000
C DIMENSIONS OF CORE CONCRETE              00006100
C -----                                00006200
C BCORKP = WIDTH OF CORE CONCRETE, MEASURED TO THE OUTSIDE 00006300
C OF PERIMETER HOOP (MM)                   00006400
C HCORKP = DEPTH OF CORE CONCRETE, MEASURED TO THE OUTSIDE 00006500
C OF PERIMETER HOOP (MM)                   00006600
C BCOREM = WIDTH OF CORE CONCRETE, MEASURED TO THE CENTRELINE 00006700
C OF PERIMETER HOOP (MM)                   00006800
C HCOREM = DEPTH OF CORE CONCRETE, MEASURED TO THE CENTRELINE 00006900
C OF PERIMETER HOOP (MM)                   00007000
C                                           00007100
C PROGRAM CONTROL PARAMETERS               00007200
C -----                                00007300
C NSEC = NUMBER OF SUB-SECTIONS             00007400
C NE = NUMBER OF STRIPS TO BE USED          00007500
C NSTEEL = NUMBER OF LEVELS OF REINFORCING BARS 00007600

```

```

C
C CONCRETE SUB-SECTION DIMENSIONS
C -----
C K = SUB-SECTION NUMBER
C YISEC = STARTING ORDINATE OF SUB-SECTION (MM)
C YJSEC = FINISHING ORDINATE OF SUB-SECTION (MM)
C BSECOP = TOTAL WIDTH OF COVER, MEASURED FROM THE FACE OF
C CONCRETE TO THE OUTSIDE OF HOOPS (MM)
C BSECOM = TOTAL WIDTH OF COVER, MEASURED FROM THE FACE OF
C CONCRETE TO THE CENTRELINE OF HOOPS (MM)
C
C LONGITUDINAL REINFORCING STEEL LEVELS
C -----
C KS = STEEL LEVEL NUMBER
C NBARS = NUMBER OF BARS IN LEVEL
C YS = ORDINATE POSITION OF STEEL LEVEL (MM)
C
C AXIAL LOADING
C -----
C RATIO = RATIO OF AXIAL LOAD LEVELS
C
C NEUTRAL AXIS DEPTH AND ULTIMATE CURVATURE DUCTILITY FACTOR
C -----
C C = INITIAL ESTIMATION OF NEUTRAL AXIS DEPTH (MM)
C CDFMAX = MAXIMUM CURVATURE DUCTILITY FACTOR FOR TERMINATING
C THE PROGRAM
C
C SECTION TYPE
C -----
C ITYPE = SECTION TYPE, SET 1 FOR SQUARE SECTION
C SET 2 FOR RECTANGULAR SECTION
C
C NUMBER OF LONGITUDINAL BARS (ONLY FOR ITYPE = 1)
C -----
C NB = NUMBER OF LONGITUDINAL BARS SUPPORTED IN THE CORNERS
C OF THE BENT TRANSVERSE HOOPS IN WHICH ARCHING ACTION
C DEVELOPS
C
C TRANSVERSE SPACING BETWEEN LONGITUDINAL BARS (ONLY FOR ITYPE = 1)
C -----
C I = NUMBER OF SPACING BETWEEN LONGITUDINAL BARS
C SS = TRANSVERSE SPACING BETWEEN LONGITUDINAL BARS, IN WHICH
C ARCHING ACTION OF CONCRETE DEVELOPS
C
C CONFINED CONCRETE STRENGTH (ONLY FOR ITYPE = 2)
C -----
C FPCC = CONFINED CONCRETE COMPRESSIVE STRENGTH (MPA)
C
C GRAPH TITLE
C -----
C GNAME = ALPHANUMERIC CAPTION FOR GRAPH
C
C X-AXIS LABEL
C -----
C XNAME = LABEL TO BE GIVEN TO X-AXIS ON GRAPH
C
C Y-AXIS LABEL
C -----
C YNAME = LABEL TO BE GIVEN TO Y-AXIS ON GRAPH
C
C
C INTEGER NBARS(10),T
C REAL FMX(1)/'F4.1'/,FMY(1)/'F4.2'/
C REAL YISEC(20),YJSEC(20),YI(80),YJ(80),BSECOP(80),BSECOM(80)
C REAL AC(80),ACONCR(80)
C REAL ACORKP(80),ACOVKP(80),ACORM(80),ACOV(80)
C REAL PHIKP(500),MKPARK(500),CDFKP(500),MRATKP(500)
C REAL PHIM(500),MMAND(500),CDFM(500),MRATM(500)
C REAL EPSC(80),FCORE(80),FCOVER(80)
C REAL SS(10),WCL(10),TOLERN(300),CC(300)
C REAL MCONCR,MSTEEL,MI,MYKP,MYMAND
C REAL TITLE(80),GNAME(10),XNAME(10),YNAME(10)
C COMMON NCODE,NYIELD,NCONCR,NSTEEL,EPST,C,HSEC,
* YC(80),YS(10),AS(10),EPSS(10),FS(10),
* EPSSYC,EPSSYT,EPSSH,EPSSU,ES,ESH,FY,FSU,
* PC(80),PS(10),PSTEEL,MCONCR,MSTEEL

```

```

C      DATA CHAR/'.'/
C      READ(5,1000) TITLE
      READ(5,/) BSEC,HSEC
      READ(5,/) T,FPC,FPC28,FPT,EPSCPL
      READ(5,/) DS,FY,FSU,ES,ESH,EPSSH,EPSSU
      READ(5,/) DCS,SCS,FYH,TLENGT
      READ(5,/) BCORKP,HCORKP,BCOREM,HCOREM
      READ(5,/) NSEC,NE,NSTEEL
C      AGROSS = 0.0
      DO 100 K = 1,NSEC
        READ(5,/) K,YISEC(K),YJSEC(K),BSECOP(K),BSECOM(K)
        ASEC = (YJSEC(K)-YISEC(K))*BSEC
        AGROSS = AGROSS+ASEC
100    CONTINUE
      YTHICK = (YJSEC(NSEC)-YISEC(1))/NE
      YI(1) = YISEC(1)
      MM = 0
      DO 110 K = 1,NSEC
        N = (YJSEC(K)-YISEC(K))/YTHICK
        IF(N.EQ. 0) N=1
        DO 105 NN = 1,N
          MM = MM+1
          YJ(MM) = YISEC(K)+NN*(YJSEC(K)-YISEC(K))/N
          YI(MM+1) = YJ(MM)
105    CONTINUE
110    CONTINUE
      NE = MM
      AST = 0.0
      DO 115 KS = 1,NSTEEL
        READ(5,/) KS,NBARS(KS),YS(KS)
        AS(KS) = 0.7854*NBARS(KS)*(DS**2)
        AST = AST+AS(KS)
115    CONTINUE
C      K = 1
      DO 135 I=1,NE
120    IF((YJ(I)-YJSEC(K)).LE.0.1.AND.(YJ(I)-YISEC(K))
      * .GE.-0.1) GO TO 125
      K = K+1
      IF(K.LE.NSEC) GO TO 120
125    AC(I) = (YJ(I)-YI(I))*BSEC
      ACNCR(I) = AC(I)
      DO 130 J = 1,NSTEEL
        IF(YS(J).LE.YJ(I).AND.YS(J).GT.YI(I)) AC(I)=AC(I)-AS(J)
130    CONTINUE
      ACOVKP(I) = (YJ(I)-YI(I))*BSECOP(K)
      ACORKP(I) = AC(I)-ACOVKP(I)
      ACOVM(I) = (YJ(I)-YI(I))*BSECOM(K)
      ACORM(I) = AC(I)-ACOVM(I)
135    CONTINUE
C      READ(5,/) RATIO
      READ(5,/) C,CDFMAX
C      -----
C      TABULATION OF INPUT DATA
C      -----
C      ACT = 0.0
      ACVKP = 0.0
      ACRKP = 0.0
      ACVM = 0.0
      ACRM = 0.0
      EPSSYC = -FY/ES
      EPSSYT = FY/ES
      PE = RATIO*FPC*AGROSS/1000.0
C      WRITE(6,6030) TITLE
      WRITE(6,6040) BSEC,HSEC
      WRITE(6,6045)

```

```

00015300
00015400
00015500
00015600
00015700
00015800
00015900
00016000
00016100
00016200
00016300
00016400
00016500
00016600
00016700
00016800
00016900
00017000
00017100
00017200
00017300
00017400
00017500
00017600
00017700
00017800
00017900
00018000
00018100
00018200
00018300
00018400
00018500
00018600
00018700
00018800
00018900
00019000
00019100
00019200
00019300
00019400
00019500
00019600
00019700
00019800
00019900
00020000
00020100
00020200
00020300
00020400
00020500
00020600
00020700
00020800
00020900
00021000
00021100
00021200
00021300
00021400
00021500
00021600
00021700
00021800
00021900
00022000
00022100
00022200
00022300
00022400
00022500

```



```

DO 145 I = 1,NE
  YC(I) = (YI(I)+YJ(I))*0.5
  ACT = ACT+AC(I)
  ACVKP = ACVKP+ACOVKP(I)
  ACRKP = ACRKP+ACORKP(I)
  ACVM = ACVM+ACOV(I)
  ACRM = ACRM+ACORM(I)
  WRITE(6,6050) I,YI(I),YJ(I),YC(I),AC(I),
    * ACOVKP(I),ACORKP(I),ACOV(I),ACORM(I)
  DO 140 J = 1,NSTEEL
    IF(YS(J).LE.YJ(I).AND.YS(J).GT.YI(I))
  * WRITE(6,6060) AS(J),YS(J)
140 CONTINUE
145 CONTINUE
C
  WRITE(6,6070) AGROSS,ACT,ACVKP,ACRKP,ACVM,ACRM,AST
  WRITE(6,6075) FYH,DCS,SCS
  WRITE(6,6078) FY,FSU,EPSSYC,EPSSYT,EPSSH,EPSSU,ES,ESH
  WRITE(6,6080) PE,RATIO
C
C =====
C DETERMINATION OF MOMENT AND CURVATURE AT THE IDEAL STRENGTH,
C USING THE CONCRETE DESIGN CODE NZS 3101:1982 APPROACH
C =====
C
  NCODE = 1
  EPST = 0.003
  BETAI = 0.85-0.008*(FPC-30.0)
  IF(FPC.LE.30.0) BETAI=0.85
  IF(BETAI.LT.0.65) BETAI=0.65
  I = 0
210 I = I+1
  IF(I.GE.40) WRITE(6,7015)
  NCONCR = 0
  PCONCR = 0.0
  FCONCR = 0.85*FPC
  YA = BETAI*C
  DO 230 M = 1,NE
    IF(YI(M).GT.YA) GO TO 220
    IF(YA.GT.YI(M).AND.YA.LT.YJ(M)) GO TO 215
    PC(M) = ACONCR(M)*FCONCR/1000.0
    GO TO 225
  215 PC(M) = ((YA-YI(M))/(YJ(M)-YI(M)))*ACONCR(M)*FCONCR/1000.0
    GO TO 225
  220 PC(M) = 0.0
  225 PCONCR = PCONCR+PC(M)
    NCONCR = NCONCR+1
  230 CONTINUE
C
  CALL SSTEEL
C
C -----
C CHECK EQUILIBRIUM OF FORCES
C -----
C
  PI = PCONCR+PSTEEL
  TOLERN(I) = PI-PE
  IF(ABS(TOLERN(I)).LE.0.01*PE) GO TO 265
  IF(I.NE.1) GO TO 255
  CC(I) = C
  250 CNEW = CC(I)-TOLERN(I)/PE*CC(I)
    GO TO 260
  255 DIF = TOLERN(I)-TOLERN(I-1)
    IF(DIF.EQ.0.0) GO TO 250
    CNEW = CC(I)-TOLERN(I)/DIF*(CC(I)-CC(I-1))
  260 CC(I+1) = CNEW
    C = CC(I+1)
    GO TO 210
C
C -----
C CURVATURE AND MOMENT AT THE IDEAL STRENGTH,PHII AND MI
C -----
C
  265 PHII = EPST/C*1000.0
C
  CALL MOMENT
C
  MI = MCONCR+MSTEEL
C
  WRITE(6,7010)
  WRITE(6,7020) EPST,I,C,YA,PI,PHII,MI

```

```
C
C
C =====
C MOMENT-CURVATURE ANALYSES USING THE STRESS-STRAIN RELATIONSHIP
C FOR CONCRETE GIVEN BY THE MODIFIED KENT-PARK MODEL
C =====
C
C STRESS-STRAIN PARAMETERS FOR CONCRETE
C
EPS50U = (3.0+0.29*FPC)/(145.0*FPC-1000.0)
RHOSKP = (TLENGT*0.7854*DCS**2)/(SCS*BCORKP*HCORKP)
EPS50H = 0.75*RHOSKP*SQRT(HCORKP/SCS)
CK      = 1.0+RHOSKP*FYH/FPC
FPCKCP  = CK*FPC
EPSCCP  = CK*0.002
Z       = 0.5/(EPS50U-0.002)
ZM      = 0.5/(EPS50U+EPS50H-0.002*CK)
EPSCU   = 0.002+1.0/Z
ECKP    = 4700.0*SQRT(FPC)
EPSCTP  = FPT/ECKP
C
WRITE(6,8010) FPC,FPT,ECKP,EPSCTP,EPS50U,EPS50H,EPSCU,
*          RHOSKP,CK,FPCKCP,EPSCCP,Z,ZM
C
C DETERMINATION OF PHIYDP AND MYKP, I.E. CURVATURE AND MOMENT
C CORRESPONDING TO THE FIRST YIELD OF THE LONGITUDINAL BARS
C
C YIELD CURVATURE PHIYP = PHIYDP*MI/MYKP
C
NCODE     = 0
NYIELD    = 1
EPSS(NSTEEL) = -EPSSYT
I         = 0
410 I      = I+1
EPST      = C/(C-YS(NSTEEL))*EPSS(NSTEEL)
IF(I.LE. 40) GO TO 515
IF(I.GT. 40) WRITE(6,7015)
C
C -----
C FIRST YIELD CURVATURE AND MOMENT,PHIYDP AND MYKP
C YIELD CURVATURE  PHIYP
C -----
C
465 PHIYDP = EPST/C*1000.0
C
CALL MOMENT
C
MYKP = MCONCR+MSTEEL
PHIYP = PHIYDP*MI/MYKP
C
WRITE(6,8020)
WRITE(6,8030) EPST,EPSS(NSTEEL),I,C,PKPARK,PHIYDP,MYKP,PHIYP
WRITE(6,8040)
WRITE(6,8050)
C
C -----
C CONCRETE STRESSES, STRAINS AND FORCES
C -----
C
NYIELD = 0
N       = 0
IF(RATIO.LE. 0.1) EPST=0.0001
IF(RATIO.GT. 0.1.AND. RATIO.LE. 0.5) EPST=0.0004
IF(RATIO.GT. 0.5) EPST=0.0010
C
505 CALL STRAIN(EPST,RATIO)
C
N       = N+1
I       = 0
ICHECK  = 0
510 I    = I+1
IF(I.LE. 40) GO TO 515
ICHECK  = ICHECK+1
IF(ICHECK.GT. 1) GO TO 575
C       = 0.5*HSEC
I       = 1
515 EPSB = (C-HSEC)/C*EPST
NCONCR  = 0
PCONCR  = 0.0
```

```

DO 540 M = 1,NE                                00038800
  EPSC(M) = (C-YC(M))/C*EPST                    00038900
  IF(EPSC(M) .LE. 0.0) GO TO 517                00039000
  IF(EPSC(M) .LE. 0.002*CK) GO TO 520           00039100
  FCMIN = CK*FPC*(1.0-ZM*(EPSC(M)-0.002*CK))    00039200
  FCMIN = 0.2*CK*FPC                             00039300
  IF(FCORE(M) .LE. FCMIN) FCMIN=FCMIN            00039400
  GO TO 525                                       00039500
517 IF(ABS(EPSB) .GT. ABS(EPSCPT)) GO TO 545      00039600
  FCMIN = ECKP*EPSC(M)                          00039700
  FCOVER(M) = FCMIN                             00039800
  GO TO 535 .                                     00039900
520 FCMIN = CK*FPC*(2.0*EPSC(M)/0.002/CK- (EPSC(M)/0.002/CK)**2) 00040000
  IF(EPSC(M) .GE. 0.002) GO TO 525              00040100
  FCOVER(M) = FPC*(2.0*EPSC(M)/0.002- (EPSC(M)/0.002)**2) 00040200
  GO TO 535                                       00040300
525 IF(EPSC(M) .GT. EPSCPL) GO TO 530            00040400
  IF(EPSC(M) .GE. EPSCU) GO TO 530              00040500
  FCOVER(M) = FPC*(1.0-Z*(EPSC(M)-0.002))       00040600
  GO TO 535                                       00040700
530 FCOVER(M) = 0.0                             00040800
535 PC(M) = (ACORCP(M)*FCORE(M)+ACOVCP(M)*FCOVER(M))/1000.0 00040900
  PCONCR = PCONCR+PC(M)                         00041000
  NCONCR = NCONCR+1                             00041100
C                                                00041200
540 CONTINUE                                     00041300
C                                                00041400
545 CALL SSTEEL                                 00041500
C                                                00041600
C ----- 00041700
C CHECK EQUILIBRIUM OF FORCES 00041800
C ----- 00041900
C                                                00042000
  PKPARK = PCONCR+PSTEEL                        00042100
  TOLERN(I) = PKPARK-PE                         00042200
  IF((ABS(TOLERN(I)) .LE. 0.01*PE) .AND. (NYIELD .EQ. 1)) 00042300
  * GO TO 465                                     00042400
  IF((ABS(TOLERN(I)) .LE. 0.01*PE) .AND. (NYIELD .NE. 1)) 00042500
  * GO TO 565                                     00042600
  IF(I .NE. 1) GO TO 555                         00042700
  CC(I) = C                                       00042800
550 CNEW = CC(I)-TOLERN(I)/PE*CC(I)              00042900
  GO TO 560                                       00043000
555 DIF = TOLERN(I)-TOLERN(I-1)                 00043100
  IF(DIF .EQ. 0.0) GO TO 550                     00043200
  CNEW = CC(I)-TOLERN(I)/DIF*(CC(I)-CC(I-1))    00043300
560 CC(I+1) = CNEW                               00043400
  IF(CC(I+1) .LT. 0.0) CC(I+1)=0.5*HSEC          00043500
  IF(CC(I+1) .GE. 1.5*HSEC) CC(I+1)=0.5*HSEC    00043600
  C = CC(I+1)                                    00043700
  IF(NYIELD .EQ. 1) GO TO 410                    00043800
  GO TO 510                                       00043900
C                                                00044000
C ----- 00044100
C CURVATURE AND MOMENT, PHIKP(N) AND MKPARK(N) 00044200
C CURVATURE DUCTILITY FACTOR AND MOMENT RATIO, 00044300
C CDFKP(N) AND MRATKP(N) 00044400
C ----- 00044500
C                                                00044600
565 PHIKP(N) = EPST/C*1000.0                    00044700
C                                                00044800
C CALL MOMENT                                     00044900
C                                                00045000
  MKPARK(N) = MCONCR+MSTEEL                      00045100
  CDFKP(N) = PHIKP(N)/PHIYP                      00045200
  MRATKP(N) = MKPARK(N)/MI                      00045300
C                                                00045400
  WRITE(6,8060) N,EPST,I,C,PKPARK,PHIKP(N),MKPARK(N), 00045500
  * CDFKP(N),MRATKP(N) 00045600
  IF(EPST .GT. 0.050 .AND. MRATKP(N) .LT. 0.8*MI) GO TO 570 00045700
  IF(CDFKP(N) .GT. CDFMAX) GO TO 570             00045800
  GO TO 505                                       00045900
570 NKP = N                                       00046000
  IF(I .GT. 40) NKP=N-1                         00046100
  IF(I .GT. 40) C=0.5*HSEC                      00046200
  GO TO 1375                                     00046300
575 WRITE(6,7018) EPST                          00046400
  IF(EPST .GT. 0.3) GO TO 1375                  00046500
  GO TO 505                                       00046600

```

```

C
C =====
C MOMENT-CURVATURE ANALYSES USING THE STRESS-STRAIN RELATIONSHIP
C FOR CONCRETE GIVEN BY THE MODEL OF MANDER, PRIESTLEY AND PARK
C =====
C
C STRESS-STRAIN PARAMETERS FOR CONCRETE
C
C
C SECTION TYPE
C -----
C
C FOR SQUARE SECTION,          ITYPE = 1
C FOR RECTANGULAR SECTION, ITYPE = 2
C
1375 READ(5,/) ITYPE
    IF(ITYPE .EQ. 2) GO TO 1385
C
    READ(5,/) NB
    SCSCCL = SCS-DCS
    SIGMA = 0.0
    DO 1380 I = 1,NB-1
        READ(5,/) I,SS(I)
        WCL(I) = SS(I)-DS
        SIGMA = SIGMA+WCL(I)**2
1380 CONTINUE
    RHOSM = (3.414*0.7854*DCS**2)/(SCS*HCOREM)
    RHOCCL = AST/(BCOREM*HCOREM)
    CKE = (1.0-SIGMA/6.0/HCOREM**2)*((1.0-0.5*SCSCCL/HCOREM)**2)/
    * (1.0-RHOCCL)
    FPL = CKE*RHOSM*FYH
    FPCO = (T/(2.5+0.93*T))*FPC28
    EPSCO = 0.002*(4.0+0.85*T)/(2.5+0.93*T)
    FPCC = FPCO*(-1.254+2.254*(SQRT(1.0+7.94*FPL/FPCO))-2.0*FPL/FPCO)
    GO TO 1390
1385 READ(5,/) FPCC
    FPCO = (T/(8.5+0.95*T))*FPC28
    EPSCO = 0.002*(4.0+0.85*T)/(8.5+0.95*T)
1390 EPSCC = EPSCO*(1.0+5.0*(FPCC/FPCO-1.0))
    SRATIO = FPCC/FPC
    ECM = 5000.0*SQRT(FPCO)
    EPSCTM = FPT/ECM
    ESEC = FPCC/EPSCC
    RM = ECM/(ECM-ESEC)
    ESECU = FPCO/EPSCO
    RMU = ECM/(ECM-ESECU)
    IF(ITYPE .EQ. 2) GO TO 1400
C
    WRITE(6,8510) FPC,FPT,ECM,EPSCCTM,T,FPCO,FPCC,EPSCO,EPSCC,
    * SRATIO,FPL,CKE,RHOSM,RHOCCL
    GO TO 1405
1400 WRITE(6,8515) FPC,FPT,ECM,EPSCCTM,T,FPCO,FPCC,EPSCO,EPSCC,
    * SRATIO
C
C DETERMINATION OF PHIYDM AND MYMAND, I.E. CURVATURE AND MOMENT
C CORRESPONDING TO THE FIRST YIELD OF THE LONGITUDINAL BARS
C
C YIELD CURVATURE PHIYM = PHIYDM*MI/MYMAND
C
C
1405 NYIELD = 1
    EPSS(NSTEEL) = -EPSSYT
    I = 0
1410 I = I+1
    EPST = C/(C-YS(NSTEEL))*EPSS(NSTEEL)
    IF(I .LE. 40) GO TO 1515
    IF(I .GT. 40) WRITE(6,7015)
C
C -----
C FIRST YIELD CURVATURE AND MOMENT, PHIYDM AND MYMAND
C YIELD CURVATURE PHIYM
C -----
1465 PHIYDM = EPST/C*1000.0
C
    CALL MOMENT
C
    MYMAND = MCONCR+MSTEEL
    PHIYM = PHIYDM*MI/MYMAND
C
    WRITE(6,8520)
    WRITE(6,8030) EPST,EPSS(NSTEEL),I,C,PMAND,PHIYDM,MYMAND,PHIYM
    WRITE(6,8540)
    WRITE(6,8550)

```

```

C
C -----
C CONCRETE STRESSES, STRAINS AND FORCES
C -----
C
NYIELD = 0
N = 0
IF(RATIO .LE. 0.1) EPST=0.0001
IF(RATIO .GT. 0.1 .AND. RATIO .LE. 0.5) EPST=0.0004
IF(RATIO .GT. 0.5) EPST=0.0010
C
1505 CALL STRAIN(EPST,RATIO)
C
N = N+1
I = 0
ICHECK = 0
1510 I = I+1
IF(I .LE. 40) GO TO 1515
ICHECK = ICHECK+1
IF(ICHECK .GT. 1) GO TO 1575
C = 0.5*HSEC
I = 1
1515 EPSB = (C-HSEC)/C*EPST
NCONCR = 0
PCONCR = 0.0
DO 1540 M = 1,NE
  EPSC(M) = (C-YC(M))/C*EPST
  IF(EPSC(M) .LE. 0.0) GO TO 1530
  FCORE(M) = FPCC*EPSC(M)/EPSCC*RM/(RM-1.0+(EPSC(M)/EPSCC)
  * **RM)
  IF(EPSC(M) .GT. 2.0*EPSCO) GO TO 1520
  FCOVER(M) = FPCO*EPSC(M)/EPSCO*RMU/(RMU-1.0+(EPSC(M)/EPSCO)
  * **RMU)
  GO TO 1535
C
C UNCONFINED CONCRETE STRESSES AT STRAINS GREATER THAN
C 2.0*EPSCO, LINEAR RELATIONSHIP
C
1520 IF(EPSC(M) .GT. EPSCPL) GO TO 1525
FCOV2 = FPCO*2.0*RMU/(RMU-1.0+2.0**RMU)
FCOVER(M) = FCOV2*(EPSCPL-EPSC(M))/(EPSCPL-2.0*EPSCO)
GO TO 1535
1525 FCOVER(M) = 0.0
GO TO 1535
1530 IF(ABS(EPSB).GT.ABS(EPSCM)) GO TO 1545
FCORE(M) = ECM*EPSC(M)
FCOVER(M) = FCORE(M)
1535 PC(M) = (ACORM(M)*FCORE(M)+ACOV(M)*FCOVER(M))/1000.0
PCONCR = PCONCR+PC(M)
NCONCR = NCONCR+1
C
1540 CONTINUE
C
1545 CALL SSTEEL
C
C -----
C CHECK EQUILIBRIUM OF FORCES
C -----
C
PMAND = PCONCR+PSTEEL
TOLERN(I) = PMAND-PE
IF((ABS(TOLERN(I)) .LE. 0.01*PE) .AND. (NYIELD .EQ. 1))
* GO TO 1465
IF((ABS(TOLERN(I)) .LE. 0.01*PE) .AND. (NYIELD .NE. 1))
* GO TO 1565
IF(I .NE. 1) GO TO 1555
CC(I) = C
1550 CNEW = CC(I)-TOLERN(I)/PE*CC(I)
GO TO 1560
1555 DIF = TOLERN(I)-TOLERN(I-1)
IF(DIF .EQ. 0.0) GO TO 1550
CNEW = CC(I)-TOLERN(I)/DIF*(CC(I)-CC(I-1))
1560 CC(I+1) = CNEW
IF(CC(I+1) .LT. 0.0) CC(I+1)=0.5*HSEC
IF(CC(I+1) .GE. 1.5*HSEC) CC(I+1)=0.5*HSEC
C = CC(I+1)
IF(NYIELD .EQ. 1) GO TO 1410
GO TO 1510

```

```

C
C -----
C CURVATURE AND MOMENT, PHIM(N) AND MMAND(N)
C CURVATURE DUCTILITY FACTOR AND MOMENT RATIO,
C CDFM(N) AND MRATM(N)
C -----
C
1565 PHIM(N) = EPST/C*1000.0
C
C CALL MOMENT
C MMAND(N) = MCONCR+MSTEEL
C CDFM(N) = PHIM(N)/PHIYM
C MRATM(N) = MMAND(N)/MI
C
C WRITE(6,8060) N,EPST,I,C,PMAND,PHIM(N),MMAND(N),
* CDFM(N),MRATM(N)
C IF(EPST.GT. 0.050 .AND. MRATM(N).LT. 0.8*MI) GO TO 1570
C IF(CDFM(N).GT. CDFMAX) GO TO 1570
C GO TO 1505
1570 NM = N
C IF(I.GT. 40) NM=N-1
C GO TO 1577
1575 WRITE(6,7018) EPST
C IF(EPST.GT. 0.3) GO TO 1577
C GO TO 1505
C
C =====
C TABULATION OF OUTPUT RESULTS
C =====
C
1577 WRITE(6,9010)
C WRITE(6,9020)
C DO 1580 J = 1,N
C WRITE(6,9030) J,PHIKP(J),PHIM(J),MKPARK(J),MMAND(J),
* CDFKP(J),CDFM(J),MRATKP(J),MRATM(J)
1580 CONTINUE
C
C =====
C PLOTTING
C =====
C
C READ(5,1010) GNAME
C READ(5,1010) XNAME
C READ(5,1010) YNAME
C CALL AINIT(5000)
C CALL AORIG(150,200)
C CALL ABOX(0,0,10,7,80,50,2)
C CALL ASCALE(65,-16,80,0,3.0,3.0,10,1,2,FMX,4)
C CALL ASCALE(-45,-5,0,50,0.0,0.2,8,1,2,FMY,4)
C CALL ALAB(115,-100,GNAME,60,1,2)
C CALL ALAB(470,-50,XNAME,40,1,2)
C CALL ALAB(-75,150,YNAME,20,1,4)
C CALL ALINE(CDFKP,MRATKP,NKP,0.0,0.0,3.75,0.4)
C CALL ALINEC(CDFM,MRATM,NM,0.0,0.0,3.75,0.4,CHAR,10,10,1,2)
C CALL AEND
C STOP
C
C =====
C OUTPUT FORMAT STATEMENTS
C =====
C
1000 FORMAT(80A1)
1010 FORMAT(10A6)
6030 FORMAT(1H1,132(1H*)//26X,80A1/1H0,132(1H*)////)
6040 FORMAT(1H0,21X,27HDIMENSIONS OF CROSS SECTION,/
* 22X,27(1H-)//
* 22X,45HWIDTH OF SECTION.....= ,F5.1,
* 1X,2HMM//
* 22X,45HVERALL DEPTH OF SECTION.....= ,F5.1,
* 1X,2HMM////)
6045 FORMAT(1H0,21X,16HSECTION ELEMENTS,/
* 22X,16(1H-)//35H STRIP YI YJ YC,
* 5X,47HACONC ACOVKP ACORKP ACOVM ACORM,
* 10X,16HASTEEL YS//)
6050 FORMAT(I5,6F10.1,2X,2F10.1)
6060 FORMAT(1H+,92X,2F10.1)
6070 FORMAT(1H1,21X,36HSECTIONAL AREA OF CONCRETE AND STEEL,/
* 22X,36(1H-)//
* 22X,45HGROSS SECTIONAL AREA.....= ,F8.1,1X,
* 3HMM2//
* 22X,45HTOTAL AREA OF CONCRETE.....= ,F8.1,1X,
* 3HMM2//
* 22X,45HAREA OF COVER CONCRETE,KENT-PARK.....= ,F8.1,1X,
* 3HMM2//
* 22X,45HAREA OF CORE CONCRETE,KENT-PARK.....= ,F8.1,1X,
* 3HMM2//

```

```

*22X,45HAREA OF COVER CONCRETE,MANDER.....= ,F8.1,1X,      00071700
*3HMM2//                                           00071800
*22X,45HAREA OF CORE CONCRETE,MANDER.....= ,F8.1,1X,      00071900
*3HMM2//                                           00072000
*22X,45HAREA OF LONGITUDINAL STEEL.....= ,F8.1,1X,      00072100
*3HMM2//)                                           00072200
6075 FORMAT(1H0,21X,24HTRANSVERSE REINFORCEMENT,/      00072300
*22X,24(1H-)//)                                     00072400
*22X,45HYIELD STRENGTH.....= ,F5.1,1X,      00072500
*3HMPA//                                           00072600
*22X,45HDIAMETER OF HOOPS.....= ,F5.1,1X,      00072700
*2HMM//                                           00072800
*22X,45HHOOP SPACINGS IN THE PLASTIC HINGE REGION..= ,F5.1,1X,      00072900
*2HMM//)                                           00073000
6078 FORMAT(1H0,21X,26HLONGITUDINAL REINFORCEMENT,/      00073100
*22X,26(1H-)//)                                     00073200
*22X,45HYIELD STRENGTH.....= ,F7.1,1X,      00073300
*3HMPA//                                           00073400
*22X,45HULTIMATE STRENGTH.....= ,F7.1,1X,      00073500
*3HMPA//                                           00073600
*22X,45HYIELD STRAIN IN COMPRESSION.....= ,F7.4//      00073700
*22X,45HYIELD STRAIN IN TENSION.....= ,F7.4//      00073800
*22X,45HSTRAIN HARDENING STRAIN.....= ,F7.4//      00073900
*22X,45HULTIMATE STRAIN.....= ,F7.4//      00074000
*22X,45HMODULUS OF ELASTICITY.....= ,F7.0,1X,      00074100
*3HMPA//                                           00074200
*22X,45HSTRAIN HARDENING MODULUS.....= ,F7.0,1X,      00074300
*3HMPA//)                                           00074400
6080 FORMAT(1H0,21X,17HAXIAL LOAD LEVELS,/      00074500
*22X,17(1H-)//)                                     00074600
*22X,45HCOLUMN AXIAL LOAD.....= ,F6.1,1X,      00074700
*2HKN//                                           00074800
*22X,45HAXIAL LOAD RATIO.....= ,F6.3,1X,      00074900
*6HFPC*AG//)                                         00075000
7010 FORMAT(1H1,132(1H*)//41X,      00075100
*50HIDEAL STRENGTH BASED ON THE NZS 3101:1982 APPROACH/1H0,      00075200
*132(1H*)//)                                         00075300
7015 FORMAT(1H0,36HDID NOT CONVERGE UP TO 40 ITERATIONS//)      00075400
7018 FORMAT(1H0,48HDID NOT CONVERGE UP TO 40 ITERATIONS FOR EPST = ,      00075500
*F6.4//)                                           00075600
7020 FORMAT(22X,      00075700
*      45HCONCRETE STRAIN AT EXT.COMPRESSION FIBRE...= ,F6.4//      00075800
*22X,45HNUMBER OF ITERATIONS.....= ,I6//      00075900
*22X,45HNEUTRAL AXIS DEPTH.....= ,F6.1,1X,      00076000
*2HMM//                                           00076100
*22X,45HEQUIVALENT COMPRESSIVE STRESS BLOCK.....= ,F6.2,1X,      00076200
*2HMM//                                           00076300
*22X,45HAXIAL LOAD AT THE IDEAL STRENGTH.....= ,F6.1,1X,      00076400
*2HKN//                                           00076500
*22X,45HCURVATURE AT THE IDEAL STRENGTH.....= ,F6.4,1X,      00076600
*5HRAD/M//                                           00076700
*22X,45HIDEAL MOMENT CAPACITY.....= ,F6.1,1X,      00076800
*3HKNM//)                                           00076900
8010 FORMAT(1H1,21X,      00077000
*56HSTRESS-STRAIN PARAMETERS IN THE MODIFIED KENT-PARK MODEL,/      00077100
*22X,56(1H-)//)                                     00077200
*22X,45HCONCRETE COMPRESSIVE STRENGTH.....= ,F7.1,1X,      00077300
*3HMPA//                                           00077400
*22X,45HCONCRETE MODULUS OF RUPTURE.....= ,F7.2,1X,      00077500
*3HMPA//                                           00077600
*22X,45HMODULUS OF ELASTICITY OF CONCRETE.....= ,F7.1,1X,      00077700
*3HMPA//                                           00077800
*22X,45HCONCRETE TENSILE STRAIN.....= ,F7.4//      00077900
*22X,45HCONCRETE STRAIN AT 50U.....= ,F7.5//      00078000
*22X,45HCONCRETE STRAIN AT 50H.....= ,F7.5//      00078100
*22X,45HMAXIMUM UNCONFINED STRAIN.....= ,F7.5//      00078200
*22X,45HVOLUMETRIC RATIO OF CONFINING STEEL.....= ,F7.5//      00078300
*22X,45HENHANCEMENT OF CONCRETE STRENGTH.....= ,F7.5//      00078400
*22X,45HPEAK STRENGTH OF CONFINED CONCRETE.....= ,F7.3,1X,      00078500
*3HMPA//                                           00078600
*22X,45HSTRAIN AT PEAK STRENGTH OF CONFINED.....= ,F7.5//      00078700
*22X,45HSLOPE OF FALLING BRANCH FOR UNCONFINED.....= ,F7.2//      00078800
*22X,45HSLOPE OF FALLING BRANCH FOR CONFINED.....= ,F7.2//)      00078900
8020 FORMAT(1H0,132(1H-)//39X,      00079000
*54HYIELD CURVATURE AND MOMENT -MODIFIED KENT-PARK MODEL-/      00079100
*1H0,132(1H-)//)                                     00079200
8030 FORMAT(22X,26HYIELD CURVATURE AND MOMENT,/      00079300
*22X,26(1H-)//)                                     00079400
*22X,45HCONCRETE STRAIN AT FIRST YIELD.....= ,F7.4//      00079500
*22X,45HSTEEL STRAIN AT FIRST YIELD.....= ,F7.4//      00079600
*22X,45HNUMBER OF ITERATIONS.....= ,I7//      00079700
*22X,45HNEUTRAL AXIS DEPTH.....= ,F7.1,1X,      00079800
*2HMM//                                           00079900
*22X,45HAXIAL LOAD.....= ,F7.1,1X,      00080000
*2HKN//                                           00080100
*22X,45HCURVATURE AT FIRST YIELD.....= ,F7.4,1X,      00080200
*5HRAD/M//                                           00080300
*22X,45HMOMENT AT FIRST YIELD.....= ,F7.1,1X,      00080400
*3HKNM//                                           00080500
*22X,45HYIELD CURVATURE.....= ,F7.4,1X,      00080600
*5HRAD/M//)                                           00080700

```

```

8040 FORMAT(1H1,132(1H=)//39X,
*53HMOMENT-CURVATURE ANALYSIS -MODIFIED KENT-PARK MODEL-/
*1H0,132(1H=)//)
00080800
00080900
00081000
8050 FORMAT(7X,1HN,7X,4HEPST,6X,1HI,3X,13HN.A.DEPTH(MM),4X,
*10HPKPARK(KN),3X,12HPHIKP(RAD/M),3X,11HMKPARK(KNM),6X,
*5HCDFKP,9X,6HMRATKP//)
00081100
00081200
00081300
8060 FORMAT(5X,I3,5X,F6.4,4X,I3,5X,F6.2,10X,F6.1,8X,F7.5,8X,
*F6.1,8X,F6.3,10X,F5.3)
00081400
00081500
8510 FORMAT(1H1,21X,44HSTRESS-STRAIN PARAMETERS IN THE MANDER MODEL,/
*22X,44(1H-)//
00081600
00081700
*22X,45HCONCRETE COMPRESSIVE STRENGTH.....=,F7.1,1X,
00081800
*3HMPA//
00081900
*22X,45HCONCRETE MODULUS OF RUPTURE.....=,F7.2,1X,
00082000
*3HMPA//
00082100
*22X,45HMODULUS OF ELASTICITY OF CONCRETE.....=,F7.1,1X,
00082200
*3HMPA//
00082300
*22X,45HCONCRETE TENSILE STRAIN.....=,F7.4//
00082400
*22X,45HAGE OF CONCRETE.....=,I7,1X,
00082500
*4HDAYS//
00082600
*22X,45HPEAK STRENGTH OF UNCONFINED CONCRETE.....=,F7.2,1X,
00082700
*3HMPA//
00082800
*22X,45HPEAK STRENGTH OF CONFINED CONCRETE.....=,F7.2,1X,
00082900
*3HMPA//
00083000
*22X,45HSTRAIN AT PEAK STRENGTH OF UNCONFINED.....=,F7.5//
00083100
*22X,45HSTRAIN AT PEAK STRENGTH OF CONFINED.....=,F7.5//
00083200
*22X,45HENHANCEMENT OF CONCRETE STRENGTH.....=,F7.5//
00083300
*22X,45HEFFECTIVE CONFINING STRESS.....=,F7.2,1X,
00083400
*3HMPA//
00083500
*22X,45HCONFINEMENT EFFECTIVENESS COEFFICIENT.....=,F7.5//
00083600
*22X,45HVOLUMETRIC RATIO OF CONFINING STEEL.....=,F7.5//
00083700
*22X,45HVOLUMETRIC RATIO OF LONGITUDINAL STEEL.....=,F7.5////)
00083800
8515 FORMAT(1H1,21X,44HSTRESS-STRAIN PARAMETERS IN THE MANDER MODEL,/
*22X,44(1H-)//
00083900
00084000
*22X,45HCONCRETE COMPRESSIVE STRENGTH.....=,F7.1,1X,
00084100
*3HMPA//
00084200
*22X,45HCONCRETE MODULUS OF RUPTURE.....=,F7.2,1X,
00084300
*3HMPA//
00084400
*22X,45HMODULUS OF ELASTICITY OF CONCRETE.....=,F7.1,1X,
00084500
*3HMPA//
00084600
*22X,45HCONCRETE TENSILE STRAIN.....=,F7.4//
00084700
*22X,45HAGE OF CONCRETE.....=,I7,1X,
00084800
*4HDAYS//
00084900
*22X,45HPEAK STRENGTH OF UNCONFINED CONCRETE.....=,F7.2,1X,
00085000
*3HMPA//
00085100
*22X,45HPEAK STRENGTH OF CONFINED CONCRETE.....=,F7.2,1X,
00085200
*3HMPA//
00085300
*22X,45HSTRAIN AT PEAK STRENGTH OF UNCONFINED.....=,F7.5//
00085400
*22X,45HSTRAIN AT PEAK STRENGTH OF CONFINED.....=,F7.5//
00085500
*22X,45HENHANCEMENT OF CONCRETE STRENGTH.....=,F7.5////)
00085600
8520 FORMAT(1H0,132(1H-)//45X,
*42HYIELD CURVATURE AND MOMENT -MANDER MODEL-/
00085700
00085800
*1H0,132(1H-)//)
00085900
8540 FORMAT(1H1,132(1H=)//45X,
*41HMOMENT-CURVATURE ANALYSIS -MANDER MODEL-/
00086000
00086100
*1H0,132(1H=)//)
00086200
8550 FORMAT(7X,1HN,7X,4HEPST,6X,1HI,3X,13HN.A.DEPTH(MM),4X,9HPMAND(KN),
*4X,11HPHIM(RAD/M),5X,10HMMAND(KNM),7X,4HCDFM,10X,5HMRATM//)
00086300
00086400
9010 FORMAT(1H1,132(1H*)//32X,
*30HMOMENT-CURVATURE RELATIONSHIPS,5X,
00086500
00086600
*31H-MODIFIED KENT-PARK AND MANDER-/
00086700
*1H0,132(1H*)//)
00086800
9020 FORMAT(8X,1HN,4X,12HPHIKP(RAD/M),4X,11HPHIM(RAD/M),4X,
*11HMKPARK(KNM),4X,10HMMAND(KNM),8X,5HCDFKP,8X,4HCDFM,
00086900
00087000
*8X,6HMRATKP,8X,5HMRATM//)
00087100
9030 FORMAT(6X,I3,7X,F6.4,9X,F6.1,9X,F6.1,9X,
*F6.3,6X,F6.3,9X,F5.3,8X,F5.3)
00087200
00087300
END
00087400

```



```

C
C
C *****
C SUBROUTINE STRAIN(EPST,RATIO)
C *****
C
C SUBROUTINE TO DETERMINE THE INCREMENT OF CONCRETE STRAIN
C AT THE EXTREME COMPRESSION FIBRE EPST
C
C IF(EPST .GE. 0.1) GO TO 1200
C IF(EPST .GE. 0.05) GO TO 1210
C IF(EPST .GE. 0.01) GO TO 1220
C EPST = EPST+0.0002
C GO TO 1230
1200 EPST = EPST+0.01
C GO TO 1230
1210 EPST = EPST+0.005
C GO TO 1230
1220 IF(RATIO .LE. 0.1) EPST=EPST+0.0002
C IF(RATIO .GT. 0.1) EPST=EPST+0.0025
1230 RETURN
C END
C
C *****
C SUBROUTINE SSTEEL
C *****
C
C SUBROUTINE TO DETERMINE THE STRESS-STRAIN RELATIONSHIP
C FOR LONGITUDINAL REINFORCING STEEL GIVEN BY THE MODEL OF
C MANDER, PRIESTLEY AND PARK
C
C COMMON NCODE,NYIELD,NCONCR,NSTEEL,EPST,C,HSEC,
C * YC(80),YS(10),AS(10),EPSS(10),FS(10),
C * EPSSYC,EPSSYT,EPSSH,EPSSU,ES,ESH,FY,FSU,
C * PC(80),PS(10),PSTEEL,MCONCR,MSTEEL
C
C PSTEEL = 0.0
C
C DO 845 J = 1,NSTEEL
C EPSS(J) = ((C-YS(J))/C)*EPST
C IF(EPSS(J) .GE. EPSSYC .AND. EPSS(J) .LE. EPSSYT) GO TO 815
C IF(EPSS(J) .GT. EPSSYT .AND. EPSS(J) .LE. EPSSH) GO TO 820
C IF(EPSS(J) .LT. EPSSYC .AND. EPSS(J) .GE. (-EPSSH)) GO TO 820
C IF(EPSS(J) .GT. EPSSH .AND. EPSS(J) .LE. EPSSU) GO TO 830
C IF(EPSS(J) .LT. (-EPSSH) .AND. EPSS(J) .GE. (-EPSSU)) GO TO 830
C
C -----
C ELASTIC BRANCH
C -----
C
C 815 FS(J) = EPSS(J)*ES
C GO TO 840
C
C -----
C YIELD PLATEAU
C -----
C
C 820 IF(EPSS(J) .GT. 0.0) GO TO 825
C FS(J) = -FY
C GO TO 840
C 825 FS(J) = FY
C GO TO 840
C
C -----
C HARDENED SKELETON BRANCH
C -----
C
C 830 P = ESH*ABS((EPSSU-EPSSH)/(FSU-FY))
C IF(EPSS(J) .GT. 0.0) GO TO 835
C IF(NCODE .EQ. 1) FS(J)=-FY
C FS(J) = -(FSU-(FSU-FY)*((EPSSU-ABS(EPSS(J)))/(EPSSU-
C * EPSSH))**P)
C IF(ABS(FS(J)) .GT. FSU) FS(J) = -FSU
C GO TO 840
C 835 IF(NCODE .EQ. 1) FS(J)=FY
C FS(J) = FSU-(FSU-FY)*((EPSSU-EPSS(J))/(EPSSU-EPSSH))**P
C IF(ABS(FS(J)) .GT. FSU) FS(J) = FSU
C 840 PS(J) = AS(J)*FS(J)/1000.0
C PSTEEL = PSTEEL+PS(J)
C 845 CONTINUE
C RETURN
C END

```

```

00087500
00087600
00087700
00087800
00087900
00088000
00088100
00088200
00088300
00088400
00088500
00088600
00088700
00088800
00088900
00089000
00089100
00089200
00089300
00089400
00089500
00089600
00089700
00089800
00089900
00090000
00090100
00090200
00090300
00090400
00090500
00090600
00090700
00090800
00090900
00091000
00091100
00091200
00091300
00091400
00091500
00091600
00091700
00091800
00091900
00092000
00092100
00092200
00092300
00092400
00092500
00092600
00092700
00092800
00092900
00093000
00093100
00093200
00093300
00093400
00093500
00093600
00093700
00093800
00093900
00094000
00094100
00094200
00094300
00094400
00094500
00094600
00094700
00094800
00094900
00095000
00095100
00095200
00095300
00095400
00095500
00095600

```

C		00095700
C	*****	00095800
	SUBROUTINE MOMENT	00095900
C	*****	00096000
C		00096100
C	SUBROUTINE TO CALCULATE MOMENT FOR EACH VALUE OF EPST	00096200
C		00096300
	REAL MCONCR,MSTEEL	00096400
	COMMON NCODE,NYIELD,NCONCR,NSTEEL,EPST,C,HSEC,	00096500
*	YC(80),YS(10),AS(10),EPSS(10),FS(10),	00096600
*	EPSSYC,EPSSYT,EPSSH,EPSSU,ES,ESH,FY,FSU,	00096700
*	PC(80),PS(10),PSTEEL,MCONCR,MSTEEL	00096800
	MCONCR = 0.0	00096900
	MSTEEL = 0.0	00097000
	DO 950 M = 1,NCONCR	00097100
	MCONCR = MCONCR+PC(M)*(HSEC/2.0-YC(M))/1000.0	00097200
950	CONTINUE	00097300
	DO 960 J = 1,NSTEEL	00097400
	MSTEEL = MSTEEL+PS(J)*(HSEC/2.0-YS(J))/1000.0	00097500
960	CONTINUE	00097600
	RETURN	00097700
	END	00097800

APPENDIX B

APPLICATION OF THE DESIGN CHARTS BY ZAHN TO OBTAIN THE
FLEXURAL STRENGTH AND DUCTILITY OF THE COLUMN UNITS

B.1 AVAILABLE CURVATURE DUCTILITY

As outlined in Section 5.5.3, the design charts for ductility⁽²⁴⁾, which were derived by Zahn from the cyclic moment-curvature analysis⁽³⁾, can be applied to solid and hollow circular columns as well as to solid rectangular columns.

Because of a large number of different possible arrangements of the longitudinal and transverse reinforcement, and a large possible range of values for the section side ratio, b/h , only one type of rectangular column section was examined by Zahn. The geometric parameters of the section were as follows (see Fig. B.1).

- section side ratio $\beta = b/h = 1.5$
- 40% of the total steel area A_{st} in each of the long faces
- extreme steel layers in long faces at distance gh apart, with $g = 0.85$
- relative concrete cover thickness = $0.06h$

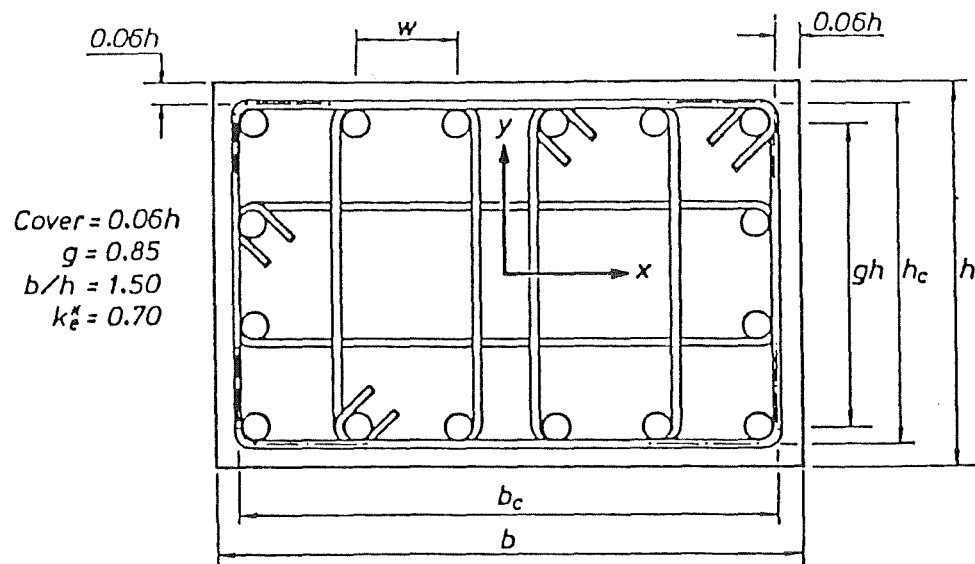


Fig. B.1 : SECTION GEOMETRY OF RECTANGULAR COLUMN INVESTIGATED

For this type of rectangular column, only bending about the weak axis was considered and two variables were investigated, namely the ratio of the effective confining stress to the unconfined concrete compressive strength f_r/f'_{co} and the axial load ratio $P_e/f'_c A_g$. The mechanical reinforcing ratio $\rho_t m$ ($m = f_y/0.85 f'_c$) was kept constant at 0.2. Also, $f'_c = 30$ MPa, $f_y = 275$ MPa, $f_{yh} = 275$ MPa and k_e^* of 0.7 were assumed. It should be noted that Zahn⁽²⁴⁾ defined k_e^* as the confinement effectiveness coefficient based on the first moments of area rather than on the effective area of confined concrete proposed by Mander et al⁽³⁾.

Clearly, the design charts for rectangular columns are strictly only valid for the determination of the available curvature ductility for the particular type of rectangular column considered by Zahn. However, the design charts can be used to approximate the available curvature ductility of the square columns tested.

The available curvature ductility ϕ_u/ϕ_y is expressed as

$$\frac{\phi_u}{\phi_y} = \gamma \left(\frac{\phi_u}{\phi_y} \right)_b \quad (B.1)$$

$$\text{in which} \quad \gamma = \gamma f'_c \quad \gamma f_y \quad \gamma f_{yh} \quad \gamma_{cover} \quad (B.2)$$

where $\left(\frac{\phi_u}{\phi_y} \right)_b$ is the available curvature ductility obtained from the basic design chart shown in Fig. B.2, and γ is a curvature ductility modification which includes the influences of variation in concrete compressive strength f'_c , yield strengths of longitudinal bars f_y and confining steel f_{yh} , and the relative concrete cover thickness. The values of $\gamma f'_c$, γf_y , γf_{yh} and γ_{cover} are found from Figs. B.3 to B.7 respectively. It is worth noting that these values were derived from results for circular columns but may be used for rectangular columns.

The values of $\gamma f'_c$, γf_{yh} and γ_{cover} for Units 1 to 4 can be found by interpolation or extrapolation of the values plotted in Figs. B.3 to B.6. As shown in Fig. B.4, the scatter of the values for γf_y was quite large and there was only a little dependence on $\rho_t m$. Therefore it may be more reasonable to neglect that influence completely and assume $\gamma f_y = 1.0$ ⁽²⁴⁾.

The mechanical reinforcing ratio $\rho_t m$ for Units 1 to 4 varied from 0.17 to 0.20; hence it may be assumed to be 0.20 as used in the charts. Table B.1 summarizes the available curvature ductility factors obtained for all units.

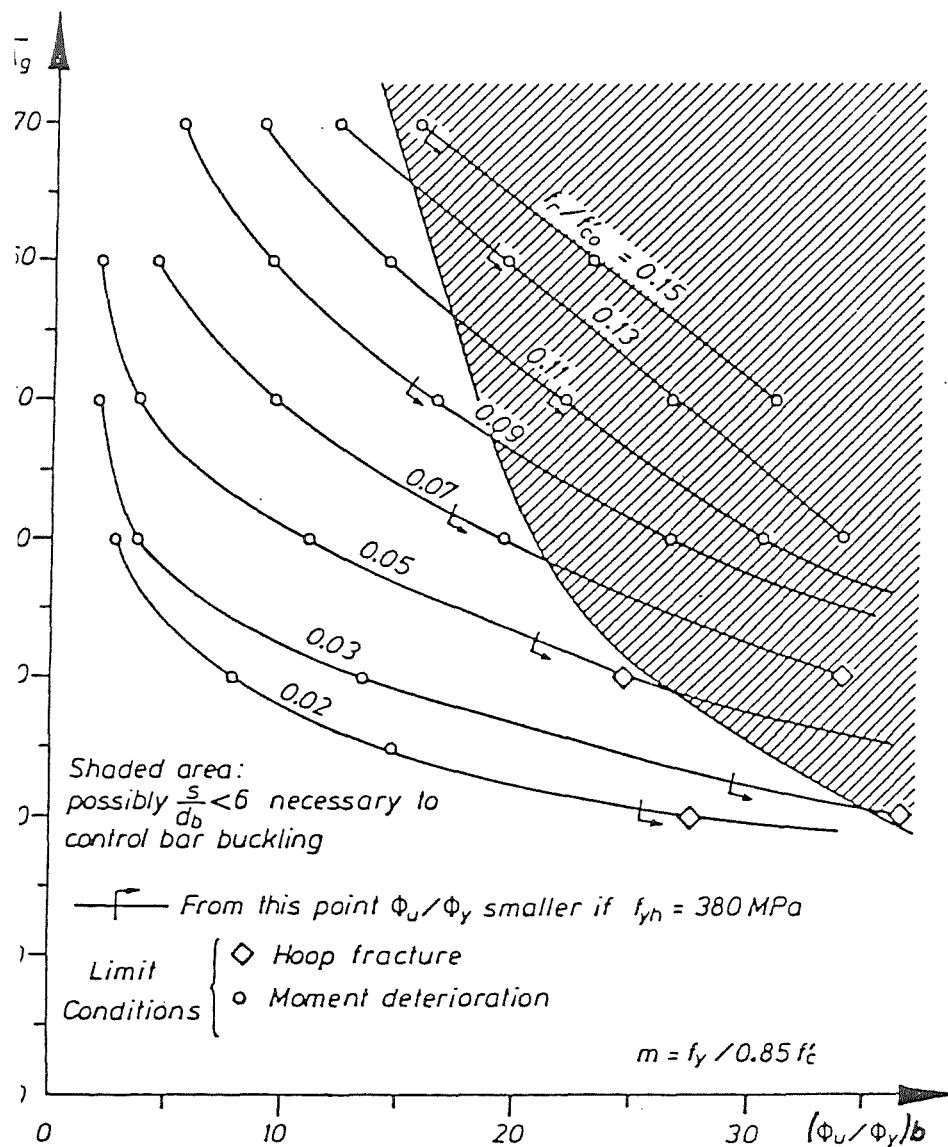


Fig. B.2 : BASIC CURVATURE DUCTILITY DESIGN CHARTS FOR RECTANGULAR COLUMNS⁽²⁴⁾

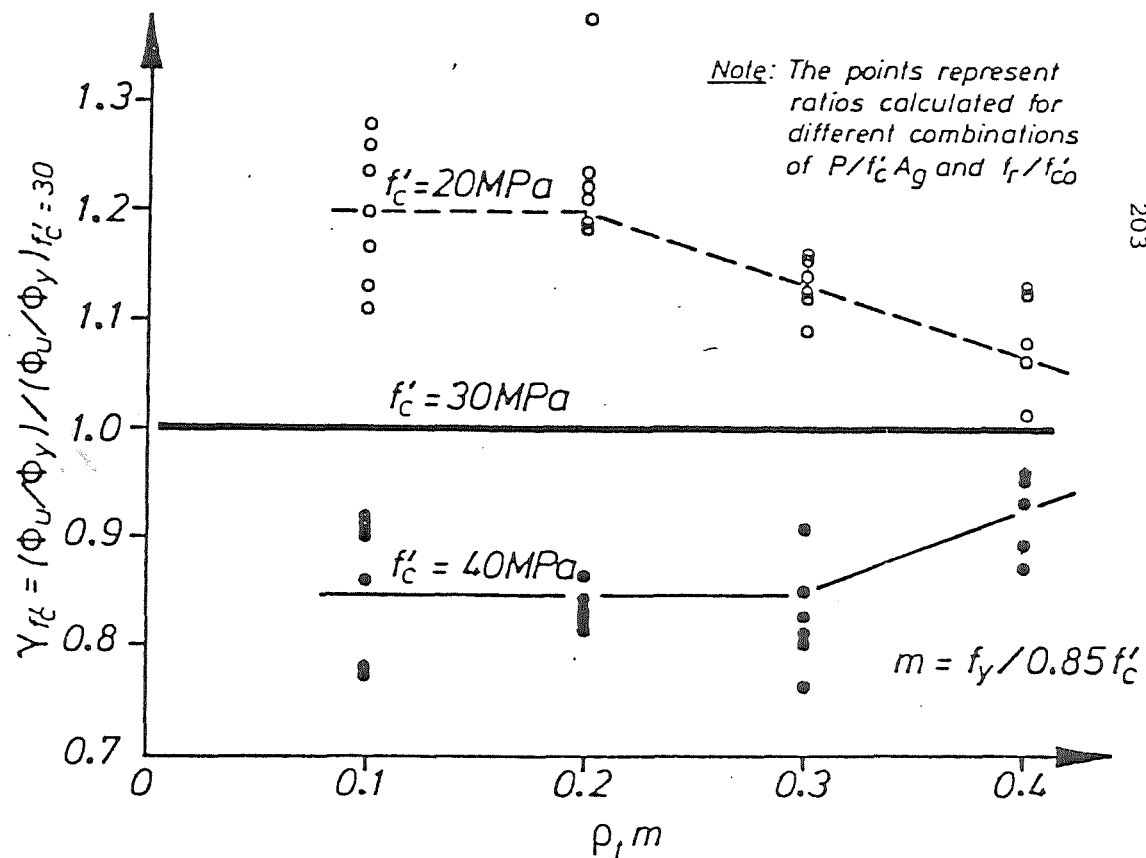


Fig. B.3 : INFLUENCE OF CONCRETE COMPRESSIVE STRENGTH ON CURVATURE DUCTILITY⁽²⁴⁾

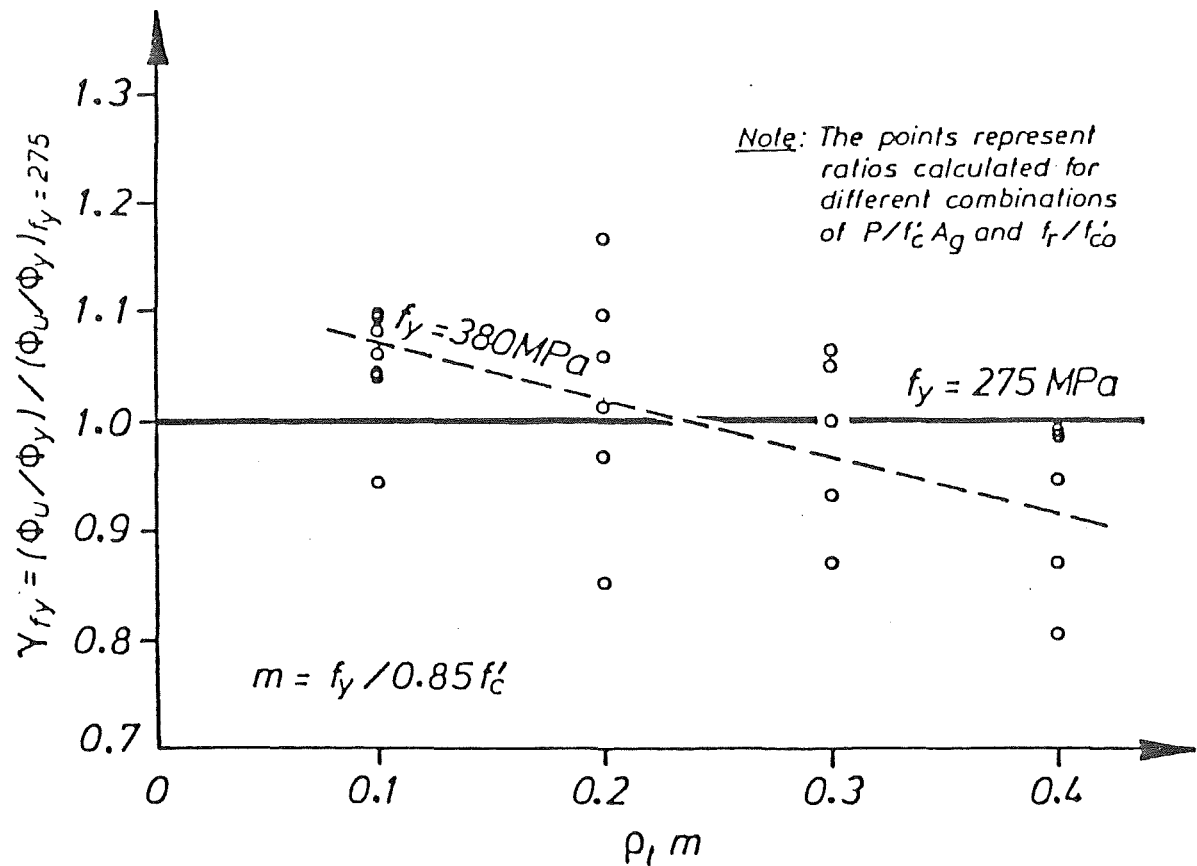


Fig. B.4 : INFLUENCE OF STEEL GRADE OF LONGITUDINAL BARS ON CURVATURE DUCTILITY⁽²⁴⁾

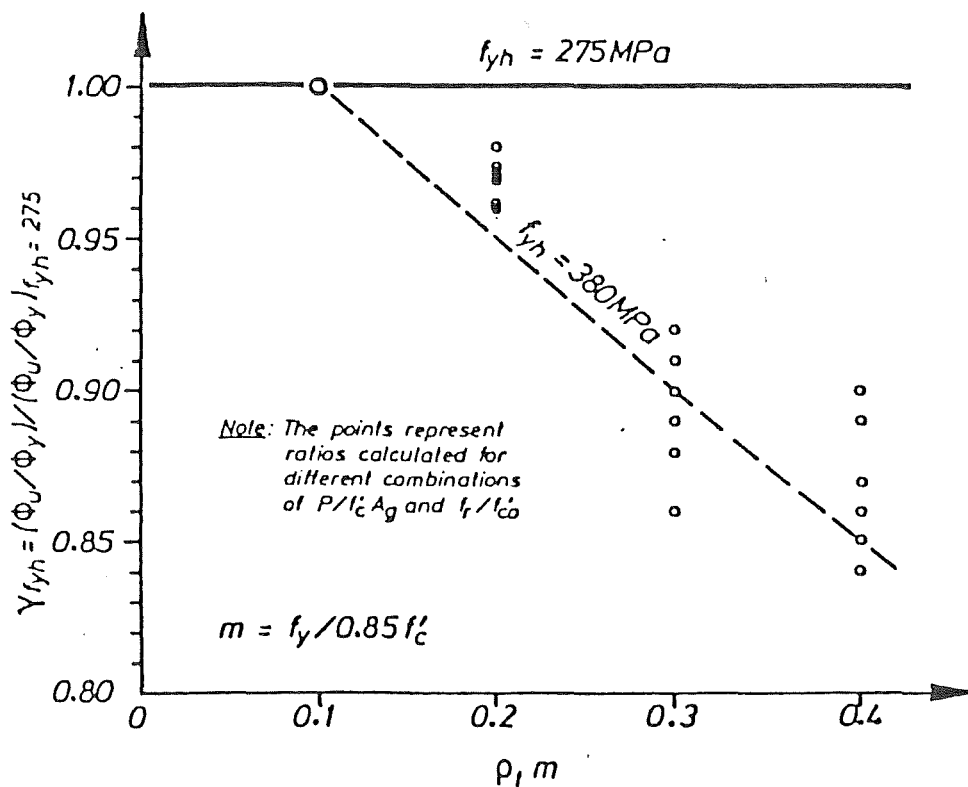


Fig. B.5 : INFLUENCE OF STEEL GRADE OF CONFINING STEEL ON CURVATURE DUCTILITY⁽²⁴⁾

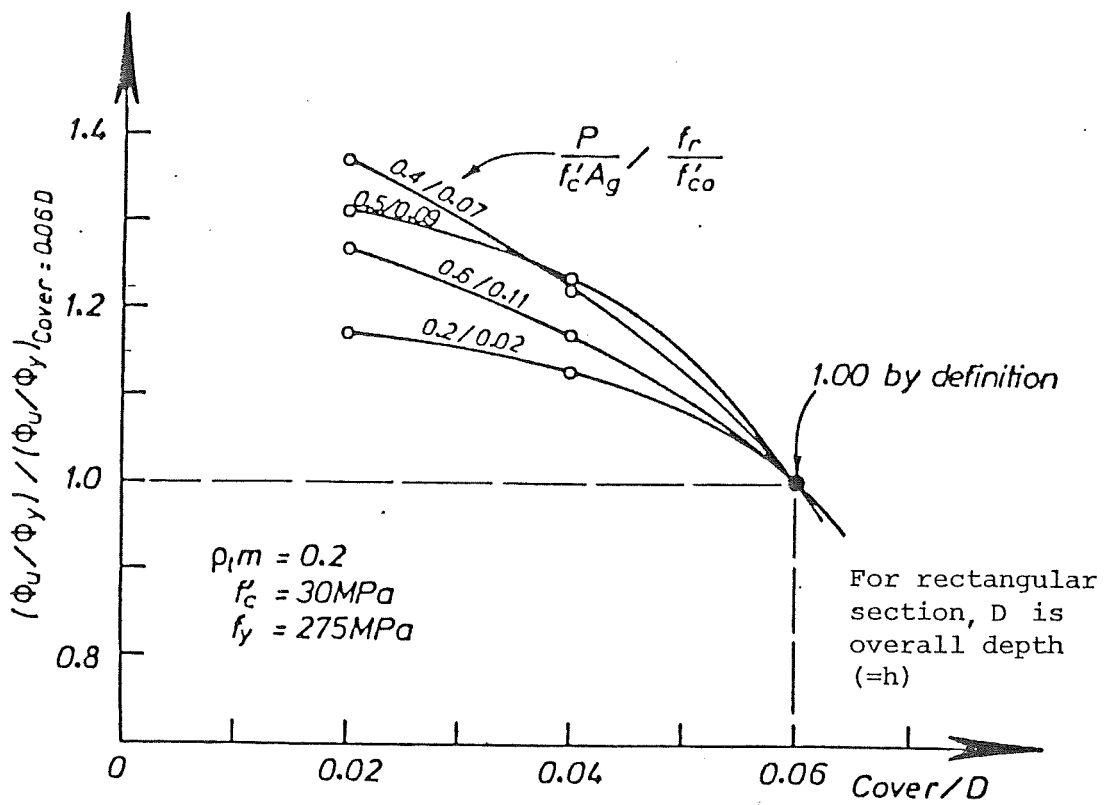


Fig. B.6 : INFLUENCE OF RELATIVE COVER THICKNESS ON CURVATURE DUCTILITY (24)

Table B.1 : AVAILABLE CURVATURE DUCTILITY FACTORS FOR UNITS 1 TO 4 OBTAINED FROM FIGS. B.2 TO B.6

Unit	$\frac{P_e}{\phi f'_c A_g}$	$\frac{f_r}{f'_{co}}$	$\left(\frac{\phi_u}{\phi_y} \right)_b$ Fig.B.2	$\gamma f'_c$ Fig.B.3	γf_y Fig.B.4	γf_{yh} Fig.B.5	γ_{cover} Fig.B.6	$\frac{\phi_u}{\phi_y}$ Eq.B.1
1	0.1	0.027	No appar- ent limits	0.75	1.0	0.96	1.15	-
2	0.3	0.043	22.5	0.79	1.0	0.96	1.22	20.8
3	0.3	0.026	12.0	0.79	1.0	0.96	1.18	10.7
4	0.3	0.013	4.0	0.85	1.0	1.01	1.15	4.0

B.2 IDEAL FLEXURAL STRENGTH AND FLEXURAL OVERSTRENGTH FACTOR

Zahn⁽²⁴⁾ defined the ideal flexural strength M_i as

$$M_i = M_{\text{code}} K_{m0} K_{m1} K_{m2} \quad (\text{B.3})$$

where M_{code} is the flexural strength based on the code⁽²⁾ approach and the specified material strengths, and K_{m0} and K_{m1} are the enhancement factors shown in Figs. B.7 and B.8 which were derived from monotonic moment-curvature analyses and take into account the effects of f_r/f'_c , $P_e/\phi f'_c A_g$, ρ_t and the actual values of f'_c and f_y . K_{m2} is a factor allowing for the strength enhancement caused by the additional confinement provided by adjacent members and can be taken as 1.05.

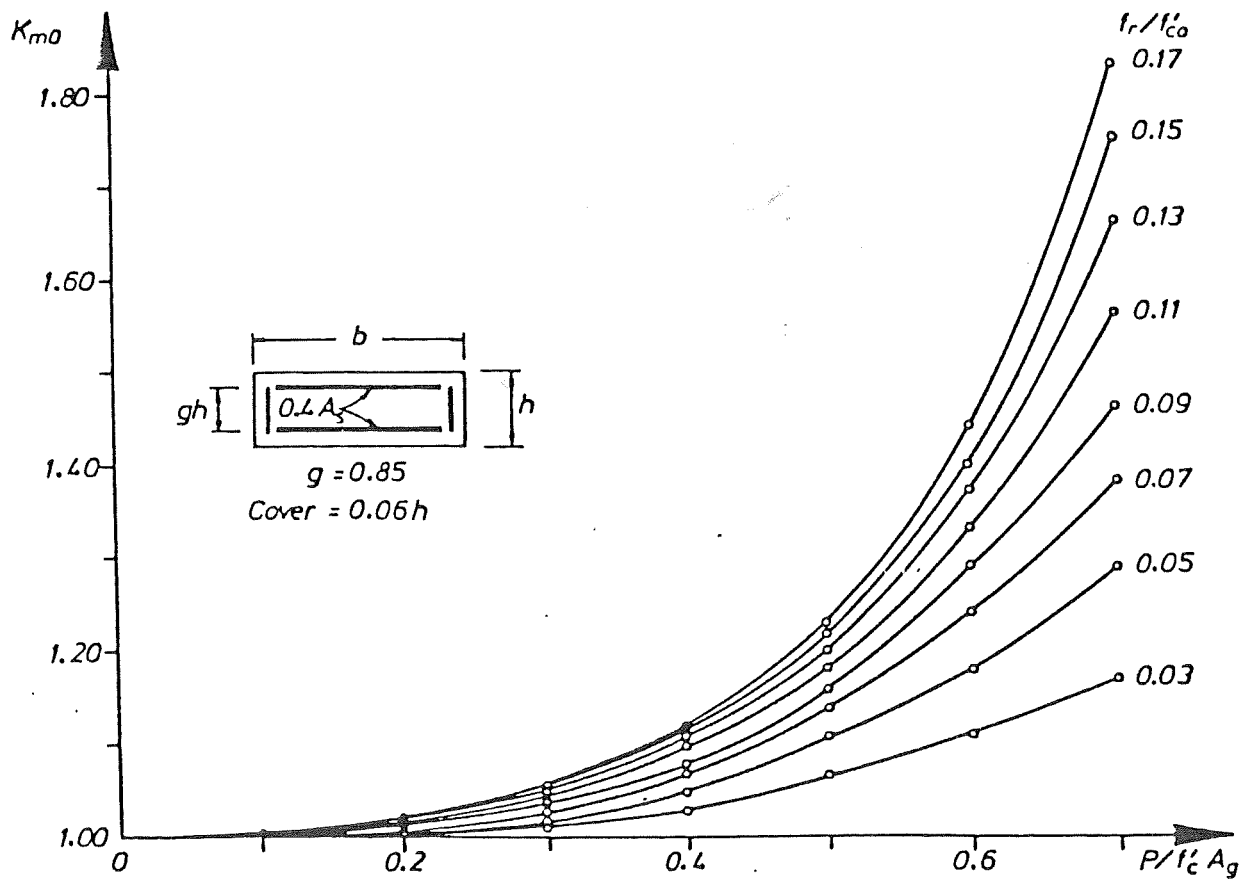


Fig. B.7 : STRENGTH ENHANCEMENT FACTOR K_{m0} FOR RECTANGULAR SECTIONS⁽²⁴⁾

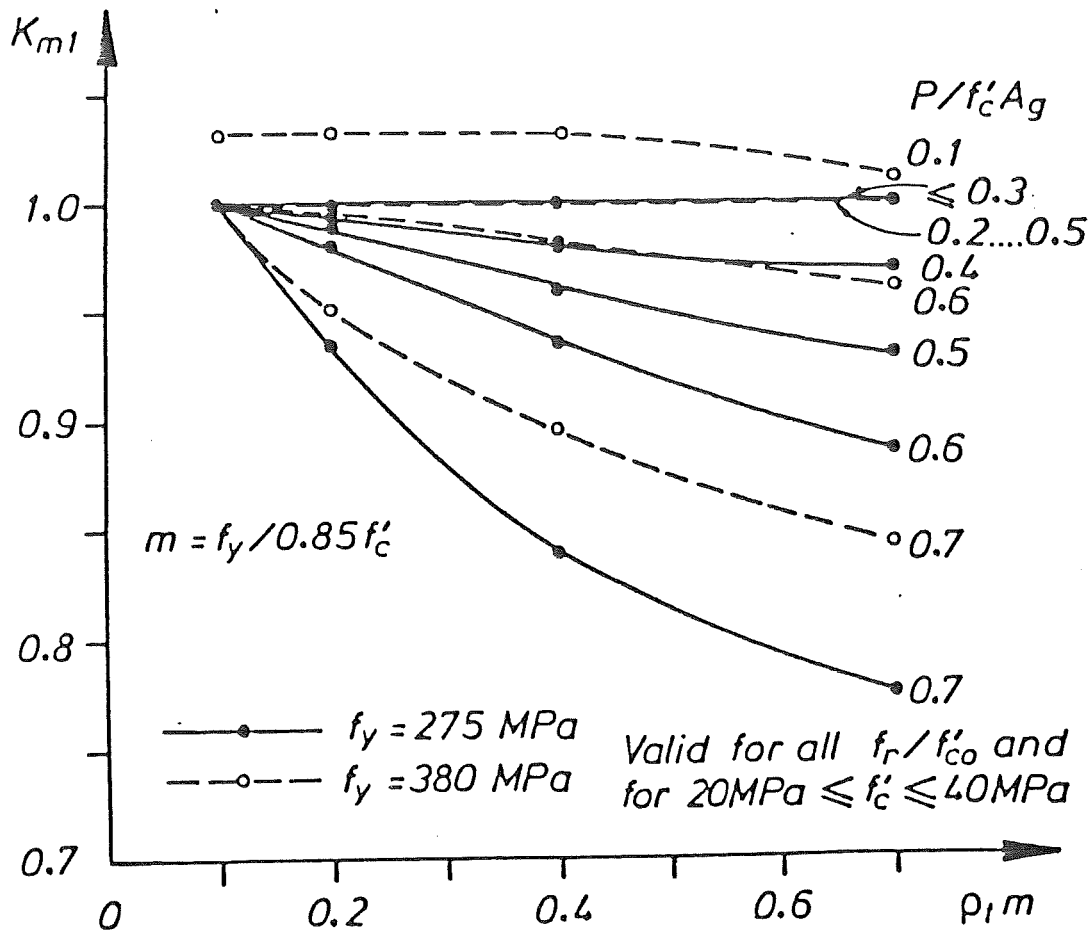


Fig. B.8 : STRENGTH ENHANCEMENT FACTOR K_{m1} FOR RECTANGULAR SECTIONS⁽²⁴⁾

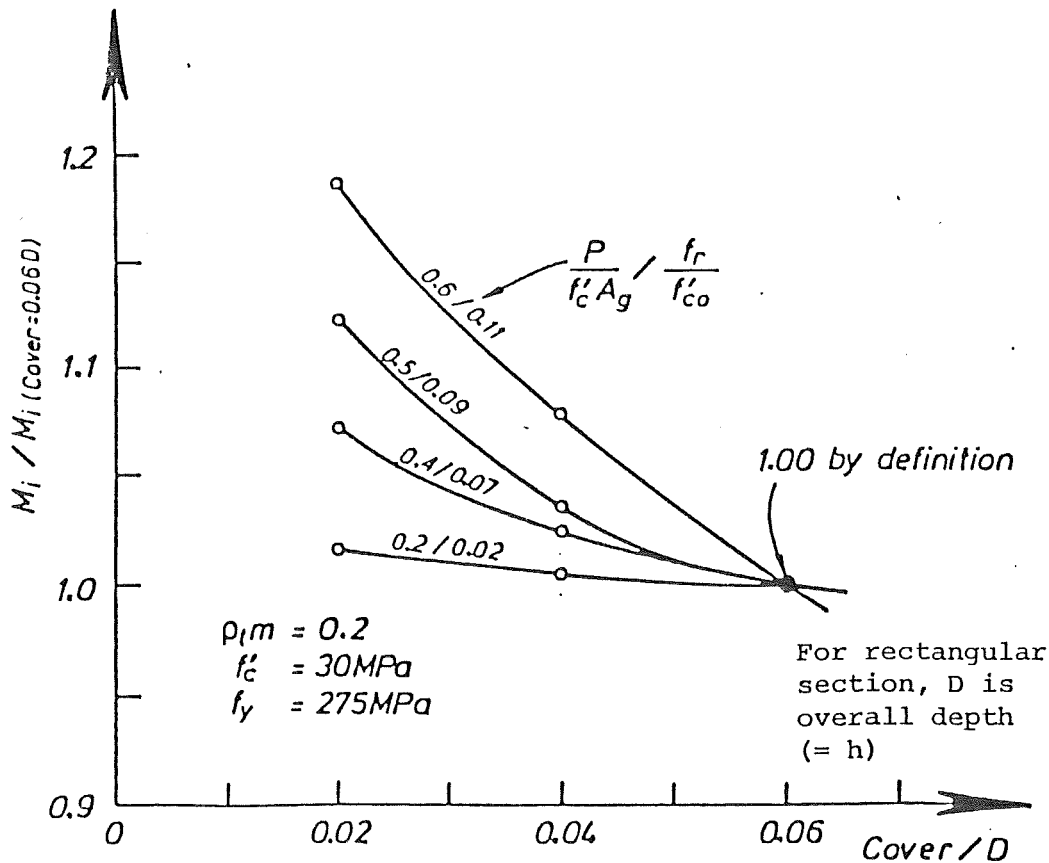


Fig. B.9 : INFLUENCE OF RELATIVE COVER THICKNESS ON FLEXURAL STRENGTH

As with the design charts for the available curvature ductility, the factors K_{m0} and K_{m1} shown in Figs. B.7 and B.8 are only valid for a particular type of rectangular column with a relative cover thickness of 0.06h. For a different cover thickness, the flexural strength can be refined as shown in Fig. B.9 which was derived for circular columns and is assumed to be applicable also to rectangular columns.

The flexural overstrength M_{max} for rectangular columns can be calculated from

$$M_{max} = M_i K_{m3} \quad (B.4)$$

where K_{m3} is a factor to allow for strain hardening of the steel which varied from 1.0 to 1.15 for Grade 275 steel and from 1.0 to 1.20 for Grade 380 steel, depending on the combination of $P_e/f'_c A_g$, ρ_t and f_r/f'_{co} . These values were derived from cyclic moment-curvature analyses for circular columns. Due to lack of information for rectangular columns, K_{m3} is assumed to be 1.10 in this study. Table B.2 shows the ideal flexural strength M_i and the flexural overstrength factor M_{max}/M_i for all units.

Table B.2 : IDEAL FLEXURAL STRENGTHS AND FLEXURAL OVERSTRENGTH FACTORS
FOR UNITS 1 TO 4

UNIT	M_{code} (kNm)	K_{m0} Fig. B.7	K_{m1} Fig. B.8	K_{m2}	$\frac{M_i}{M_i(\text{cover}=0.06h)}$ Fig. B.9	M_i (kNm) Eq. B.3	$K_{m3} = \frac{M_{max}}{M_i}$ Eq. B.4
1	302	1.0	1.06	1.05	1.0	336	1.10
2	405	1.01	1.0	1.05	1.01	434	1.10
3	406	1.01	1.0	1.05	1.01	435	1.10
4	383	1.01	1.0	1.05	1.01	410	1.10

Classn:

LIMITED DUCTILITY DESIGN OF REINFORCED CONCRETE COLUMNS

M.T. Soesianawati

ABSTRACT: Results of experimental and analytical investigations of the seismic performance of reinforced concrete square columns are presented. Conclusions are made with regard to the ductility available from columns containing substantially less transverse confining steel than recommended in the New Zealand concrete design code.

Department of Civil Engineering, University of Canterbury,
Master of Engineering Report, 1986.